Institute for Nuclear Sciences
Laboratory of Analytical Chemistry

A critical comparison and evaluation of methods for the annual radiation dose determination in the luminescence dating of sediments

Syed Mohammod Hossain

Thesis submitted in fulfillment of the requirements for the degree of Doctor (Ph.D.) in Science

Promoters: Prof. Dr. Frans De Corte
Prof. Dr. P. Van den haute

Academic year: 2002-2003

Acknowledgements

In writing these acknowledgements and looking back at the many years of struggle to prepare this thesis, I feel heartily indebted to my supervisor Prof. Dr. Frans De Corte for his guidance, encouragement, support and suggestions throughout this work. His meticulous efforts to solve all those problems, which I faced throughout this work, are very well appreciated. This thesis would not be what it is without him.

I would like to express my sincere thanks to my co-supervisor Prof. Dr. Peter Van den haute for his guidance, cooperation, valuable suggestions, and the team spirit throughout this endeavour.

I also wish to express my gratitude to Prof. Dr. Richard Dams for allowing me to undertake my studies in the Institute for Nuclear Sciences (INW) and for his support and cooperation.

I am very grateful to my nearest colleague Dimitri Vanden Berghe for his continuous help and support throughout this work.

I wish to express my very special gratitude to Tony De Wispelaere for his friendly, sincere and tireless efforts to solve all the technical problems. The technical assistance of Jochem Temmerman and Nicole Vindevogel, and the cooperation of Line Vancraeynest and Caroline Lievens with the measurements are highly appreciated.

Grateful acknowledgment is made to Prof. Dr. G. Wagner and co-workers at the Max Planck Institute (MPI), Heidelberg and to Dr. M. Tite and co-workers at the Research Laboratory for Archaeology and the History of Art (RLAHA), Oxford, for giving us the opportunity to use their calibration blocks. Thanks are due to Dr. E. Rhodes (RLAHA) for his help with the interpretation of the Oxford measurements, and to Dr. A. Murray and Dr. S. Bowman for informing us about the composition of the Oxford calibration blocks.

Thanks are due to R. Dolieslager, J. Dewaele and J. De Donder for helping me to irradiate my samples in the Reactor Thetis.

I would like to take this opportunity to thank all of my friends and colleagues of the INW, especially, M. Van Hulle, L. Mees, C. Chery, K. De Cremer, J. Courtyn, C. Hufkens and M. Dejaeger for their cooperation.

In particular I would like to thank Mrs. Igna De Corte. Igna together with Frans made my life easy and enjoyable in Belgium.

Sincere thanks and gratitude are addressed to my family members and colleagues in the Bangladesh Atomic Energy Commission for their encouragement to finish up this work. Especially, I would like to remember the root of my inspiration – my mother who has enormous efforts and prayer behind all of my success.

My wife, Rubaiyat Jahan Biswas and my sons, Syed Anagh Albab and Syed Rubric Albab deserve special mention for their support, patience, sacrifice and love throughout the period of this work.

The work was sponsored by the Fund for Scientific Research-Flanders, the Bangladesh Atomic Energy Commission and by the Ghent University.

Contents

- CHAPTER 1 -

INTRODUCTION

Human beings are now under the threat of the effects of global warming of the Earth. Therefore, dating the deposition of Quaternary sediments is quite relevant, since it provides a timescale for palaeoclimatic studies, which leads to improved modeling and eventual prediction of future trends, with associated implications for global warming. In the above context, the appropriate examples of climatically significant deposits are “loess” and “coversands”. The deposition of both sediments is indicative of dry windy conditions. Loess is generally associated with glacial climate, whereas coversand can document arid periods. Although numerous methods are existing in geochronological dating, the luminescence method is one of the very few that is suitable for the case of sediment. It provides a direct means for determining the time of deposition and is not based on the age determination of associated materials, as it is the case for e.g. ^{14}C dating.

Luminescence dating is a method that can be used to determine the time that has elapsed since a sediment was last exposed to sunlight as a “clock resetting event” [Aitken, 1985, 1998]. Such a clock resetting exposure may occur between the time of erosion of silt or sand grains and the time of their subsequent deposition in a sedimentary deposit. For example sunlight exposure occurs during the transportation of the loess particles through the air.

The primary materials used for luminescence dating of sediments are either quartz or feldspars. These minerals have a crystalline structure such that they are capable of producing a luminescence signal, and they are present in the majority of sedimentary environments. The amount of luminescence emitted is proportional to the mineral’s intrinsic sensitivity to radiation and the total amount of radiation absorbed (= the radiation dose). In this way, the mineral is used as a natural radiation dosimeter. The

luminescence can be observed and measured when the minerals are stimulated either thermally (TL) or optically (OSL). The age equation can be written as:

$$\mathrm{TL/OSL-age} = \frac{\text{palaeodose} \quad (\mathrm{Gy})}{\text{annual radiation dose} \quad (\mathrm{Gy/unit\ of\ time})} \tag{1.1}$$

where Gray (symbol: Gy) is the amount of energy absorbed per unit of mass (Joule/kg). The palaeodose is the amount of radiation dose that is responsible for the sample's natural luminescence signal. It is accumulated at a rate characteristic of the sample itself and of the environment in which the sample is buried. Therefore, the palaeodose is proportional to the age of the sample, i.e. the time elapsed since the last clock resetting event. It can be evaluated from the division of two measured quantities: the natural luminescence signal (counts) emitted by the sample and the sample's sensitivity (counts/Gy) as derived via administering a known artificial radiation dose.

The palaeodose and the annual radiation dose have their origin in the γ-, β- and/or α-radiation of the naturally occurring long-lived radionuclides ^{40}K, ^{232}Th+daughters and ^{235,238}U+daughters [the contribution by ^{87}Rb and cosmic radiation usually being less critical] present in the samples and their immediate surroundings. The role of radioactivity in luminescence dating is that it provides a constant dose rate for the production of luminescence, assuming that the geological processes have not altered the radioactive concentrations during the burial period.

The above considerations are the subject of Chapter 2, where a concise outline is given of the basic principles of the luminescence dating method, and of its use in sediment dating.

From the age equation [Eq. (1.1)], it is clear that the assessment of the annual radiation dose is an important step in luminescence dating, since its relative uncertainty is linearly propagated to the age result. Therefore, adequate methodologies have to be chosen and dedicated working procedures should be

followed in order to arrive at dose rate values with sufficient precision and accuracy. In the course of the years, much attention went to the development and optimization of various methods for the determination of the dose rate [Aitken, 1985, 1998]. Occasionally, some comparisons of these methods were made, mostly in the context of dating work e.g. by Hutton and Prescott [1992] and Prescott and Hutton [1995]. Since then, new methods came into use and others were optimized, while the recently developed protocols for improved palaeodose determination at the same time impose a more stringent accuracy and precision on the determination of the annual radiation dose.

As outlined in Chapter 3, evaluation of the annual radiation dose is possible by using:

an indirect method:

- via determining the concentrations of the radioactive elements [Goedicke, 1988; Olley et al., 1997; Pernicka and Wagner, 1982; Preusser and Kasper, 2001];
- via alpha-, beta- and gamma- ray counting [Bøtter-Jensen and Mejdahl, 1985, 1988; Chiozzi et al., 2000; Chowdhury et al., 1982; De Corte et al., 2001, 2002; Guibert and Schvoerer, 1991; Meakins et al., 1979; Murray et al., 1987; Murray and Aitken, 1988; Sanderson, 1988; Sanzelle et al., 1988; Wintle and Dijkmans, 1988];

a direct method:

- via thermoluminescence dose monitors e.g. $CaSO_4$:Dy, CaF_2:Dy, α-Al_2O_3:C, etc. [Aitken, 1968, 1969; Bailiff, 1976; Bailiff and Aitken, 1980; Bøtter-Jensen, 2000; Bowman, 1976; Kalchgruber, 2002; Mejdahl, 1978; Murray, 1981].

With the above considerations in mind, and also depending on the availability of experimental facilities, a detailed study of some commonly applied methods for the determination of the annual radiation dose was undertaken in the framework of this doctoral thesis. It reports on our findings for the determination of the annual radiation

dose in two typical aeolian (windblown) deposits, loess and coversand, using the following methods:

- NaI(Tl) gamma-ray spectrometry both in field (in-situ) and in low-background laboratory conditions, for the measurement of K, Th and U;

- extended energy-range Ge gamma-ray spectrometry in low-background laboratory conditions, for the measurement of K, Th and U, and also for the detection of possible disequilibria in the Th- and especially the U-decay series;

- thick source ZnS alpha-counting, both in the integral and in the pair-counting mode (the latter for the discrimination between Th and U);

- low-background GM beta-counting, for the measurement of K + Th + U;

- instrumental reactor neutron activation analysis (INAA) for the determination of K, Th, U and Rb;

- atomic absorption spectrometry (AAS), for the determination of K.

It should be noted that the contribution from cosmic radiation was not investigated. This contribution amounts to a few percent only and can with sufficient accuracy be adopted from existing tabulations [Prescott and Hutton, 1994].

The present systematic study on the annual radiation dose determination in luminescence dating of sediments was performed via the analysis of two sediment profiles: a loess profile at Volkegem, in the southern part of East Flanders, Belgium and a coversand profile at Ossendrecht, in the south-western part of the Netherlands. The case of the loess sediment is dealt with in Chapter 4, whereas the study of the coversand is described in Chapter 5.

Finally, Chapter 6 summarizes our findings and deals with the overall conclusions.

- CHAPTER 2 -

THE LUMINESCENCE DATING METHOD

2.1. Principle

The luminescence dating method is based on the time-dependent accumulation of radiation energy stored in some non-conducting crystalline materials as a result of natural radioactivity. In the laboratory, the deposited energy can be released in the form of luminescence by stimulation, either via heating [thermoluminescence] or illumination [optically stimulated luminescence]. As a result, the TL/OSL signal acquired over geological time - i.e. since the last clock resetting event (e.g. signal zeroing by heating in the case of pottery or by exposure to sunlight in the case of windblown sediment) - is removed and can be measured. This is schematically shown in Fig. 2.1.

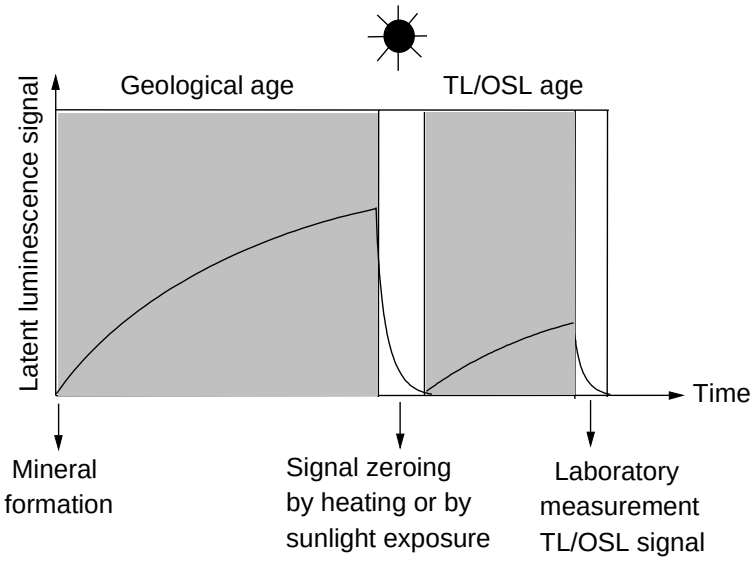

Fig. 2.1. Schematic representation of the luminescence dating principle (based on Vancraeynest, 1998).

The amount of TL/OSL signal observed in the sample estimates the amount of total absorbed radiation dose - termed as palaeodose. As outlined in the Introduction [Eq. (1.1)], comparison of the palaeodose with the dose received per year or the annual radiation dose (assumed to be constant with time) permits determination of the age of the sample:

$$\mathrm{TL/OSL-age} = \frac{\text{palaeodose} \quad (\mathrm{Gy})}{\text{annual radiation dose} \quad (\mathrm{Gy/unit\ of\ time})} \tag{2.1}$$

2.2. The palaeodose

TL/OSL measurements are used to estimate the radiation dose that the sample has absorbed since the event that is being dated. This quantity is known as the palaeodose or equivalent dose. It can be evaluated from measurement of the natural luminescence signal (counts) and the sensitivity (counts/Gy). The palaeodose can be expressed by the equation:

$$\text{palaeodose} = \frac{\text{natural TL/OSL signal (counts)}}{\text{TL/OSL sensitivity (counts/Gy)}} \tag{2.2}$$

The TL/OSL sensitivity, i.e. the TL/OSL signal per unit radiation dose, is measured after exposing the sample to a known dose of radiation from an artificial radioisotope.

2.2.1. Physical mechanism of luminescence

Although the mechanisms responsible for luminescence are much more complex, it is convenient to use a simplified model for explaining the behaviour of luminescent crystals in the context of the dating method. In this model, an ideal insulating crystal is characterized by an occupied valence band and an empty conduction band, with an energetically forbidden zone in between. Natural crystals, however, are not perfect

and have structural defects (such as vacancies, dislocations and substitutional impurities), which lead to localized energy levels within the forbidden zone.

The first step in the luminescence process is the creation of electrons and holes due to the interaction of ionizing radiation with the mineral lattice (Fig. 2.2.a). These electrons and holes subsequently can get "trapped" at defects T and L, respectively in the forbidden zone (Fig. 2.2.a). The longer the mineral is exposed to ionizing radiation, the more charges are accumulating in the traps. The efficiency by which the electrons are stored in the electron traps, is determined by the depth E (Fig. 2.2.b) below the conduction band. In the context of dating, we are only concerned with those traps which are deep enough so as to have insignificant leakage during the time span that is being dated.

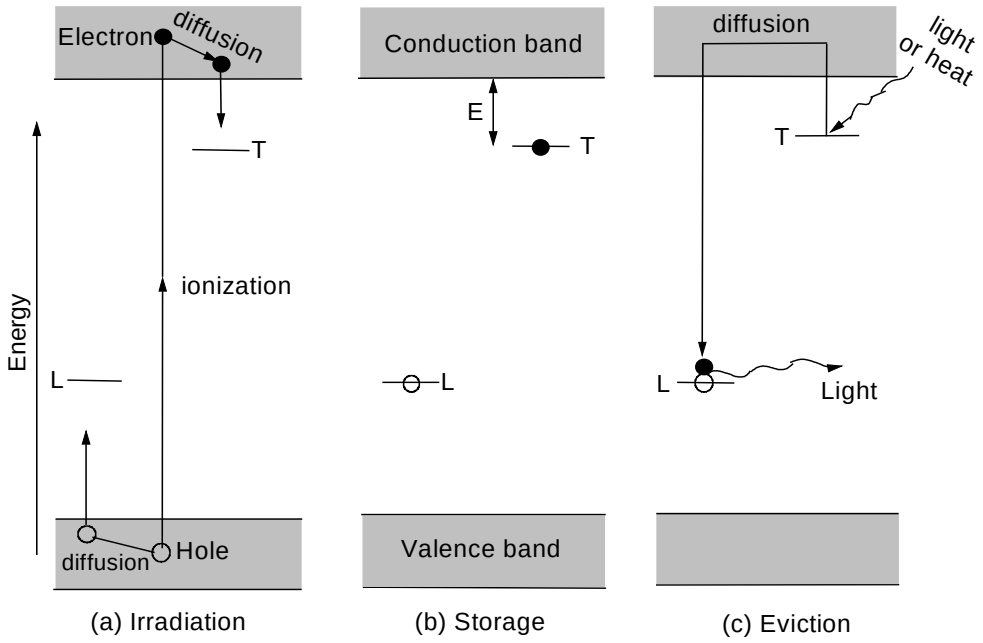

Fig. 2.2. Energy-level diagram of TL and OSL processes (based on Aitken, 1998): a) ionization due to exposure to nuclear radiation with trapping of electrons and holes at crystal defects; b) storage during antiquity; c) the electron is evicted from its trap by heating or shining light and recombines with a luminescence center under emission of TL/OSL signal.

The trapped electrons can become free once again if the crystal is heated to a certain temperature or is exposed to light of a specific wavelength (Fig. 2.2.c). Luminescence finally occurs if the released electrons recombine with hole centers also called

luminescence centers. When the luminescence is stimulated by applying heat or light, the resulting signal is known as thermoluminescence (TL) or optically stimulated luminescence (OSL), respectively. The amount of luminescence emitted is proportional to the total absorbed radiation dose (ignoring the effects of signal saturation). This is the fundamental basis of TL and OSL dating.

2.2.2. The luminescence processes

2.2.2.1. Thermally stimulated luminescence (TL)

In the early 1950s, Daniels et al. [1953] launched the use of thermoluminescence (TL) to measure nuclear radiation doses and they suggested to use it for geological and archaeological age determination. Afterwards, it was extensively applied to date archaeological and geological materials (pottery, burnt flint, burnt stones, volcanic lava, stalagmitic calcite, etc.) [Aitken et al., 1964, 1968; Debenham and Aitken, 1984; Göksu et al., 1974; Mejdahl, 1969; Miallier et al., 1983] and sediments [Morozov, 1968; Wintle and Huntley, 1979, 1980]. The methodology of thermoluminescence dating has been reviewed by Aitken [1985]. If a sample is heated at a constant rate to some temperature (e.g. 500^{o}C), there is emission of light. The luminescence emitted as a function of temperature is termed as "glow curve". The glow curve observed in a loess sample collected from Volkegem (southern part of East Flanders, Belgium) is shown in Fig. 2.3. During the heating, traps of increasing depth are emptied and thus the glow curve peaks reflect the thermal stability of the electron traps involved. Normally, glow peaks lower than 200^{o}C are not useful for dating Quaternary deposits, as electrons can be liberated from the traps over a prolonged time even at environmental temperatures. Stable glow peaks suitable for dosimetry usually occur at higher than 300^{o}C. However, anomalous fading of high temperature glow peaks at room temperature has been observed in some feldspars. In principle, TL-dating covers a wide age range of a few 100 a up to ca. 1 Ma, the upper limit being caused by long-term fading and/or saturation of the TL-signal.

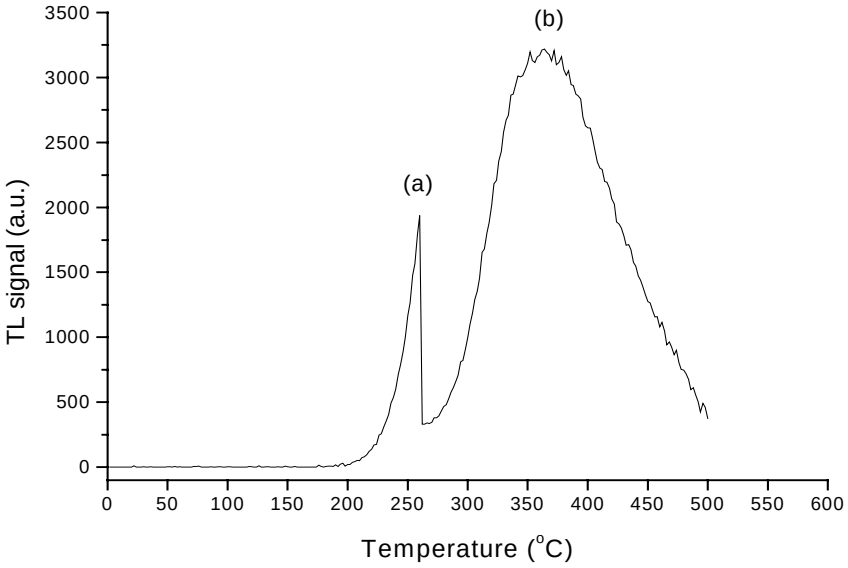

Fig. 2.3. Thermoluminescence glow-curve observed in a loess sample taken from Volkegem (background subtracted); curve (a) shows the light emission observed during preheat and curve (b) light observed during the second heating.

2.2.2.2. Optically stimulated luminescence (OSL)

Although thermoluminescence dating of sediments was well underway in the 1970s, problems associated with incomplete zeroing made the technique difficult to apply. Huntley et al. (1985) and Hütt et al. (1988) opened a new era of optical dating, showing that quartz and feldspar grains in sediments exhibit luminescence signals which are rapidly and completely zeroed by a few minutes of daylight exposure, thus avoiding the main problem of TL dating.

If the OSL intensity of a sample is directly measured as the stimulation proceeds, a decreasing curve, the so-called "shine-down curve", is obtained with increasing exposure time. The OSL shine-down curve of a sand sample taken from Ossendrecht (south-western part of the Netherlands) and stimulated by blue light is shown in Fig. 2.4. The OSL signal of quartz and feldspars is completely bleached away by stimulation for a few minutes with a light intensity of ca. 10 mW cm^{-2} [Aitken, 1998]. Due to this characteristic, the OSL dating method enables the dating of very recent events (<100 a), whereas the upper limit should be the same as for TL.

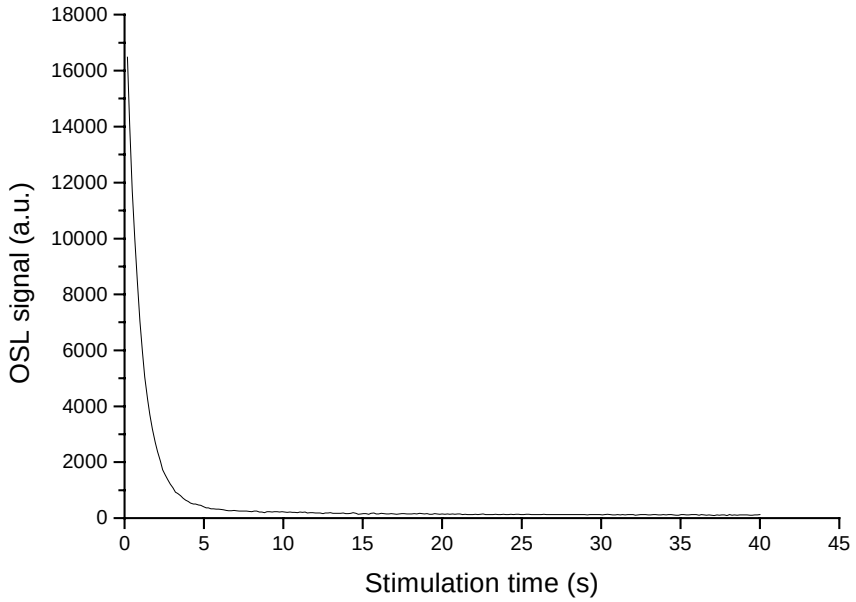

Fig.2.4. Optically stimulated luminescence (OSL) shine-down curve of sand sample (stimulated with blue light) taken from Ossendrecht.

2.3. The annual radiation dose

2.3.1. Natural radioactivity

Various kinds of radioactive nuclides are present in nature, and they can be placed in the following categories:

primordial: existing since the last event of nucleosynthesis preceding the formation of our Solar System;

cosmogenic: formed as a result of cosmic ray interactions with our atmosphere and lithosphere;

human made: enhanced or formed due to human activities.

The annual radiation dose in luminescence dating originates from the ionizing radiation (γ-, β- and α-radiation) of naturally occurring, long-lived primordial

radionuclides (^{235}U, ^{238}U, ^{232}Th, ^{40}K and ^{87}Rb) present in the sample and its immediate surroundings and from cosmic radiation (the contribution from ^{87}Rb and cosmic radiation usually being less critical).

When nuclei of ^{40}K with a natural atomic abundance of 0.0117% undergo radioactive decay, beta particles and a gamma ray with an energy of 1460.8 keV are emitted. For ^{87}Rb, there is emission of β-particles only. The radioactive decay schemes of ^{40}K and ^{87}Rb are shown in Fig. 2.5.

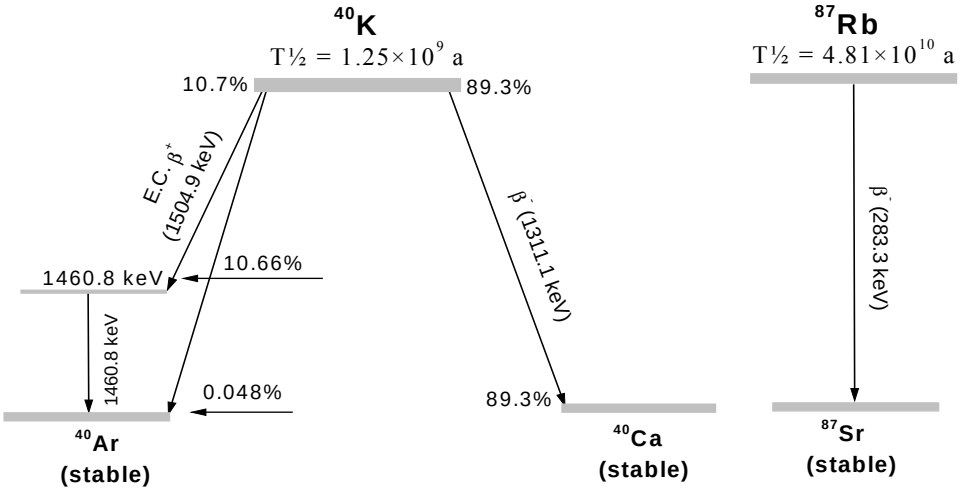

Fig. 2.5. Decay schemes of ^{40}K and ^{87}Rb.

Natural uranium and thorium consist of three radioactive series headed by ^{235}U, ^{238}U and ^{232}Th and ending in ^{207}Pb, ^{206}Pb and ^{208}Pb, respectively. It is generally assumed that the ^{238}U to ^{235}U ratio is constant in nature. Even though ^{235}U accounts for only 0.72% of the atoms in the natural uranium, it contributes to as much as ~ 4.4% in the combined uranium activity, because of the shorter half-life of ^{235}U compared to ^{238}U. During transformation of the U concentration to the annual radiation dose, the constant ^{238}U/^{235}U ratio is taken into account.

The natural Th to U concentration ratio in the earth crust is about 4:1, and the limited variability of this ratio plays a role in the calibration of the ZnS alpha counting.

When the nucleus of ^{235}U undergoes radioactive decay, with emission of an α-particle, the daughter nucleus formed, ^{231}Th, is also radioactive. This process continues through radioactive daughters until the stable ^{207}Pb isotope is reached. Linking the start and end of the chains there are several radioactive daughters of ^{235}U, ^{238}U and ^{232}Th that are significant since they emit a variety of α-, β- and γ-radiations. The radioactive decay series of ^{235}U, ^{238}U and ^{232}Th are shown in Figs 2.6 - 2.8.

α-Particles emitted by an unstable nucleus belong to one or more mono-energetic groups. Most naturally occurring α-ray emitters emit particles in the range of 3 to 8 MeV. Being highly charged and relatively heavy, they interact intensely with electrons within the atoms of the materials they encounter without getting scattered, giving up their energy gradually over a very short but well-defined penetration range that is significant in the context of luminescence dating. In silicate minerals their travel distances are limited to about 25 μm.

A β-particle emitted from the nucleus of radioactive atoms has a continuum energy spectrum up to about 2 MeV. β-Particles are much less massive and less charged than α-particles and interact less intensely with atoms in the material they pass through, which gives them a longer range than α-particles. Their range in minerals is about 2 mm. When β-particles decelerate by interaction with electrons and protons, part of their energy is converted into electromagnetic radiation in the form of bremsstrahlung. The intensity of bremsstrahlung radiation is proportional to the energy of the beta particles and the atomic number of the material through which the β-particles are passing.

In many instances, γ-rays are accompanying the emission of α- and β-particles. Like all forms of electromagnetic radiation, γ-rays have no rest mass or charge and interact less intensively with minerals than ionizing particles, which gives them a large material penetrating capability. For the case of sediment material, the γ-ray penetrates to a distance of about 50 cm [(for E_γ = 2614.5 keV (^{208}Tl in the ^{232}Th decay series)] [De Corte et al., 1994]. The interaction behaviour of γ-rays with matter is in marked

contrast to the α- and β- particles, which slow down gradually through continuous, multiple interaction with many absorber atoms. By the interaction the photon disappears entirely or is scattered through a significant angle. There are three types of significant interaction mechanisms, which play an important role in the field of radiation research, namely photoelectric effect, Compton effect and pair production. Photoelectric effect predominates for low-energy gamma rays, pair production predominates for high-energy gamma rays, and Compton scattering is the most probable process over the range of intermediate energies between these extremes.

All these three types of radiation (α, β, γ) discussed above are quite important for the luminescence dating methods, and the amount of luminescence induced in the sample depends both on the rate of emission and the energy carried by these radiations. The share of the α- and β- radiation dose rate to the total annual radiation dose is mostly coming from the radionuclides present within the sample, whereas the share of the γ-radiation dose rate is mostly coming from the radionuclides present in the surrounding materials from where the samples have been collected.

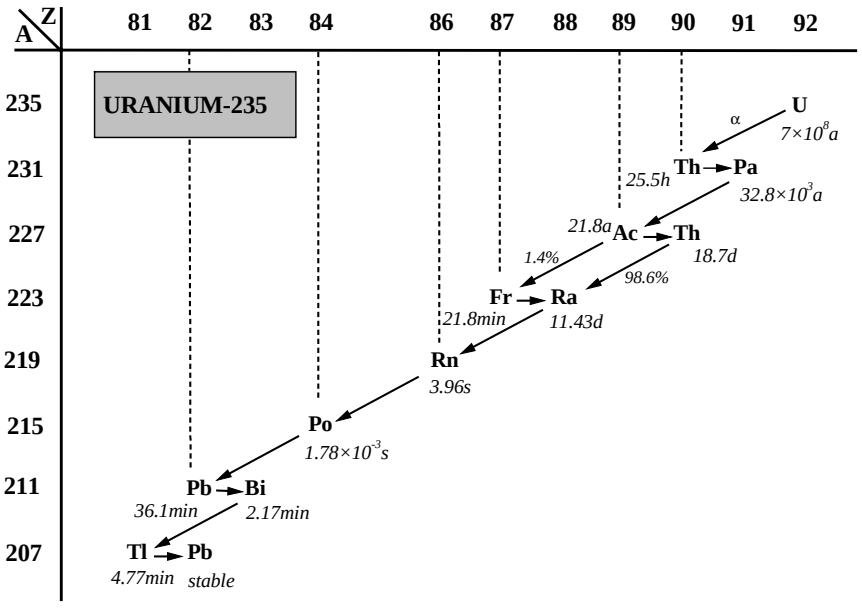

Fig. 2.6. Decay chain of ^{235}U (branchings with a probability of less than 1% are omitted).

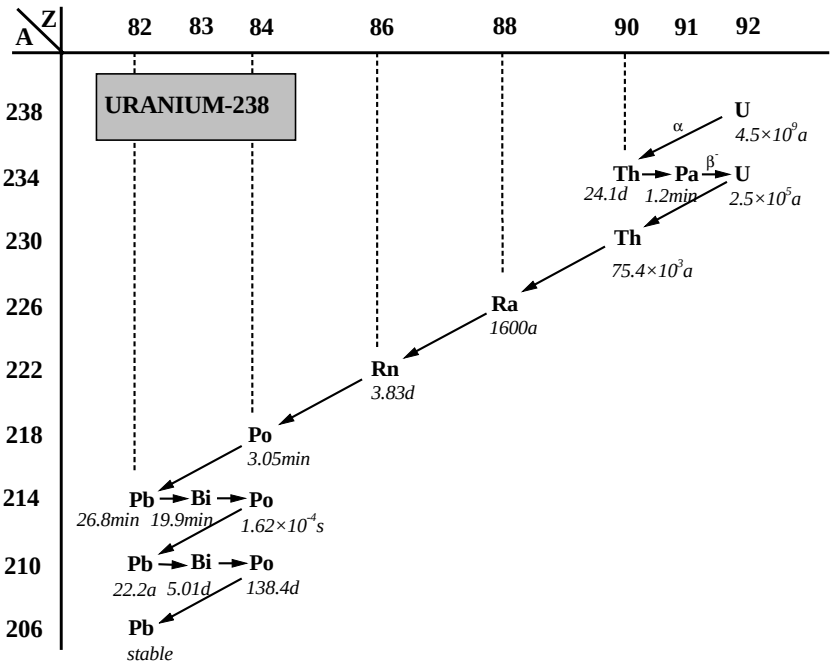

Fig. 2.7. Decay chain of ^{238}U (branchings with a probability of less than 1% are omitted).

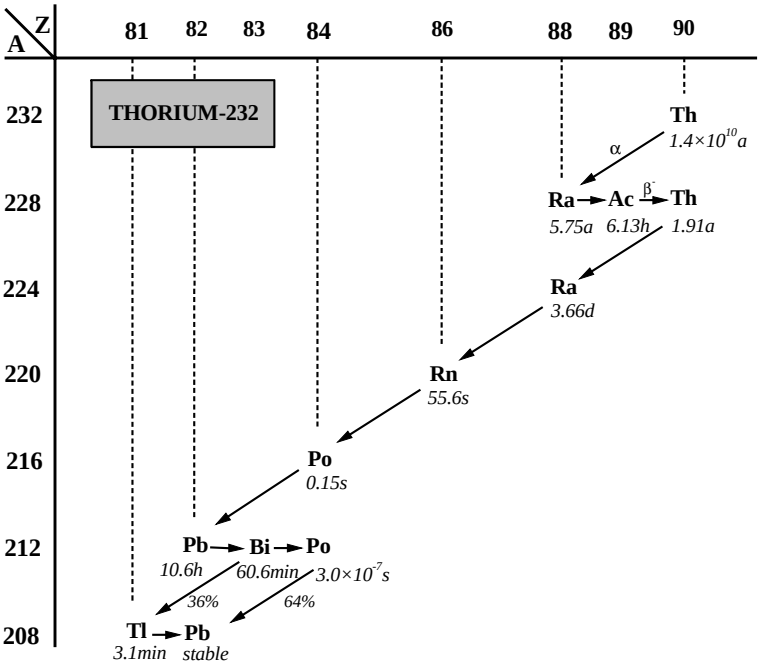

Fig. 2.8. Decay chain of ^{232}Th (branchings with a probability of less than 1% are omitted).

2.3.2. Radioactive equilibrium

In the radioactive decay chains as shown above (Figs 2.6 – 2.8), each parent decays into a daughter nucleus which itself is radioactive, until the chain ends with a stable lead isotope. If the system is closed, a radioactive equilibrium is reached in which $\lambda_1 N_1 = \lambda_2 N_2 = \lambda_i N_i$ [where $\lambda = (\ln 2)/T_{½}$ is the decay constant and N is the number of nuclei], i.e. all decaying radionuclides have the same activity. Obviously, in case of branched decay, a multiplication has to be done with the branching factor.

It is important to note that, if the half-life of the parent radionuclide is much longer than that of the daughter, the latter determines the time after which equilibrium is reached. Indeed, beyond about 10 half-lives of the daughter radionuclide it decays at the same rate as it is produced - a state called secular equilibrium. A relevant example is the mother-daughter pair ^{226}Ra ($T_{½}$ = 1600 a) which decays to ^{222}Rn (3.83 days), for which equilibrium is thus reached after about one month.

2.3.3. Radioactive disequilibrium

As mentioned above, the role of radioactivity in luminescence dating is that it provides a constant dose rate, assuming that geological processes have not altered the radioactive concentrations during the entire burial period. Unfortunately, this simple assumption may become violated by the possibility of disequilibria in the radioactive decay series.

In a geochemically closed system, the concentration of ^{40}K will remain effectively constant over the entire burial period and - consequently - the dose rate from this nuclide will also remain effectively constant.

For the ^{232}Th decay series the risk of disequilibrium is comparatively low due to its relatively short-lived daughters (the longest-lived being ^{228}Ra with a half-life of 5.75

years). Thus, the dose rate derived from the ^{232}Th decay series will also be likely to remain effectively constant over the entire burial period.

The equilibrium conditions of the ^{238}U decay series, however, can be more easily disrupted by physical and chemical processes. Mobility of individual nuclides in the decay series can result in parts of the series being broken by depletion or enrichment of radionuclides.

An obvious example is the loss of ^{222}Rn ($T_{1/2}$ = 3.83 d) due to gaseous diffusion, which would reduce the lower part of the uranium series relative to the parent ^{238}U. This emanation is particularly likely if the sample is porous rather than compact. Due to the short half-life of ^{220}Rn ($T_{1/2}$ = 55.6 s) in the ^{232}Th series and of ^{219}Rn ($T_{1/2}$ = 3.96 s) in the ^{235}U series, migration out of the material is not very likely to occur in these cases.

Another example is that of ^{226}Ra which may be leached out (then all subsequent members of the series are depleted) or leached in (all subsequent members of the series are then present in excess) by the action of ground water. In fact, this is also true for its predecessor ^{234}U, for instance as a result of α-recoil leading to weaker binding in the crystal lattice, or even to migration to the pore filling, or as a result of the enhanced leachability of its +6 oxidation state which forms water soluble complexes [Krbetschek et al., 1994].

High-resolution gamma-ray spectrometry with a low-background extended-energy Ge-detector is a suitable method for checking the occurrence of disequilibria in the ^{232}Th and ^{235,238}U series. In practice, this comes down to measuring the concentrations of certain key isotopes at different positions in the decay series. The measurement of the gamma-lines from ^{226}Ra and its daughters ^{214}Bi and ^{214}Pb e.g. is respectively directly and indirectly indicating any depletion or enrichment of ^{226}Ra. On the other hand, ^{210}Pb is a suitable indicator for Rn emanation in geological times. The problem remaining is that due to many low-intensity gamma-rays and spectral interferences, only a limited number of gamma-lines can be measured with sufficient statistical

uncertainty via Ge gamma-ray spectrometry (the experimental details will be discussed further in Chapter 4 Section 4.3).

Another technique which can provide information on possible radioactive disequilibria is alpha-spectrometry. In this case, one looks at the various α-emitters throughout the decay chains. For instance, a valid alternative for ^{210}Pb as a Rn indicator, is ^{210}Po (see Fig. 2.7).

Although the degree of radioactive disequilibrium can in principle be serious, it should be noted that in many cases small-scale disequilibria (partial emanation of radon, partial leaching of radium) do not have a significant effect on the annual radiation dose.

2.3.4. Cosmic radiation

The contribution of cosmic rays to the annual radiation dose is usually very small compared to that from the radioelements ^{235,238}U + daughters, ^{232}Th +daughters, ^{40}K and ^{87}Rb. The primary cosmic ray particles interact with the upper atmosphere and produce showers of secondary particles. Many of these secondary particles having lower energy are absorbed by the earth's atmosphere. At sea level, cosmic radiation is composed of hard and soft components. The hard component is mainly consisting of muons, the soft component of electrons. The latter are fully absorbed by 50 cm of sediment layer [Aitken, 1985]. In the context of luminescence dating one is concerned with the hard component, which shows a dependency on altitude and geographical latitude. Because the earth's atmosphere acts as a shield, the exposure to cosmic rays is greater at higher elevations then at sea level. In a typical sediment at a depth of 1m, the average cosmic radiation dose rate is 0.150 Gy.ka^{-1} for latitudes above 40^{o}, at sea level [Aitken, 1985]. The variation of cosmic radiation dose rate with depth is shown in Fig. 2.9.

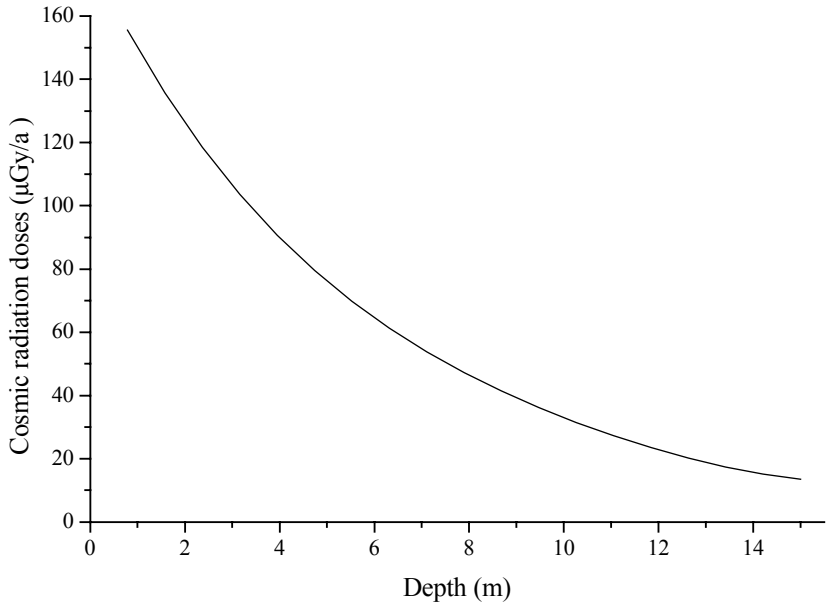

Fig. 2.9. Variation of cosmic radiation dose rate with depth under the earth's surface (taken from Vancraeynest, 1998), for latitudes above 40^o, at sea level.

- CHAPTER 3 -

SURVEY OF METHODS FOR THE ANNUAL RADIATION DOSE DETERMINATION

3.1. Classification of methods

There are many analytical methods that have been adopted in the past for determining the annual radiation dose. In practice, they can be classified in the following categories:

Indirect determination:

1) concentration determination of radioelements;
2) α-, β- and γ-ray counting;

Direct determination

3) α-, β- and γ-dose determination via dose monitors e.g., α-Al_2O_3:C, $CaSO_4$:Dy, CaF_2:Dy, etc.

3.1.1. Indirect determination

3.1.1.1. Concentration determination of radioelements

A large number of analytical methods are available to assess the annual radiation dose via the determination of the U, Th and K. Although Rb can be determined as well, this is rarely done because its contribution to the annual dose is quite small (of the order of 1%), so that in general a K:Rb concentration ratio of 200:1 [Warren, 1978] can safely be assumed without introducing a significant inaccuracy.

The most frequently applied determination methods are: (n,γ) reactor neutron activation analysis (NAA) - for K, U and Th, fission track counting (FT) – for U, Th, and delayed neutron analysis (DNA) – for U [Pernicka and Wagner, 1982]; inductively coupled plasma mass spectrometry (ICP-MS) – for K, U and Th [Preusser and Kasper, 2001]; X-ray fluorescence (XRF) – for K, U and Th [Olley et al., 1997]; and atomic absorption spectrometry (AAS) and flame photometry – for K [Aitken, 1985].

Evidently, all of these methods yield, next to K, only the U and Th parent nuclide concentrations, and they are therefore only reliable on condition that the U and Th decay series are in equilibrium. For more detailed information on the NAA and AAS instrumentation and protocols used in this work, see Chapter 4 Sections 4.7 and 4.8, respectively.

3.1.1.2. α-, β- and γ-ray counting

Thick source α-counting (TSAC) using a ZnS screen is the most common approach for the assessment of the alpha dose rate directly from the alpha activity itself. Alpha counting was adopted for luminescence dating in the early 1960s [Tite and Waine, 1962]. In the early stage of luminescence history most of the laboratories were using it for the determination of not only the alpha dose rate but also of the beta and gamma dose rate of U and Th in conjunction with chemical analysis of K (usually by flame photometry). Strictly speaking, for assessing the U and Th beta and gamma dose rate, the conversion of count rate to dose rate depends on the U:Th concentration ratio in the sample. Fortunately, the alpha counting technique can be applied both in the integral mode (for determining the gross alpha activity from U, Th and their daughters) and in the pair counting mode (to discriminate between U and Th) [Aitken, 1985]. In spite of suffering from the effect of "overcounting" [Pernicka and Wagner, 1982; Wintle and Dijkmans, 1988; Zöller and Pernicka, 1989], the technique keeps a central place in most of the luminescence laboratories. It should be noted that if the U and Th decay chains are not in equilibrium, the accuracy of the annual radiation dose

determination obtained via α-counting (where the whole of alpha radiation is measured) is not so much deteriorating as in the case of chemical analysis only yielding the parents.

The ZnS alpha counting system can not be applied as a spectrometer due to its poor resolution and incapability for distinguishing different energies of alpha emission. It is, however, possible to make use of high-resolution alpha spectrometry [Desai, 1975; Murray, 1981] with silicon surface barrier detectors, in order to distinguish between different alpha-energies. In this way, the count rates (and finally the concentrations) from individual members of the Th and U decay series can be obtained, thus enabling the examination of equilibrium conditions in both the U and Th decay chains. Evidently, the main disadvantage of the method is that a laborious destruction and chemical treatment of the sample is required in order to prepare a source which is thin compared to the alpha ranges. In spite of this, alpha spectrometry is frequently used for the measurement of ^{210}Po, the grand-daughter of ^{210}Pb, as an indicator for radon in the ^{238}U decay series. The reason for this popularity is that polonium can easily and selectively be isolated from the solution obtained after digestion of the sample, by spontaneous deposition on a silver foil [García-Orellana and García-León, 2002; Mangini et al., 1983].

Thick source beta counting (TSBC) using wafers of NE102A plastic scintillator developed by Sanderson [Sanderson, 1988], or using the Risø beta GM multicounter system developed by Bøtter-Jensen and Mejdahl [1985, 1988], are the most common approaches for beta dose determination. The methods are convenient due to their capability of handling a small amount of sample, the low cost of high-efficiency counters and the low background levels that can be obtained (using an anti-coincidence "guard detector" in the case of the Risø beta GM multicounter system). Here too, the reliability of the results is bound to the establishment of equilibrium in the U and Th decay series.

The most common approaches for the dose-rate assessment via gamma-ray counting are NaI(Tl) and Ge gamma-ray spectrometry.

Highly efficient but poor resolution NaI(Tl) gamma-ray counting systems are especially suitable for the on-site determination of the in-situ environmental gamma dose rate [Chiozzi et al., 2000; De Corte et al., 2001; Sanzelle et al., 1988]. Although in the literature [Aitken, 1985] it is mentioned that, when working in auger hole geometry, gamma-rays from a volume of 30 cm radius around the sample location are measured, this radius is rather of the order of 60-80 cm, depending on the gamma-ray energy [De Corte et al., 2001]. An important advantage of on-site measurements is that any effects of heterogeneity in radioactivity within this radius are automatically taken into account. Next to the 1460.8 keV line of ^{40}K, the technique only measures the decay of two radionuclides in the lower half of the U and Th decay chains [1764.5 keV for ^{214}Bi in the ^{238}U series and 2614.5 keV for ^{208}Tl in the ^{232}Th series]. This makes that accurate results for the dose rate are only obtained in case of equilibrium in the decay series. Evidently, in addition to its use as a portable instrument in field work, the NaI(Tl) detector can also be operated for measuring samples in low-background conditions in the laboratory. In this case, the same type of information is obtained as outlined above, albeit for a more limited sample volume.

Ge gamma-ray spectrometry, apart from yielding elemental concentrations, is capable - thanks to its excellent energy-resolution - of individually measuring a number of radionuclides in the U and Th decay chains, so that information on the radioactive equilibrium is obtained [Chowdhary et al., 1982; Guibert and Schvoerer, 1991; Meakins et al., 1979; Murray et al., 1987; Murray and Aitken, 1988; Olley et al. 1997; Prescott and Hutton, 1995]. The measurements must obviously be done in low-background conditions. Moreover, in order to have a precise and accurate response of the low-energetic gamma-lines (the 63.3 keV line of ^{234}Th, and especially the 46.5 keV line of ^{210}Pb), use should be made of a specially designed Ge-detector: either a low-energy photon detector (LEPD), or – preferably, so as keep at the same time a good efficiency for the high-energy gamma-rays - an extended-energy range detector (such as the XtRa Ge detector of Canberra). Even so, in order to reduce the counting times, use is frequently made of samples brought in so-called Marinelli geometry, i.e. surrounding the detector. Finally, let it be remarked that the use of Ge gamma-ray

spectrometry is generally limited to laboratory measurements, due to its high cost and its cumbersome and impractical use in the field.

For more detailed information on the operation principles and characteristics of the γ-, α- and β- counting systems and measurements dealt with in this work, see Chapter 4 Sections 4.2-4.3, 4.5 and 4.6, respectively.

3.1.2. Direct determination

3.1.2.1. α-, β- and γ-dose determination via dose monitors

Thermoluminescence dosimetry phosphors (TLDs), primarily developed for nuclear hazard monitoring and personnel dosimetry, are applicable to determine alpha-, beta- and gamma-dose rates [Aitken, 1968,1969; Bailiff, 1976; Bailiff and Aitken, 1980; Bowman, 1976; Mejdahl, 1978; Murray, 1981]. Traditionally, two types of TLDs are in common use in this context: dysprosium-activated calcium fluoride (CaF_2:Dy) and calcium sulphate ($CaSO_4$:Dy) [Aitken, 1985]. This direct method is attractive due to its low cost and because no extra electronics are involved. Beta- and gamma-dose rate estimation using these TLDs has been proved effective, whereas for alpha-radiation the sensitivity is less [Murray, 1981]. The major disadvantage of this method is that, because of its poor sensitivity, the encapsulated TLD has to be buried on-site for several months or even a year in order to get a proper response (but on the other hand, this procedure – although quite impractical – has the advantage to level out seasonal variations in water content and radon emanation).

Akselrod et al. (Akselrod et al., 1990) have introduced the anion deficient aluminium oxide doped with carbon (α-Al_2O_3:C) as a material for thermoluminescence dosimetry. They improved the dosimetric characteristics of Al_2O_3 significantly by the inclusion of oxygen vacancies into its structure. The advantage of single-crystal α-Al_2O_3:C is that it possesses a very high TL-sensitivity making it suitable for short

term exposure (of the order of days) in environmental dosimetry [Bøtter-Jensen, 2000; Kalchgruber, 2002]. Several authors have investigated the material and found that it has a high sensitivity to gamma-radiation [Akselrod et al., 1993; Kitis et al., 1994; Kortov et al., 1994; Moscovitch et al., 1993a,b; Musk, 1993], beta-radiation [Brown et al., 1993] and alpha-radiation [O'Brien et al., 1993; Mukherje and Lucas, 1993]. Moreover, it possesses a photon energy response nearly identical to that of quartz and feldspar [Akselrod et al., 1990], which is particularly interesting for dating applications. The limitation of using this material in TL-dosimetry is that the higher heating reduces the TL-sensitivity [Kortov et al., 1994]. However, Bøtter–Jensen [2000] recently found that the emission of luminescence by optical stimulation is much more sensitive than by thermal stimulation. The material can be completely emptied of trapped charges by exposure to daylight for some hours, which effectively improves the minimum detection limit of the dosimeter.

- CHAPTER 4 -

ANNUAL RADIATION DOSE DETERMINATION IN THE LUMINESCENCE DATING OF LOESS SEDIMENT

4.1. Selection of the loess site and sampling of the material

4.1.1. Selection of the loess site

For the present study, a loess profile was selected at Volkegem, in the southern part of East-Flanders (more specific to the south-east of Oudenaarde), Belgium. From the geological context it was believed that the selected profile is homogeneous with respect to its composition. Fig. 4.1.1 is a part taken from the topographic map of Horebeke-Zottegem. An excerpt of the geological map of the area around Volkegem is shown in Fig. 4.1.2 [Marechal, 1992].

The studied loess is a yellow-gray, fine-grained aeolic sediment (average grain size < 50 μm) that was deposited through the action of wind during the latest glacial times, more precisely in the Young-Pleistocene (Weichselian), a part of the Quaternary. It consists mostly of decarbonated homogeneous loess, with traces of glauconite (potassium containing silicate).

Fig.4.1.1. Topographic situation of the investigated site at Volkegem. The place where the NaI(Tl) field gamma spectrometry was performed and where the sampling was made is marked on the map. Fragment of the topographic map produced by Marechal [1992] (Scale 1:25000).

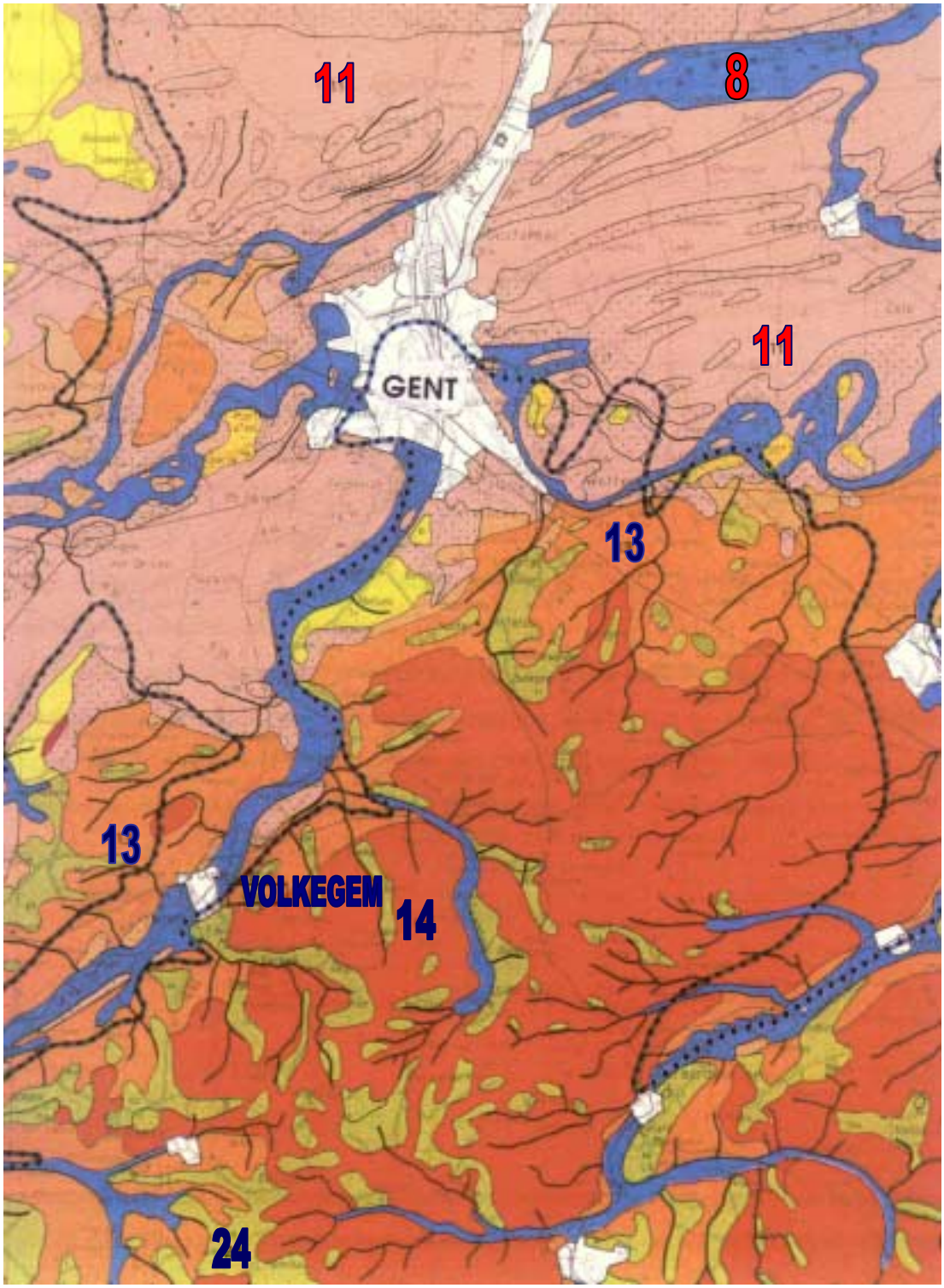

Fig. 4.1.2. Geological setting of the investigated site at Volkegem produced by Marechal [1992] (Volkegem is marked; scale 1: 250000).
Legend: orange (13) = Young-Pleistocene, sandy loess; green (24) = Quaternary, mostly sandy loess or loess on clay and/or sand; red (14) = Young-Pleistocene, loess; blue (8) = alluvial deposits; brown (11) = Young-Pleistocene, sand or loessy sand.

4.1.2. Sampling of the material

Five main locations were chosen, horizontally separated by at least 1 meter. At each location, three sampling points were selected with vertical separations of ~ 25 cm, whereby the "middle point" was the one where NaI(Tl) field gamma-ray spectrometry was performed (see Chapter 4, section 4.2) as shown in Fig. 4.1.3. After cleaning the surface of the profile, sampling was done by hammering steel cylinders of 50 mm diameter × 50 mm length into the profile (Fig. 4.1.4); after removal, they were capped and wrapped in plastic to retain the natural moisture content of the loess samples. Each sample ring contained about 190 gram of undisturbed loess material, which was then brought to the laboratory.

Fig 4.1.3. The Volkegem loess profile showing the sample location. The NaI(Tl) detector is inserted into the borehole of one of the sample locations.

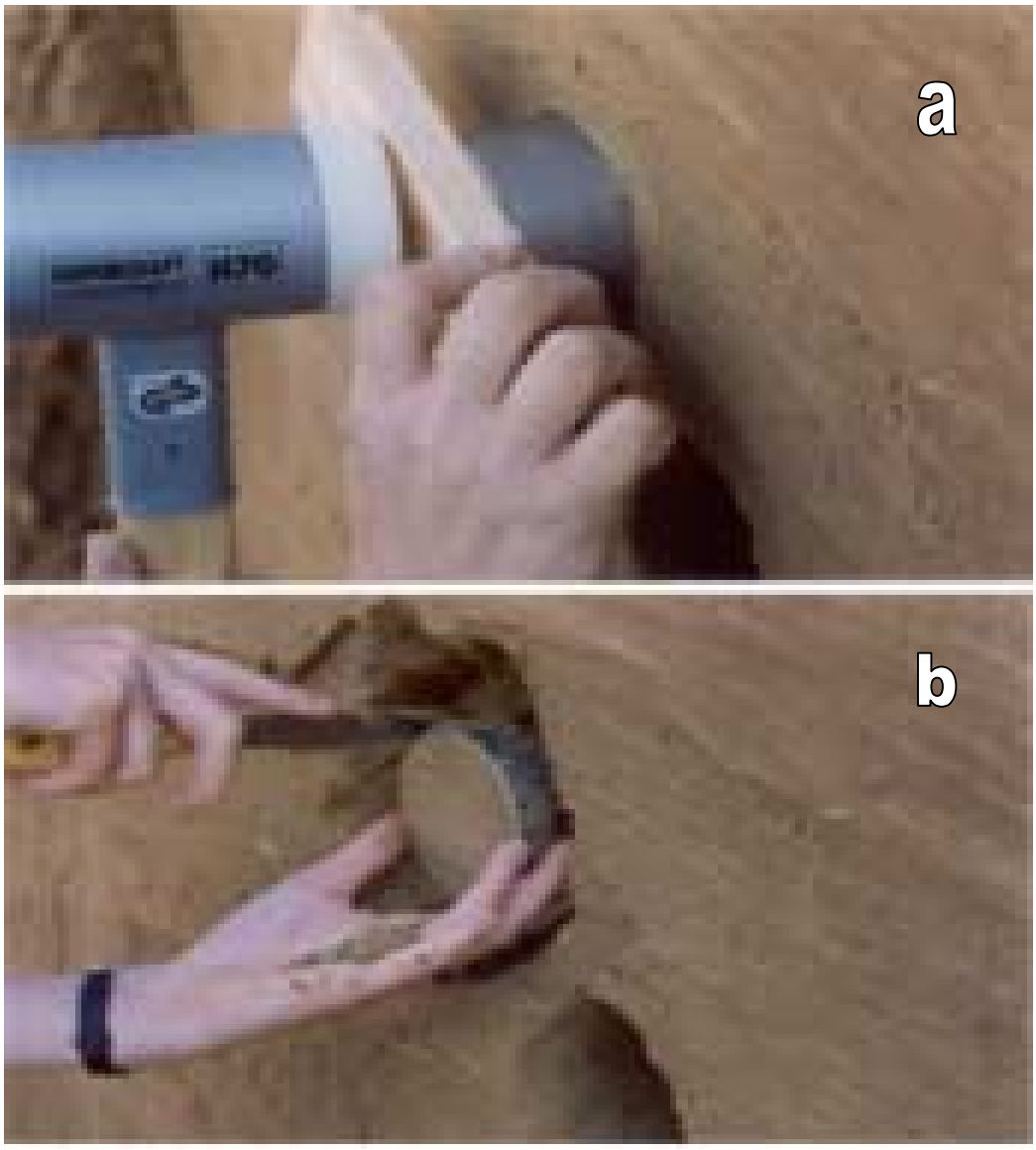

Fig. 4.1.4. Sample collection: a) by hammering a steel cylinder of 50 mm diameter × 50 mm length into the profile; b) digging out the steel cylinder with loess sample.

4.2. NaI(Tl) gamma-ray spectrometry

4.2.1. Field gamma-ray spectrometry

4.2.1.1. Introduction

Field gamma-ray spectrometry with a NaI(Tl) detector in auger hole geometry is a traditional but still valuable technique to evaluate the annual radiation dose. A major advantage of this method is its capability of measuring the individual contributions of K, Th and U simultaneously on the sampling site. A portable multichannel analyzer combined with a notebook PC and powerful software is nowadays available, thus allowing reliable data acquisition and gamma-ray spectrum analysis.

The primary output of NaI(Tl) field gamma-ray spectrometry is a number of counts associated with well-defined γ-rays emitted by indicator isotopes of the radioelements, namely ^{40}K, ^{214}Bi (in the ^{238}U decay series) and ^{208}Tl (in the ^{232}Th decay series).

4.2.1.2. Collection of spectra in the field

Field gamma-ray spectra were collected using a Canberra Portable Plus γ-spectrometry system Model 1150, equipped with a 3 × 3 inch NaI(Tl) detector. Measurements of 2 hours each were performed in five auger holes of 40 cm depth and 8 cm diameter which were made at exactly the same spot as the earlier mentioned "middle sampling points" (section 4.1.2), after the samples had been taken with the steel cylinders. Fig. 4.2.1 shows that, in the recorded gamma-ray spectra, the peaks of interest are at 1460.8 keV (^{40}K), 1764.5 keV (^{214}Bi, in the ^{238}U series) and 2614.5 keV (^{208}Tl, in the ^{232}Th series). The latter two are, in spite of the numerous γ-rays emitted in the ^{232}Th, ^{235}U and ^{238}U decay series, the only ones that are quasi interference-free and hence useful for the measurement of U and Th, respectively. It is also fortunate that the 1460.8 keV gamma, the only one emitted by ^{40}K, is not significantly interfered by γ-rays from the U and Th decay series.

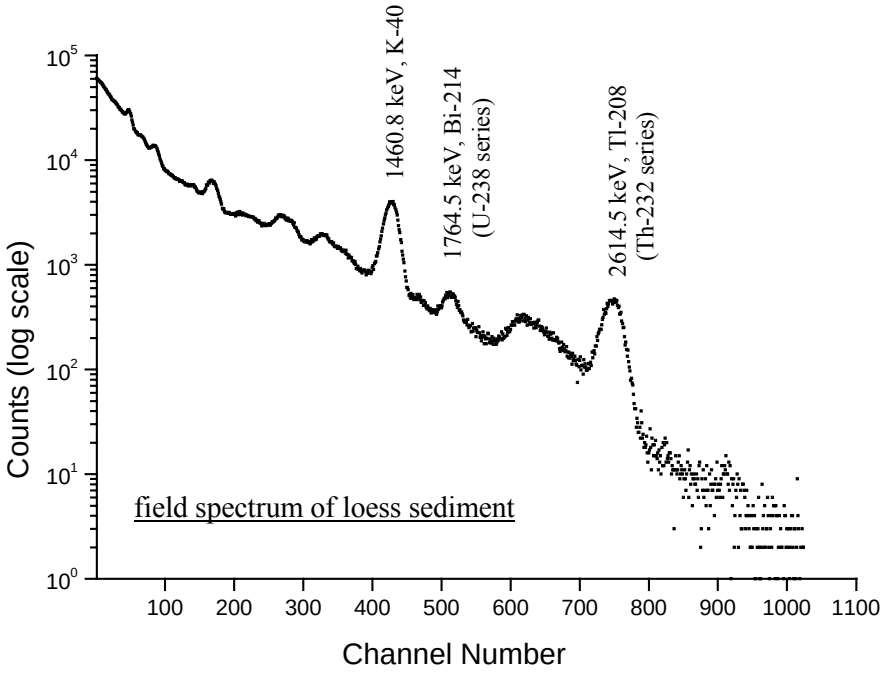

Fig. 4.2.1. NaI(Tl) field spectrum of loess sediment collected during 2 h, showing the useful peaks of the radioelements K, U and Th.

4.2.1.3. Calibration of field gamma-ray spectra

In order to derive the K-, U- and Th- concentrations (and finally the annual radiation dose)[Aitken, 1998] from the measured number of counts (via window counting - using spectrum stripping -, or via γ-ray spectrometry) corresponding to the above mentioned γ-rays, calibration methods have been developed in the past making use of voluminous blocks with known contents of these radioelements and containing a "borehole" for inserting the NaI(Tl) detector. Evidently, such blocks should simulate the field measurements, i.e., the counting conditions with respect to geometry, composition and density of the materials should not differ significantly. Only in this case, it is possible to determine the concentrations using the following equation:

$$[\mathrm{conc}_{\mathrm{K,U,Th}}]_{\mathrm{field}} = [\mathrm{conc}_{\mathrm{K,U,Th}}]_{\mathrm{block}} \times \frac{[\mathrm{cps}_{\mathrm{K,U,Th}}]_{\mathrm{field}}}{[\mathrm{cps}_{\mathrm{K,U,Th}}]_{\mathrm{block}}} \qquad (4.2.1)$$

with cps = measured counts per second.

4.2.1.3.1. Selection of calibration blocks

In the frame of this study, the performance of two setups of calibration blocks was investigated and compared:

1) at the Forschungsstelle Archäometrie, MPI, Heidelberg, Germany: a natural granite block [Flossenburg Granite] of 1 × 1 × 1 m, with K, U and Th concentrations of, respectively, 4.08 ± 0.11% (by weight), 18.8 ± 1.3 $mg.kg^{-1}$ and 14.0 ± 0.9 $mg.kg^{-1}$ [Pernicka]. In its "borehole" of 50 cm depth × 8.5 cm diameter, several measurements of 1 up to 4 hours were performed [Fig. 4.2.2];

2) at the Research Laboratory for Archaeology and the History of Art, Oxford University, UK: three concrete blocks of 0.51 × 0.51 × 0.51 m doped with respectively K, U and Th [plus one undoped "background" block], for which so called "effective doping concentrations are given of 5.71 % (by weight) K, 117 $mg.kg^{-1}$ U and 126 $mg.kg^{-1}$ Th (additionally including 4.8 $mg.kg^{-1}$ U), respectively, with no uncertainties specified [Allsop]. In their "borehole" of 29 cm depth × 10.2 cm diameter, measurements of 45 minutes (3 hours for the background block) were performed in duplicate.

When performing measurements in the Heidelberg block, peak shifting during counting was minimized by working at constant temperature, which was controlled by attaching a thermocouple to the NaI(Tl) detector. Counting was started when the temperature of the detector became stable.

Fig. 4.2.2. The natural granite block [Flossenburg Granite] of 1 × 1 × 1 m at Forschungsstelle Archäometrie, MPI, Heidelberg, Germany, performing the measurement in its "borehole" of 50 cm depth × 8.5 cm diameter using a Canberra Portable Plus γ-spectrometry system Model 1150, equipped with a 3 x 3 inch NaI(Tl) detector.

The spectra measured in the field and in the calibration blocks were analyzed in two different ways according to the calibration procedure that was used. For the "Heidelberg" calibration, gamma-spectrometry was performed, and all net peak area determinations of the relevant gamma-peaks were performed with the Hypermet-PC software package [Fazekas et al., 1997]. The spectrum collected from the Heidelberg calibration block is shown in Fig. 4.2.3.

On the other hand, the Oxford calibration blocks were rather developed for "window counting" with spectrum stripping [Aitken, 1985], and – since in each case a full spectrum was measured - the setting of the windows could be easily based on the location of the peaks, so that effects of possible temperature shift were minimized. The spectra collected from the Oxford concrete blocks (K-, U-, Th-doped blocks and background block) are shown in Figs 4.2.4 – 4.2.7. Full details on the calculational

methodology and on the results obtained in the case of the Volkegem measurements are given in Appendix A.

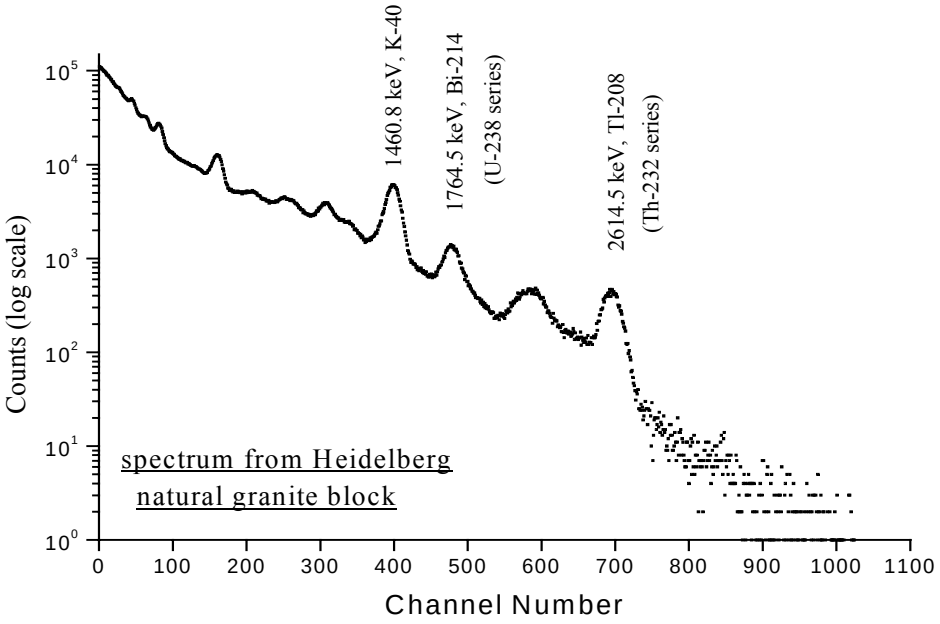

Fig. 4.2.3. NaI(Tl) spectrum collected from the Heidelberg natural granite block during 1 h, showing the useful peaks of the radioelements K, U and Th.

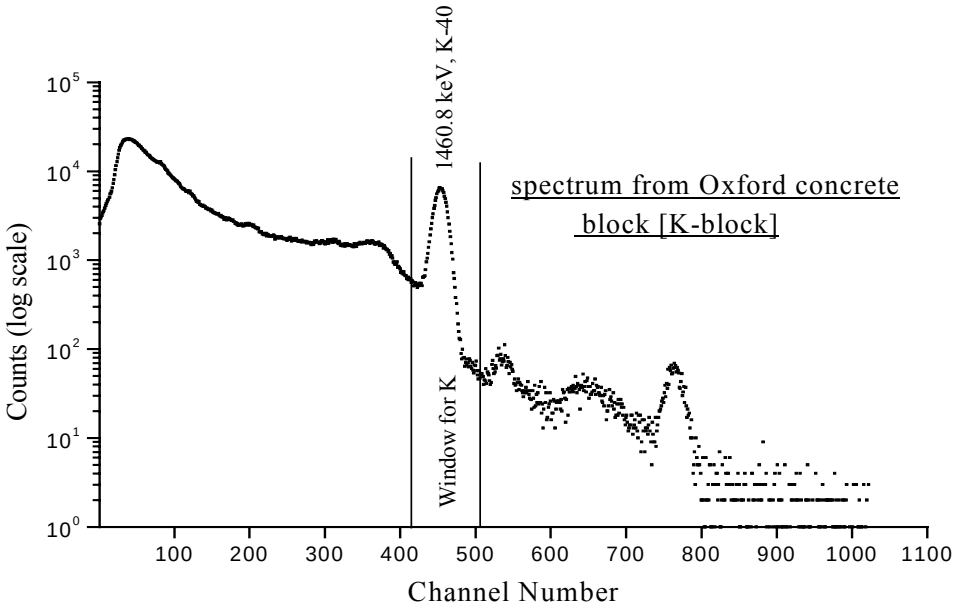

Fig. 4.2.4. NaI(Tl) spectrum collected from the Oxford concrete K-doped block during 45 min, showing the window of the radioelement K.

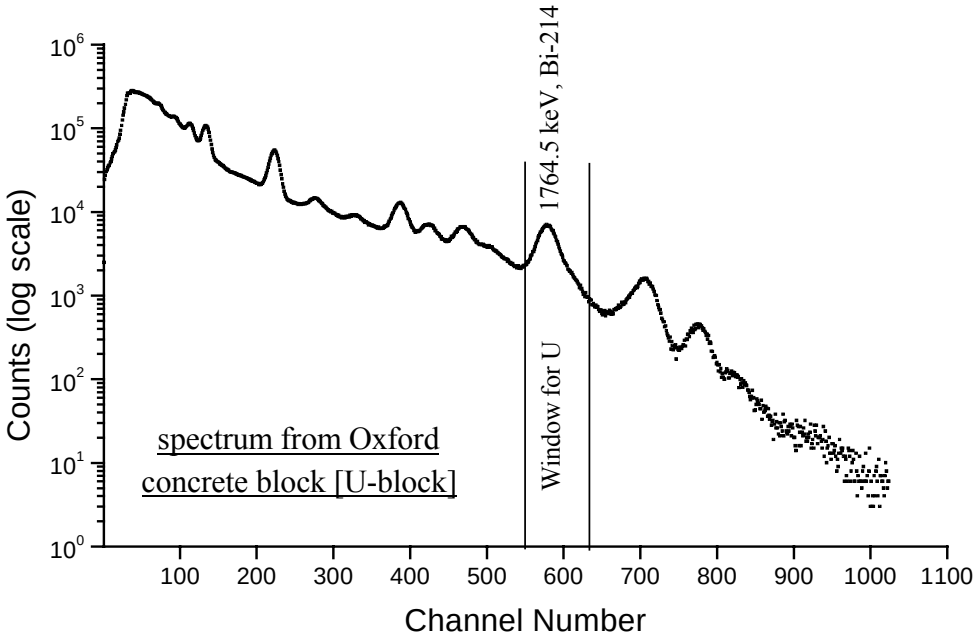

Fig. 4.2.5. NaI(Tl) spectrum collected from the Oxford concrete U-doped block during 45 min, showing the window of the radioelement U.

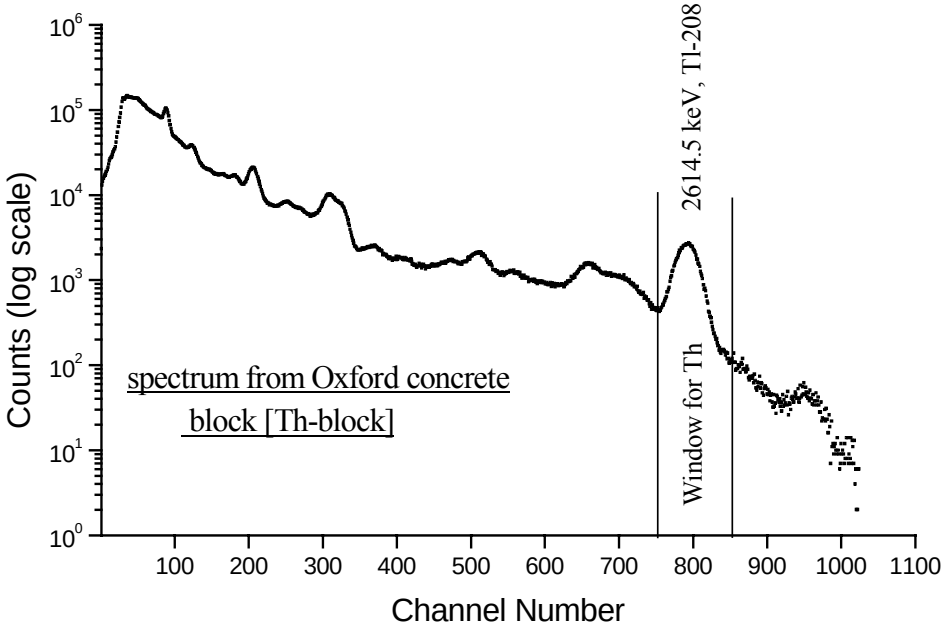

Fig. 4.2.6. NaI(Tl) spectrum collected from the Oxford concrete Th-doped block during 45 min, showing the window of the radioelement Th.

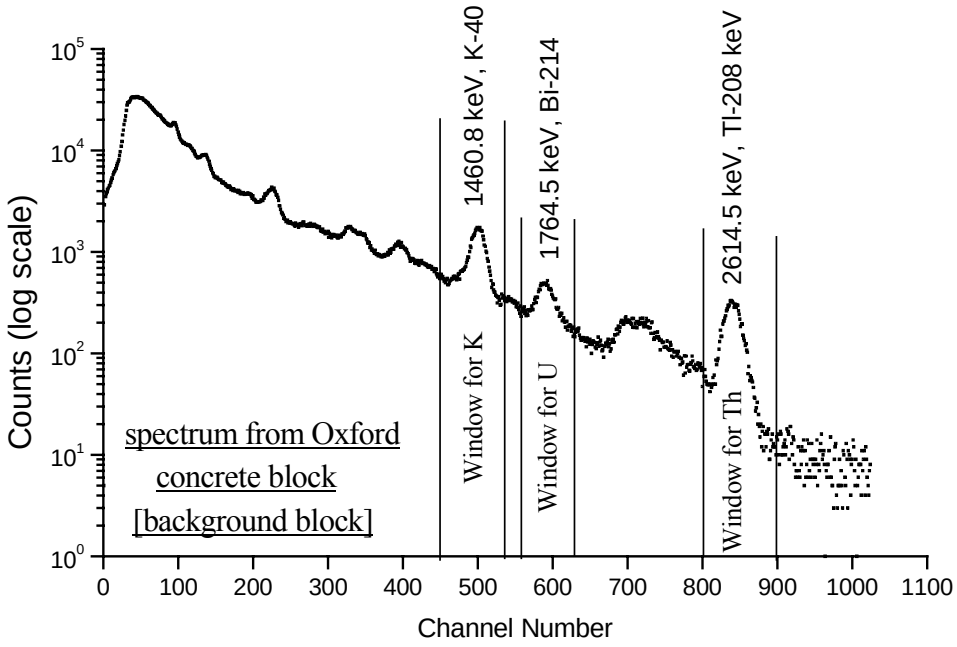

Fig. 4.2.7. NaI(Tl) spectrum collected from the Oxford concrete background-block during 3 h, showing the windows of the radioelements K, U and Th.

4.2.1.3.2. The introduction of Marinelli effective solid angles

In principle, corrections are needed in the evaluation of the elemental concentration and the annual radiation dose via NaI(Tl) field gamma-ray spectrometry, calibrated via voluminous blocks that are simulating the auger hole measurements, because there are distinct differences between both counting conditions.

In terms of the effective solid angle $\overline{\Omega}$, introduced in the early 1980s in the k_0-methodology [Moens et al., 1981], the calculation of the K, Th and U concentration is based on the fact that for a given gamma-ray energy, $\overline{\Omega}$ is - by definition - proportional to the peak detection efficiency. Thus, the observed count rate (cps) is proportional to $\overline{\Omega}V\rho$ and – of course – also to the concentration of the gamma-emitting radioelement. Hence, one can write:

$$[\text{conc}]_{\text{field}} = [\text{conc}]_{\text{block}} \times \frac{[\text{cps}]_{\text{field}}}{[\text{cps}]_{\text{block}}} \times \frac{[\overline{\Omega}V\rho]_{\text{block}}}{[\overline{\Omega}V\rho]_{\text{field}}} \qquad (4.2.2)$$

where $\overline{\Omega}$ is the effective solid angle, V is the volume of the source and ρ is its density.

The calculations were based on Marinelli geometries (see Chapter 5) for which $\overline{\Omega}$ was obtained via the software ANGLE [Jovanović et al., 1997], originally designed for Ge-detectors but modified in this work for NaI(Tl) [Jovanović et al., 1992] .To realise this, however, the following transformations had to be made (see Fig. 4.2.8):

1) in the case of loess, the field auger hole measurement clearly can be seen as a Marinelli geometry with infinite dimensions (Fig. 4.2.8a). The question is then: for which d-value (see Fig. 4.2.8b) is a Marinelli beaker with loess "infinite"?. The answer to this is given by calculating and plotting for this configuration $\overline{\Omega}V$ versus d (for composition and density of loess, see below), from which it can be concluded that d = 80 cm is more than sufficient to be considered as "infinite" (Fig. 4.2.9). However, it can be seen that in practice d = 60 cm will not lead to significant errors. As expected, Fig. 4.2.9 shows that "infinity" is more readily reached for the less energetic gamma-ray of ^{40}K at 1460.8 keV, followed by ^{214}Bi at 1764.5 keV and finally ^{208}Tl at 2614.5 keV. From the curves in Fig. 4.2.9, it can also be concluded that the formerly mentioned [Aitken, 1985] 0.3 meter external gamma-dose contribution is somewhat underestimated.

2) in the case of the calibration blocks, their cubic shape (Fig. 4.2.8c) was converted to an equivalent cylindrical Marinelli beaker shape – i.e. with the same total volume - (Fig. 4.2.8d).

For the above calculations, the compositions and densities of loess (at the Volkegem site), of granite (the 'Heidelberg" calibration block) and of concrete (the "Oxford" calibration blocks) were introduced as listed in Table 4.2.1. It should be remarked that

at Oxford, at the time of preparing the concrete, no coarse aggregates were added to the mix, which explains the low density of the final material [Bowman, 1976; Murray, 1981]. With the above assumptions and input parameters, the following correction factors were obtained and introduced in case of calibration with the "Heidelberg" granite block:

$$\frac{\left[\overline{\Omega}\,V\,\rho\right]_{\text{Heid.block}}}{\left[\overline{\Omega}\,V\,\rho\right]_{\text{loess}}} = 1.033 \text{ for } {}^{40}\text{K at 1460.8 keV,}$$

$$= 1.038 \text{ for } {}^{214}\text{Bi at 1764.5 keV, and}$$

$$= 1.047 \text{ for } {}^{208}\text{Tl at 2614.5 keV.}$$

Taking into account that "non-infiniteness" of the calibration block would make the correction factors smaller than 1, it can be concluded that the "Heidelberg" calibration block can be considered as infinite; the small correction factor larger than 1 is mainly caused by the higher density of the granite as compared to loess. In this context, it should be mentioned that the composition and the density of the source material are implicitly present in the $\overline{\Omega}$-value.

As to the "Oxford" concrete blocks, the calculation yields:

$$\frac{\left[\overline{\Omega}\,V\,\rho\right]_{\text{Oxf.block}}}{\left[\overline{\Omega}\,V\,\rho\right]_{\text{loess}}} = 0.933 \text{ for } {}^{40}\text{K at 1460.8 keV,}$$

$$= 0.917 \text{ for } {}^{214}\text{Bi at 1764.5 keV, and}$$

$$= 0.870 \text{ for } {}^{208}\text{Tl at 2614.5 keV.}$$

This indicates that the "Oxford" blocks, with their dimensions of 0.51×0.51×0.51 m, are far from infinite. This was formerly recognized at the Oxford lab, and therefore the doping concentrations that are specified (see above) are "effective" values, which

were empirically estimated with the aim to yield the correct dosimetry response [Allsop]. This use of "effective" concentrations means that, in this work, principally no $\overline{\Omega}V\rho$-correction was required in case of the "Oxford" calibration.

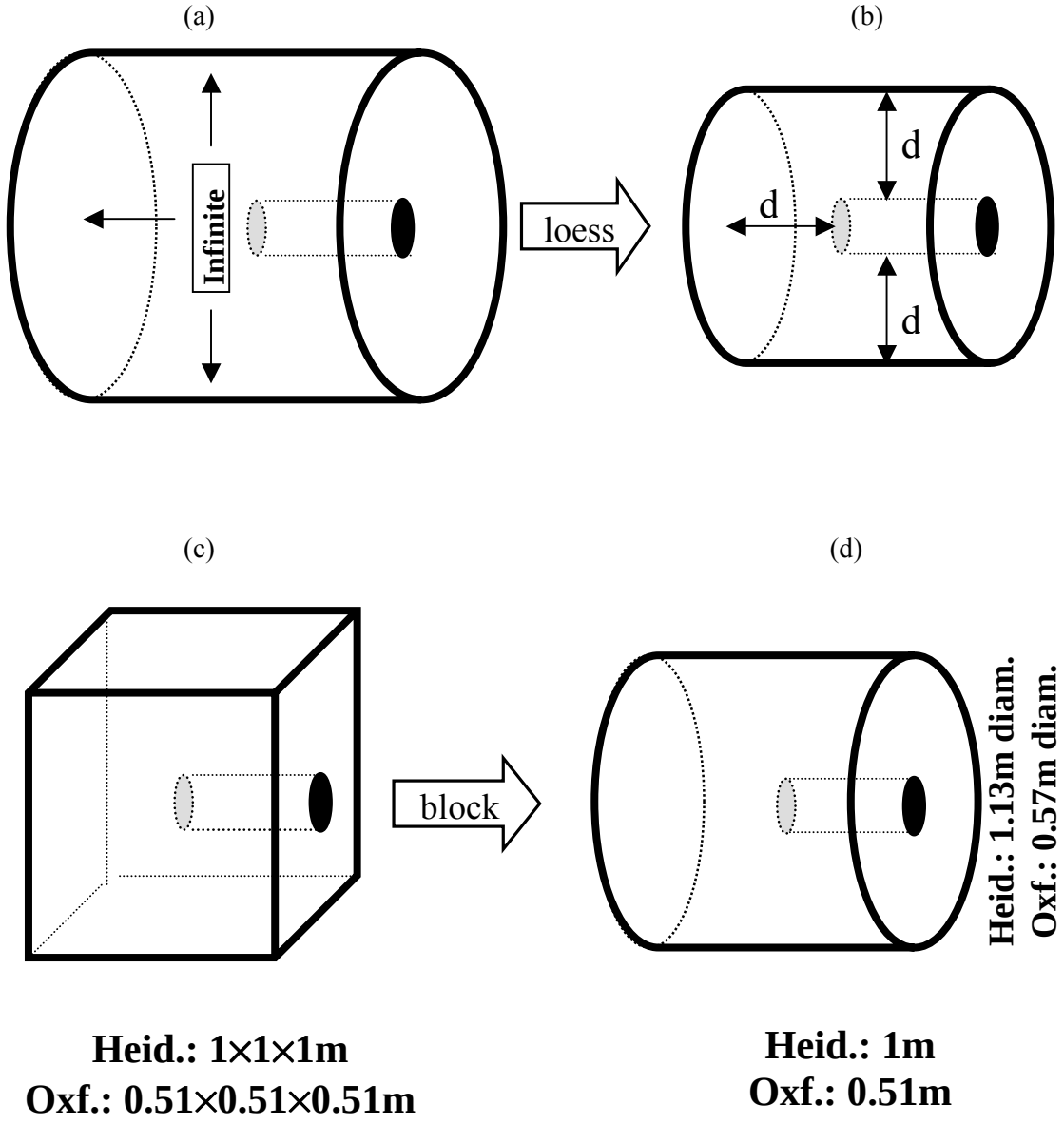

Fig. 4.2.8. Transformation of the counting conditions for an auger hole in field conditions and for the "Heidelberg" or "Oxford" calibration blocks, to a Marinelli geometry.

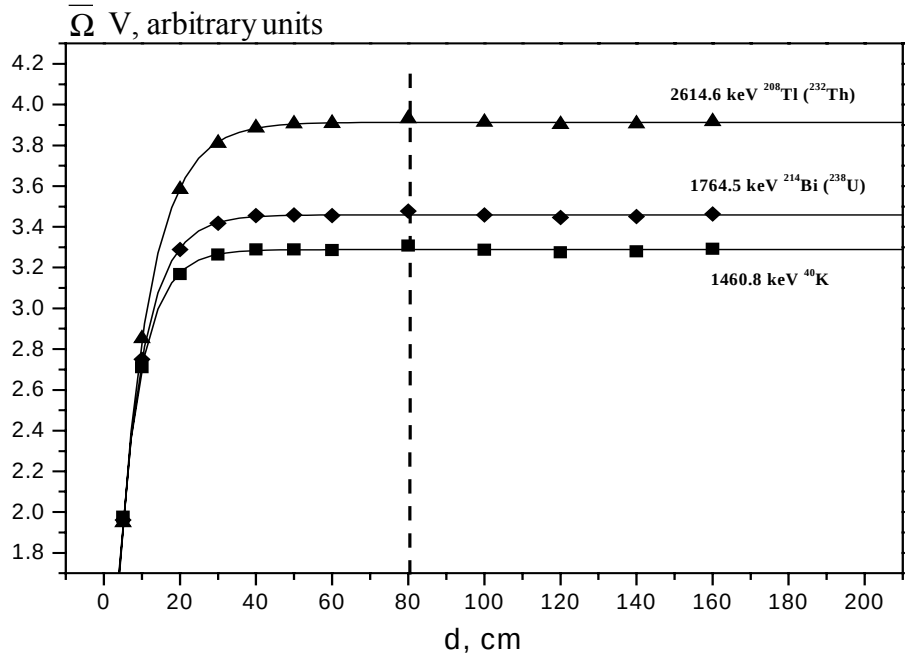

Fig. 4.2.9. Replacement of the infinite dimensions in field conditions by a finite Marinelli geometry (d – see Fig. 4.2.8b).

Table 4.2.1. Composition and density of loess (Volkegem site) [Duchesne], granite ("Heidelberg" calibration block) [Cox et al.. 1981] and concrete ("Oxford" calibration blocks) [Bowman, 1976; Murray, 1981].

Elemental composition	Material		
	Loess (Volkegem)	Granite (Heidelberg)	Concrete (Oxford)
Si, %	31.55	33.33	29.16
Ti, %	0.37	0.19	-
Al, %	4.01	7.58	4.42
Fe, %	2.33	2.12	1.10
Mg, %	0.35	0.43	-
Ca, %	0.41	1.32	7.64
Na, %	0.67	2.73	1.56
K, %	1.49	3.38	1.75
H, %	1.90	0.09	1.44
O, %	56.92	48.83	52.93
Density, g.cm^{-3}	1.95	2.70	1.93

4.2.1.4. Results

The above-described procedure obviously leads to K, U and Th concentrations in "wet loess", i.e. loess having its natural moisture content in the field.

Table 4.2.2. shows the results of the finally achieved K-, U-, and Th-concentration results (recalculated to the dry weight by introducing the moisture content – see section 4.4) based on the auger hole field measurements with the "Heidelberg" and the "Oxford" calibration. The uncertainties quoted on K, U and Th concentrations resulting from both calibrations are only based on the counting statistics.

Table 4.2.2. The results of the K, U and Th concentration in the Volkegem loess based on the auger hole field measurements with the "Heidelberg" and the "Oxford" calibration.

No. of field spec-trum	Calibration via the Oxford concrete blocks			Calibration via the Heidelberg granite block		
	K (%) ± 2s (dry weight)	U (mg/kg) ± 2s (dry weight)	Th (mg/kg) ± 2s (dry weight)	K (%) ± 2s (dry weight)	U (mg/kg) ± 2s (dry weight)	Th (mg/kg) ± 2s (dry weight)
S.31	1.665±0.017	2.447±0.079	9.67±0.15	1.745±0.025	2.57±0.17	10.42±0.37
S.34	1.635±0.016	2.481±0.080	10.08±0.15	1.789±0.026	2.50±0.16	10.61±0.38
S.39	1.670±0.017	2.482±0.080	9.90±0.15	1.768±0.025	2.55±0.17	10.47±0.37
S.29	1.622±0.016	2.400±0.077	9.98±0.15	1.741±0.024	2.64±0.17	10.38±0.37
S.27	1.608±0.017	2.371±0.076	9.96±0.15	1.803±0.026	2.47±0.16	10.62±0.38

4.2.2. NaI(Tl) gamma-ray spectrometry in low-background laboratory conditions

4.2.2.1. Counting of the sample in cylindrical geometry

The 15 undisturbed loess samples that were brought to the laboratory in the steel cylinders of 50 mm diam. × 50 mm height (see Fig. 4.1.4 in Section 4.1.2) were counted in this cylindrical geometry, during a period of 4 days each, with the portable NaI(Tl) detector. The instrumentation is the same as the one used in the field except that the detector is mounted in a low-background lead castle. The castle, which has a vertical detector chamber and a removable door, is designed to accommodate the NaI(Tl) detector. The main features of the lead castle are as follows: thickness = 100 mm instead of usual 50 mm; net weight = 390 kg; inner dimension = 120 mm dia × 250 mm height. The steel cylinder base facing the detector was uncapped and the cap was replaced by a thin Mylar foil (6 μm thickness). The spectrum obtained is similar to the one obtained in the field, with the same peaks of interest. The background was measured for two weeks with the blank cylinder in the same counting position as the samples.

4.2.2.2. Calibration of NaI(Tl) gamma-ray laboratory measurements

Calibration was done in an absolute way via calculation of the peak detection efficiency and correction for true-coincidence with the software package Kayzero/Solcoi Version 4 [1996], and with introduction of nuclear data taken from Isotope Explorer [Chu et al., 1999].

4.2.2.2.1. Peak detection efficiency

To perform an absolute calibration, it is necessary to determine the full-energy peak detection efficiency (ε_p) of the counting arrangement for the considered gamma energy (E_γ). This determination is performed in two steps:

i. Experimental determination of the peak detection efficiency curve ("$\varepsilon_{p,ref}$" versus E_γ, in log-log representation) in "reference" conditions i.e., for a point source at a large distance from the detector where true-coincidence effects are negligible;

ii. Conversion of "$\varepsilon_{p,ref}$" to "$\varepsilon_{p,geo}$" for the counting geometry at hand, based on the concept of the "effective solid angle" $\overline{\Omega}$.

4.2.2.2.1.1. Experimental determination of peak detection efficiency curve at reference position ($\varepsilon_{p,ref}$)

For the determination of the reference peak detection efficiency curve ($\log\varepsilon_p$ versus $\log E_\gamma$), commercially available absolutely calibrated point sources ^{22}Na, ^{60}Co, ^{137}Cs, ^{241}Am and a secondary calibration source ^{24}Na (home-made) were used with energies ranging from 59.5 keV to 2754.0 keV. The secondary calibration point source ^{24}Na (E_γ = 1368.6 keV and 2754.0 keV) was used [De Corte and Simonits, 1994] to obtain an extra efficiency point in the high-energy region [De Corte, 1987a], in view of the determination of Th via the 2614.5 keV gamma-ray of ^{208}Tl. For the present work, 20.95 cm source-to-detector distance was selected as the "reference position" (where the true coincidence effects are undoubtedly negligible).

The peak detection efficiency for the point sources can be determined on the basis of the equation:

$$\varepsilon_p = \frac{N_p / t_m}{A\,\gamma\,C} \qquad (4.2.3)$$

where: N_p - net number of counts collected under the full-energy peak;

t_m - counting time;

A - present activity of the point source;

$= A_0 e^{-\lambda t_d}$

with:

A_0 - activity at the time of certification of the point source;

λ - decay constant = $\frac{\ln 2}{T½}$; T½ - half life;

t_d - decay time;

γ - absolute intensity of the gamma-emission;

C - counting factor;

$= \frac{[1 - e^{-\lambda t_m}]}{\lambda t_m}$

The radionuclides used and their relevant nuclear data are listed in Table 4.2.2.

Table 4.2.2. Decay data of primary and secondary calibration point sources, taken from Isotope Explorer [Chu et al., 1999].

Radionuclide	Half-life	Gamma energy (keV)	Gamma intensity (%)
^{22}Na	2.602 a	511.0 1274.5	181 99.94
^{60}Co	5.275 a	1173.2	99.9
		1332.5	99.98
^{137}Cs	30.07 a	661.7	85.1
^{241}Am	432.2 a	59.5	35.9
^{24}Na	14.96 h	1368.6	100
		2754.0	99.94

Experimentally determined efficiency values for the NaI(Tl) detector at reference position were plotted as a function of gamma energy (in log-log representation). A reference efficiency curve ranging from 59.5 to 2754.0 keV was obtained by fitting a second-order polynomial as shown in Fig. 4.2.10.

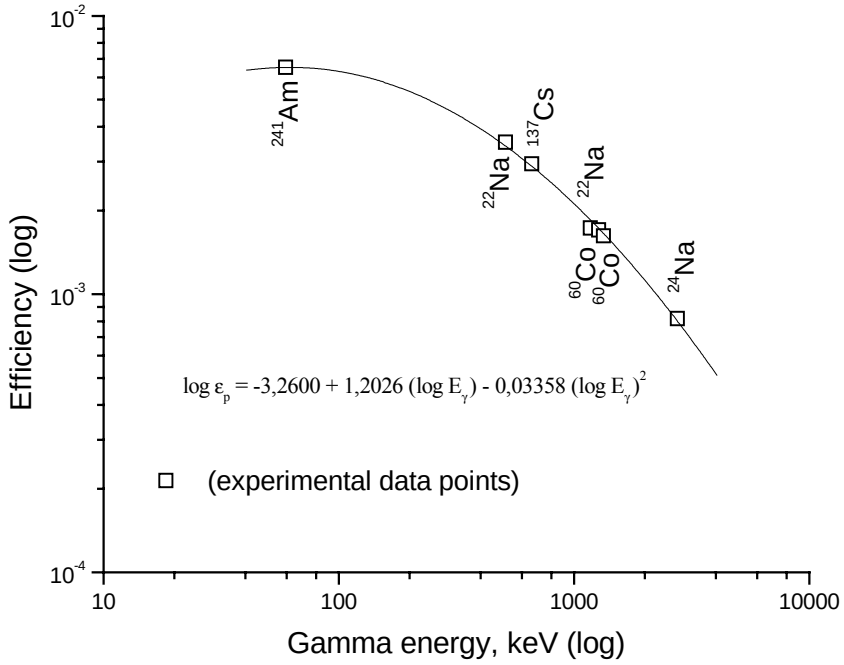

Fig. 4.2.10. Experimentally determined efficiency curve for the NaI(Tl) detector in "reference conditions".

4.2.2.2.1.2. Conversion of "$\varepsilon_{p,ref}$" to "$\varepsilon_{p,geo}$"

The experimentally determined reference detection efficiency, $\varepsilon_{p,ref}$, can be converted to $\varepsilon_{p,geo}$ for the cylindrical geometry using the following equation [Moens et al., 1981]:

$$\varepsilon_{p,geo} = \varepsilon_{p,ref} \cdot \frac{\overline{\Omega}_{geo}}{\overline{\Omega}_{ref}} \qquad (4.2.4)$$

where $\overline{\Omega}$ is the effective solid angle subtended by the detector at the source. The effective solid angles for reference ($\overline{\Omega}_{ref}$) and cylindrical geometry ($\overline{\Omega}_{geo}$) are calculated by integration of an infinitesimal solid angle element, weighted with a

factor for gamma-attenuation and detector response, over the volume of the source and the detector:

$$\overline{\Omega} = \int_{\substack{\text{source} \\ \text{detector}}} F_{att}\, F_{eff}\, d\Omega \qquad (4.2.5)$$

with $d\Omega$ - infinitesimal solid angle element;

F_{att} - weighing factor taking into account gamma attenuation before a gamma ray hits the active zone of the detector;

F_{eff} - weighing factor taking into account detector response when a gamma ray hits the active zone of the detector.

In practice, the calculation of $\overline{\Omega}$ is based on a multiple numerical integration according to the Gauss-Legendre Quadrature. For this, the software package Kayzero/Solcoi Version 4 [1996] was used, which is adopted from the computer program SOLANG written in FORTRAN IV for a VAX machine [Moens et al., 1981].

The applicability of above described ε_p- conversion is bound to the following conditions:

The detector body must be cylindrical and concentric with its housing and its geometric parameters must be known. The characteristics of the 3×3 inch NaI(Tl) detector used in the present work are shown in Fig. 4.2.11.

The method applies to cylindrically symmetrical sources (cylinders, disks, points) with a rotation axis coinciding with the detector axis and a radius smaller than or equal to the detector radius. The source composition (with respect to the major elements) and its density must be known.

The thickness, major element composition and density of all gamma-absorbing layers interposed between the source and the active detector body should be known.

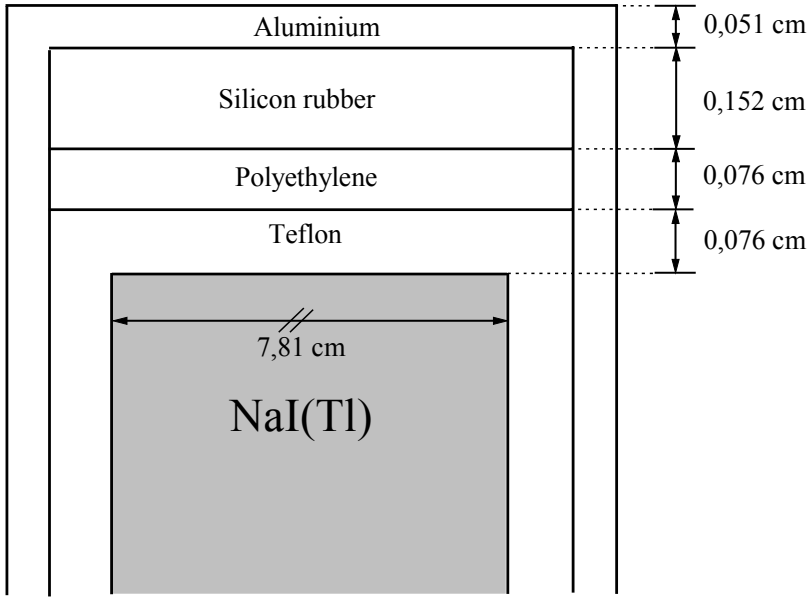

Fig. 4.2.11. Characteristics of the 3×3 inch NaI(Tl) detector.

4.2.2.2.2. Correction for true-coincidence effects

True-coincidence effects originate from the simultaneous detection of pulses generated in the detector by cascading photons. These are geometry dependent and the correction is needed for any absolute standardization especially when sources are positioned close to the detector. For instance, if in the decay scheme of Fig. 4.2.12(a), A is the measured gamma ray under consideration, a count in its associated photopeak may be gained due to the simultaneous detection of fully deposited cascading gamma rays B and C. On the other hand, Fig. 4.2.12(b) illustrates that a pulse may be lost due to the simultaneous detection of the preceding gamma ray D or/and the following gamma ray E.

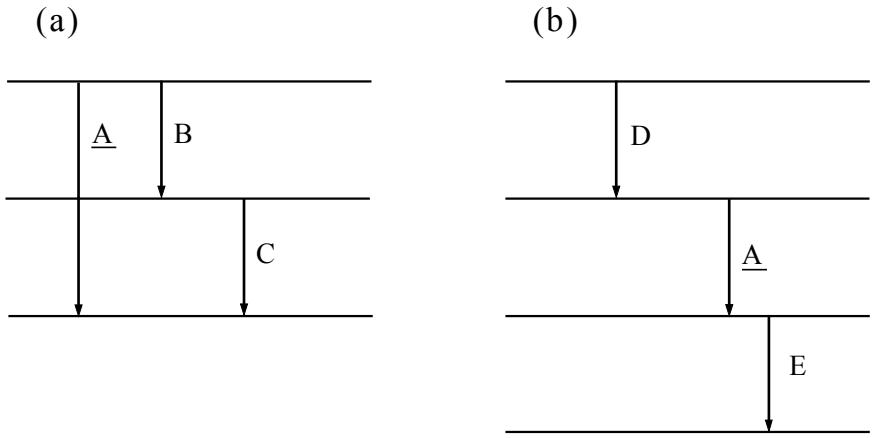

Fig. 4.2.12. Simplified decay scheme, illustrating true-coincidence effects: a) "summing-in" – the probability of counts gained due to simultaneous detection of fully deposited cascading gamma rays; b) "summing-out" – the probability of counts lost due to simultaneous detection of preceding or/and following gamma rays.

It is possible to correct mathematically for these effects, notably to calculate the probabilities for loss ("summing-out") and gain ("summing-in") of pulses in the peak [De Corte, 1987a]. If these probabilities are denoted by L($\underline{A}$) and S($\underline{A}$), respectively, the true-coincidence correction factor is given by the relation:

$$\mathrm{COI}(\underline{A}) = [1 - \mathrm{L}(\underline{A})][1 + \mathrm{S}(\underline{A})] \qquad (4.2.6)$$

Thus, the measured counts (N_p) in the associated photopeak of $\underline{A}$ can be corrected for true-coincidence as:

$$\mathrm{N}_{\mathrm{p},\underline{A}}(\mathrm{corrected}) = \frac{\mathrm{N}_{\mathrm{p},\underline{A}}(\mathrm{measured})}{\mathrm{COI}\ (\underline{A})} \qquad (4.2.7)$$

For the calculation of true-coincidence "summing-out" effects, the total detection efficiency ε_t is required as an input parameter, which is obtained from the peak detection efficiency ε_p and the so-called peak-to-total ratio P/T:

$$\varepsilon_t = \frac{\varepsilon_p}{\mathrm{P/T}} \qquad (4.2.8)$$

The peak-to-total ratio P/T is an experimentally measurable quantity, which is significantly depending on the photon energy and the source-to-detector distance. Its dependence on the source geometry (if not too extended) and composition, and on the presence of absorbing and scattering materials can be neglected in practice [De Corte, 1987a].

An experimental P/T curve for point sources and a home made source ^{49}Ca (for an extra point at 3084.4 keV; T½ = 8.72 min and absolute gamma intensity = 0.92) at reference position (= 20.95 cm) from the NaI(Tl)-detector is shown in Fig. 4.2.13. The point sources used are similar to those used for determination of the peak detection efficiency at reference position – see Section 4.2.2.2.1.1.

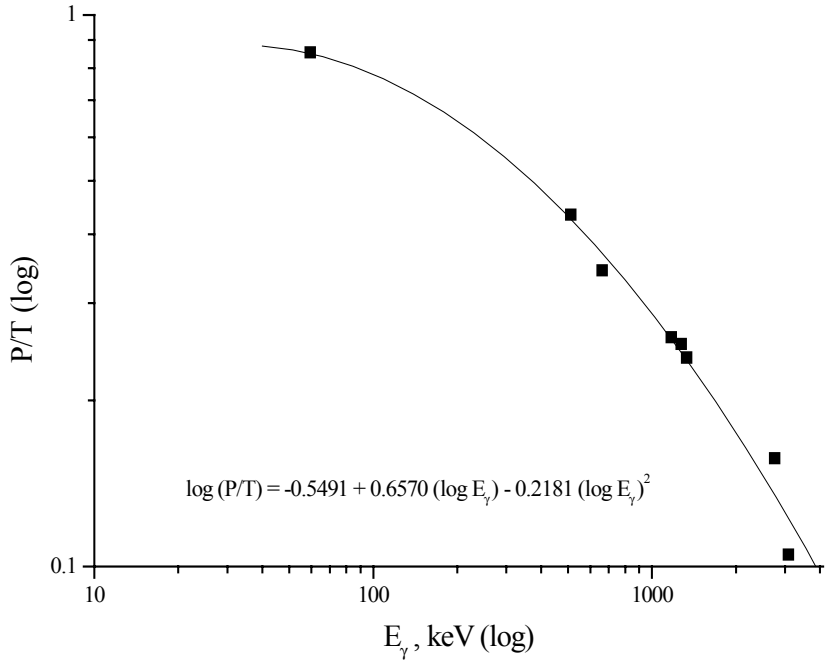

Fig. 4.2.13. Experimental peak-to-total curve for point sources and a home made source ^{49}Ca measured at 20.95 cm distance from the NaI(Tl)-detector.

In the present work the NaI(Tl) detection system was used for the measurement of the natural gamma activity of loess samples with a voluminous cylindrical geometry (50 × 50 mm) on top of the detector. In such a case the coincidence correction factor

significantly varies with the distance (in fact: with the detection efficiency). Therefore, the true-coincidence effects or COI-factors for the 1764.5 keV gamma line of ^{214}Bi (^{238}U decay series) and the 2614.5 keV gamma line of ^{208}Tl (^{232}Th decay series) were calculated based on dividing the cylinder in a number of layers and then applying a numerical integration procedure [De Corte et al., 1994, De Wispelaere et al., 1997] – as the weighted mean of COIs for infinitesimal thin source layers parallel to the detector surface (the detection efficiency – in fact, the effective solid angle – being the weighing factor). The underlying reasoning is as follows.

In general, the measured count rate (cps) for a source is given by:

$$cps = dps \,.\, \gamma \,.\, \varepsilon_p \,.\, COI \qquad (4.2.9)$$

with: dps - disintegrations per second;
γ - gamma-ray intensity;
ε_p - peak detection efficiency;
COI - correction factor for true coincidence.

At the height h (Fig. 4.2.14), one considers a disk with an infinitesimal thickness δh and volume δv. Then, the infinitesimal count rate δ[cps(h)] contributing to the total count rate is:

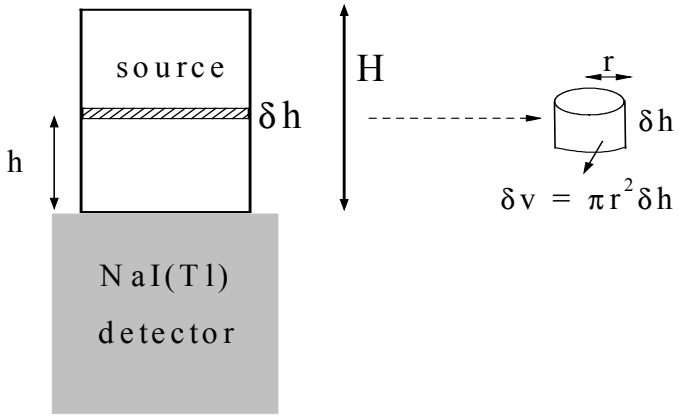

Fig. 4.2.14. Cylindrical sample positioned on top of the detector.

$$\delta[\mathrm{cps}\,(h)] = \frac{\mathrm{dps}}{V} \,.\, \gamma \,.\, \varepsilon_p\,(h) \,.\, \mathrm{COI}\,(h) \,.\, \delta v \qquad (4.2.10)$$

where $\frac{\mathrm{dps}}{V}.\delta v$ is the disintegration rate in the volume element δv.

When considering that $V = \pi.r^2.H$ and $\delta v = \pi.r^2.\delta h$, one gets:

$$\delta[\mathrm{cps}\,(h)] = \frac{\mathrm{dps}}{H} \,.\, \gamma \,.\, \varepsilon_p\,(h) \,.\, \mathrm{COI}\,(h) \,.\, \delta h \qquad (4.2.11)$$

Integrating over the total height yields:

$$\int_0^H \delta[\mathrm{cps}\,(h)] = \mathrm{cps} = \frac{\mathrm{dps}}{H}.\gamma \int_0^H \varepsilon_p\,(h).\mathrm{COI}(h).\delta h \qquad (4.2.12)$$

where cps is the total observed count rate originating from the cylinder. Thus, combining Eq. (4.2.9) with Eq. (4.2.12) leads to:

$$\mathrm{dps}.\gamma.\varepsilon_p.\mathrm{COI} = \frac{\mathrm{dps}}{H} \,.\, \gamma \int_0^H \varepsilon_p\,(h) \,.\, \mathrm{COI}(h) \,.\, \delta h \qquad (4.2.13)$$

and:

$$\mathrm{COI} = \frac{\int_0^H \varepsilon_p\,(h) \,.\, \mathrm{COI}(h) \,.\, \delta h}{\varepsilon_p \,.\, H} \qquad (4.2.14)$$

With the peak detection efficiency (ε_p) proportional to the effective solid angle ($\overline{\Omega}$), one obtains finally:

$$COI = \frac{\int_0^H \overline{\Omega}(h) \,.\, COI(h) \,.\, \delta h}{\overline{\Omega} \,.\, H} \qquad (4.2.15)$$

As mentioned before, $\overline{\Omega}(h)$ to be introduced in Eq. (4.2.15) can be obtained from the output of computer code Kayzero/Solcoi Version 4 [1996]. In the present work, Eq. (4.2.15) was worked out by numerical integration, after determining the P/T curve as a function of the (point) source-detector distance [De Corte et al., 1994].

In the measuring conditions of the present work, the COI factor for the 2614.5 keV gamma line of ^{208}Tl (^{232}Th-decay series) was found to be 0.889. For the 1764.5 keV gamma line of ^{214}Bi (^{238}U-decay series), the COI factor of 0.999 is hardly different from unity, and the 1460.8 keV line of ^{40}K is coincidence-free, so that in this case COI ≡ 1.

4.2.2.3. Calculation of concentrations

The concentrations of K, Th and U are obtained through the equation:

$$\text{conc.}\,(g.g^{-1}) = C \,.\, \frac{cps / W}{\varepsilon_p . COI} \qquad (4.2.16)$$

where W is the sample mass and C is a combined factor, given by:

$$C = \frac{M}{N_{Av} \,.\, \gamma \,.\, \theta \,.\, F \,.\, \lambda} \qquad (4.2.17)$$

with:

	M	-	molar mass;
	N_{Av}	-	Avogadro's number;
	γ	-	absolute gamma-ray intensity;
	θ	-	isotopic abundance;

λ - decay constant;

F - branching factor.

The combined factor amounts to 3.022×10^{-1} g.s for K, 6.863×10^{-4} g.s for Th (taking into account the $^{212}Bi\rightarrow{}^{208}Tl$ branching ratio F = 0.362) and 5.257×10^{-4} g.s for U, taking the values from Isotope Explorer [Chu et al., 1999] as shown in Table 4.2.4.

Table 4.2.4. Relevant parameters for the calculation of concentrations, taken from Isotope Explorer [Chu et al., 1999].

	^{232}Th	^{238}U	^{40}K
M ($g.mol^{-1}$)	Th: 232.04	U: 238.03	K: 39.10
θ	1	0.992745	0.000117
λ (s^{-1})	1.564×10^{-18}	4.918×10^{-18}	1.721×10^{-17}
γ	^{208}Tl: 0.9916	^{214}Bi: 0.154	^{40}K: 0.1067
F	0.362 (branching $^{212}Bi \rightarrow {}^{208}Tl$)		

Evidently, here again "wet loess weight" concentrations are obtained, to be recalculated to dry weight (see Section 4.4.1). The concentrations of K, U and Th in 15 Volkegem loess samples determined via low background NaI(Tl) gamma-spectrometry in the laboratory are shown in Table 4.2.5. The uncertainties quoted are only based on counting statistics. The spectra for sample S.31 and S.34 are lost due to a computer problem.

Table 4.2.5. K, U and Th concentrations in loess from Volkegem determined via low- background NaI(Tl) gamma-spectrometry in the laboratory.

No. of Volkegem loess sample	K (%) ± 2s (dry weight)	U ($mg.kg^{-1}$) ± 2s (dry weight)	Th ($mg.kg^{-1}$) ± 2s (dry weight)
S.31	-	-	-
S.35	1.684±0.023	2.48±0.25	10.19±0.45
S.30	1.763±0.026	2.45±0.26	10.00±0.58
S.34	-	-	-
S.28	1.662±0.022	2.58±0.26	9.79±0.46
S.32	1.710±0.024	2.33±0.25	9.52±0.44
S.39	1.678±0.024	2.41±0.27	10.17±0.44
S.33	1.759±0.027	2.51±0.27	10.18±0.51
S.38	1.813±0.030	2.46±0.29	10.43±0.46
S.29	1.700±0.026	2.49±0.27	10.21±0.66
S.17	1.782±0.025	2.51±0.28	10.45±0.48
S.5	1.769±0.026	2.68±0.24	9.58±0.41
S.27	1.703±0.025	2.42±0.28	10.36±0.49
S.16	1.723±0.026	2.42±0.28	10.18±0.56
S.10	1.797±0.025	2.26±0.23	10.31±0.47

4.3. Extended-energy range Ge gamma-ray spectrometry in low-background laboratory conditions

4.3.1. Detection system

For the present work, use was made of an extended-energy range high-purity p-type coaxial Ge detector (XtRa HPGe) with a thin carbon-epoxy entrance window (0.5 mm thickness). This detector is suitable for measuring the different gamma-lines of K and of U and Th and their daughters. Notably, the carbon-epoxy window makes it possible to efficiently measure the low-energetic gamma-rays, such as the one at 46.5 keV emitted by ^{210}Pb (in the ^{238}U-series). This is important, because it is an indicator for possible radon escape in the geological times. The detection system is locally called "Bertha". The schematic representation and the characteristics of "Bertha" as quoted by the supplier (Canberra) are shown in Fig. 4.3.1 and Table 4.3.1, respectively.

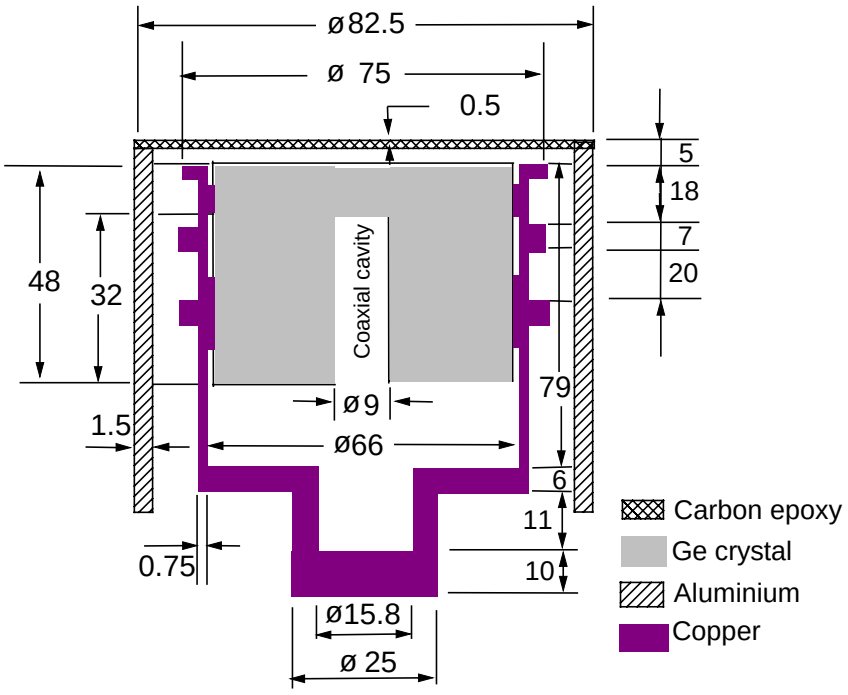

Fig. 4.3.1. Schematic representation of detector Bertha. The dimensions are in mm.

Table 4.3.1. Characteristics of detector Bertha.

Active volume	163 cm^3
Entrance window	0.5 mm carbonepoxy
Resolution (FWHM) at 122 keV	0.801 keV
Resolution (FWHM) at 1332.5 keV	1.78 keV
Relative efficiency at 1332.5 keV	45.7 %

The detector is mounted in a low-background lead castle supplied by Canberra. The shielding arrangement, shown in Fig. 4.3.2, is an ultra low-background shield with 150 mm thick lead [130 mm thick lead with activity <50 mBq/g + 20 mm thick lead with activity < 10 mBq/g]. The inner surface of the lead shield is covered with a 5 mm-thick Cu-liner to absorb secondary radiation. Nitrogen is continuously flushing through the shielding against radon contamination. For sample chamber access, the shielding is equipped with a swing-top door, allowing it to fit tightly against the shield body.

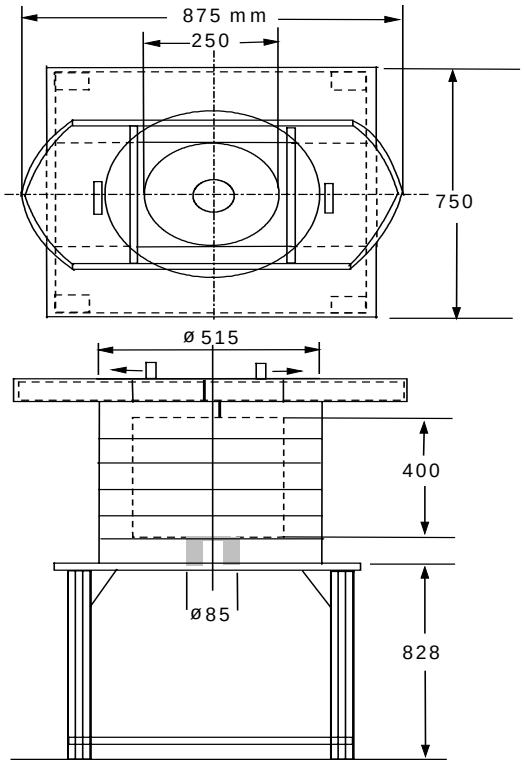

Fig. 4.3.2. Shielding arrangement of detector Bertha. The dimensions are in mm.

4.3.2. Choice of gamma lines to check disequilibria

High-resolution gamma-ray spectrometry can be used to obtain information on the state of equilibrium of the ^{235,238}U and ^{232}Th decay series, as is explained in Chapter 2 Section 2.3.

In the following three sections, a survey of the measured γ-lines is given, together with comments on their sensitivity, spectral interferences and ability to detect disequilibria. The gamma-ray energies and intensities (denoted hereafter as γ) are taken from Isotope Explorer [Chu et al., 1999].

4.3.2.1. ^{238}U-decay series

^{234}Th: E_γ = 63.3 keV, with γ = 4.84 %

The concentration determination via this gamma-line (with a small contribution of the ^{234}Th 62.9 keV line, with γ = 0.021 %) provides conclusive information for the mother isotope ^{238}U. It is interfered (with a contribution of up to 10 % [Murray, 1981]) by the ^{232}Th 63.8 keV line (with γ = 0.263 %) and a correction for this spectral interference is thus needed in case of both absolute and relative standardization (unless in the latter the Th/U ratio happens to be the same in sample and standard).

^{226}Ra: E_γ = 186.2 keV, with γ = 3.59 %

As said above, ^{226}Ra is mobile by the action of ground water. Therefore, measurement of the ^{226}Ra 186.2 keV line (the only choice) gives an indication of disequilibrium. Unfortunately, this gamma-line is strongly interfered by the ^{235}U 185.7 keV line, with a contribution of several tens of percents. Although, in principle, a correction for this spectral interference is possible, it leads to results with relatively poor accuracy and precision.

^{214}Pb: E_γ = 242.0 keV, with γ = 7.43 %
295.2 keV, with γ = 19.3 %
351.9 keV, with γ = 37.6 %

and

^{214}Bi: E_γ = 609.3 keV, with γ = 46.1 %
1120.3 keV, with γ = 15.1 %
1764.5 keV, with γ = 15.4 %

These two radionuclides are quite important, because they are (indirect) indicators for depletion or enrichment of ^{226}Ra. In this case, it is indeed clear that, when considering the series ^{230}Th (T½ = 75.4×10^3 a) → ^{226}Ra (T½ = 1600 a) → ^{222}Rn (T½ = 3.83 d) → ^{218}Po (T½ = 3.05 min) → ^{214}Pb (T½ = 26.8 min) → ^{214}Bi (T½ = 19.9 min), the activities of both ^{214}Pb and ^{214}Bi will follow any change in the activity of ^{226}Ra and will thus be different from the ^{234}Th activity. Also, it is obvious that, in view of the half-lives involved, the ^{230}Th → ^{226}Ra equilibrium - if disturbed in geological times - cannot be re-established in the laboratory after collection and preparation of the sample. ^{210}Pb, on the other hand, which is the next radionuclide measurable via gamma-ray spectrometry and which is formed via ^{214}Bi (T½ = 19.9 min) → ^{214}Po (T½ = 1.62×10^{-4} s) → ^{210}Pb (T½ = 22.2 a), is not suitable as a Ra-indicator since its activity can in addition be changed due to Rn-emanation (see further). It should be noted that in the latter case also the ^{214}Pb and ^{214}Bi activities are decreased. However – due to their short half-lives - their equilibrium in the series ^{226}Ra → ^{222}Rn → ^{218}Po → ^{214}Pb → ^{214}Bi is re-established after ~1 month (about 8 half-lives of the ^{222}Rn-daughter) when (leak-tight) encapsulating the sample for laboratory measurements (a re-establishment that does not happen with the long-lived ^{210}Pb).

All the above listed gamma-lines can be applied for the use of ^{214}Pb and ^{214}Bi as radium indicators. With some peaks, however, there are some small inconveniences: the ^{214}Pb 242.0 keV peak is situated in a complex triplet with

the ^{212}Pb 238.6 keV and ^{224}Ra 241.0 keV peaks (from the ^{232}Th-series), so that the use of powerful software for spectrum deconvolution is required (such as Hypermet-PC; see later). On the other hand, the ^{214}Bi 1120.3 keV peak has a rather weak intensity and its use is not recommended.

Because the ^{214}Pb and ^{214}Bi gamma-lines are measurable with good counting statistics, their analysis provides a better check of radium depletion or enrichment than the direct measurement of ^{226}Ra – in view of the cumbersome spectral interference of its 186.2 keV line, as outlined above. On the other hand, it would still be interesting to measure the ^{226}Ra isotope directly, so as to absolutely eliminate possible artifacts caused by the occurrence around the Ge detector (unwanted, and usually eliminated by flushing with N_2 from the Dewar) of ^{222}Rn (decaying to ^{214}Pb and ^{214}Bi).

^{210}Pb: $E_\gamma = 46.5$ keV, with $\gamma = 4.25$ %

If radon emanation occurs in geological times, it results in a decreased activity - compared to ^{234}Th – of the ^{210}Pb radionuclide, which is formed via ^{222}Rn ($T_{½}$ = 3.83 d) → ^{218}Po ($T_{½}$ = 3.05 min) → ^{214}Pb ($T_{½}$ = 26.8 min) → ^{214}Bi ($T_{½}$ = 19.9 min) → ^{214}Po ($T_{½} = 1.62\times10^{-4}$ s) → ^{210}Pb ($T_{½}$ = 22.2 a). In fact, this decrease of activity holds for all radionuclides situated between ^{222}Rn and ^{210}Pb, among which the gamma-emitters ^{214}Pb and ^{214}Bi. However, due to the short half-lives of these, their equilibrium in the series ^{226}Ra ($T_{½}$ = 1600 a) → ^{222}Rn → ^{218}Po → ^{214}Pb → ^{214}Bi is reached again (i.e. they get again the same activity as ^{234}Th) after about 1 month in leak-tight laboratory measuring conditions (see above). This re-establishment is not happening for the long-lived ^{210}Pb radionuclide, which is therefore to be considered as the only suitable ^{222}Rn indicator [at least, in the context of gamma-ray spectrometry; when performing alpha-spectrometry, ^{210}Po - formed via ^{210}Pb ($T_{½}$ = 22.2 a) → ^{210}Bi ($T_{½}$ = 5.01 d) → ^{210}Po ($T_{½}$ = 138.4 d) – is equally suitable]. It should be noted that the ^{210}Pb activity will not significantly change when the ^{222}Rn-loss happens during collection and preparation of the sample in the laboratory,

in view of the limited duration of these operations as compared to the long half-life of ^{210}Pb. On the other hand, when in geological times Ra-depletion or -enrichment (see above) occurs simultaneously with Rn-emanation, the three groups of activities ^{234}Th, ^{214}Bi-^{214}Pb and ^{210}Pb activities will be different (even when taking into account the 1 month period in the laboratory for re-establishing the possible Rn-emanation caused by sampling), and in these "mixed" conditions the difference between the activities of ^{234}Th and ^{210}Pb (the latter disturbed via both Ra-depletion/enrichment and Rn-emanation) does no longer provide a direct measure for the Rn-emanation. The only disadvantage of ^{210}Pb as a Rn-indicator is the low-energy of its gamma-line, not only requiring an appropriate Ge-detector but also leading to significant gamma-attenuation in the measured sample (usually of extended geometry) which is upon correction yielding a somewhat decreased accuracy.

4.3.2.2. ^{235}U-decay series

^{235}U: E_γ = 143.8 keV, with γ = 10.96 %
185.7 keV, with γ = 57.2 %
205.3 keV, with γ = 5.01 %

As mentioned above, the only high-intensity gamma-line of ^{226}Ra in the ^{238}U decay series is at 186.2 keV, which is strongly interfered by ^{235}U at 185.7 keV. In general, correction for this type of spectral interference can be made via other undisturbed gamma-lines of the interfering radionuclide, taking into account gamma-ray intensities, detection efficiencies and coincidence correction factors. Unfortunately, the other measurable gamma-lines of ^{235}U show serious inconveniences. The gamma-line at 143.8 keV is of moderate intensity and is itself interfered by gamma-lines from ^{230}Th at 143.9 keV and ^{223}Ra at 144.2 keV - thus requiring a second-order correction that leads to questionable results. On the other hand, the use of the 205.3 keV gamma-line, which is actually interference-free, is quite cumbersome for low active

samples due to its very low intensity – requiring long counting times and still leading to poor counting statistics.

As an alternative to the above suggested possibilities for the interference correction, another approach is the calculation of the ^{238}U activity via measurement of the ^{234}Th 63.3 keV line (see above). This is then followed by conversion to the ^{235}U-activity (based on the constant ^{235}U/^{238}U ratio), from which then the 185.7 keV gamma-peak area can be calculated – to be subtracted from the measured counts for the 186.2 keV + 185.7 keV doublet, so as to obtain the net number of counts for the ^{226}Ra 186.2 keV gamma-line.

4.3.2.3. ^{232}Th-decay series

As mentioned above, disequilibria in the decay chain are much less likely for ^{232}Th than for ^{238}U. The relevant daughter radionuclides and their analytically interesting gamma-lines are listed below.

^{232}Th: E_γ = 63.8 keV, with γ = 0.263 %

As outlined in the discussion of the ^{238}U decay series, the ^{232}Th 63.8 keV peak is an interference when measuring the ^{234}Th 63.3 keV peak, so that a correction is needed to obtain the correct number of counts for the latter. Unfortunately, there is no other suitable undisturbed ^{232}Th peak available. Thus the correction is based on the measurement of the undisturbed ^{228}Ac peak at 338.3 keV (introducing then gamma-ray intensities, detection efficiencies and coincidence correction factors). This interference correction is possible if ^{232}Th and ^{228}Ac are in equilibrium.

^{228}Ac: E_γ = 129.1 keV, with γ = 2.42 %
209.3 keV, with γ = 3.89 %
328.0 keV, with γ = 2.95 %

338.3 keV, with $\gamma = 11.27$ %

463.0 keV, with $\gamma = 4.40$ %

911.2 keV, with $\gamma = 25.8$ %

969.0 keV, with $\gamma = 15.8$ %

The most reliable and interference free gamma-lines of ^{228}Ac are at 338.3 keV, 911.2 keV and 969.0 keV. Other gamma-lines are of low intensity. The gamma-line at 328.0 keV is interfered by Bi-212 at 328.0 keV.

^{224}Ra: $E_\gamma = 241.0$ keV, with $\gamma = 4.10$ %

This gamma line is a rather weak component of a triplet with the 238.6 keV line of ^{212}Pb and the 242.0 keV line of ^{214}Pb, so that reliable software for spectrum analysis is required (such as Hypermet-PC; see later).

^{212}Pb: $E_\gamma = 238.6$ keV, with $\gamma = 43.3$ %

300.1 keV, with $\gamma = 3.28$ %

The highly intense 238.6 keV peak is part of the triplet mentioned above. It can be measured with good counting statistics. The gamma-line at 300.1 keV is not very useful because of its very low intensity.

^{212}Bi: $E_\gamma = 727.3$ keV, with $\gamma = 6.58$ %

This gamma-line is not useful, since its gamma-intensity is very low and the peak is interfered by ^{228}Ac at 726.9 keV.

^{208}Tl: $E_\gamma = 583.2$ keV, with $\gamma = 84.5$ %

860.5 keV, with $\gamma = 12.4$ %

2614.5 keV, with $\gamma = 99.2$ %

The gamma-lines of 583.2 keV and 2614.5 keV are measurable without any difficulties, whereas the line at 860.5 keV has a very low gamma intensity, which makes it practically useless.

4.3.3. Counting of a sample in a cylindrical geometry

The 15 cylindrical, undisturbed loess samples were measured on top of detector Bertha for a period of 7 days each. The software Genie-2000 [Model S500, spectroscopy system, Canberra] was used for data acquisition. A spectrum collected for loess sample number S.31 is shown in Fig. 4.3.3.

In order to detect possible radon loss from the loess material in the laboratory, during the period of time between the uncapping of the cylinder and the covering of its base (facing the detector) with Mylar foil (6 μm thickness), two measurements were performed with 4 weeks interval. No significant differences were observed. Invariably, the Hypermet-PC software package [Fazekas et al., 1997] was used for peak analysis.

The background was counted for 12 days with the same cylindrical steel container (not containing the sample) at the same counting position of the sample. The spectrum is shown in Fig. 4.3.4. The background count rate was subtracted from the sample count rate for each gamma line to get the net peak count rate.

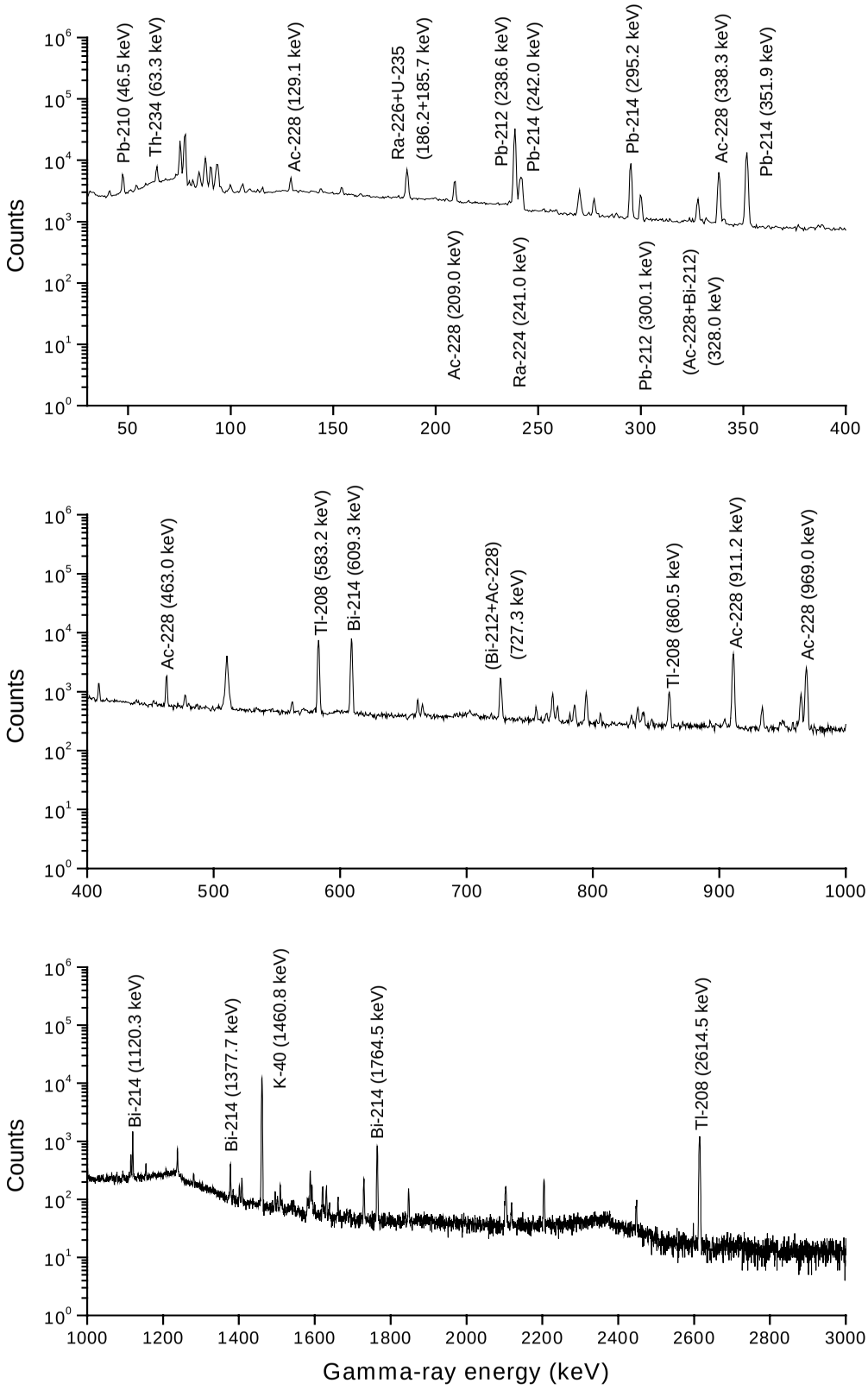

Fig. 4.3.3. Spectrum of Volkegem loess material (190 g) counted in cylindrical geometry during 7 days on top of XtRa Ge detector "Bertha".

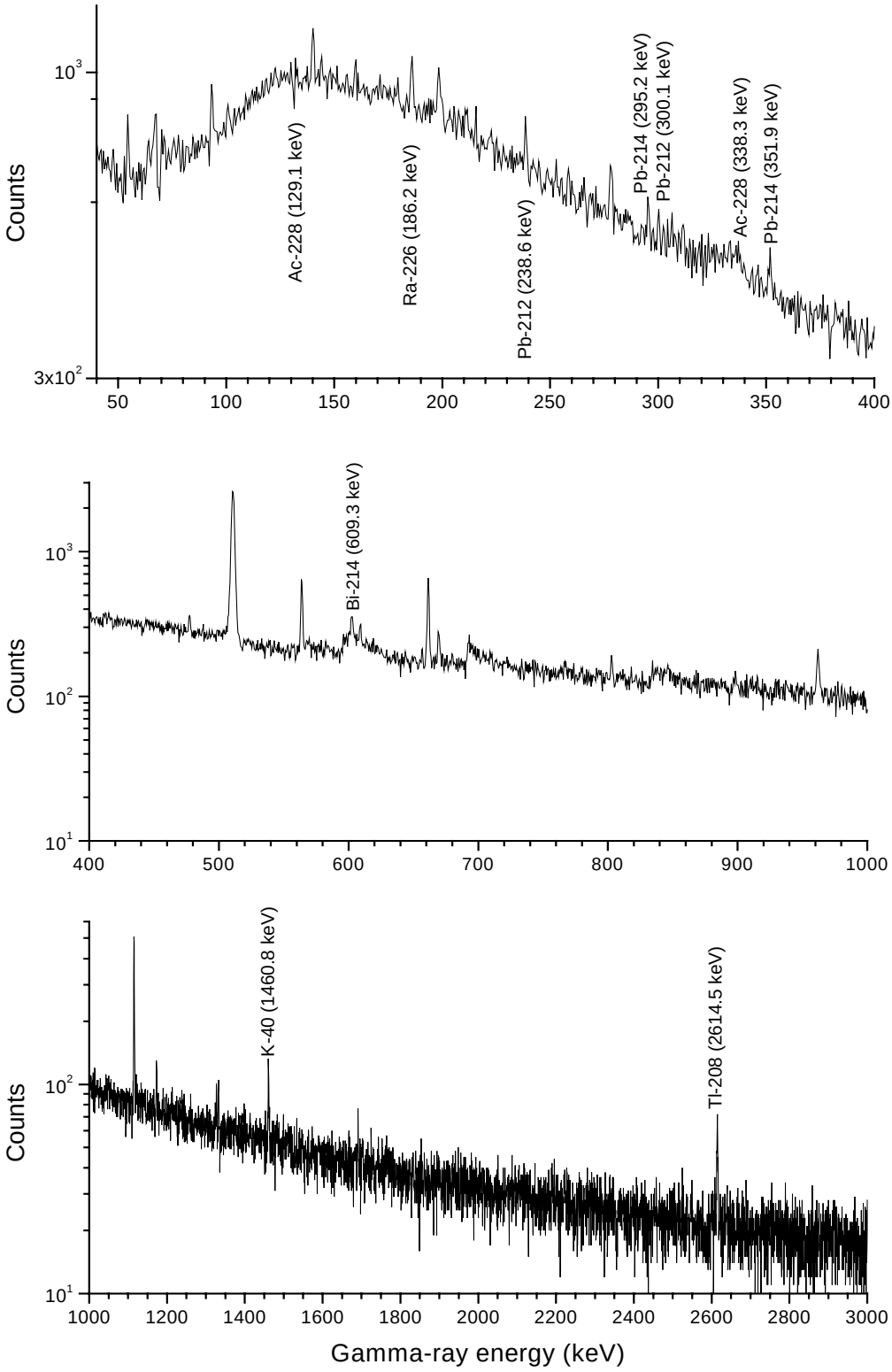

Fig. 4.3.4. Background spectrum recorded for the XtRa HPGe detector Bertha using the shielding shown in Fig. 4.3.2. The counting time was 12 days, with the same cylindrical steel container (without the sample) at the same counting position (on top of the detector) as for the sample.

4.3.4. Calibration

Calibration was done in two ways: absolute and relative.

4.3.4.1. Absolute calibration

Absolute calibration was performed as described above for the NaI(Tl) laboratory measurements [see also Eq. (4.2.16)]. Let it be recalled here that the absolute calibration is based on peak detection efficiency, true-coincidence correction and nuclear data. In view of their importance when discussing the results obtained in this way (see further), the absolute intensities of the gamma-lines measured are shown in Table 4.3.2. The other relevant parameters, taken from Isotope Explorer [Chu et al. 1999], and the experimentally determined coincidence corrections (COI) of different gamma-lines of U and Th daughters, are shown in Table 4.3.3. The peak detection efficiency curve at reference position (24.03 cm) was determined using commercially available absolutely calibrated point sources (^{60}Co, ^{133}Ba, ^{134}Cs, ^{152}Eu, ^{166}Ho, ^{226}Ra) and a home- made source ^{56}Co. The gamma-lines that were used with their absolute intensities for these point sources are shown in Table 4.3.4. The peak detection efficiency curve for detector Bertha at the reference position (24.03 cm), together with the result of the polynomial fittings (divided into 3 regions), is shown in Fig. 4.3.5.

Just as in the protocol described for the measurements with the NaI(Tl) detector (see Section 4.2.2.2), the reference efficiencies were converted to efficiencies for the actual counting geometries (voluminous source on top of the detector) via the calculation of effective solid angles. Also here, corrections had to be performed for true-coincidence effects, for which knowledge of the peak-to-total ratio curve was required. An example of such an experimentally measured P/T-curve for detector Bertha is shown in Fig. 4.3.6. The used gamma-lines with their absolute intensities for the sources used for P/T curve are shown in Table 4.3.6.

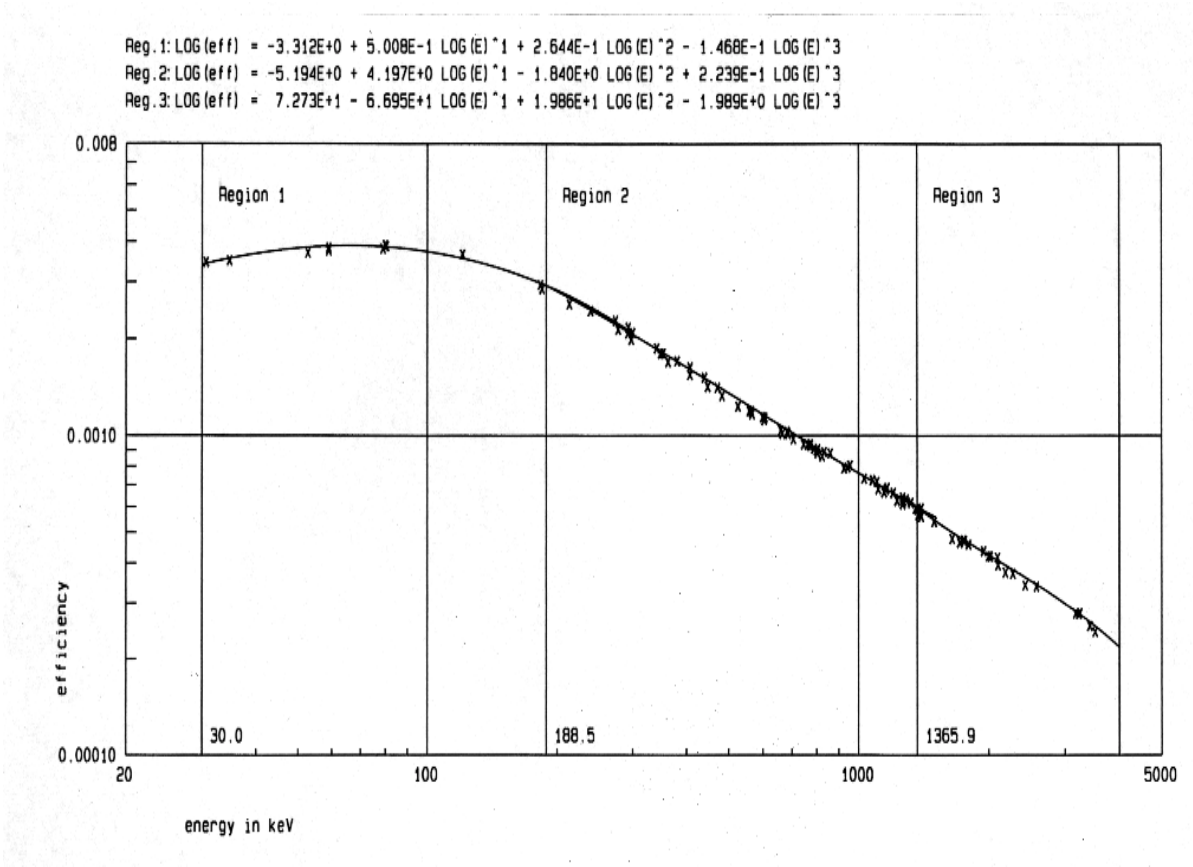

Fig. 4.3.5. Experimental detection efficiency curve of detector Bertha using point sources at reference position (24.03 cm).

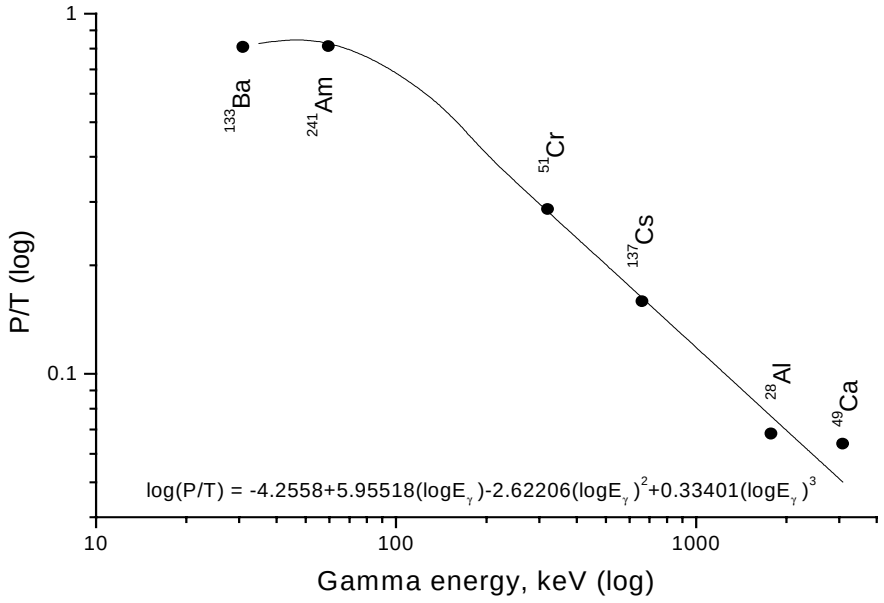

Fig. 4.3.6. Experimental peak-to-total curve of detector Bertha using point sources at reference position (24.03 cm).

Table 4.3.2. Gamma-energies and intensities of ^{40}K, of the measured radionuclides in the ^{232}Th and ^{238}U decay series, and of the interfering gamma rays based on Isotope Explorer [Chu et al., 1999].

Radio-nuclide	Measured gamma-line		Interfered by			Corrected via	
	Energy, keV	Intensity[1)], %	Radio-Nuclide	Energy, keV	Intensity[1)], %	Energy, keV	Intensity[1)], %
^{40}K	1460.8	1.158 *20*	-	-	-	-	-
^{232}Th series							
^{228}Ac	338.3	11.27 *19*	-	-	-	-	-
	911.2	25.8 *4*	-	-	-	-	-
	969.0	15.8 *3*	-	-	-	-	-
^{224}Ra	241.0	4.10 *5*	-	-	-	-	-
^{212}Pb	238.6	43.3 *3*	-	-	-	-	-
^{208}Tl	583.2	84.5 *7*	-	-	-	-	-
	2614.5	99.2 -	-	-	-	-	-
^{238}U series							
^{234}Th	63.3 + 62.9	4.84 *6* 0.021 *4*	^{232}Th	63.8	0.263 *13*	338.3[2)]	11.27 *19*
^{226}Ra	186.2	3.59 *6*	^{235}U	185.7	57.2 *8*	205.3[3)]	5.01 *10*
^{214}Pb	242.0	7.43 *11*	-	-	-	-	-
	295.2	19.3 *2*	-	-	-	-	-
	351.9	37.6 *4*	-	-	-	-	-
^{214}Bi	609.3	46.1 *5*	-	-	-	-	-
	1764.5	15.4 *2*	-	-	-	-	-
^{210}Pb	46.5	4.25	-	-	-	-	-

[1)] with *last digit uncertainty*

[2)] from ^{228}Ac (in the ^{232}Th series)

[3)] the line at 143.8 keV, with a higher intensity of 10.96 %, is itself interfered by the ^{230}Th 143.9 keV and ^{223}Ra 144.2 keV lines

Table 4.3.3. Gamma-ray energies and other relevant parameters, together with the experimentally determined true-coincidence factor (COI).

Radio-nuclide	Gamma energy (keV)	Isotopic abundance θ (%)	Decay constant λ (s^{-1})	Molar mass ($g.mol^{-1}$)	Branching factor F	Coincidence correction factor COI
^{40}K	1460.8	0.0117	1.72082×10^{-17}	39.1	1	1
^{232}Th series		100	1.56405×10^{-18}	232.04		
^{228}Ac	338.3				1	0.986
	911.2				1	0.979
	969.0				1	0.980
^{224}Ra	241.0				1	0.997
^{212}Pb	238.6				1	1
^{208}Tl	583.2				0.362	0.882
	2614.5				0.362	0.889
^{238}U series		99.2745	4.91828×10^{-18}	238.03		
^{234}Th	63.3				1	1
^{226}Ra	186.2				1	1
^{214}Pb	242.0				1	0.992
	295.2				1	0.999
	351.9				1	1
^{214}Bi	609.3				1	0.921
	1764.5				1	0.999
^{210}Pb	46.5				1	1
^{235}U series	185.7	0.7200	3.12232×10^{-17}	238.03	1	0.996

Table 4.3.4. Decay data of primary and secondary calibration point sources used for measuring the peak detection efficiency curve of the XtRa HPGe-detector Bertha at reference position (24.03 cm).

Point Source	Gamma energy keV	Gamma intensity %	Point Source	Gamma energy keV	Gamma intensity %	Point Source	Gamma energy keV	Gamma intensity %
^{60}Co	1173.2	99.85		80.6	12.33		1385.3	0.757
	1332.5	99.98		184.4	72.6		1401.5	1.27
	30.9	97.1		215.9	2.61		1408.0	2.15
	35.0	23.2		280.5	29.77		1509.2	2.11
	53.2	2.199		300.8	3.732		1661.3	1.15
	79.6	2.62		365.8	2.476	^{226}Ra	1729.6	2.92
^{133}Ba	81	34.06		410.9	11.43		1764.5	15.4
	276.4	7.164		451.5	2.984		2118.6	1.14
	302.9	18.33	^{166}Ho	529.8	9.69		2204.2	5.08
	356.0	62.05		571.0	5.55		2293.4	0.305
	383.9	8.94		611.5	1.408		2447.9	1.57
	475.4	1.486		670.5	5.48		1771.4	15.47
	563.3	8.35		691.3	1.343		1810.8	0.638
	569.3	15.38		711.7	55.32		1963.7	0.724
	604.7	97.62		752.3	12.29		2015.2	3.04
^{134}Cs	795.9	85.53		778.8	3.078		2034.8	7.89
	802.0	8.69		810.3	58.08	^{56}Co	2113.1	0.376
	1038.6	0.988		830.6	9.82		2598.5	17.3
	1168.0	1.789		951.0	2.755		3202.0	3.32
	1365.2	3.014		186.2	3.59		3253.4	8.12
	121.8	28.67		242.0	7.43		3273.0	1.93
	344.3	26.56		295.2	19.3		3451.4	0.972
	411.1	2.237		351.9	37.6		3547.9	0.200
	444.0	2.830		487.1	0.42			
	688.7	0.859		609.3	46.1			
	778.9	12.96		768.4	4.97			
^{152}Eu	867.4	4.258	^{226}Ra	806.2	1.22			
	964.1	14.65		839.0	0.587			
	1085.9	10.24		1120.3	15.1			
	1112.1	13.69		1155.2	1.646			
	1213.0	1.426		1238.1	5.79			
	1299.1	1.626		1281.0	1.43			
	1408.0	21.07		1377.7	4			

Source	Half-life
^{60}Co	5.275 a
^{133}Ba	10.52 a
^{134}Cs	2.065 a
^{154}Eu	13.54 a
^{166}Ho	1200 a
^{226}Ra	1600 a
^{56}Co	77.23 d

Table 4.3.5. Decay data of primary and secondary calibration sources used for measuring the P/T curve of the XtRa HPGe-detector Bertha at reference position (24.03 cm).

Source	Half-life	Gamma energy keV	Gamma intensity %
^{241}Am	432.2 a	59.5	35.9
^{51}Cr	27.7 d	320.1	9.9
^{137}Cs	30.04 a	661.7	85.1
^{28}Al	2.24 min.	1778.9	100
^{49}Ca	8.72 min.	3084.4	92

4.3.4.2. Relative calibration

Relative calibration was also performed, by measuring K, Th and U standards. Therefore, three steel cylinders identical to the ones used for the loess sampling, were completely filled with RGK-1, RGTh-1 and RGU-1 material, respectively. These are radiometric reference materials issued by the IAEA, Vienna [IAEA, 1987], with reported K, Th and U contents – expressed on dry weight basis - of (44.8±0.3) %, (800±16) mg.kg^{-1} and (400±2) mg.kg^{-1}, respectively, where the uncertainties are 1s. In these standards, the U- and Th- decay series are reported to be in radioactive equilibrium. Measurement of the reference materials (8 hours for RGK-1, 16 hours for RGTh-1 and 18 hours for RGU-1) was done in duplicate, and the spectra obtained were analyzed using the Hypermet-PC software.

4.3.5. Calculation of concentrations

The concentrations of K, U and Th via absolute calibration were obtained according to Eq. (4.2.16).

By applying the relative calibration, the concentrations of K, Th and U in the loess were obtained from:

$$[\text{conc.}]_{\text{loess}} = [\text{conc.}]_{\text{ref.mat.}} \times \frac{[\text{cps}/\text{W}]_{\text{loess}}}{[\text{cps}/\text{W}]_{\text{ref.mat.}}} \times \frac{[\overline{\Omega}]_{\text{ref.mat.}}}{[\overline{\Omega}]_{\text{loess}}} \qquad (4.3.1)$$

where W is the sample mass of loess and reference material (in the steel cylinder), and where the differences in true-coincidence correction factors for loess and the reference material (both in the same geometrical configuration versus the detector) are considered to be negligible.

As mentioned above, there are two cases (both in the ^{238}U-decay series) where corrections have to be made for spectral interference (overlapping gamma-peaks). In general, the conversion of the measured to the correct peak area (N_p) is performed as:

$$[N_{p,a}]_{\text{correct}} = [N_{p,a+b}]_{\text{meas.}} - [N_{p,\text{ref}}]_{\text{meas.}} \times \frac{[\gamma \times \varepsilon_p \times \text{COI}]_b}{[\gamma \times \varepsilon_p \times \text{COI}]_{\text{ref}}} \qquad (4.3.2)$$

with γ the gamma-ray intensity, and where “a” denotes the interfered peak, “b” the interfering peak and “ref” is an undisturbed peak from the interfering radionuclide. In the case of the ^{234}Th 63.3 keV (+ 62.9 keV) peak, which is interfered by a gamma-ray at 63.8 keV from ^{232}Th, there is no suitable undisturbed ^{232}Th peak available, and therefore the peak at 338.3 keV from ^{228}Ac (in the ^{232}Th series) was chosen as the reference. In the case of the ^{226}Ra 186.2 keV peak, which is interfered by a gamma-ray at 185.7 keV from ^{235}U, there are two (low intense) ^{235}U lines that can be used as reference: one at 143.8 keV, which is however itself interfered by lines from both ^{230}Th (143.9 keV) and ^{223}Ra (144.2 keV); the other, at 205.3 keV, is interference-free and can as such be used as reference. However, when doing so, its poor counting statistics leads to a large uncertainty, thus hampering the precise and accurate quantification of U via ^{226}Ra. Note that in this case no gamma-line from another radionuclide in the ^{238}U series can be used as reference (as done above for Th), because it can a priori not be excluded that Ra is enriched or depleted. Let it be mentioned that, here too, the detection efficiency and the coincidence correction factors were calculated via the program Solcoi and the absolute gamma-intensity data

were taken from Isotope Explorer. Finally, it is clear that the method yields "wet loess weight" K, Th and U-concentrations, to be converted to dry weight based on the moisture content (see Section 4.4.1). The concentrations of U and Th determined via different daughter-products/gamma-lines followed by absolute and relative calibration, are shown in Tables 4.3.6 – 4.3.9. The uncertainties specified refer only to the counting statistics (2s).

The final results obtained are shown in Table 4.3.10. The uncertainties quoted on the K concentrations resulting from both the absolute and the relative calibration are only based on counting statistics. In the case of U and Th, both the expected uncertainty (from the counting statistics) and the observed uncertainty (from the variation of U, Th concentrations via different daughters/gamma-lines) were calculated and the larger of the two was adopted.

Table 4.3.6. Concentration of U (± 2s counting statistics), using absolute calibration, from HPGe γ-spectrometry of the daughter radionulcides in the ^{238}U decay chain (the "S.xy" notations refer to the sampling points).

Sample No.	^{234}Th 63.3 keV (mg/kg) Dry weight	^{226}Ra 186.2 keV (mg/kg) Dry weight	^{214}Pb 242.0 keV (mg/kg) Dry weight	^{214}Pb 295.2 keV (mg/kg) Dry weight
S.31	2.35±0.20	3.3±1.1	2.47±0.10	2.503±0.041
S.35	2.30±0.13	3.4±1.0	2.49±0.13	2.381±0.044
S.30	2.46±0.21	3.1±1.5	2.44±0.16	2.323±0.048
S.34	2.25±0.26	3.4±1.4	2.463±0.086	2.396±0.049
S.28	2.245±0.070	2.9±1.2	2.42±0.12	2.262±0.047
S.32	2.23±0.21	2.7±1.1	2.34±0.11	2.363±0.053
S.39	2.25±0.22	2.8±1.2	2.44±0.16	2.387±0.059
S.33	2.21±0.17	3.2±1.2	2.34±0.14	2.249±0.055
S.38	2.25±0.19	2.9±1.5	2.48±0.14	2.380±0.044
S.29	2.21±0.30	3.1±1.4	2.73±0.14	2.401±0.064
S.17	2.48±0.19	3.1±1.0	2.434±0.095	2.350±0.048
S.5	2.29±0.19	3.1±1.1	2.38±0.12	2.266±0.056
S.27	2.35±0.16	3.1±1.6	2.53±0.13	2.445±0.045
S.16	2.13±0.17	3.3±1.2	2.318±0.086	2.381±0.044
S.10	2.76±0.14	3.4±1.0	2.59±0.11	2.426±0.050

Sample No.	^{214}Pb 351.9 keV (mg/kg) Dry weight	^{214}Bi 609.3 keV (mg/kg) Dry weight	^{214}Bi 1764.5 keV (mg/kg) Dry weight	^{210}Pb 46.5 keV (mg/kg) Dry weight
S.31	2.488±0.045	2.366±0.029	2.733±0.082	3.07±0.20
S.35	2.405±0.044	2.253±0.028	2.523±0.096	3.03±0.19
S.30	2.369±0.034	2.282±0.055	2.572±0.093	2.88±0.18
S.34	2.366±0.043	2.332±0.029	2.527±0.076	2.87±0.13
S.28	2.245±0.045	2.238±0.050	2.39±0.10	2.96±0.14
S.32	2.371±0.043	2.303±0.037	2.441±0.088	2.92±0.19
S.39	2.343±0.024	2.283±0.028	2.474±0.059	3.19±0.18
S.33	2.272±0.032	2.202±0.040	2.352±0.085	2.77±0.21
S.38	2.477±0.040	2.327±0.029	2.61±0.12	3.00±0.16
S.29	2.457±0.025	2.33±0.12	2.66±0.12	2.94±0.18
S.17	2.372±0.029	2.264±0.041	2.480±0.099	2.92±0.22
S.5	2.280±0.023	2.160±0.035	2.52±0.11	3.01±0.28
S.27	2.488±0.030	2.342±0.057	2.68±0.10	3.12±0.19
S.16	2.427±0.034	2.270±0.041	2.57±0.10	2.72±0.12
S.10	2.505±0.035	2.399±0.044	2.65±0.11	2.76±0.14

Table 4.3.7. Concentration of Th (± 2s counting statistics), using absolute calibration, from HPGe γ-spectrometry of the daughter radionulcides in the ^{232}Th decay chain (the "S.xy" notations refer to the sampling points).

Sample No.	^{228}Ac 338.3 keV (mg/kg) Dry weight	^{228}Ac 911.2 keV (mg/kg) Dry weight	^{228}Ac 969.0 keV (mg/kg) Dry weight	^{224}Ra 241.0 keV (mg/kg) Dry weight
S.31	10.42±0.23	10.56±0.13	10.83±0.29	10.35±0.50
S.35	10.44±0.44	10.61±0.13	10.41±0.30	9.59±0.68
S.30	10.05±0.24	10.25±0.19	10.57±0.32	9.72±0.96
S.34	10.62±0.28	10.64±0.15	10.68±0.33	10.89±0.46
S.28	10.41±0.25	10.03±0.20	10.25±0.33	9.67±0.64
S.32	10.40±0.19	10.24±0.23	10.44±0.30	10.16±0.57
S.39	10.25±0.29	10.45±0.21	10.36±0.32	10.95±0.88
S.33	10.07±0.21	10.05±0.20	9.80±0.26	10.13±0.71
S.38	10.41±0.21	10.67±0.17	10.79±0.33	10.18±0.72
S.29	10.75±0.28	10.74±0.17	10.44±0.26	10.37±0.71
S.17	9.94±0.22	10.29±0.21	9.97±0.21	10.67±0.47
S.5	10.00±0.36	9.89±0.20	9.80±0.24	9.87±0.66
S.27	10.58±0.23	10.52±0.21	11.00±0.31	10.82±0.63
S.16	10.38±0.38	10.87±0.22	10.47±0.34	10.34±0.42
S.10	10.82±0.22	10.82±0.22	11.09±0.32	10.46±0.55

Sample No.	^{212}Pb 238.6 keV (mg/kg) Dry weight	^{208}Tl 583.2 keV (mg/kg) Dry weight	^{208}Tl 2614.5 keV (mg/kg) Dry weight
S.31	10.67±0.11	10.25±0.16	10.18±0.19
S.35	10.58±0.11	10.18±0.20	9.77±0.24
S.30	10.22±0.12	9.93±0.18	9.60±0.30
S.34	10.50±0.30	10.19±0.18	9.73±0.20
S.28	10.10±0.10	9.72±0.16	9.27±0.29
S.32	10.38±0.17	9.67±0.12	9.43±0.29
S.39	10.27±0.12	10.32±0.19	9.88±0.27
S.33	9.96±0.10	9.53±0.17	9.29±0.33
S.38	10.64±0.13	10.21±0.20	9.90±0.25
S.29	10.73±0.15	10.19±0.20	10.00±0.29
S.17	10.35±0.084	9.82±0.14	9.41±0.27
S.5	9.91±0.12	9.55±0.15	9.26±0.25
S.27	10.58±0.086	10.46±0.17	9.80±0.24
S.16	10.49±0.085	10.58±0.17	9.55±0.28
S.10	10.77±0.087	10.13±0.18	10.11±0.27

Table 4.3.8. Concentration of U (± 2s counting statistics), using relative calibration, from HPGe γ-spectrometry of the daughter radionulcides in the ^{238}U decay chain (the "S.xy" notations refer to the sampling points).

Sample No.	^{234}Th 63.3 keV (mg/kg) Dry weight	^{226}Ra 186.2 keV (mg/kg) Dry weight	^{214}Pb 242.0 keV (mg/kg) Dry weight	^{214}Pb 295.2 keV (mg/kg) Dry weight
S.31	2.62±0.21	3.5±1.4	2.49±0.10	2.601±0.047
S.35	2.56±0.15	3.2±1.3	2.52±0.13	2.474±0.049
S.30	2.75±0.10	3.0±1.5	2.46±0.13	2.414±0.052
S.34	2.50±0.23	3.0±1.6	2.49±0.12	2.490±0.057
S.28	2.504±0.093	3.2±1.6	2.45±0.13	2.351±0.051
S.32	2.49±0.22	3.5±1.4	2.37±0.12	2.456±0.058
S.39	2.51±0.23	3.5±1.6	2.47±0.17	2.481±0.063
S.33	2.50±0.19	3.0±1.6	2.40±0.14	2.371±0.060
S.38	2.51±0.20	3.6±1.9	2.51±0.14	2.473±0.049
S.29	2.47±0.30	3.2±1.8	2.76±0.15	2.510±0.069
S.17	2.76±0.20	3.1±1.3	2.462±0.097	2.441±0.053
S.5	2.56±0.22	2.8±1.5	2.41±0.14	2.355±0.061
S.27	2.619±0.070	3.3±1.8	2.56±0.13	2.541±0.050
S.16	2.37±0.18	3.2±1.6	2.344±0.088	2.474±0.049
S.10	2.54±0.25	3.1±1.4	2.62±0.11	2.521±0.054

Sample No.	^{214}Pb 351.9 keV (mg/kg) Dry weight	^{214}Bi 609.3 keV (mg/kg) Dry weight	^{214}Bi 1764.5 keV (mg/kg) Dry weight	^{210}Pb 46.5 keV (mg/kg) Dry weight
S.31	2.566±0.048	2.456±0.032	2.669±0.085	2.64±0.18
S.35	2.481±0.047	2.400±0.031	2.464±0.098	2.60±0.17
S.30	2.443±0.051	2.431±0.055	2.51±0.11	2.48±0.13
S.34	2.440±0.048	2.484±0.038	2.468±0.083	2.46±0.15
S.28	2.316±0.048	2.384±0.054	2.33±0.10	2.54±0.13
S.32	2.445±0.046	2.454±0.041	2.383±0.090	2.51±0.17
S.39	2.417±0.027	2.432±0.031	2.478±0.065	2.75±0.16
S.33	2.378±0.050	2.380±0.044	2.330±0.088	2.42±0.19
S.38	2.555±0.038	2.479±0.032	2.55±0.12	2.58±0.15
S.29	2.535±0.029	2.486±0.051	2.60±0.12	2.52±0.16
S.17	2.447±0.032	2.411±0.045	2.42±0.10	2.51±0.19
S.5	2.352±0.027	2.301±0.035	2.457±0.086	2.59±0.20
S.27	2.566±0.034	2.495±0.061	2.62±0.10	2.68±0.17
S.16	2.504±0.038	2.418±0.045	2.51±0.10	2.34±0.11
S.10	2.584±0.039	2.556±0.047	2.59±0.11	2.37±0.13

Table 4.3.9. Concentration of Th (± 2s counting statistics), using relative calibration, from HPGe γ-spectrometry of the daughter radionulcides in the ^{232}Th decay chain (the "S.xy" notations refer to the sampling points).

Sample No.	^{228}Ac 338.3 keV (mg/kg) Dry weight	^{228}Ac 911.2 keV (mg/kg) Dry weight	^{228}Ac 969.0 keV (mg/kg) Dry weight	^{224}Ra 241.0 keV (mg/kg) Dry weight
S.31	10.32±0.29	10.28±0.27	10.50±0.42	10.07±0.63
S.35	10.34±0.49	10.33±0.27	10.09±0.42	9.34±0.75
S.30	9.96±0.32	9.98±0.31	10.25±0.46	9.46±0.73
S.34	10.39±0.32	10.27±0.30	10.21±0.41	10.45±0.71
S.28	10.32±0.34	9.76±0.30	9.94±0.44	9.41±0.73
S.32	10.31±0.29	9.97±0.33	10.12±0.42	9.89±0.68
S.39	10.09±0.36	10.13±0.32	10.00±0.43	10.59±0.95
S.33	10.13±0.30	9.92±0.31	9.64±0.39	10.00±0.81
S.38	10.32±0.30	10.38±0.30	10.22±0.44	9.91±0.80
S.29	10.68±0.36	10.48±0.30	10.18±0.39	10.13±0.80
S.17	9.85±0.31	10.01±0.31	9.67±0.35	10.38±0.61
S.5	9.91±0.33	9.63±0.31	9.51±0.40	9.60±0.84
S.27	10.48±0.32	10.24±0.32	10.67±0.44	10.53±0.74
S.16	10.29±0.44	10.59±0.33	10.15±0.45	10.09±0.57
S.10	10.72±0.32	10.53±0.33	10.75±0.45	10.18±0.67

Sample No.	^{212}Pb 238.6 keV (mg/kg) Dry weight	^{208}Tl 583.2 keV (mg/kg) Dry weight	^{208}Tl 2614.5 keV (mg/kg) Dry weight
S.31	10.38±0.16	10.38±0.21	10.54±0.34
S.35	10.29±0.17	10.31±0.25	10.12±0.37
S.30	9.94±0.17	10.05±0.21	9.94±0.39
S.34	10.07±0.23	10.21±0.22	10.02±0.39
S.28	9.83±0.16	9.84±0.20	9.60±0.38
S.32	10.10±0.21	9.79±0.17	9.76±0.40
S.39	9.92±0.18	10.40±0.23	10.21±0.38
S.33	9.83±0.16	9.79±0.22	9.76±0.43
S.38	10.35±0.19	10.34±0.25	10.25±0.37
S.29	10.47±0.20	10.32±0.25	10.57±0.33
S.17	10.07±0.15	9.94±0.19	9.75±0.38
S.5	9.64±0.18	9.67±0.22	9.59±0.37
S.27	10.30±0.16	10.59±0.22	10.14±0.37
S.16	10.20±0.16	10.71±0.22	9.89±0.39
S.10	10.47±0.16	10.25±0.23	10.47±0.39

Table 4.3.10. Concentrations of K (± 2s counting statistics), U and Th (± 2s uncertainties), using absolute and relative calibration, from HPGe γ-spectrometry. Concentrations of U and Th are based on different dughters/gamma lines in the ^{238}U and ^{232}Th decay chains (the "S.xy" notations refer to the sampling points).

No. of sample	Absolute calibration			Relative calibration		
	K ± 2s % Dry weight	U ± 2s mg/kg Dry weight	Th ± 2s mg/kg Dry weight	K ± 2s % Dry weight	U ± 2s mg/kg Dry weight	Th ± 2s mg/kg Dry weight
S.31	1.786 ± 0.022	2.57 ± 0.19	10.46 ± 0.18	1.770 ± 0.019	2.557 ± 0.076	10.35 ± 0.14
S.35	1.768 ± 0.021	2.48 ± 0.20	10.23 ± 0.30	1.752 ± 0.019	2.468 ± 0.039	10.12 ± 0.27
S.30	1.868 ± 0.015	2.475 ± 0.048	10.05 ± 0.25	1.851 ± 0.018	2.452 ± 0.038	9.94 ± 0.15
S.34	1.846 ± 0.019	2.46 ± 0.15	10.47 ± 0.29	1.829 ± 0.017	2.474 ± 0.033	10.23 ± 0.15
S.28	1.775 ± 0.018	2.40 ± 0.20	9.92 ± 0.30	1.756 ± 0.017	2.367 ± 0.047	9.81 ± 0.15
S.32	1.845 ± 0.015	2.42 ± 0.17	10.10 ± 0.30	1.828 ± 0.016	2.421 ± 0.038	9.99 ± 0.15
S.39	1.781 ± 0.018	2.48 ± 0.25	10.35 ± 0.24	1.765 ± 0.017	2.455 ± 0.038	10.19 ± 0.18
S.33	1.752 ± 0.017	2.342 ± 0.046	9.83 ± 0.24	1.735 ± 0.017	2.372 ± 0.038	9.87 ± 0.16
S.38	1.853 ± 0.029	2.50 ± 0.19	10.40 ± 0.24	1.836 ± 0.024	2.513 ± 0.039	10.25 ± 0.16
S.29	1.787 ± 0.018	2.53 ± 0.19	10.46 ± 0.23	1.770 ± 0.017	2.578 ± 0.099	10.41 ± 0.16
S.17	1.868 ± 0.015	2.47 ± 0.16	10.06 ± 0.31	1.851 ± 0.016	2.436 ± 0.032	9.95 ± 0.18
S.5	1.855 ± 0.015	2.42 ± 0.22	9.75 ± 0.20	1.838 ± 0.016	2.375 ± 0.054	9.65 ± 0.16
S.27	1.772 ± 0.014	2.57 ± 0.21	10.54 ± 0.29	1.756 ± 0.017	2.556 ± 0.039	10.42 ± 0.15
S.16	1.761 ± 0.021	2.40 ± 0.15	10.38 ± 0.15	1.745 ± 0.019	2.449 ± 0.061	10.27 ± 0.22
S.10	1.793 ± 0.022	2.52 ± 0.12	10.60 ± 0.28	1.777 ± 0.019	2.575 ± 0.035	10.48 ± 0.16

4.4. Chemical composition of the loess

4.4.1. Moisture content

After finishing the NaI(Tl) and Ge gamma-ray spectrometric measurements in the laboratory, the loess was removed from the steel cylinders and dried in an oven at 110 °C until constant weight. This was required so as to obtain dry material for further analysis, namely alpha- and beta-counting, neutron activation analysis and atomic absorption spectrometry. Also, the drying procedure yielded information on the moisture content of the wet material, which is necessary to convert the K, Th and U concentrations (determined via gamma-spectrometry) from "wet weight" to "dry weight". The dry/wet ratios for the 15 collected Volkegem loess samples are shown in Table 4.4.1. The average water content of the wet loess was thus 13.8 %.

Table 4.4.1. Moisture content of Volkegem loess samples.

Number of sample	Dry/wet ratio
S.31	0.851
S.35	0.854
S.30	0.845
S.34	0.848
S.28	0.855
S.32	0.848
S.39	0.855
S.33	0.861
S.38	0.849
S.29	0.850
S.17	0.887
S.5	0.879
S.27	0.862
S.16	0.892
S.10	0.887

4.4.2. Elemental composition

The content of the major and minor elements in the dried Volkegem loess material was determined via XRF analysis at the Université de Liège [Duchesne]. Based on these results, the matrix composition of the wet material, taking into account an average water content of 13.8 % (see 4.4.1), was calculated. The result is presented in Table 4.4.2. This information on the (approximate) elemental composition is required for the calculation of the effective solid angles in the gamma-spectrometric measurements [Sections 4.2 and 4.3].

Table 4.4.2. Matrix composition of wet Volkegem loess.

Component	%
Si, %	38.12
Ti, %	0.450
Al, %	4.843
Fe, %	2.812
Mg, %	0.428
Ca, %	0.500
Na, %	0.809
K, %	1.801
O, %	50.37

4.5. Thick source alpha-counting

4.5.1. α-Counting system

For α-counting, use was made of two Elsec 7286 low-level α-counting systems, each equipped with three scintillation/PM tube measuring units designed by Littlemore Scientific Engineering. Each PM tube has its own individually adjustable high voltage supply and discriminator circuit. Ready-made scintillation screens (plastic screens impregnated with ZnS), purchased from Littlemore, were used.

The schematic experimental setup is shown in Fig. 4.5.1. Counting is performed by homogeneously spreading a 1 mm thick layer of dried finely powdered sample on a 42 mm diameter ZnS screen, positioned in a sealed Plexiglas holder. The sample layer of 1 mm is considered as infinitely thick ("Thick Source Alpha Counting – TSAC") because the most energetic α-particles in the U and Th decay series have a maximum range of 50 μm [Bowman, 1982]. The PM tube plus the sample are enclosed in a dark box. The pulses are fed into a preamplifier, amplifier and discriminator and then to timers and counters, and finally the results (number of counts and counting statistics) are printed. Next to the main timer/counter, giving the total counts for U + Th, there is a slow and a fast timer/counter, allowing to electronically discriminate Th [with its slow α-pairs from $^{220}Rn \rightarrow {}^{216}Po$ ($T½ = 0.15$ s) in the ^{232}Th-decay series] from U [with its fast α-pairs from $^{219}Rn \rightarrow {}^{215}Po$ ($T½ = 0.0018$ s) in the ^{235}U-decay series], so that the individual number of counts for Th and U (and their counting statistics) are obtained as well. Full details on the methodology, electronic setup and application of the alpha pair counting technique can be found in Aitken [985], Huntley and Wintle [1981] and the ELSEC 7286 User Manual [1993].

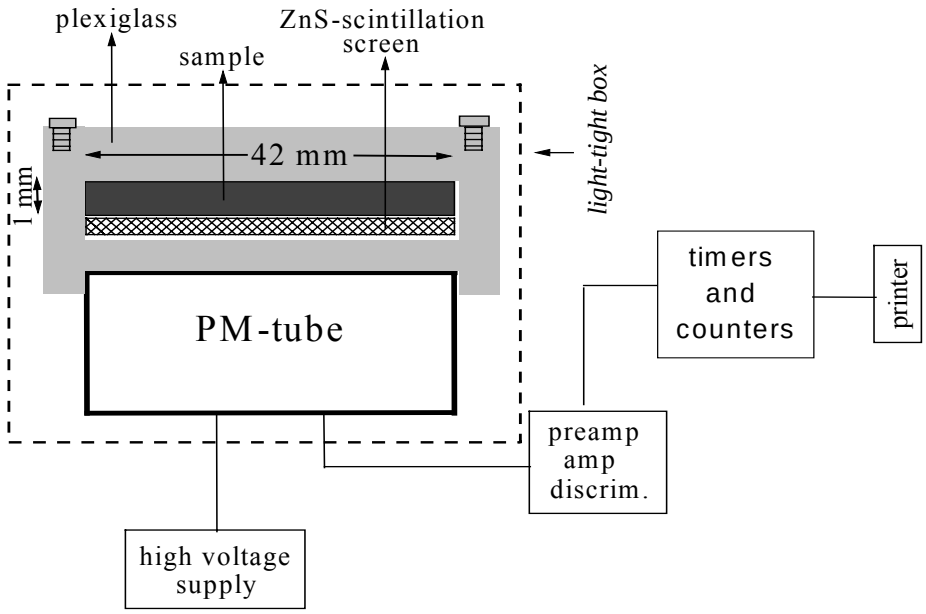

Fig.4.5.1. Schematic diagram of the thick source ZnS alpha counting system (based on Aitken, 1985).

4.5.2. Calibration of the α-counting system

For each α-counter, calibration was performed in two steps: i) determination of the high-voltage plateau and ii) adjustment of the threshold voltage. To eliminate a long counting period, geostandard Granite GS-N was used for this purpose, with 42 $mg.kg^{-1}$ Th and 8 $mg.kg^{-1}$ U [Govindaraju, 1989]. For performing both calibration steps, the standard is gently scraped onto the ZnS screen.

As a first step, the high-voltage plateau was determined by lowering the voltage in steps of 25 V, from 1400 V to 800 V for counter 1, 1375 V to 775 V for counter 2, 1250 V to 700 V for counters 3-4, 1350 V to 750 V, for counters 5-6. Each time the count rate was recorded. The plateau values are chosen as 1275 V, 1200 V, 1150 V, 1075V, 1175 V and 1075 V for counters 1-6, respectively, as shown in Figs 4.5.2 - 4.5.3.

A second step of the calibration procedure is the determination of the threshold voltage. By setting a proper threshold value, the pulses corresponding to β-particles, γ-rays and photomultiplier noise are eliminated, but a part of the α-particle pulses are rejected as well.

The threshold setting [Bowman, 1982] is usually adjusted in such a way that for a Th standard, with the ^{232}Th decay series in equilibrium, 85% of the α-pulses are counted. This setting then yields 82% of the pulses for a pure U standard in equilibrium and 83.5% for a sample with equal Th and U activity. Taking into account its Th/U ratio, it was calculated that 83.8% of the α-pulses should lie above the threshold value for the standard Granite GS-N.

The threshold value is determined by setting the plateau value and increasing the threshold voltage in steps of 0.25 V, from 0.25 V to 2.50 V. For each of the ten steps the count rate was recorded. After performing a linear regression on these data points (count rate versus threshold voltage) the crossing with the y-axis gives the maximum count rate where no threshold voltage would have been set, which means that all pulses would have been led through.

The threshold values corresponding with the fraction 0.838 (for counters 1-6) of the maximum count rate were set for all further measurements, which means a setting of 0.595 V, 1.012 V, 1.808 V, 1.861 V, 1.175 V and 0.853 V for counters 1-6, respectively, as shown in Figs 4.5.4 –4.5.5.

The calibration setting of counters 1-6 was validated by comparing the observed count rate (directly measured via alpha counting) to the predicted count rate (calculated from the certified concentrations of U and Th) using a set of standards: RGU-1 [IAEA, 1987], RGTh-1 [IAEA, 1987] and Biotite Mica-Fe [Govindaraju, 1988]. The count rate was predicted by using the following relation [Aitken, 1998]:

$$\left[\dot{\alpha}\ (\text{counts} / \text{ks})\right]_{\text{predicted}} = 0.513\times[\text{conc.}(\text{mg.kg}^{-1})]_{\text{Th}} + 1.78\times[\text{conc.}(\text{mg.kg}^{-1})]_{\text{U}} \quad (4.5.1)$$

The consistency between the observed and predicted count rates (Table 4.5.1) gave confidence in using the above-mentioned calibration settings for further measurement of unknown samples.

Table 4.5.1. Validation of the calibration of the alpha counters (the unit of observed and predicted count rate is counts/10ks). The uncertainties are ± 2s, unless otherwise specified.

No. of α-Counter	RGU-1 U = 400±2 mg/kg (1s)			RGTh-1 Th = 800±16 mg/kg (1s) U = 6.3±0.4 mg/kg (1s)			Biotite Mica-Fe* Th = 150 mg/kg U = 80 mg/kg		
	Obser-ved Count rate	Predi-cted count rate	Ratio Obs./ Pred.	Obser-ved Count rate	Predi-cted count rate	Ratio Obs./ Pred.	Obser-ved Count rate	Predi-cted count rate	Ratio Obs./ Pred.
1	6963 ±42	7120 ±83	0.978 ±0.013	3948 ±30	4216 ±165	0.936 ±0.037	2292 ±32	2194*	1.045 ±0.015
2	6935 ±60		0.974 ±0.011	3918 ±56		0.929 ±0.039	2232 ±34		1.017 ±0.016
3	6957 ±34		0.977 ±0.011	3979 ±32		0.944 ±0.038	2286 ±36		1.042 ±0.016
4	6877 ±38		0.967 ±0.011	3856 ±26		0.915 ±0.036	2198 ±55		1.002 ±0.025
5	6811 ± 34		0.957 ±0.011	3891 ±34		0.923 ±0.037	2289 ±30		1.043 ±0.014
6	7203 ±36		1.012 ±0.011	4070 ±28		0.965 ±0.038	2449 ±30		1.116 ±0.014
Mean ratio			0.978 ±0.015			0.935 ±0.015			1.044 ±0.032
Grand mean = 0.986±0.063									

** For Biotite Mica-Fe no uncertainty specified with the concentrations of U and Th*

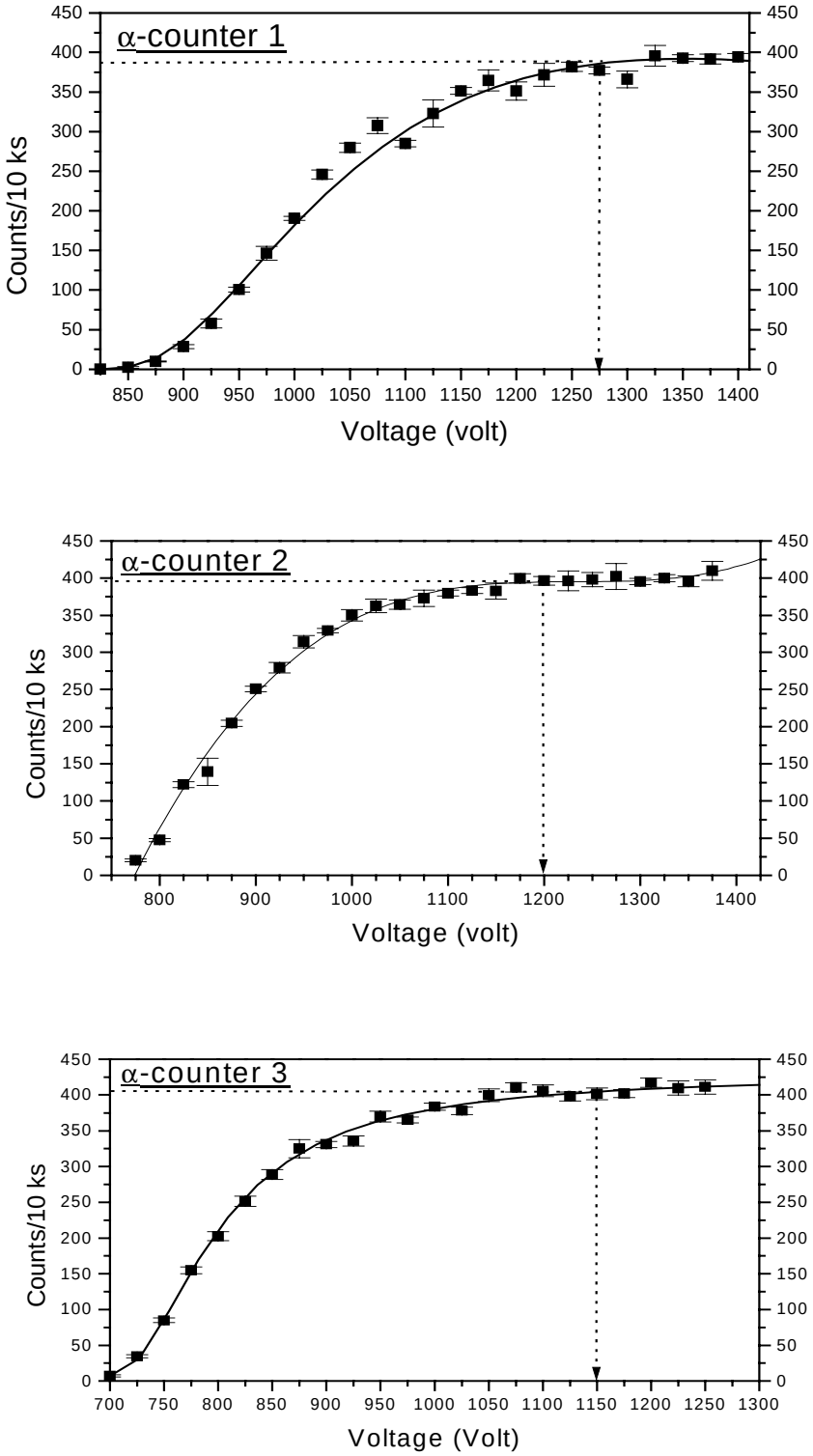

Fig. 4.5.2. High-voltage plateau of alpha-counters 1-3.

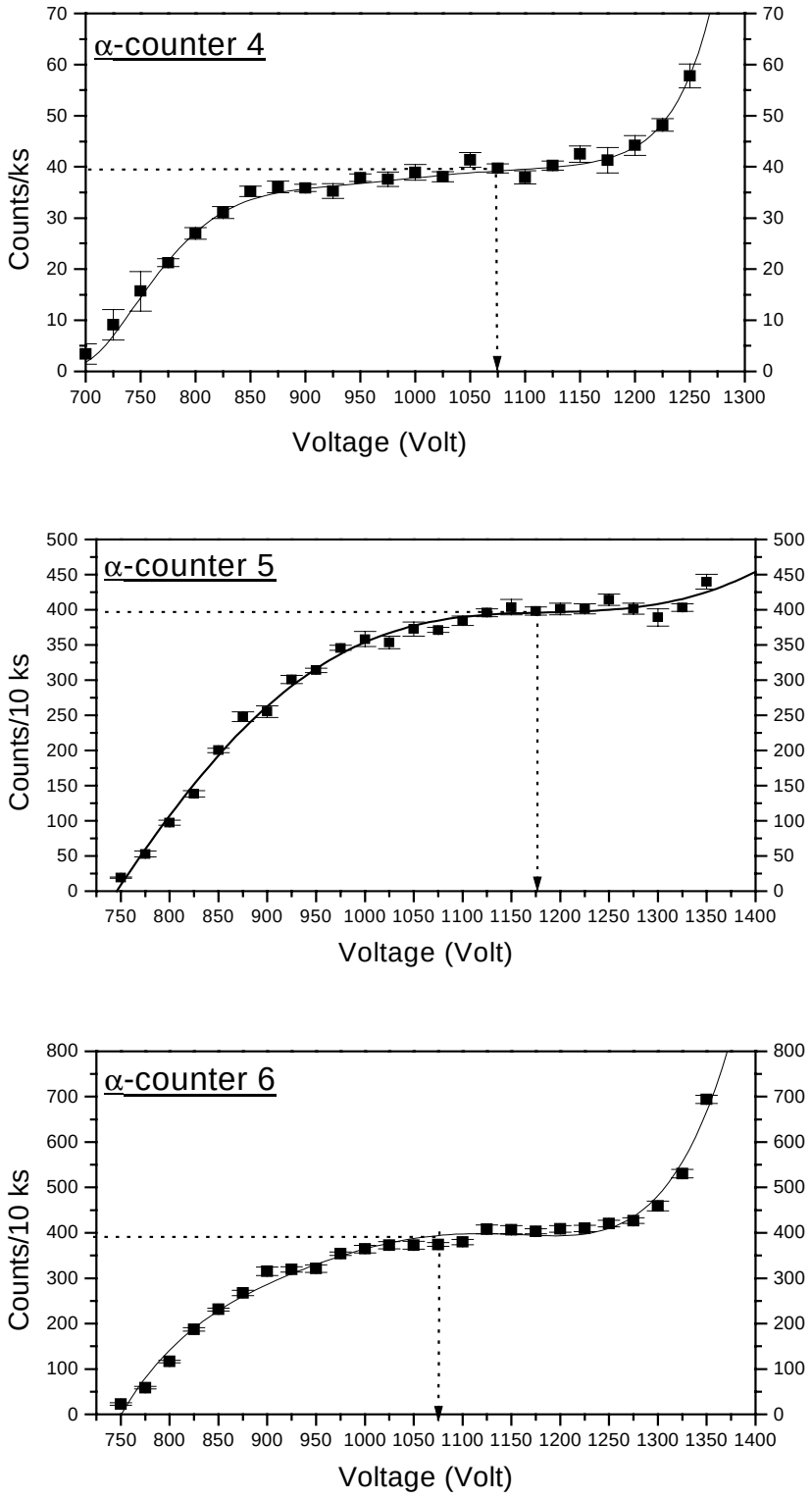

Fig. 4.5.3. High-voltage plateau of alpha-counters 4-6.

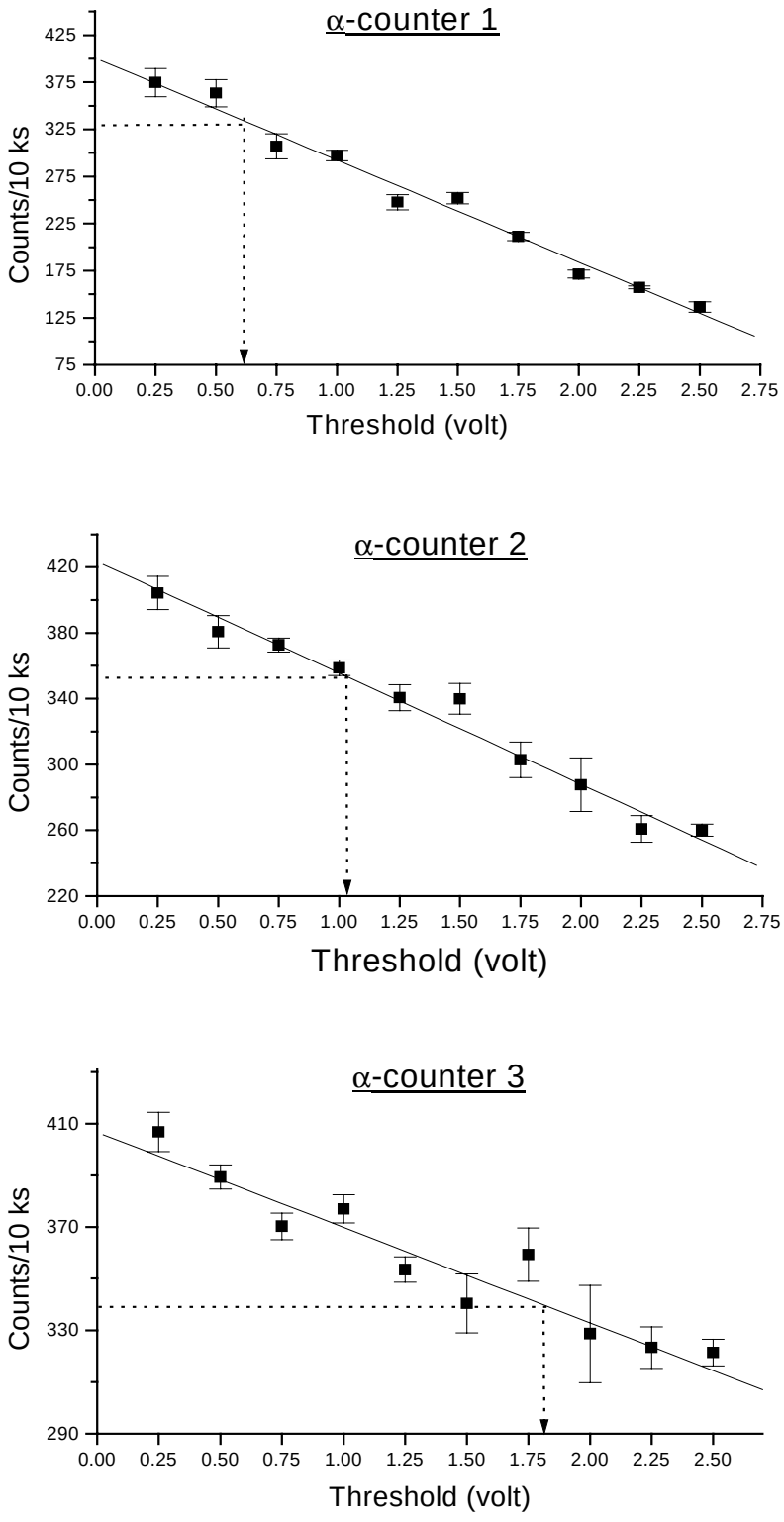

Fig. 4.5.4. Threshold voltage for alpha-counters 1-3.

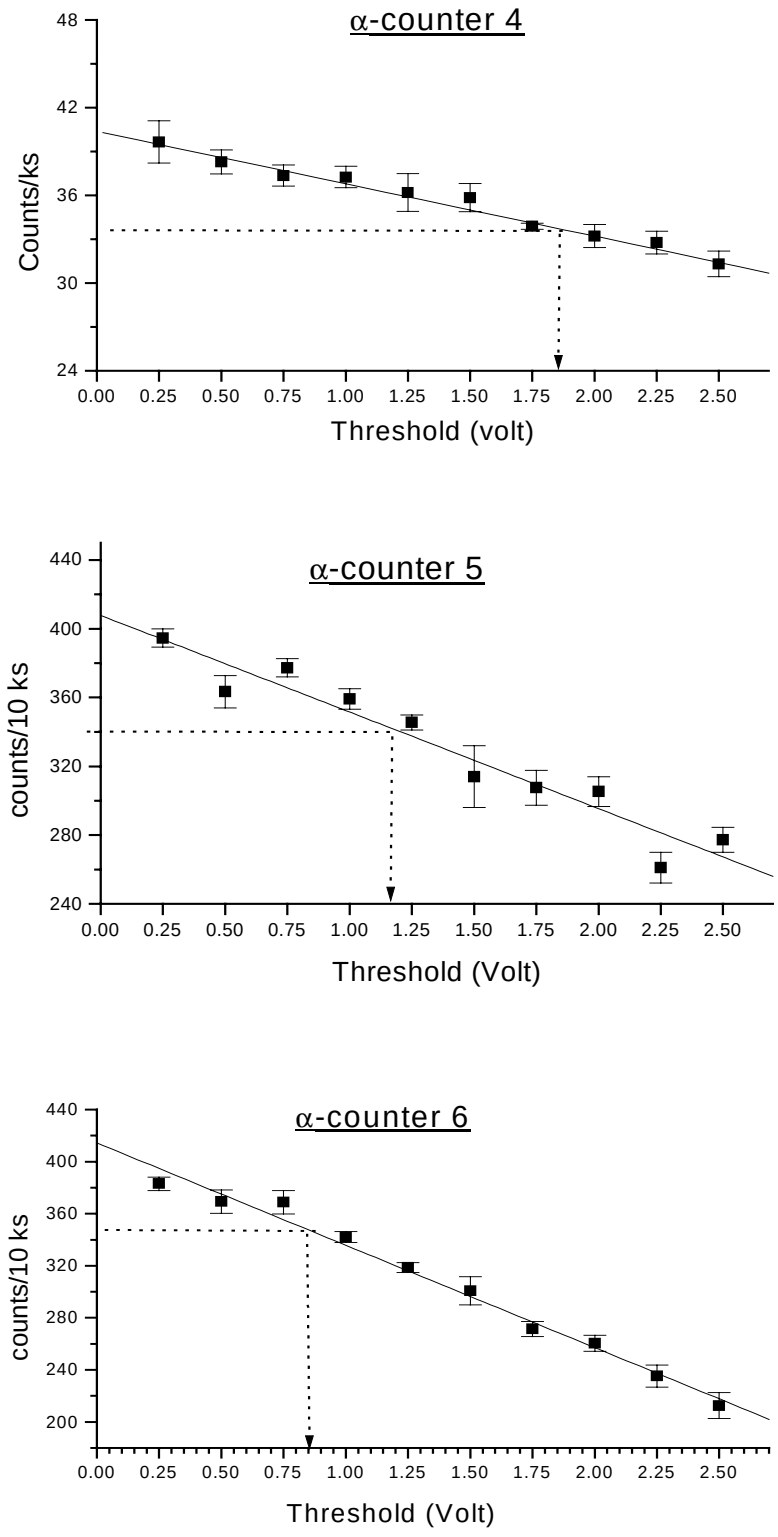

Fig. 4.5.5. Threshold voltage for alpha-counters 4-6.

4.5.3. Sample and background measurements

Thick source ZnS α-counting was performed for the 15 loess samples both in integral and pair mode to discriminate between U and Th. The dried sample was ground and homogenized (manually in a porcelain mortar), and finally sieved to get a particle size of less than 63 μm. The grinding was continued until all material passed through the sieve. In alpha counting, particle size reduction is performed in order to eliminate the phenomenon of "overcounting" [Aitken, 1985; Pernicka and Wagner, 1982; Wintle and Dijkmans, 1988; Zöller and Pernicka, 1989], which would lead to the observation that the ratio of the measured (directly via ZnS α-counting) to the predicted (from the U and Th concentration) α-activity is substantially higher than the unity. "Overcounting" is normally associated with two principal phenomena: i) the non-homogeneous distribution of U and Th with respect to grain size in the sample under investigation and ii) radioactive disequilibrium (whereby the daughters of U and Th in the decay series are in excess). The possible reasons to have "overcounting" due to sample inhomogeneity are: i) fine particles (possibly feldspars) may contain higher radioactivity than the coarse ones (possibly quartz, which is low in radioactivity) and these fines can preferentially be located directly on the ZnS screen in the holes between the larger particles; ii) the α-radioactivity is preferentially located in the surface layer of the large particles (this means with a diameter larger than the α-particle range) so that the effective radioactivity, as seen by the ZnS screen, is higher than the average. In addition, radon gas accumulation can occur in the free holes between the particles close to the scintillation screen [Murray, 1982; Pernicka and Wagner, 1982; Zöller and Pernicka, 1989].

As to the loess samples, counting times of 7 days were applied to get at least 5000 integral counts and 100 pair counts. In order to detect possible radon escape from the sample in the laboratory, each sample was counted twice, the first time immediately after sealing, the second time minimum 4 weeks later. The background was also counted for each counter for two weeks. The background count rates for all counters were found to be 1-2 counts.10 ks^{-1}.

4.5.4. Results of alpha-counting

As outlined above, by using the Littlemore Elsec 7286 low-level α-counting system, the experimentally obtained quantities are the integral count rate $\dot{\alpha}$, the slow-pair count rate $\dot{p}_{Th}$, the fast pair count rate $\dot{p}_{U}$, and the count rates due to Th series, $\dot{\alpha}_{Th}$, and the U series, $\dot{\alpha}_{U}$.

The integral count rates for 15 loess samples are shown in Table 4.5.2. The first count rate was recorded immediately after sealing and the second one at least 4 weeks later. Since no significant difference between both was observed, the mean of the two count rates was converted to the annual radiation doses.

Table 4.5.2. Comparison of alpha count rates.

Sample Number	First integral count rate (counts/10 ks) $\dot{\alpha}_{1st} \pm 2s$	Second integral count rate (counts/10 ks) $\dot{\alpha}_{2nd} \pm 2s$	Ratio of integral Count rate $(\dot{\alpha}_{2nd}/\dot{\alpha}_{1st}) \pm 2s$	Mean integral count rate (counts/10 ks) $\dot{\alpha} \pm 2s$
S.31	102.2±3.4	102.3±3.1	1.000±0.045	102.2±2.3
S.35	99.1±2.8	98.6±3.0	0.994±0.041	98.9±2.1
S.30	100.7±2.7	102.5±2.5	1.018±0.036	101.6±1.8
S.34	101.9±2.5	93.3±2.7	0.916±0.035	97.6±1.9
S.28	102.3±3.1	103.7±2.5	1.013±0.039	103.0±2.0
S.32	104.5±3.3	89.0±3.0	0.851±0.039	96.7±2.2
S.39	108.2±3.2	102.4±3.1	0.947±0.040	105.3±2.2
S.33	107.1±2.8	106.9±3.0	0.998±0.039	107.0±2.1
S.38	91.0±2.5	99.5±2.6	1.094±0.041	95.2±1.8
S.29	96.8±2.5	98.1±2.4	1.013±0.036	97.5±1.7
S.17	100.7±2.8	101.0±2.8	1.003±0.039	100.8±2.0
S.5	103.7±3.2	103.5±2.8	0.999±0.041	103.6±2.1
S.27	99.4±2.5	109.9±2.8	1.105±0.040	104.7±1.9
S.16	97.4±3.0	95.6±2.9	0.981±0.042	96.5±2.1
S.10	107.6±3.4	111.8±2.9	1.039±0.044	109.7±2.2

4.5.4.1. Annual radiation doses

The α-count rate $\dot{\alpha}$ (counts.ks^{-1}) measured via a 42 mm diam. ZnS screen with standard electronics settings (threshold fractions of 85% and 82% for the Th and U decay series, respectively), can be converted to the actual annual α-radiation dose (Gy/ka) by the relation:

$$\dot{D}_{\alpha} = 1.56 \times \dot{\alpha} \qquad (4.5.2)$$

This equation is valid for a sample containing an equal activity of the Th and U series (Th:U concentration ratio = 4:1).

In evaluating the effective annual α-dose $\dot{D}_{\alpha,eff}$ (Gy.ka^{-1}) from the α-count rate $\dot{\alpha}$ (counts.ks^{-1}) it is necessary to use the a-value system (referring to the α-effectiveness: α-radiation is less effective in inducing luminescence than β- and γ- radiation) [Aitken, 1985]:

$$\dot{D}_{\alpha,eff} = 1.28 \times a \times \dot{\alpha} \qquad (4.5.3)$$

The beta component of the annual radiation dose, $\dot{D}_{\beta}$, as derived from ZnS α-counting for a sample containing equal activities of the Th and U series is:

$$\dot{D}_{\beta} = 0.067 \times \dot{\alpha} \qquad (4.5.4)$$

In case that only the Th series is present in the sample, this equation will overestimate the beta annual dose by about 20% compared to the true value, whereas, for the other extreme (only the U series present) it will be underestimated by about 20%. The combined Th and U contribution to the gamma annual dose $\dot{D}_{\gamma}$ for the case of equal activities of the two series is:

$$\dot{D}_{\gamma} = 0.078 \times \dot{\alpha} \qquad (4.5.5)$$

The effect of the Th and U ratio is about the same as in the case of the beta annual dose but in the opposite way.

The measured integral count rates $\dot{\alpha}$ (counts/10 ks) were converted to the α-, β- and γ- annual radiation doses $\dot{D}_{\alpha,\mathrm{eff}}$ (a = 0.1 was taken from recent literature [Aitken, 1998]), $\dot{D}_{\beta(\mathrm{U,Th})}$ and $\dot{D}_{\gamma(\mathrm{U,Th})}$ by using Eqs (4.5.3) - (4.5.5), respectively, and the results are shown in Table 4.5.3. The quoted uncertainties refer only to the counting statistics.

Table 4.5.3. The α-, β- and γ- annual radiation doses measured via thick source α-counting.

Sample Number	Measured α dose-rate $\dot{D}_{\alpha,\mathrm{eff}}$ (Gy/ka) ± 2s	Measured β dose-rate $\dot{D}_{\beta(\mathrm{U,Th})}$ (Gy/ka) ± 2s	Measured γ dose-rate $\dot{D}_{\gamma(\mathrm{U,Th})}$ (Gy/ka) ± 2s
S.31	1.309±0.029	0.685±0.015	0.797±0.018
S.35	1.265±0.026	0.662±0.014	0.771±0.016
S.30	1.300±0.023	0.681±0.012	0.792±0.014
S.34	1.249±0.024	0.654±0.013	0.761±0.015
S.28	1.319±0.025	0.690±0.013	0.803±0.015
S.32	1.238±0.028	0.648±0.015	0.755±0.017
S.39	1.310±0.029	0.685±0.015	0.798±0.018
S.33	1.327±0.026	0.695±0.014	0.809±0.016
S.38	1.219±0.023	0.638±0.012	0.743±0.014
S.29	1.248±0.022	0.653±0.012	0.760±0.013
S.17	1.290±0.025	0.675±0.013	0.786±0.015
S.5	1.326±0.027	0.694±0.014	0.808±0.017
S.27	1.340±0.024	0.701±0.013	0.816±0.015
S.16	1.236±0.027	0.647±0.014	0.753±0.017
S.10	1.404±0.028	0.735±0.015	0.856±0.017

4.5.4.2. Concentrations of U and Th

With the Elsec/Littlemore system used, the count rate $\dot{\alpha}_{Th}$ associated with the Th series is obtained directly from the slow pairs using the following relation [Aitken, 1985]:

$$\dot{\alpha}_{Th} = 21.1 \times \left[\dot{p}_{Th} - \frac{\dot{\alpha}^2 (\text{counts / unit of time})^2 \times C_t (\text{time})}{\text{period time}} \right] \tag{4.5.6}$$

where $\dot{p}_{th}$ is the slow pair count rate, C_t is the coincidence time (= 0.38 s) and the period time used for the present work was 10 ks.

The count rate $\dot{\alpha}_U$ associated with the U series is given by:

$$\dot{\alpha}_U = \dot{\alpha} - \dot{\alpha}_{Th} \tag{4.5.7}$$

The concentrations of Th and U, the results of which are shown in Table 4.5.4, were determined using the following relations [Aitken, 1998]:

$$[\text{conc.}(\text{mg.kg}^{-1})]_{Th} = \frac{\dot{\alpha}_{Th} (\text{counts / ks})}{0.513} \tag{4.5.8}$$

$$[\text{conc.}(\text{mg.kg}^{-1})]_{U} = \frac{\dot{\alpha}_{U} (\text{counts / ks})}{1.78} \tag{4.5.9}$$

where the calculation of the U-concentration includes the contribution from both ^{235}U and ^{238}U to the overall U-activity.

Here too, the "first count rate" was recorded immediately after sealing and the "second count rate" at least 4 weeks later, and again no significant difference between both was observed.

Table 4.5.4. Concentrations of Th and U via thick source ZnS alpha counting in the pair mode.

Sample number	First count rate due to Th series (Counts/10 ks) $\dot{\alpha}_{Th,1st}$ ± 1s	Second count rate due to Th series (Counts/10 ks) $\dot{\alpha}_{Th,2nd}$ ± 1s	Mean count rate due to Th series (Counts/10 ks) $\dot{\alpha}_{Th}$ ± 1s	Th conc. $mg.kg^{-1}$ dry weight ± 1s
S.31	58.3 ± 5.0	47.3 ± 4.9	52.8 ± 3.5	10.29 ± 0.69
S.35	52.3 ± 4.9	50.8 ± 4.9	51.5 ± 3.5	10.05 ± 0.68
S.30	56.2 ± 5.0	56.3 ± 5.1	56.3 ± 3.6	10.96 ± 0.70
S.34	44.5 ± 3.8	47.0 ± 4.3	45.7 ± 2.7	8.91 ± 0.56
S.28	53.1 ± 5.0	57.5 ± 5.2	55.3 ± 3.6	10.78 ± 0.70
S.32	51.6 ± 4.9	54.3 ± 5.4	52.9 ± 3.7	10.32 ± 0.71
S.39	54.8 ± 4.4	48.9 ± 5.3	51.8 ± 3.5	10.10 ± 0.68
S.33	65.7 ± 5.5	57.4 ± 5.2	61.6 ± 3.8	12.01 ± 0.74
S.38	55.3 ± 4.8	46.2 ± 4.7	50.8 ± 3.4	9.90 ± 0.66
S.29	48.0 ± 4.2	48.6 ± 4.0	48.3 ± 2.9	9.42 ± 0.57
S.17	54.3 ± 5.1	49.1 ± 4.8	51.7 ± 3.5	10.08 ± 0.68
S.5	62.5 ± 5.2	42.4 ± 4.6	52.4 ± 3.6	10.22 ± 0.70
S.27	51.2 ± 5.3	48.6 ± 4.3	49.9 ± 3.4	9.72 ± 0.67
S.16	50.5 ± 4.8	54.5 ± 5.0	52.5 ± 3.5	10.24 ± 0.68
S.10	55.1 ± 5.1	62.1 ± 5.4	58.6 ± 3.7	11.42 ± 0.72

Sample number	First count rate due to U series (Counts/10 ks) $\dot{\alpha}_{U,1st}$ ± 1s	Second count rate due to U series (Counts/10 ks) $\dot{\alpha}_{U,2nd}$ ± 1s	Mean count rate due to U series (Counts/10 ks) $\dot{\alpha}_{U}$ ± 1s	U conc. $Mg.kg^{-1}$ dry weight ± 1s
S.31	43.9 ± 4.9	55.0 ± 4.9	49.5 ± 3.6	2.78 ± 0.20
S.35	46.3 ± 5.0	48.4 ± 4.9	47.3 ± 3.5	2.66 ± 0.20
S.30	44.00 ± 5.0	46.2 ± 5.2	45.1 ± 3.6	2.53 ± 0.20
S.34	57.4 ± 4.1	46.3 ± 4.0	51.9 ± 2.9	2.91 ± 0.16
S.28	49.2 ± 5.0	46.2 ± 5.2	47.7 ± 3.6	2.68 ± 0.20
S.32	53.0 ± 5.0	47.8 ± 5.4	50.4 ± 3.7	2.83 ± 0.21
S.39	47.6 ± 4.5	59.4 ± 5.5	53.5 ± 3.5	3.01 ± 0.20
S.33	41.4 ± 5.5	49.5 ± 5.1	45.4 ± 3.8	2.55 ± 0.21
S.38	44.2 ± 4.8	44.2 ± 4.8	44.2 ± 3.4	2.48 ± 0.19
S.29	49.6 ± 4.1	48.8 ± 4.2	49.2 ± 2.9	2.76 ± 0.16
S.17	46.4 ± 5.1	51.9 ± 4.8	49.1 ± 3.5	2.76 ± 0.20
S.5	41.2 ± 5.3	61.1 ± 4.8	51.1 ± 3.8	2.87 ± 0.22
S.27	48.2 ± 5.4	61.3 ± 4.4	54.8 ± 3.7	3.08 ± 0.20
S.16	46.9 ± 4.8	41.1 ± 5.0	44.0 ± 3.5	2.47 ± 0.20
S.10	52.5 ± 5.1	49.3 ± 5.4	50.9 ± 3.7	2.86 ± 0.21

4.6. Beta-counting

4.6.1. Risø low-level beta GM-25-5 multicounter system

Use was made of the Risø low-level beta GM-25-5 multicounter system, shown in Fig. 4.6.1 [Bøtter-Jensen and Mejdahl, 1985, 1988]. It is a gas-flow counter unit containing five GM sample counter elements (provided with a window of <1 mg.cm^{-2} density and a diameter of 25 mm) and a common guard counter gated in anticoincidence mode to reduce the cosmic-ray background. The counters are gas-flow types operating with 99% Ar/1% isobutane. For counting, about 2 gram finely powdered material is placed in the plastic sample holder of 21 mm inner diameter and is then covered first with thin Al foil (15 μm thickness) and then with mylar foil (6 μm thickness) for mechanical stability. For the beta-energies to be measured, this sample geometry behaves as "infinitely thick" [[Bøtter-Jensen and Mejdahl, 1988]. A sample slide allows to insert five samples into the multicounter and to measure them simultaneously. A lift mechanism minimizes the sample-window separation so as to obtain maximum detection efficiency. The whole counting system is positioned inside a lead shielding of 100 mm thickness. A bubble chamber at the gas outlet controls a stable gas flow through the counter elements. The incident beta particles are converted by the GM counters to electronic pulses, which are further processed in an electronic module incorporating a high voltage supply and multiple counting channels each with pre-amplifier, anticoincidence gate, scaler and microprocessor-controlled printer interface.

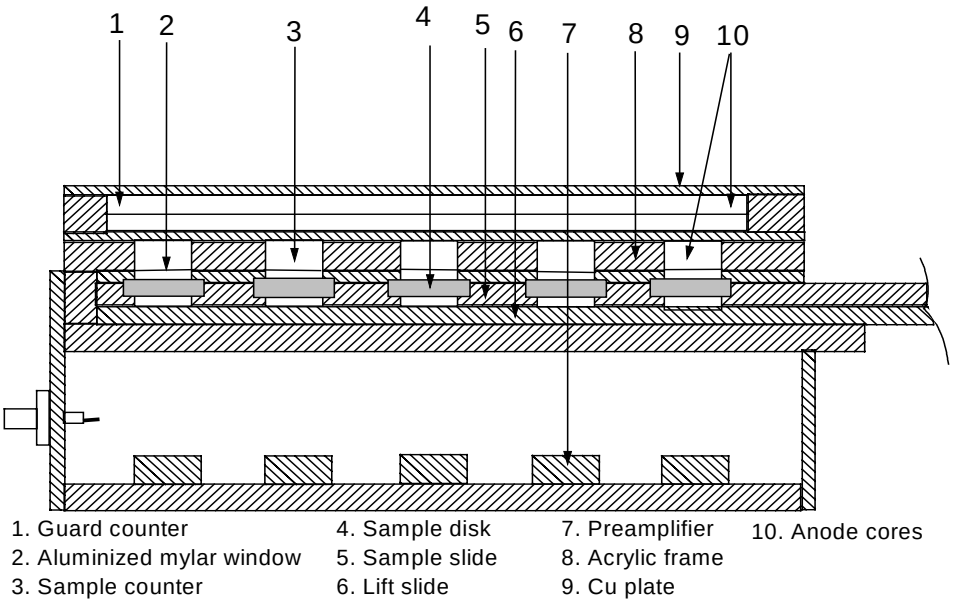

Fig. 4.6.1. Risø low-level beta GM-25-5 counter unit, based on Bøtter-Jensen and Mejdahl [1988].

4.6.2. Calibration of the beta GM-25-5 multicounter system

Calibration was done with a number of K, Th and U standards, from which 5 sub samples of ~ 2 g each were measured for 24 hours in each of the 5 counting positions to minimize the variability of the counters. For U, use was made of RGU-1 [IAEA, 1987] and CRM 105-A [NBL, 1981a], with U-contents of 400 ± 2 $mg.kg^{-1}$ and 10.23 ± 0.23 $mg.kg^{-1}$, respectively. For Th, use was made of RGTh-1 [IAEA, 1987] and CRM 109-A [NBL, 1981b], with Th-contents of 800 ± 16 $mg.kg^{-1}$ and 105.26 ± 0.98 $mg.kg^{-1}$, respectively. The uncertainties quoted with the certified concentrations for all the standards mentioned above are based on 1s. For K, use was made of a series of K standards prepared by adding potassium biphtalate ($C_8H_5KO_4$) to SiO_2 (Aldrich; average particle size 5-25 μm), so as to obtain K-contents of 0.25, 0.50, 1.00, 2.00, 3.00, and 5.00 %. Homogenization of these mixtures was done for 48 hours each in a turbulent mixer (Turbula Type T2A, W.A. Bachofen). In order to check the homogeneity, 6 aliquots of 1 gram of the 0.25% K home-made standard were

analysed via k_0-NAA, the results of which are shown in Table 4.6.1. The background, in the case of the K-dilutions, was measured with the SiO_2, which was used to prepare these home-made standards.

Table 4.6.1. Homogeneity checked for K concentration in home-made standard via k_0-NAA.

# Aliquot	K concentrations (%) ± 2s
1	0.245 ± 0.003
2	0.249 ± 0.003
3	0.248 ± 0.003
4	0.256 ± 0.003
5	0.251 ± 0.003
6	0.256 ± 0.004
Mean	0.251 ± 0.004

The beta dose rates $\dot{D}_\beta$ (Gy.ka^{-1}) for the standards, as shown in Table 4.6.2, were calculated from the concentrations of the U, Th and K using the following relation [Aitken, 1998]:

$$\left[\dot{D}_\beta\,(\mathrm{Gy.ka^{-1}})\right]_{\text{predicted}} = 0.0273\times[\mathrm{conc.(mg.kg^{-1})}]_{\mathrm{Th}} + 0.145\times[\mathrm{conc.(mg.kg^{-1})}]_{\mathrm{U}} + 0.782\times[\mathrm{conc.(\%)}]_{\mathrm{K}} \qquad (4.6.1)$$

The calibration factors (cpm/Gy.ka^{-1}) were then obtained by calculating the count rate per unit dose rate. Ideally, the calibration factors should be the same for all standards. As seen in Table 4.6.2, the average results for U (2.936 ± 0.097 cpm/Gy.ka^{-1}) and K (3.223 ± 0.046cpm/Gy.ka^{-1}) are about 4.7 % lower and higher, respectively, than the one for Th (3.072 ± 0.103 cpm/Gy.ka^{-1}), although the differences are hardly significant. On the other hand, the calibration factors do not depend on the concentration. The final calibration factor was obtained by taking the average of the

values obtained for the U, Th and K standards and amounted to 3.077 ± 0.083 cpm/Gy.ka^{-1}. The uncertainty with the final "overall" calibration factor quoted (2s) corresponds to the largest of the internal or external uncertainty.

Table 4.6.2. Calibration factors (cpm/Gy.ka^{-1}) for standards of Th, U and K measured with the GM-25-5 multi counter system. The conversion factors (concentration → beta dose rate) are taken from recent literature [Aitken, 1998].

Standard	Concentration [U, Th = mg.kg^{-1} and K = %] ± 1s	Calculated beta dose-rate $\dot{D}_\beta$, in Gy.ka^{-1} ± 2s	Counts per minute cpm ± 2s	Cpm/Gy.ka^{-1} ± 2s
RGTh-1 (Th standard)	Th = 800 ± 16 U = 6.3 ± 0.4 K = 0.02 ± 0.01	22.77 ± 0.88	71.12 ± 1.34	3.12 ± 0.13
CRM109A (Th standard)	Th = 105.2_6 ± 0.98 U = 4.18	3.480 ± 0.065	10.51 ± 0.18	3.020 ± 0.077
Average calibration factor for Th ± 2s = 3.072 ± 0.103				
RGU-1 (U standard)	U = 400 ± 2	58.00 ± 0.58	170.8 ± 3.3	2.945 ± 0.064
CRM105A (U standard)	U = 10.2_3 ± 0.2_3	1.483 ± 0.067	4.34 ± 0.19	2.93 ± 0.18
average calibration factor for U ± 2s = 2.936 ± 0.097				
Home-made mixtures of SiO_2+ $C_8H_5KO_4$ (K-standards)	K = 0.25 K = 0.50 K = 1.00 K = 2.00 K = 3.00 K = 5.00	0.196 0.391 0.782 1.564 2.346 3.910	0.611 ± 0.015 1.263 ± 0.034 2.525 ± 0.049 5.008 ± 0.095 7.67 ± 0.13 12.83 ± 0.21	3.125 ± 0.077 3.230 ± 0.086 3.229 ± 0.062 3.202 ± 0.061 3.270 ± 0.054 3.281 ± 0.054
average calibration factor for K ± 2s = 3.223 ± 0.046				
Final "overall" calibration factor (average of Th, U and K) ± 2s = 3.077 ± 0.083				

4.6.3. Sample measurements

Five sub samples of about 2g finely powdered (particle size <63 μm) dry material of each the 15 loess samples were counted for 24 hours in each of the five counting positions i.e. a total of five days were needed for counting each sample. In order to re-establish the equilibrium after possible radon escape in the laboratory, the sample was counted minimum 4 weeks after preparing the disc. For the measurement of the background, five sub samples of ultra pure quartz [MERCK A.G., 7536] were prepared in the same way as the sample discs. They were counted for 48 hours in each of the five counting positions. The mean background count-rate was found to be [0.153 ± 0.008 (2s)] cpm (counts per minute). The detailed calculation of the mean beta count rate is shown in Appendix B.

4.6.4. Determination of the annual radiation doses by beta counting

The mean beta count rates $\dot{\beta}$ (cpm) for the 15 loess samples were converted to the beta annual radiation doses $\dot{D}_\beta$ using the following relation:

$$\left[\dot{D}_\beta(\mathrm{Gy.ka^{-1}})\right]_{\mathrm{measured}} = \frac{\dot{\beta}(\mathrm{cpm})}{\mathrm{CF(cpm/Gy.ka^{-1})}} \qquad (4.6.2)$$

where CF is the overall calibration factor of 3.077 determined using different U, Th and K standards (Table 4.6.2). The results are shown in Table 4.6.3.

Table 4.6.3. Beta count rate and beta dose rate determined by the Risø low-level beta GM-25-5 multicounter system.

Sample Number	Net beta count rate $\dot{\beta} \pm 2s$ (cpm)	Calibration factor $CF \pm 2s$ (cpm/Gy.ka^{-1})	Beta dose rate $\dot{D}_\beta \pm 2s$ (Gy.ka^{-1})
S.31	6.62±0.14	3.077±0.083	2.150±0.046
S.35	6.82±0.15		2.217±0.047
S.30	6.89±0.19		2.239±0.062
S.34	6.80±0.15		2.209±0.049
S.28	6.57±0.16		2.134±0.052
S.32	6.72±0.16		2.182±0.052
S.39	6.73±0.15		2.188±0.047
S.33	6.61±0.15		2.147±0.048
S.38	6.75±0.16		2.195±0.051
S.29	6.62±0.16		2.150±0.053
S.17	6.33±0.14		2.057±0.045
S.5	6.59±0.15		2.141±0.048
S.27	6.74±0.40		2.191±0.129
S.16	6.59±0.16		2.140±0.053
S.10	6.41±0.14		2.083±0.045

4.7. Neutron activation analysis (NAA)

4.7.1. Principle

Reactor neutron activation analysis (NAA) is a nearly matrix-independent, multi-elemental determination method. The procedure is based on irradiation of the sample with reactor neutrons, to produce unstable radioactive nuclides, mostly via (n,γ) reaction. Many of these nuclides emit, in their decay, gamma-rays with characteristic energies, which can be measured by performing gamma-ray spectrometry on the irradiated sample. The rate at which the gamma-rays are emitted from an element in the sample is directly proportional to its concentration. NAA is suitable to determine elemental concentrations in complex matrices via various standardization approaches, namely relative standardization, single-comparator standardization, absolute standardization and k_0-standardization. The merits and demerits of each approach are briefly discussed by De Corte [2001]. The k_0-method combines the advantages of the other standardizations, while eliminating most of their disadvantages. Important aspects are that it is versatile for multi-element analysis (just as the single-comparator and the absolute method) and that it has nearly the same accuracy as attained by the relative standardization [De Corte, 1987a].

The analysis technique used in the present work was k_0-standardized instrumental neutron activation analysis (k_0-INAA), solely based on long irradiation of bare (i.e. not Cd-covered) samples together with IRMM-530 Al-0.1%Au alloyed foils (serving as neutron flux monitors) [Ingelbrecht et al., 1991]. Counting of the irradiated samples is done with a conventional Ge detector (i.e. not suitable for efficient measurement of low-energetic photons).

4.7.2. Basic equation of the NAA k_0-standardization

When using the k_0-method for standardization in neutron activation analysis, the concentration of an element in a sample is obtained as:

$$\rho_a(mg.kg^{-1}) = \frac{\left(\frac{N_p / t_m}{SDCW}\right)_a}{\left(\frac{N_p / t_m}{SDCW}\right)_m} . \frac{1}{k_{0,m}(a)} . \frac{G_{th,m}.f + G_{e,m}.Q_{0,m}(\alpha)}{G_{th,a}.f + G_{e,a}.Q_{0,a}(\alpha)} . \frac{\varepsilon_{p,m}}{\varepsilon_{p,a}} .10^6 \qquad (4.7.1.)$$

where

ρ_a - concentration of analyte a (in $mg.kg^{-1}$);

N_p - measured net peak area, corrected for pulse losses [dead time, random coincidence (pulse pile-up), true coincidence (cascade summing)];

t_m - counting time;

S - saturation factor; = $1-\exp(-\lambda t_{irr})$;

$\lambda = (\ln 2)/T½$;

T½ - half-life;

t_{irr} – irradiation time;

D - decay factor = $\exp(-\lambda t_d)$;

t_d – decay time (from end of irradiation to start of counting);

C - counting factor; = $[1-\exp(-\lambda t_m)]/\lambda t_m$ (correcting for decay during counting);

W_m - mass of the comparator (in g);

W_a - mass of the sample (in g);

$k_{0,m}(a)$ - k_0 factor of analyte a versus monitor m, theoretically defined as:

$$k_{0,m}(a) = \frac{M_m \theta_a \sigma_{0,a} \gamma_a}{M_a \theta_m \sigma_{0,m} \gamma_m}, \text{ with}$$

M - molar mass;

θ - isotopic abundance;

γ - absolute gamma intensity;

σ_0 - (n,γ) cross-section at 2200 $m.s^{-1}$;

(note that k_0-factors contain only well-defined invariable nuclear constants and are not related to the experimental conditions of irradiation and counting);

G_{th} - correction factor for thermal neutron self shielding;

G_e - correction factor for epithermal neutron self shielding;

f - ϕ_{th}/ϕ_e, the thermal (subcadmium) to epithermal neutron flux ratio;

$Q_0(\alpha)$ - $\{(Q_0 - 0.429)\,\overline{E}_r^{-\alpha} + 0.429/[(0.55)^{\alpha}(2\alpha+1)]\}\ (1eV)^{\alpha}$, where

$Q_0 = I_0/\sigma_0$, with I_0 – resonance integral, defined as:

$$I_0 = \int_{0.55eV}^{\infty} \sigma(E)\frac{dE}{E}$$

$\overline{E}_r$ - effective resonance energy in eV;

α - measure for the deviation of the epithermal neutron flux distribution from the 1/E shape, approximately by a $1/E^{1+\alpha}$ dependence;

ε_p - full-energy peak detection efficiency.

If the coirradiated monitor in Eq. 4.7.1 is different from the ultimate gold comparator [$^{197}Au(n,\gamma)^{198}Au$; 411.8 keV], the factor $k_{0,m}(a)$ has to be replaced by:

$$k_{0,m}(a) = \frac{k_{0,Au}(a)}{k_{0,Au}(m)} \qquad (4.7.2)$$

where the $k_{0,Au}$-factors were experimentally measured with great accuracy for all the analytically interesting radionuclides/gamma-lines and are tabulated in the literature [De Corte and Simonits, 1989; De Corte et al., 1989; De Corte et al., 1993; Van Lierde et al., 1999; De Corte and Van Lierde, 2000].

In the practice of the Kayzero software (see Section 4.7.4.4), a comparator factor is defined as

$$F_{c,Au} = \frac{\left(\frac{N_p / t_m}{SDCW}\right)_m}{k_{0,Au}(m)[G_{th,m}.f + G_{e,m}.Q_{0,m}(\alpha)] \,.\, \varepsilon_{p,m}} \,.\, 10^{-6} \qquad (4.7.3.)$$

which simplifies Eq.(4.7.1) to

$$\rho_a(\mu g.g^{-1}) = \frac{\left(\frac{N_p / t_m}{SDCW}\right)_a}{F_{c,Au} \,.\, k_{0,Au}(a)[G_{th,a}.f + G_{e,a}.Q_{0,a}(\alpha)] \,.\, \varepsilon_{p,a}} \qquad (4.7.4.)$$

The theoretical value of the comparator factor is:

$$F_{c,Au} = \frac{N_A.\theta_{Au}.\gamma_{Au}.\sigma_{0,Au}}{M_{Au}}.\phi_e.10^{-6} \cong \frac{\phi_{th}/f}{3.47\times10^6} \qquad (4.7.5)$$

where N_A is Avogadro's number. Thus, comparison of the $F_{c,Au}$-factor estimated from the knowledge of ϕ_{th} and f (Eq. 4.7.5) with the one experimentally obtained in the actual analysis (Eq. 4.7.4), allows to control the accuracy of the latter.

The implementation of the k_0-standardization in NAA is subtle and requires the accurate knowledge of some irradiation and counting parameters [De Corte, 1987a]: on the one hand, of the thermal-to-epithermal neutron flux ratio (f) and the shape of the epithermal neutron flux distribution (α); on the other hand, of the peak detection efficiency and the correction factor for true-coincidence effects – requiring, in their turn, knowledge of a number of characteristics related to the geometry and composition of the sample and the detector.

4.7.3. Accuracy of k_0-NAA

The accuracy of the k_0-standardization in NAA was formerly evaluated [De Corte et al., 1987] and experimentally determined [De Corte et al., 1984] and it was found that the contribution to the overall uncertainty on the analysis result is less than 5%.

Also, the traceability of k_0-NAA was examined in detail [De Corte, 1987b] and it was significantly enhanced by the introduction of the IRMM-530 Al-0.1%Au certified reference material [Ingelbrecht et al., 1991]

In fact, the above considerations form the basis of the recently formulated statement [Robouch et al., 2001] that k_0-NAA is a valuable tool for reference-material producers.

Let it suffice here to give one example demonstrating the reliability of k_0-NAA. It concerns the formerly reported analysis of NIST SRM 1633a Coal Fly Ash, as performed via k_0-NAA at the Institute for Nuclear Sciences (INW), Gent and the Central Research Institute for Physics (KFKI), Budapest, in diversified experimental conditions [De Corte et al., 1984]. Fig. 4.7.1 shows the results obtained for K, Rb, Th and U expressed as the ratio of the average INW-KFKI value versus the NIST certified value. As seen, k_0-NAA indeed offers a potential accuracy of better than 5%. A more detailed discussion on the advantages and limitations of k_0-NAA (also compared to relative NAA) can be found in a recent survey paper [De Corte, 2001] and references therein.

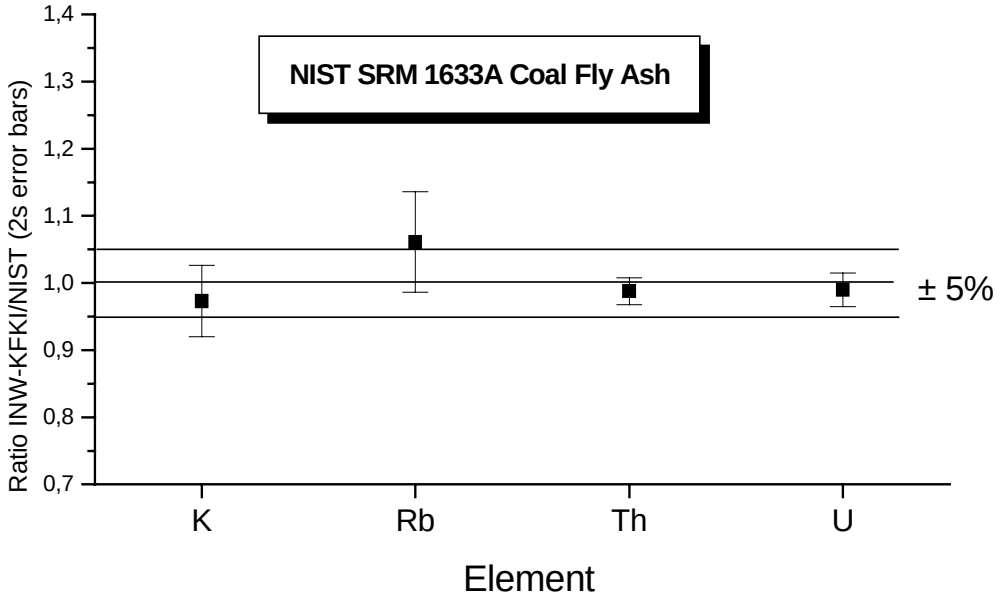

Fig.4.7.1. Concentration of K, Rb, Th and U in NIST SRM 1633A Coal Fly Ash determined independently at INW and KFKI via k_0-INAA and compared with NIST certified values.

4.7.4. Experimental procedure

4.7.4.1. Sample preparation

One of the features of k_0-INAA is the simplicity of sample preparation. As mentioned in Section 4.4.1, the loess samples were dried at 110°C until constant weight for k_0-INAA, alpha counting, beta counting and AAS. Whereas for alpha and beta counting the samples had to be ground and sieved to get a particle size less than 63 micrometer, and for AAS the samples had to be digested with $HClO_4$/HF (see Section 4.8), for k_0-INAA simply about 500 mg of dried sample was packed for irradiation in an ultra-clean polyethylene vial. For each sample three sub-samples were prepared. As shown in Fig. 4.7.2, each of the sub-samples was sandwiched between two Al-Au monitors, and by averaging the thus obtained comparator factors (see Section 4.7.2), the effect of neutron flux gradients was eliminated. The monitors were IRMM-530 Al - 0.1%Au

alloyed foils of 0.1 mm thickness, with a certified gold content of 0.100 ± 0.002% [Ingelbrecht et al., 1991].

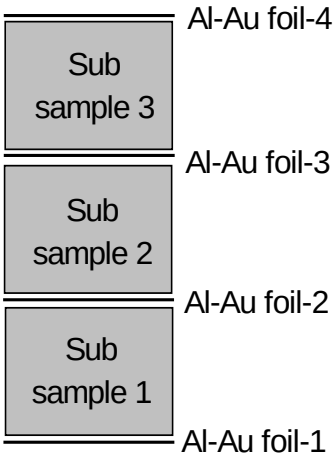

Fig. 4.7.2. Preparation of the loess samples for irradiation.

4.7.4.2. Irradiation

Irradiation was performed during 7 hours in channel 3 of reactor Thetis (Gent), with a nominal thermal neutron flux of 1.2×10^{12} $cm^{-2}.s^{-1}$. The relevant neutron spectrum characteristics for use in the k_0-method, determined by De Corte et al. [1987, 1994a] and De Wispelaere and De Corte [2001], were f = 24.3 and α = -0.0045.

4.7.4.3. Gamma-ray spectrometry

After irradiation, the samples were transferred to clean polyethylene vials and then measured three times with Ge detector "Amanda" (the schematic presentation and the characteristics of which are shown in Fig. 4.7.3. and Table 4.7.1.), equipped with an ND599 LFC (loss-free counting) module for dead-time correction: 1) after a decay time of ~ 65 hours, with a measuring time = 30 min and a source-detector separation of about 14 cm, for the determination of K [^{42}K (T½ = 12.36 h): 1524.6 keV]; 2) after

a decay time of ~ 5 days, with a measuring time = 1.5 h on top of the detector, for the determination of U [^{239}U (T½ = 23.45 min)→^{239}Np(T½ = 2.36 d): 228.2 keV and 277.6 keV]; 3) after a decay time of ~ 3 weeks, with a measuring time = 1 h on top of the detector, for the determination of Th [^{232}Th(T½ = 22.3 min)→^{233}Pa(T½ = 27.0 d): 300.3 keV and 312.2 keV]. Also Rb was detected (in the third measurement) [^{86}Rb(T½ = 18.6 d): 1077.0 keV]. It is to be considered as a distinct advantage of k_0-standardized INAA that also this element could thus be quantified, based on the k_0-factor existing in the nuclear data library (just as this can be done "automatically" for all detected elements, whereas for all others detection limits can be calculated). The co-irradiated gold monitors were also measured [^{198}Au 411.8 keV (T½ = 2.695 d)] at the same counting positions as the samples. Data acquisition was performed via the software Accuspec. An example of the spectra obtained for 7 h irradiated loess material from the first, second and third measurements, are shown in Figs 4.7.4. – 4.7.6. The analyses were done in triplicate. Spectrum analysis was performed with the software package Hypermet-PC [Fazekas et al., 1997].

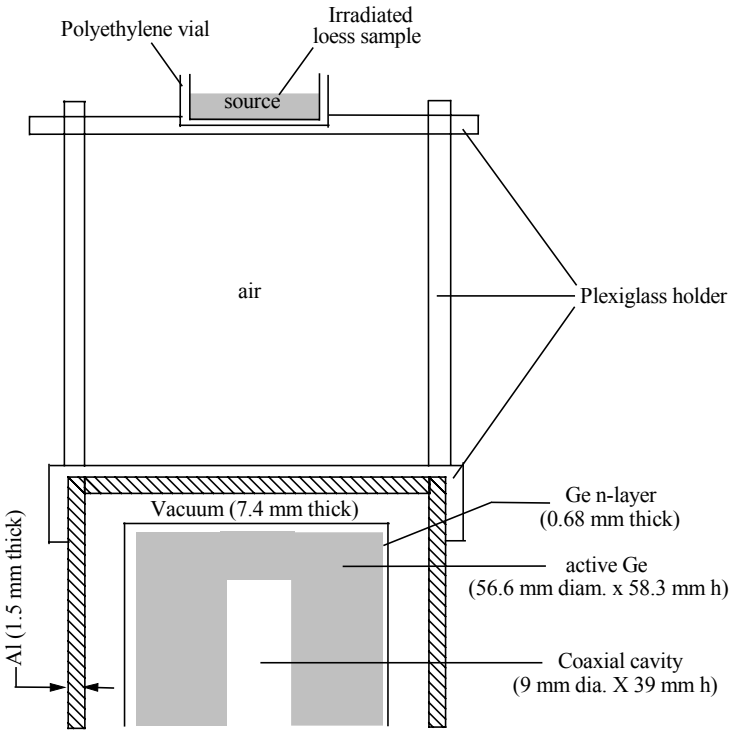

Fig. 4.7.3. Schematic representation of Ge detector "Amanda".

Table 4.7.1. Characteristics of Ge detector "Amanda'.

Detector type	P-type Hyperpure Ge with coaxial cavity
Supplier	Canberra
Active volume	156 cm^3
Entrance window	1.5 mm Al
Resolution (FWHM)	
At 1332.5 keV	1.77 keV
Relative efficiency at 1332.5 keV	38.2 %

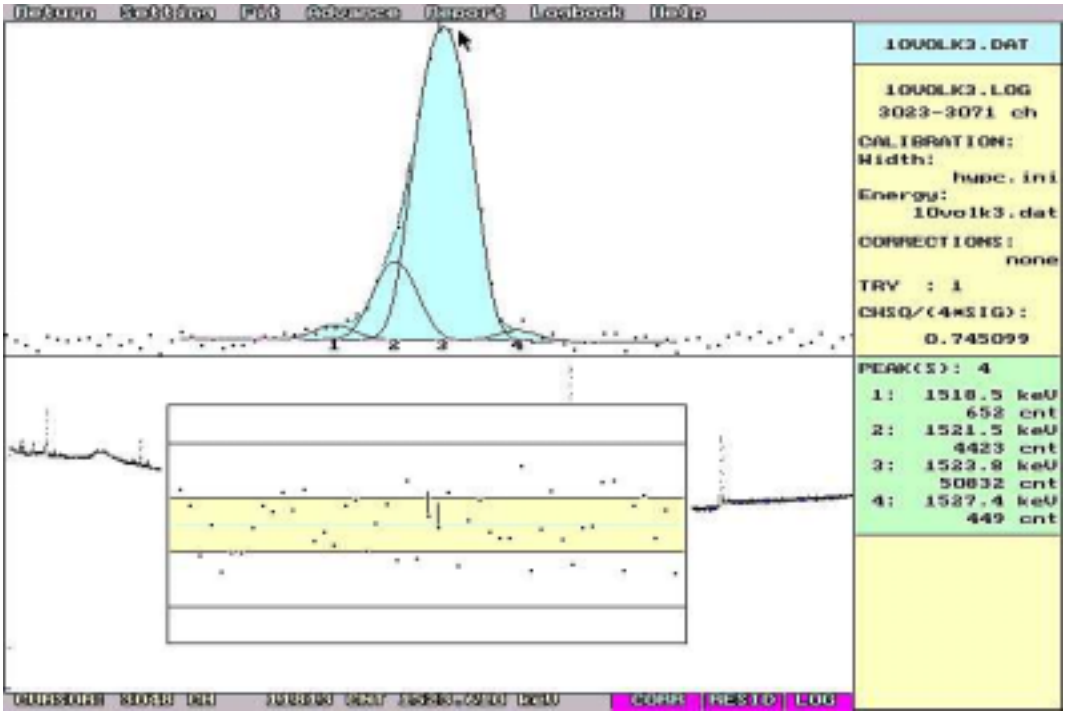

Fig. 4.7.4. Volkegem loess gamma-ray spectrum (excerpt) for the determination of K [^{42}K: 1524.6 keV]. See text for irradiation and counting details. Spectrum analysis was performed with the software package Hypermet-PC.

Fig. 4.7.4 shows the spectrum analysis performed with the software package Hypermet PC for the determination of K in the loess sample. The right column is representing the peak parameters. Sometimes the program is unable to fit the peak properly in automatic mode and in that case the normalized chi-square of the fit (CHSQ/4*SIG) becomes larger than unity. This can happen due to peak broadening. In that case a new try is justified to improve the fit until the normalized chi-square of the fit becomes smaller than unity. The peaks 1 - 4 were summed for the analysis of K

because the peak is divided into several parts when trying to improve its normalized chi-square value [CHSQ/(4*SIG) = 0.745099] and there is no interfering gamma line close to the gamma line of ^{42}K at 1524.6 keV.

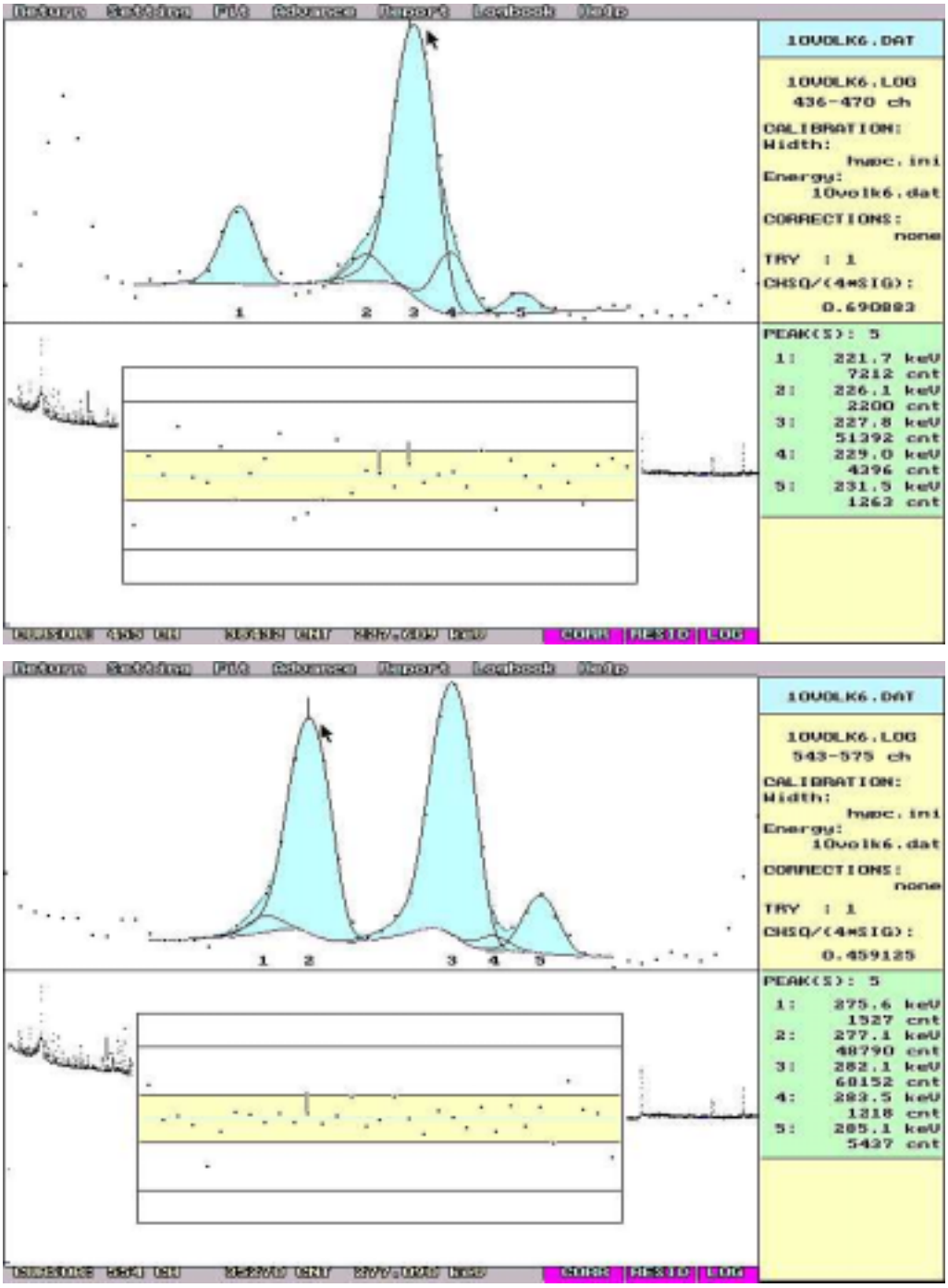

Fig. 4.7.5. Volkegem loess gamma-ray spectrum (excerpts) for the determination of U [^{239}Np: 228.2 keV and 277.6 keV]. See text for irradiation and counting details. Spectrum analysis was performed with the software package Hypermet-PC.

The top and bottom parts of Fig. 4.7.5 represent the fitted spectrum for the determination of U via 226.4+228.2 and 277.6 keV gamma-lines, respectively. From the top spectrum the peaks 2, 3 and 4 were summed for the 226.4+228.2 keV gamma line, which is interfered by ^{182}Ta and ^{132}Te (see details in Section 4.7.4.4). In the bottom spectrum the peaks 1 and 2 were summed for the 277.6 keV gamma line.

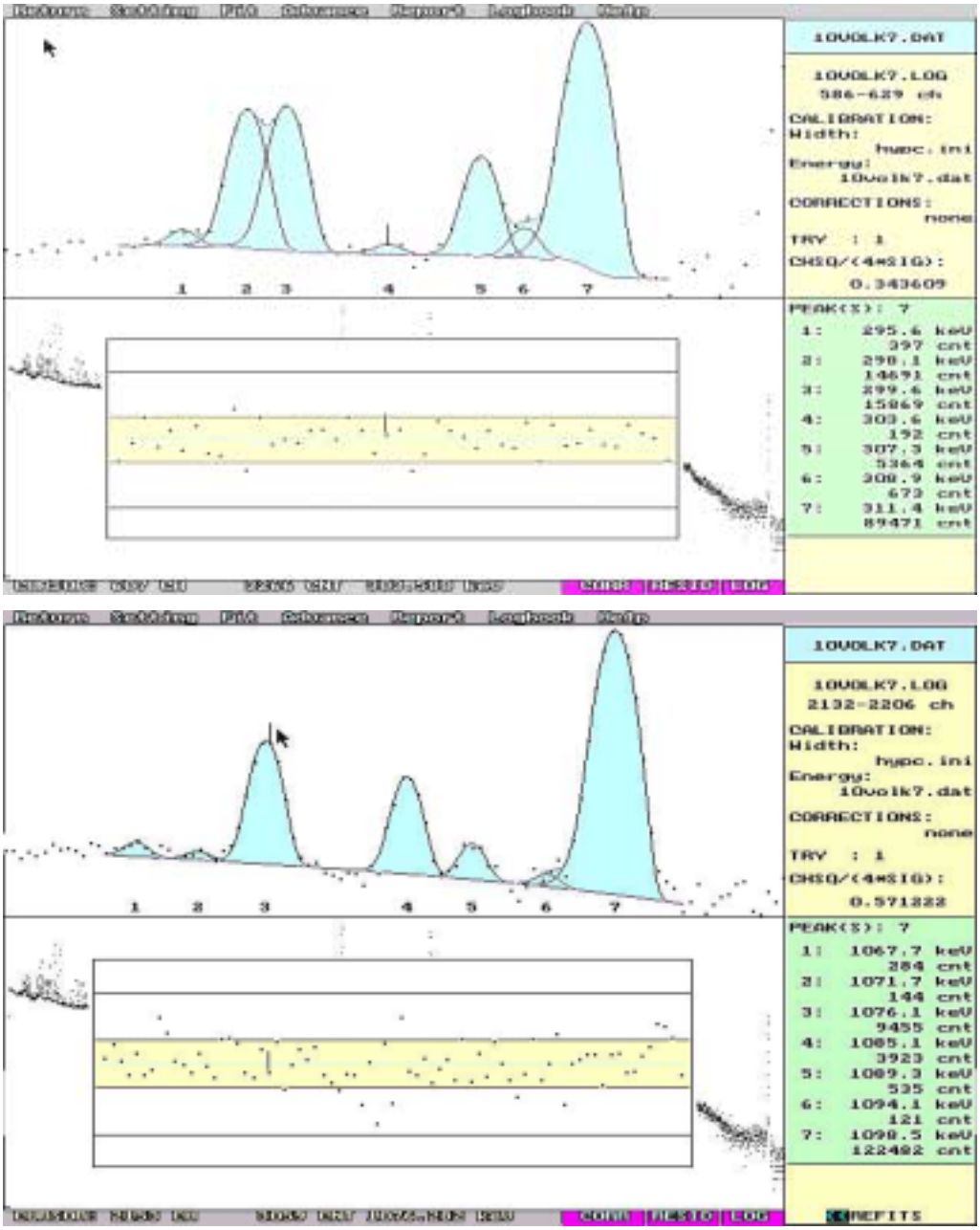

Fig. 4.7.6. Volkegem loess gamma-ray spectrum (excerpts) for the determination of Th [^{233}Pa: 300.3 keV and 312.2 keV] and Rb [^{86}Rb: 1077.0 keV]. See text for irradiation and counting details. Spectrum analysis was performed with the software package Hypermet-PC.

The top spectrum of Fig. 4.7.6 is for the determination of Th in which the peak 3 is belonging to the 300.3 keV gamma line and the peak 7 to the 312.2 keV gamma line. The peak of ^{233}Pa at 300.3 keV is in a doublet with the 298.6 keV ^{160}Tb line (T½ = 72.3 d). The deconvolution of this doublet was possible using Hypermet PC. The bottom spectrum is for the determination of Rb where the peak 3 is the1077.0 keV line of ^{86}Rb.

4.7.4.4. Concentration calculation: Kayzero/Solcoi software

For the calculations, use was made of the Kayzero/Solcoi software package Version 4 [1996]. The Solcoi subroutine computes the peak detection efficiencies (via the calculation of the effective solid angles) and the true-coincidence correction factors. These, together with the irradiation and counting parameters, have to be given as input for Kayzero, from which the K, U, Th and Rb elemental concentrations were then obtained. The relevant nuclear data for the measured radioelements are shown in Table 4.7.2.

*Table 4.7.2. Nuclear data of the measured radioelements (*sum of 226.4 and 228.2 keV).*

Element	Target isotope	Q_0	$\bar{E}_r$, eV	Formed isotope	Half-life T½	Gamma energy E_γ, keV (intensity, %)	$k_{0,Au}$
K	^{41}K	0.97	2960	^{42}K	12.36 h	1524.6 (100)	9.46×10^{-4}
U	^{238}U	103.4	16.9	^{239}U	23.45 min		
				β^- ↓			
				^{239}Np	2.356 d	228.2* (11.55) 277.6 (14.38)	2.76×10^{-3} 3.40×10^{-3}
Th	^{232}Th	11.53	54.4	^{233}Th	22.3 min		
				β^- ↓			
				^{233}Pa	26.97 d	300.3 (6.62) 312.2 (38.6)	4.37×10^{-3} 2.52×10^{-2}
Rb	^{85}Rb	14.80	839	^{86}Rb	18.64 d	1077.0 (8.64)	7.65×10^{-4}

For the determination of U, two corrections had to be applied to the ^{239}Np 228.2 keV peak area: 1) for a contribution by the 229.3 keV line from ^{182}Ta; and 2) for a contribution by the 228.2 keV line from ^{132}Te, formed via the ^{235}U(n,f) reaction.

For the first case, the correct peak area was determined exactly according to the procedure outlined in the chapter on Ge gamma-spectrometry of undisturbed loess in the laboratory (see Eq. 4.3.2). Let it be repeated that here the interfered peak is the one of ^{239}Np at 228.2 keV, the interfering peak is the one of ^{182}Ta at 229.3 keV, whereas two undisturbed (i.e. interference-free) peaks can be chosen, namely the ^{182}Ta peaks at 1221.4 and 1231.0 keV. The thus calculated correction amounted to 5.5%.

For the second case, De Corte [1992] introduced the following correction:

$$[(\text{peak area})_{228.2\ \text{keV}}]_{\text{corrected}} = \frac{[(\text{peak area})_{228.2\ \text{keV}}]_{\text{observed}}}{1+X} \tag{4.7.6}$$

with

$$X = \frac{\theta_{235}}{\theta_{238}} . \frac{\sigma_{0,235}}{\sigma_{0,238}} . \frac{f + Q_{0,235}(\alpha)}{f + Q_{0,238}(\alpha)} . Y_{Te} . \frac{\gamma_{Te}}{\gamma_{Np}} . \frac{(SDC)_{Te}}{(SDC)_{Np}} \tag{4.7.7}$$

where θ - isotopic abundance [$\theta_{235} = 0.00720$; $\theta_{238} = 0.9927$];

σ_0 - 2200 ms^{-1} cross section [^{235}U(n,fission) = 585 barn; ^{238}U(n,γ) = 2.68 barn];

f - thermal-to-epithermal neutron flux ratio [for channel 3, f = 24.3]

$Q_0(\alpha)$ = $I_0(\alpha)/\sigma_0$; $I_0(\alpha)$ – resonance integral corrected for a non-1/E epithermal neutron flux distribution approximated by $1/E^{1+\alpha}$ [channel 3: $Q_{0,235}(\alpha) = 0.45$; $Q_{0,238}(\alpha) = 100$];

Y_{Te} - cumulative ^{235}U fission yield for ^{132}Te [= 0.04312];

γ_{Te} - gamma-ray intensity of the ^{132}Te 228.2 keV gamma-line [= 0.880];

γ_{Np} - gamma-ray intensity of the ^{239}Np 228.2 keV gamma-line [= 0.116];

S,D,C - saturation, decay and counting factors [for ^{132}Te ($T_{½}$ = 3.26 d) and ^{239}Np ($T_{½}$ = 2.356 d)].

In the measuring conditions outlined above, this correction amounted to about 11 %.

4.7.5. k_0-NAA results for K, U, Th and Rb in loess material

4.7.5.1. Survey of concentrations

Table 4.7.3 shows the results of the U, Th, K and Rb concentrations in the 15 Volkegem loess samples. The k_0-NAA procedure obviously leads to concentrations in "dry loess". The uncertainties mentioned (2s) correspond to the largest of the internal (from the counting statistics) or external (from the replication of the determination) uncertainty, which are obtained according to the classical laws of error propagation.

Table 4.7.3. Results of U, Th, K and Rb concentrations in the 15 Volkegem loess samples, as determined via k_0-standardized instrumental neutron activation analysis.

No. of sample	K ± 2s % Dry weight	U ± 2s mg/kg Dry weight	Th ± 2s mg/kg Dry weight	Rb ± 2s mg/kg Dry weight
S.31	1.872 ± 0.031	2.692 ± 0.092	10.93 ± 0.20	82.2 ± 2.4
S.35	1.827 ± 0.027	2.67 ± 0.13	10.54 ± 0.12	80.5 ± 3.1
S.30	1.870 ± 0.056	2.585 ± 0.070	10.21 ± 0.27	77.5 ± 4.4
S.34	1.879 ± 0.036	2.64 ± 0.10	10.63 ± 0.30	81.6 ± 2.4
S.28	1.845 ± 0.017	2.741 ± 0.042	10.92 ± 0.16	84.0 ± 2.9
S.32	1.880 ± 0.044	2.620 ± 0.064	10.50 ± 0.14	79.2 ± 3.9
S.39	1.809 ± 0.025	2.624 ± 0.056	10.26 ± 0.15	80.2 ± 1.8
S.33	1.806 ± 0.039	2.560 ± 0.092	10.50 ± 0.21	82.0 ± 2.4
S.38	1.911 ± 0.038	2.778 ± 0.079	10.47 ± 0.24	82.5 ± 2.5
S.29	1.830 ± 0.040	2.683 ± 0.044	10.15 ± 0.24	77.7 ± 2.6
S.17	1.840 ± 0.047	2.506 ± 0.054	10.10 ± 0.11	80.7 ± 3.2
S.5	1.875 ± 0.040	2.575 ± 0.065	10.45 ± 0.35	77.1 ± 2.3
S.27	1.814 ± 0.026	2.71 ± 0.11	10.90 ± 0.28	77.4 ± 2.7
S.16	1.860 ± 0.047	2.611 ± 0.065	10.41 ± 0.51	79.0 ± 1.9
S.10	1.826 ± 0.046	2.542 ± 0.061	10.16 ± 0.35	79.2 ± 1.7

4.7.5.2. The concentration of Rb

In the assessment of the annual radiation dose, usually a K:Rb ratio of 200 is tacitly assumed [Warren, 1978] – although mention is also made of ratios ranging from 200 to 400 [Aitken, 1998]. However, as mentioned in 4.7.4.3, Rb can be determined via k_0-NAA, which is - among the methods used in this work - the only one which is capable of doing so.

Fig. 4.7.7 represents the correlation of K and Rb in 15 loess samples determined via k_0-INAA. As seen, the K:Rb ratio varies from 220 to 244. Although, in view of the small contribution from Rb, this variation does not make a significant difference to the total annual radiation dose, the possibility of determining Rb nevertheless provides an "automatic" control for the correctness of the assumption that the ratio K:Rb = 200:1.

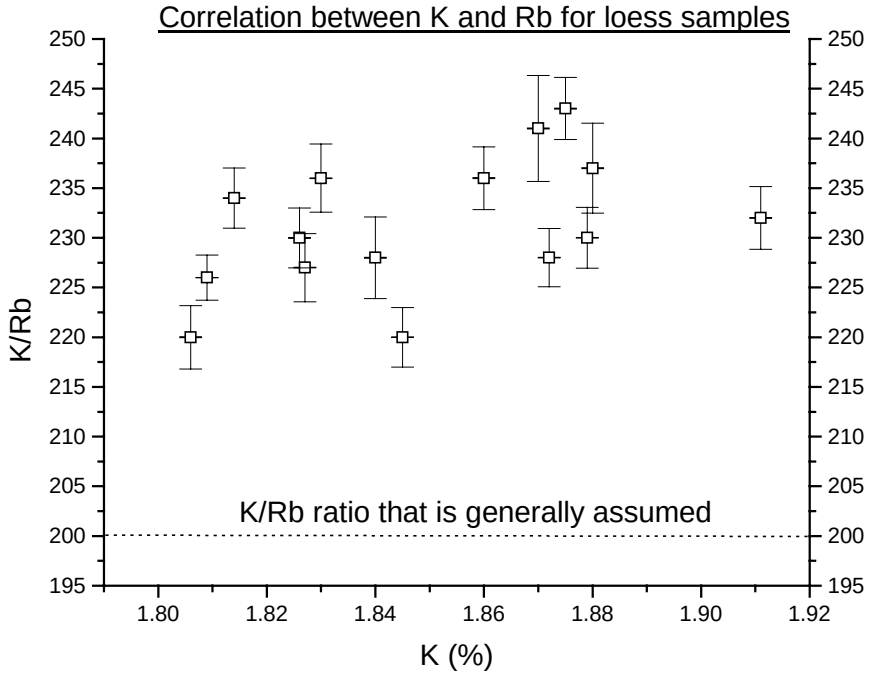

Fig.4.7.7. Ratio of K:Rb concentration in Volkegem loess samples determined via k_0-INAA.

4.8. Atomic absorption spectrometry

4.8.1. Instrumentation and basic equation

Atomic absorption spectrometry (AAS) was applied for the determination of K in the 15 loess samples collected from Volkegem.

Use was made of a Varian SpectrAA-600 instrument (Geological Institute), which is a double beam spectrometer equipped with a hollow (K) cathode lamp and an acetylene-air flame ionization system. The flame acts as an atomizer, leading to atoms of the sample in the ground state, which are capable of absorbing incident light through "resonance lines". The sample, in the form of a solution, was aspirated by a pneumatic nebulizer and transported into the flame.

In ideal conditions, the absorbance of light is proportional to the concentration of the element, according to the law of Bouger-Lambert-Beer:

$$A = \log\frac{1}{T} = \log\frac{I_0}{I} = k.c.d. \qquad (4.8.1)$$

where:
A = absorbance; the logarithm of the reciprocal of the transmission T;
I_0 = intensity of the incident light;
I = intensity of the transmitted light;
k = absorption coefficient;
c = concentration of element in the absorbing substance
d = thickness of the absorbing layer.

4.8.2. Preparation of samples and standards

As to the sample preparation, about 100 mg dried material was digested in a mixture of 1 ml $HClO_4$ (70 %, A.G.) and 20 ml HF (48 %, A.G.). The acid mixture was evaporated to dryness overnight on a heating plate at 150 $^{\circ}$C. After adding 1 ml HCl (37 %, A.G.), a dilution was made with "Milli-Q" water so as to reach a final K-concentration of the order of 1 $\mu g.ml^{-1}$. For each solution thus obtained, the absorbance measurements were performed in five-fold.

A K-standard solution was prepared by treating 15.499 mg of potassium biphtalate ($C_8H_5KO_4$) exactly as described above for the sample preparation, to get a final K concentration of 2.967 $\mu g.ml^{-1}$. Further dilutions were made with "Milli-Q" water to get a series of K standards of 0.119, 0.237, 0.475, 0.742, 0.979, 1.246, 1.484, 1.780, 1.988 and 2.967 $\mu g.ml^{-1}$. A blank was also prepared in the same way.

4.8.3. Calibration

Quantification was done via a calibration line obtained with the series of the above-mentioned K standard solutions. All measurements were carried out in five-fold. According to Eq. 4.8.1, the absorbance should linearly increase with an increasing concentration. However, as Fig. 4.8.1 reveals, in the present work a deviation from linearity at higher absorbance values is observed. This non-linearity situation could not be improved by further dilution, due to the relatively high blank value.

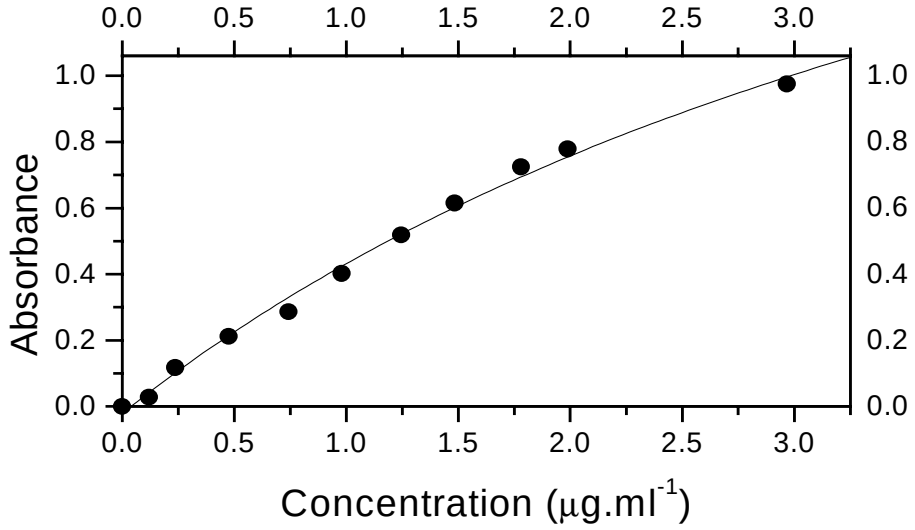

Fig. 4.8.1. Calibration line obtained with the series of K standards.

4.8.4. K-concentration results

The results of the K-concentrations determined via AAS in the 15 Volkegem loess samples are shown in Table 4.8.1. The uncertainties (2s) were obtained from quadratically combining the uncertainties on the absorbance (from the replication of the measurements) with those originating from the calibration curve (i.e. from the uncertainties on the parameters of the polynomial fitting).

Table 4.8.1. K-concentrations in the 15 Volkegem loess samples as determined via atomic absorption spectrometry.

Number of sample	K-content ± 2s % Dry weight
S.31	1.88±0.16
S.35	1.66±0.15
S.30	1.78±0.15
S.34	1.77±0.15
S.28	1.66±0.15
S.32	1.80±0.15
S.39	1.63±0.15
S.33	1.87±0.16
S.38	1.72±0.15
S.29	1.78±0.15
S.17	1.60±0.15
S.5	1.83±0.15
S.27	1.92±0.16
S.16	1.66±0.15
S.10	1.98±0.16

4.9. Comparison of results

4.9.1. Elemental concentrations

For all the methods yielding individual elemental contents, the overall results, expressed as "dry weight" concentrations, are shown in Figs 4.9.1 – 4.9.3 for K, Th and U, respectively. Whereas the NaI(Tl) field gamma-spectrometry results refer to the five "middle sampling points" at the Volkegem loess site, the other methods give results for the 15 (=5 × 3) samples brought to the laboratory. In general, the error bars give the ± 2s uncertainty, which is obtained according to the classical laws of error propagation; in case both the observed uncertainty (from the replication of the measurements) and the expected uncertainty (from the counting statistics) could be calculated, the larger of the two was adopted and plotted.

Figs 4.9.1 – 4.9.3 allow a comparison of the K, Th and U concentrations obtained with the different techniques.

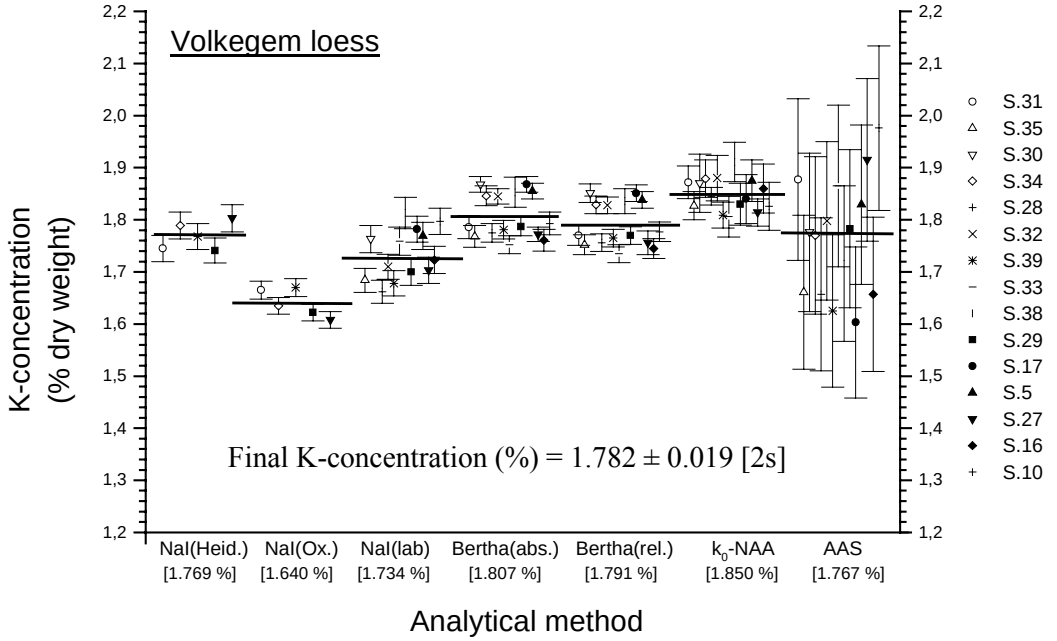

Fig. 4.9.1. Results of K concentration determinations (± 2s uncertainties) using different analytical techniques. The mean values are given in square brackets. The "S.xy" notations refer to the sampling points.

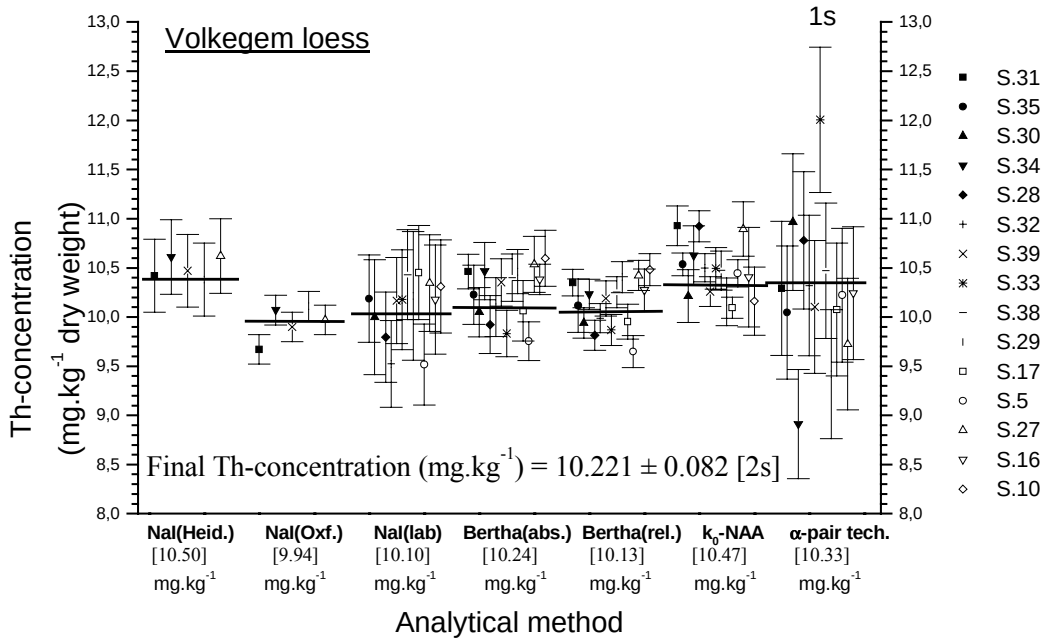

Fig. 4.9.2. Results of Th concentration determinations (± 2s uncertainties, unless otherwise specified) using different analytical techniques. The mean values are given in square brackets. The "S.xy" notations refer to the sampling points.

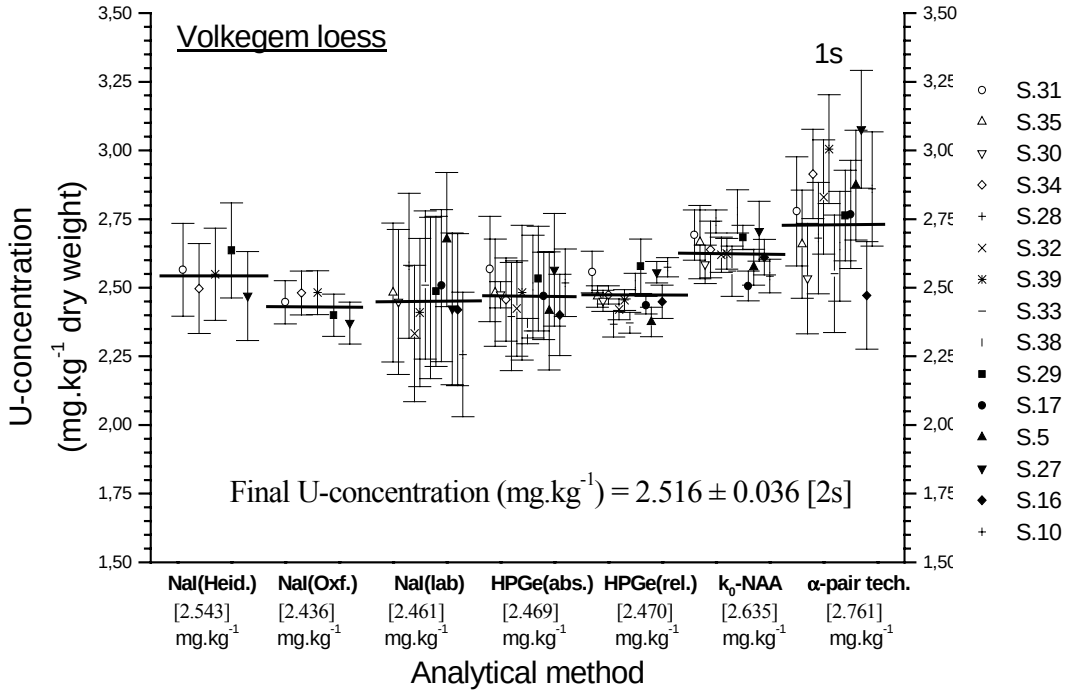

Fig. 4.9.3. Results of U concentration determinations (± 2s uncertainties, unless otherwise specified) using different analytical techniques. The mean values are given in square brackets. The "S.xy" notations refer to the sampling points.

A first observation concerns the results of the field measurements with the Heidelberg and Oxford calibrations. Within the analytical uncertainties, these results are consistent and in agreement with the laboratory measurements, except for K where a rather low concentration was obtained via the Oxford blocks. Note that the uncertainties on the concentrations resulting from both the Oxford and Heidelberg calibration are only based on the counting statistics.

As to AAS, the results of the K-determination not only bear rather large uncertainties, but also show a significant scattering. A possible explanation is the non-linearity of the calibration curve; as said in Section 4.8.3, this situation could not be improved by further dilution, due to the relatively high blank value. Nevertheless, the average K-concentration thus obtained is consistent with the results from the other determination methods.

The large uncertainties observed for the Th and U results (Figs 4.9.2 and 4.9.3) obtained with the ZnS alpha counting via the pair technique, can be completely attributed to the poor counting statistics. In addition to this, the U-content appears to be overestimated.

The concentrations obtained via k_0-NAA turn out to be somewhat at the high side, but there is a fair consistency with the results from the Heidelberg-calibrated field measurements, although less so for K. This is somewhat puzzling, since the method, when tested for its accuracy by analysis of NIST SRM 1633a Coal Fly Ash, yielded results for K, Th and U which are within 3 % consistent with the certified values [Chapter 4.7, Fig. 4.7.1].

As to the results of gamma-spectrometry in the lab, there seem to be no problems for any of the elements. This holds for the low-background measurements with both the NaI(Tl)- and the HPGe-detector ("Bertha"), although for the former the uncertainties are rather large for Th and U, because of view of the poor counting statistics achieved for their measured gamma-lines.

In the case of the measurements with "Bertha" it is, however, more interesting to look at the concentration results obtained via the individual gamma-peaks of the daughter nuclides in the ^{232}Th and ^{238}U decay series. This is shown in Figs 4.9.4 –4.9.7.

A first observation, when comparing Figs 4.9.4 and 4.9.5, and Figs 4.9.6 and 4.9.7, is that the results obtained via the relative calibration are definitely superior (a better consistency between different isotopes and gamma-lines) to those via the absolute method.

This is especially striking in the case of U, where the absolute method would even point at an increased Rn-content, which – however – seems to be an artifact when looking at the relatively calibrated results.

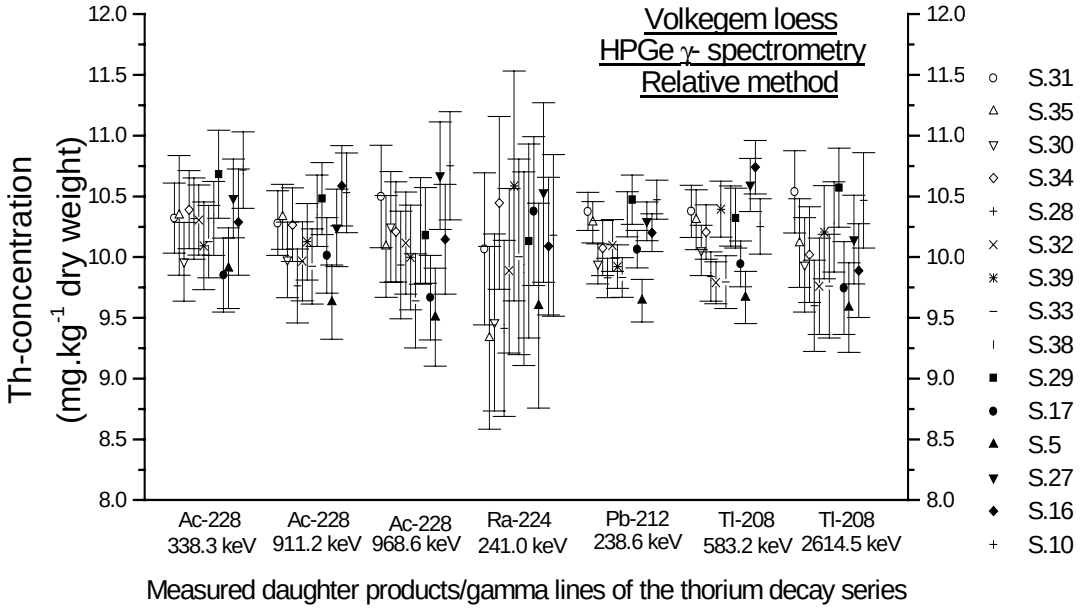

Fig. 4.9.4. Concentration of Th (± 2s counting statistics), using relative calibration, from HPGe γ-spectrometry of the daughter radionuclides in the ^{232}Th decay chain (the "S.xy" notations refer to the sampling points).

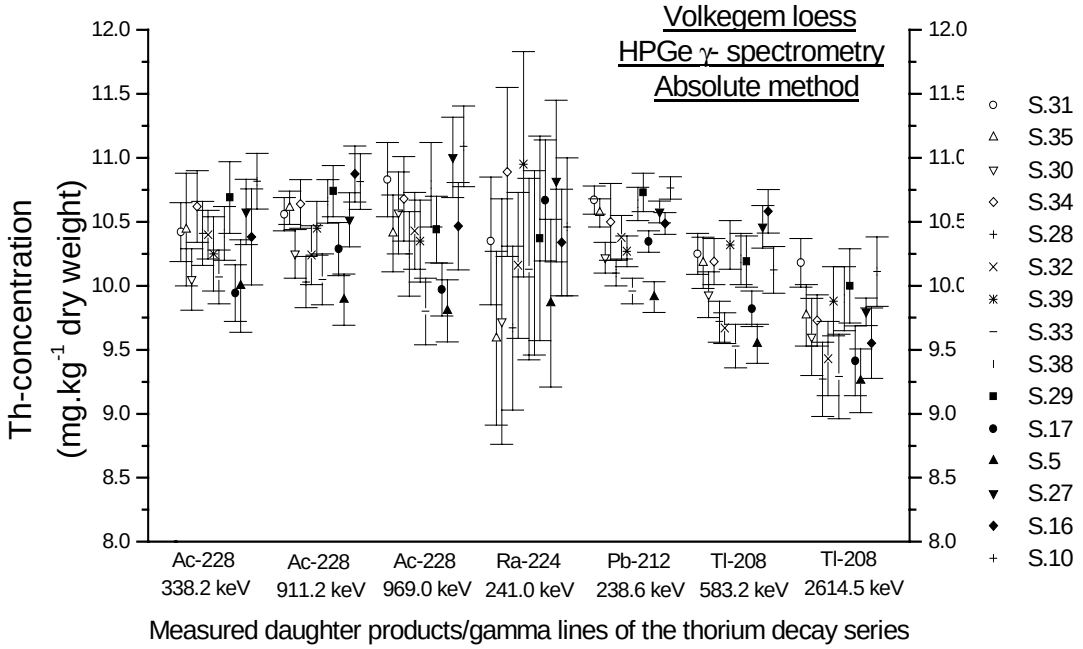

Fig. 4.9.5. Concentration of Th (± 2s counting statistics), using absolute calibration, from HPGe γ-spectrometry of the daughter radionuclides in the ^{232}Th decay chain (the "S.xy" notations refer to the sampling points).

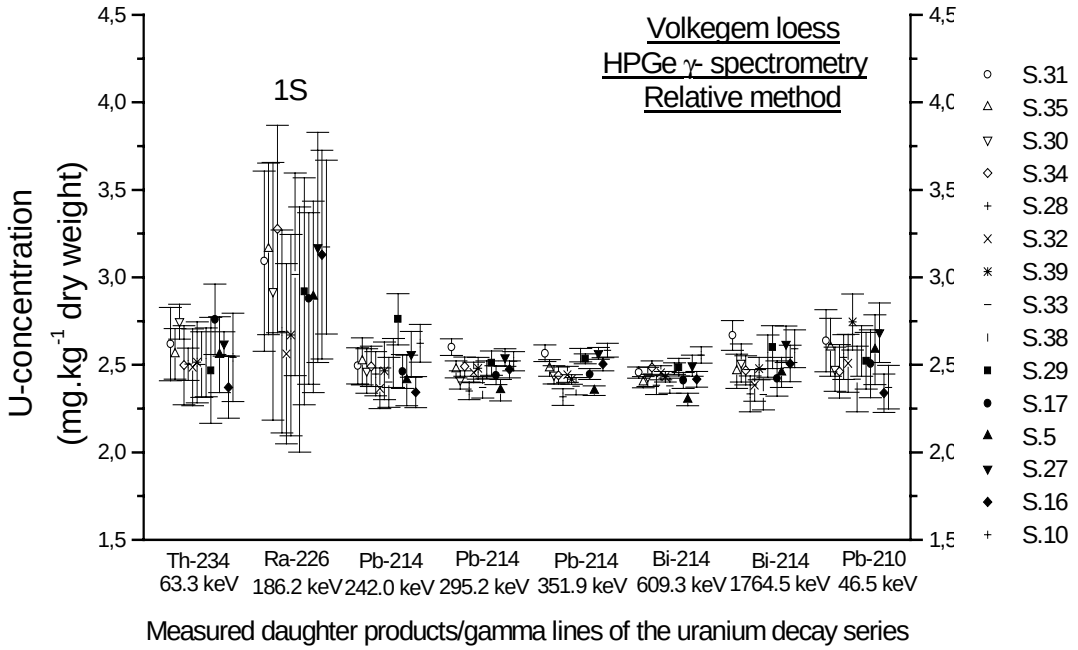

Fig. 4.9.6. Concentration of U (± 2s counting statistics, unless specified), using relative calibration, from HPGe γ-spectrometry of the daughter radionuclides in the ^{238}U decay chain (the "S.xy" notations refer to the sampling points).

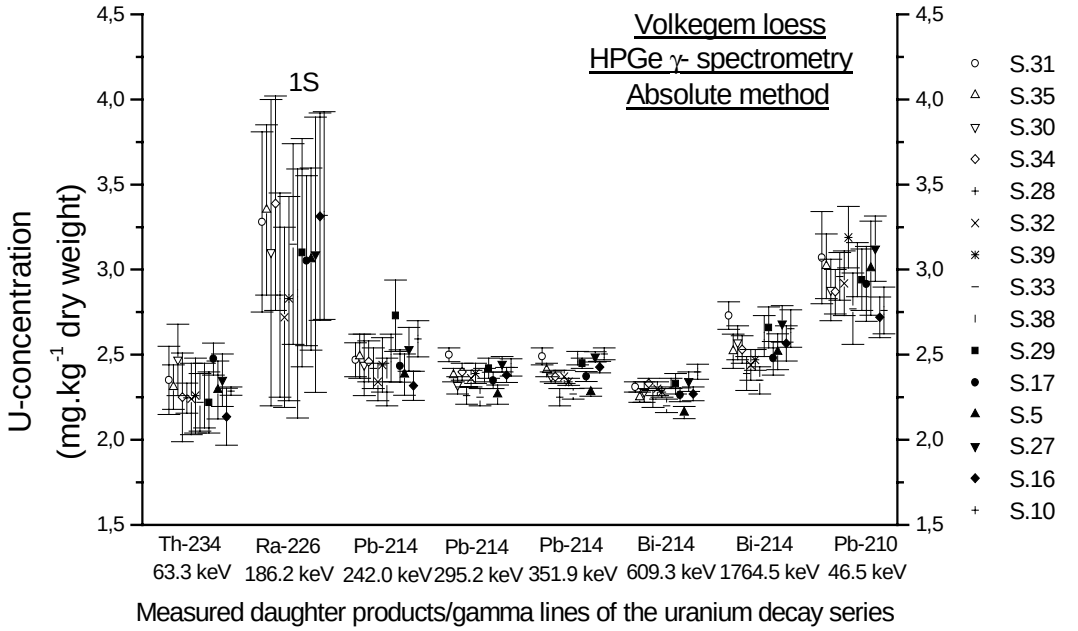

Fig. 4.9.7. Concentration of U (± 2s counting statistics, unless specified), using absolute calibration, from HPGe γ-spectrometry of the daughter radionuclides in the ^{238}U decay chain (the "S.xy" notations refer to the sampling points).

To all probability, the poorer and anomalous results from the absolute calibration are caused by inaccuracies in the literature data for the gamma-ray intensities, although some contribution from the calibration of the Ge-detector, especially in the very low energy region, can also play a role. A second observation, in the case of U, is the very large uncertainty on the result for the 186.2 keV line of ^{226}Ra, which – as explained in Section 4.3.5 – is caused by a troublesome correction for spectral interference. Anyhow, from Figs 4.9.4 and 4.9.6 – showing the results of the relative calibration - it can be concluded that neither U nor Th exhibits a disequilibrium in their decay series. Finally, it is important to mention that, in Figs 4.9.2 and 4.9.3, the "HPGe(rel.)"- and "HPGe(abs.)"-concentrations for Th and U are obtained by averaging the results for all daughters/gamma lines, except the ^{226}Ra/186.2 keV value for U. That the thus obtained "HPGe(abs.)"-results are bearing a larger uncertainty, is simply reflecting the above mentioned inferiority of the absolute calibration method.

Finally, let it be repeated that k_0-NAA "automatically" generates the concentration of Rb, as discussed in Section 4.7.5.2.

4.9.2. Annual radiation doses

A comparison was made of the results of alpha [from integral counting] and beta counting with those of the elemental determination methods, based on the transformation to annual radiation doses for the dry loess. The alpha and beta radiation dose-rates are calculated from the average elemental concentrations determined via NaI(Tl) field measurements [both Oxford and Heidelberg calibration], NaI(Tl) laboratory measurements, laboratory HPGe gamma-ray spectrometry (relative calibration only) and k_0-NAA. Dose conversion factors (Table 4.9.1) were taken from recent literature [Aitken, 1998], whereby it should be noted that, when U-concentrations are converted to annual radiation doses, the contribution from the ^{235}U series is taken into account. The results are shown in Table 4.9.2. As seen, the ratio of the calculated (from elemental concentrations) and the measured values amounts on the average to 1.043 ± 0.023 (2s) for the alpha dose rate and 1.045 ± 0.014 (2s) for the

beta dose rate. Although both ratios are higher than unity (about 4.5 %), it is concluded that for the loess studied here the results from alpha and beta counting are of sufficient accuracy and can be relied upon in radiation dose rate determination, especially when checking (the equilibrium) and combining them with the results obtained via one or more elemental determination methods.

Table 4.9.1. Conversion factors to obtain annual radiation doses from elemental contents [Aitken, 1998].

Radio-element	Annual radiation doses ($Gy.ka^{-1}$)		
	$D_{\alpha,effective}$	D_β	D_γ
U (per $mg.kg^{-1}$)	0.231	0.145	0.113
Th (per $mg.kg^{-1}$)	0.0644	0.0273	0.0478
K (per %)	-	0.782	0.243
Rb (per 50 $mg.kg^{-1}$)	-	0.019	-

Table 4.9.2. Comparison of measured and calculated alpha and beta annual radiation doses (± 2s uncertainties).

Sample number	Measured α dose-rate (Gy/ka)	Calculated α dose-rate (Gy/ka)	Measured/ Calculated α dose-rate (Gy/ka)	Measured β dose-rate (Gy/ka)	Calculated β dose-rate (Gy/ka)	Measured/ Calculated β dose-rate (Gy/ka)
S.31	1.309±0.029	1.258±0.036	1.040±0.038	2.150±0.046	2.067±0.065	1.041±0.039
S.35	1.265±0.026	1.248±0.032	1.014±0.033	2.217±0.047	2.051±0.068	1.081±0.042
S.30	1.300±0.023	1.224±0.022	1.063±0.027	2.239±0.062	2.095±0.053	1.068±0.040
S.34	1.249±0.024	1.251±0.023	0.998±0.026	2.209±0.049	2.078±0.078	1.063±0.046
S.28	1.319±0.025	1.247±0.061	1.057±0.056	2.134±0.052	2.053±0.090	1.039±0.052
S.32	1.238±0.028	1.212±0.047	1.022±0.046	2.182±0.052	2.072±0.083	1.053±0.049
S.39	1.310±0.029	1.234±0.021	1.061±0.029	2.188±0.047	2.033±0.042	1.077±0.032
S.33	1.327±0.026	1.229±0.036	1.080±0.039	2.147±0.048	2.051±0.039	1.047±0.031
S.38	1.219±0.023	1.266±0.046	0.963±0.039	2.195±0.051	2.139±0.054	1.026±0.035
S.29	1.248±0.022	1.249±0.026	0.999±0.027	2.150±0.053	2.037±0.052	1.055±0.038
S.17	1.290±0.025	1.228±0.018	1.051±0.025	2.057±0.045	2.095±0.035	0.982±0.027
S.5	1.326±0.027	1.223±0.049	1.084±0.049	2.141±0.048	2.096±0.056	1.021±0.035
S.27	1.340±0.024	1.250±0.033	1.071±0.034	2.191±0.129	2.038±0.057	1.075±0.070
S.16	1.236±0.027	1.238±0.028	0.998±0.031	2.140±0.053	2.061±0.069	1.038±0.043
S.10	1.404±0.028	1.232±0.048	1.139±0.050	2.083±0.043	2.076±0.037	1.003±0.028
Grand mean			1.043±0.023	Grand mean		1.045±0.014

4.9.3. Conclusions

From the comparative study performed in the present work, it can be concluded that the following methods for the determination of the annual radiation dose in loess sediment are giving reliable results: NaI(Tl) field gamma-ray spectrometry, both via the "Heidelberg" and the "Oxford" K-Th-U calibration blocks (although for the "Oxford" blocks especially the result for K tends to be rather low); low-background NaI(Tl) gamma-ray spectrometry in the laboratory; low-background extended-range Ge gamma-ray spectrometry (also allowing to assess the equilibrium in the Th and U decay series) via the relative calibration; k_0-standardized reactor neutron activation analysis; thick source ZnS alpha counting in the integral mode; and low-background GM beta counting. Methods of somewhat poorer quality, which were rejected for making concentration averages, were found to be: absolutely calibrated Ge gamma-ray spectrometry, ZnS alpha counting in the pair mode (for Th and U) and atomic absorption spectrometry (for K). Obviously, for all three elements the best technique is low-background extended-energy range Ge gamma-ray spectrometry with relative calibration: it offers good precision and accuracy and it simultaneously allows studying the equilibrium of the Th and U decay series.

From the results shown above, it can also be concluded that the material studied at the Volkegem loess site is quite homogeneous (in fact, this *a priori* assumption was a criterion for its selection – see Section 4.1). This follows indeed from Figs 4.9.8-4.9.10, where the K, Th and U concentrations (dry weight basis), obtained via the above listed elemental determination methods, are plotted for the 15 sampling points studied, leading to averages of 1.784 ± 0.074 % for K, 10.22 ± 0.31 $mg.kg^{-1}$ for Th and 2.52 ± 0.14 $mg.kg^{-1}$ for U. As seen, the relative standard deviations (2s) on these grand means are of the order of 3-5 %. This means in fact that, for the homogenized material, the standard errors (2s) on the concentrations are as low as about 1%.

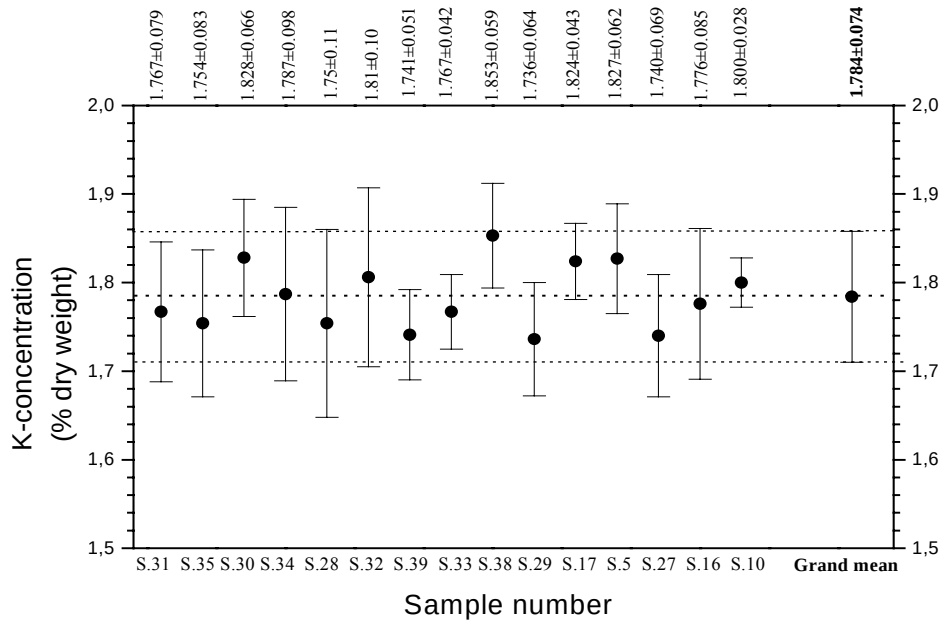

Fig.4.9.8. K concentration in the 15 loess samples, and grand mean (± 2s standard deviation), showing the homogeneity of the collected material (the "S.xy" notations refer to the sampling points).

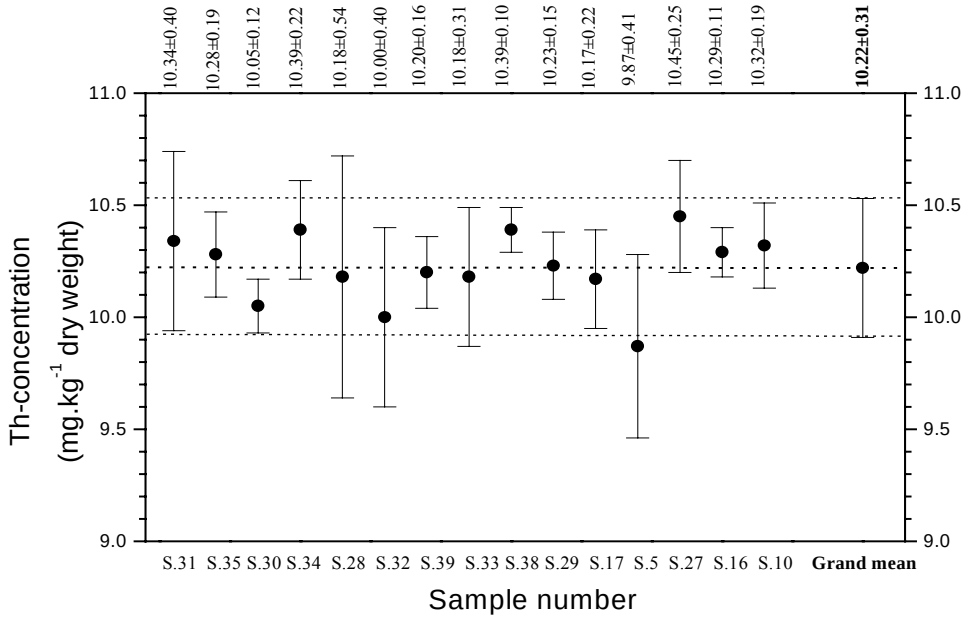

Fig. 4.9.9. Th concentration in the 15 loess samples, and grand mean (± 2s standard deviation), showing the homogeneity of the collected material (the "S.xy" notations refer to the sampling points).

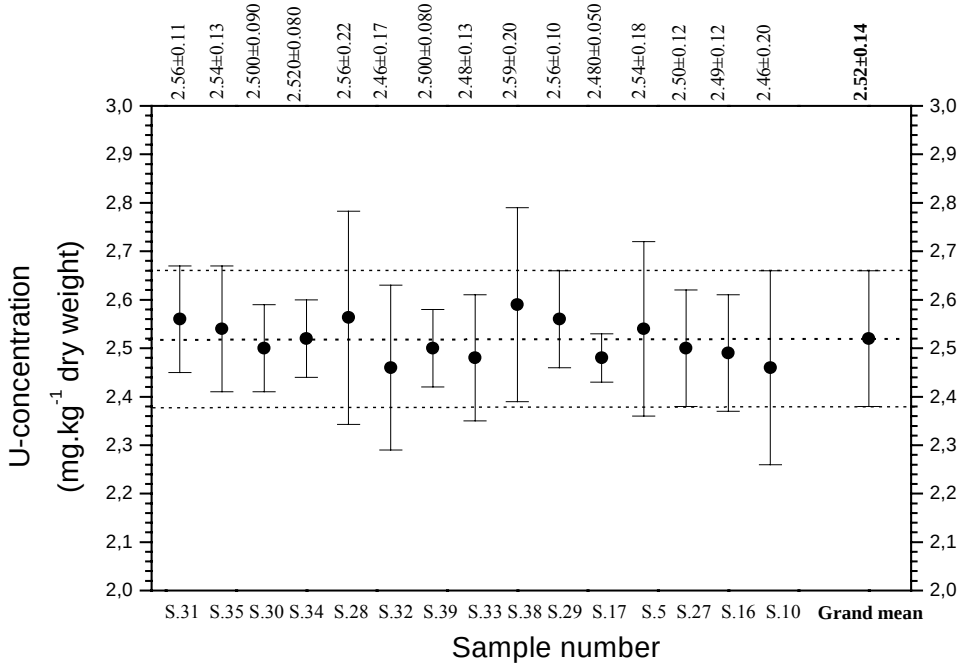

Fig. 4.9.10. U concentration in the 15 loess samples, and grand mean (± 2s standard deviation), showing the homogeneity of the collected material (the "S.xy" notations refer to the sampling points).

- CHAPTER 5 -

ANNUAL RADIATION DOSE DETERMINATION IN THE LUMINESCENCE DATING OF COVERSAND FROM OSSENDRECHT: SPECIFIC PROBLEMS AND PROCEDURES

5.1. Introduction

In Chapter 4, a detailed examination was made of the performance of some commonly applied techniques for determining the annual radiation dose in the case of loess sediment. In the present chapter, this exercise was extended to sand, for which the following methods were dealt with:

- NaI(Tl) gamma-ray spectrometry in field conditions, for the measurement of K, U and Th;

- low-background extended energy-range (XtRa) HPGe gamma-ray spectrometry in Marinelli geometry, assisted by relative calibration, for the measurement of K, U and Th, and also for the detection of possible disequilibria in the Th- and especially in the U-decay series;

- k_0-standardized instrumental reactor neutron activation analysis (k_0-INAA) for the determination of K, U, Th and Rb;

- low-background GM beta counting, for the measurement of K + U + Th;

- ZnS alpha counting in the integral mode, for the measurement of U + Th.

Methods of poorer quality, as formerly observed in the analysis of loess sediment [Chapter 4], were cancelled in the analysis of sand: absolutely calibrated XtRa HPGe gamma-ray spectrometry, ZnS alpha counting in the pair mode (for the individual counting of U and Th) and atomic absorption spectrometry (for K). Due to the low concentration of K, U and Th present in the here investigated sand samples, low background NaI(Tl) gamma-ray spectrometry in the laboratory was also cancelled.

5.2. Sampling site and samples

5.2.1. Selection of the sampling site

In the framework of an ongoing study of luminescence dating of sediment materials in the Ghent luminescence laboratory, a coversand profile was selected at Ossendrecht, in the southwestern part of the Netherlands. The location and geomorphological setting of the study area is shown in Fig. 5.1.a and 5.1.b, resprctively. The profile is situated in the sand quarry "Boudewijn" close to the village of Ossendrecht.

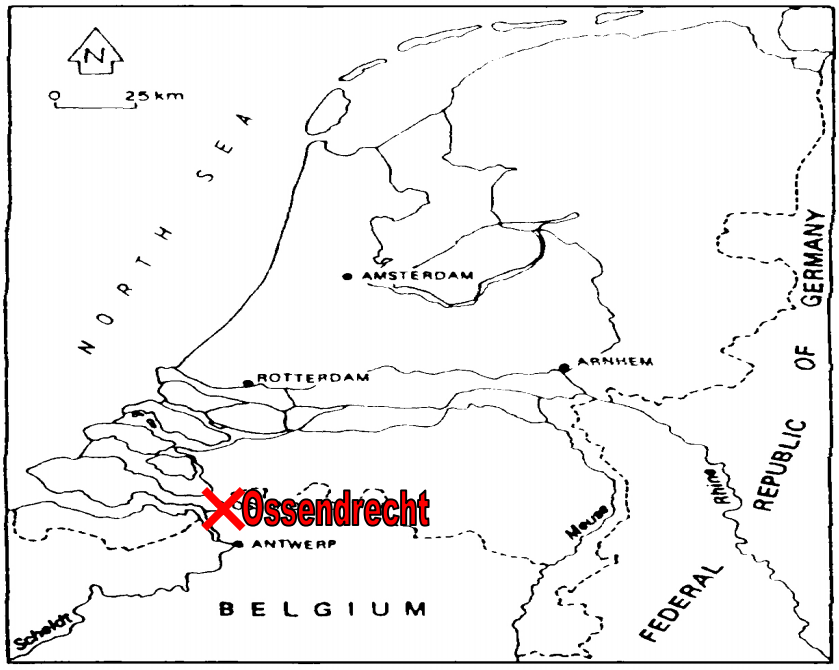

Fig. 5.1.a. Location map of the study area.

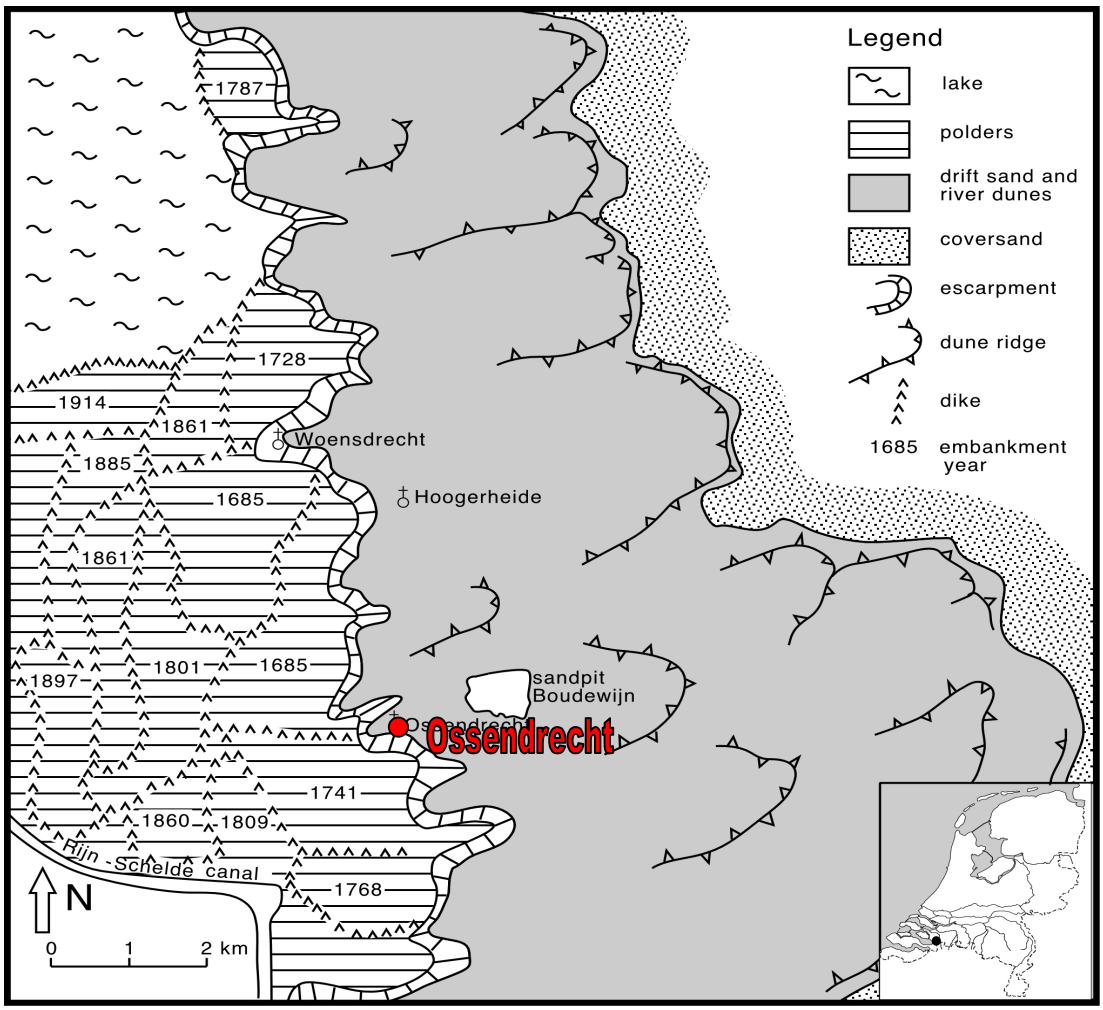

Fig. 5.1.b. Geomorphological setting of the investigated site.

5.2.2. Sample collection and measurement of field spectra

Four spots (S.2, D, S.1 and S.3) were selected for sample collection, as shown in Fig. 5.2. The sampling points S.2, D and S.3 are vertically separated by ~ 20 cm and S.1 is located at ~ 21 cm beside the central sample D.

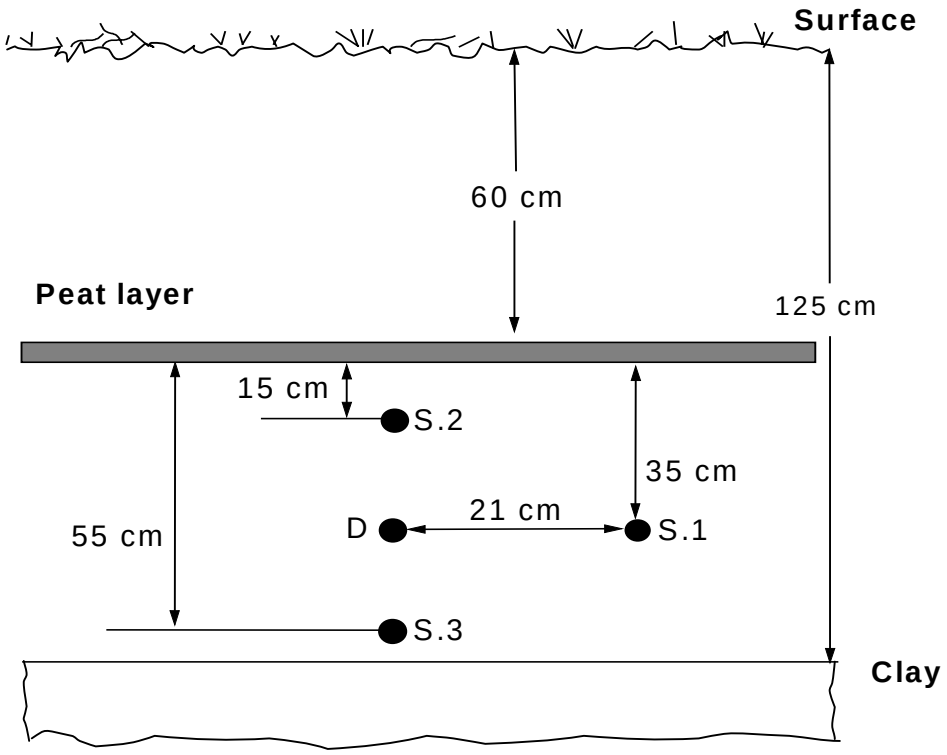

Fig. 5.2. Position of sampling spots in the Ossendrecht sand profile.

After cleaning the surface of the profile, two auger hole field gamma-ray countings (3 hours each) were performed in the vicinity of D and S.1 and at the same stratigraphic level, using the portable NaI(Tl) gamma spectrometry system described in Chapter 4 Section 4.2 (see also Fig. 5.3). After the gamma spectrometry measurements, about 3 kg of sand from each sampling point was collected in a plastic bag and brought to the laboratory.

Fig. 5.3. Picture of the sampled sand profile at Ossendrecht; the peat layer (black) is clearly visible. Shown is the experimental setup for the NaI(Tl) γ-spectrometry system.

5.2.3. Treatment of samples

In the laboratory the samples were dried at 110°C until constant weight. The moisture content was found to be 12%.

Contrary to what was formerly experienced in the case of loess sediment, the coversand revealed two specific problems during the determination of the annual radiation dose (see further): 1) the low concentration of K, U and Th in the sand, and 2) sample inhomogeneity at the gram level. As the analyses progressed and the specific problems were encountered, appropriate procedures for preparing the samples had to be found. The following sample treatment approaches ("steps") were consecutively carried out for each of the 4 samples:

1. step 1: stirring of the total amount of dried sand in a bucket, aiming at homogenization. This "raw" material was then analysed via low-background XtRa HPGe gamma-ray spectrometry in Marinelli geometry and via k_0-NAA;

2. step 2: manually grinding, in a porcelain mortar, of a portion (~ 20 g) of the material obtained in step 1, followed by sieving (using a 63 μm diameter sieve) and further stirring. The grinding was continued until all material passed through the sieve. This manually ground material was analysed via k_0-NAA , alpha and beta counting;

3. step 3: ball-milling, in a Pulverizer6 (Planetary Mono Mill, Fritsch), of a portion (~200 g, randomly sampled from the bucket) of the material obtained in step 1. This was done by loading the agate beaker (500 ml) of the Pulverizer with ~66 g of sand together with 6 agate balls (20 mm diam.) and grinding for 10 minutes, with one repetition, at a frequency of 400 rpm. A total of 3 such cycles was used, and the ~200 g milled sand thus obtained was finally further homogenized in a turbulent mixer (Turbula Type T2A, W.A. Bachofen) for 24 hours. This ball-milled material was again analysed via k_0-NAA, alpha and beta counting.

5.3. Analysis of "step 1" material (stirred sand)

5.3.1. Ge gamma-ray spectrometry in Marinelli geometry

Due to the low concentrations of K, U and Th in the samples, the cylindrical measurement geometry (as was used for loess) was replaced by a Marinelli geometry. In this Marinelli geometry (see Fig. 5.4) a large volume of sample (1.5 kg) was measured with the XtRa HPGe gamma-ray spectrometer "Bertha" (see Chapter 4 Section 4.3).

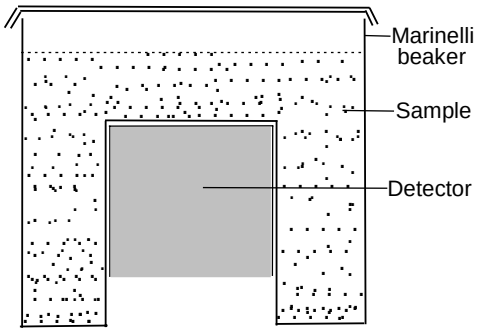

Fig. 5.4. Schematic representation of a Marinelli geometry.

Standardization was done in a relative way. Since such a large mass of standard is not easy to find commercially, the well-characterized Volkegem loess sediment was used as a secondary standard [K = 1.782 ± 0.019 %; U = 2.516 ± 0.036 mg.kg^{-1}; Th = 10.221 ± 0.082 mg.kg^{-1}], of which 1.3 kg was leading to the same packing height as the sample. The standard was prepared in two-fold and each was counted for 1 week. Each sample was counted for as long as 2 weeks. It should be noted that, before counting samples and standards, the Marinelli beaker was tightly closed and stored for at least 4 weeks to re-establish radioactive equilibrium after possible radon escape in the laboratory.

The spectra were processed as explained in Chapter 4 Section 4.3. Because of a serious spectral interference, the U-concentration based on the 186.1 keV gamma-line of ^{226}Ra is of questionable accuracy and was omitted in the processing of the data. The calculation of the elemental concentrations was performed in analogy with Eq. 4.3.1:

$$[\text{conc}]_{\text{sand}} = [\text{conc}]_{\text{loess stand.}} \times \frac{[\text{cps}/\text{W}]_{\text{sand}}}{[\text{cps}/\text{W}]_{\text{loess stand.}}} \times \frac{[\overline{\Omega}]_{\text{loess stand.}}}{[\overline{\Omega}]_{\text{sand}}} \qquad (5.1)$$

where the effective solid angle $\overline{\Omega}$ [see Chapter 4 Section 4.2.2.3.2, and De Corte et al., 2001] was obtained via the software package MARSANGLE [Jovanović et al., 1992]. Whereas the counting geometry for the samples and the standards was identical, their chemical composition and packing density - to be introduced in the calculation of $\overline{\Omega}$ - were different, as shown in Table 5.1.

Table 5.1. Composition and density of loess standard (Volkegem site) and coversand (Ossendrecht site).

	Material (dry)	
	Loess (Volkegem)	Sand (Ossendrecht)
Si, %	31.55	39.76
Ti, %	0.37	0.12
Al, %	4.01	0.70
Fe, %	2.33	0.22
Mg, %	0.35	0.005
Ca, %	0.41	0.02
Na, %	0.67	0.17
K, %	1.49	0.49
H, %	1.90	1.33
O, %	56.92	57.18
Packing density, $g.cm^{-3}$	1.37	1.54

The concentrations of K, U and Th (± 2s uncertainties) determined in this Marinelli geometry are shown in Figs 5.5-5.7, respectively. The measurements of the ^{238}U (Fig. 5.6) and ^{232}Th (Fig. 5.7) daughters show that both series are in equilibrium, although a tendency of a small but systematic decrease can be observed for ^{210}Pb in the ^{238}U decay series. This might indicate a (hardly significant) disequilibrium caused by a slight ^{222}Rn escape in the geological past after the burial of the sediment. The concentrations of U and Th via all the daughters/gamma-lines of their respective decay series, except ^{210}Pb in the ^{238}U decay series, were taken into account for obtaining the average. The average concentrations (± 2s uncertainties) of U and Th for each sample were put in the boxes of Fig.5.6 - Fig. 5.7, respectively.

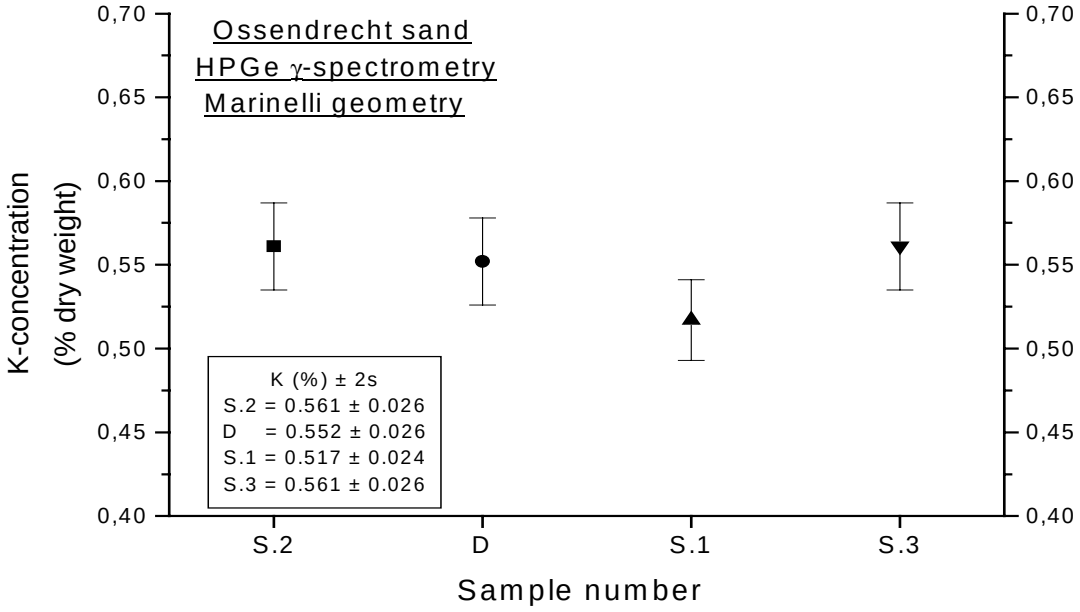

Fig. 5.5. Concentration of K (± 2s uncertainties) as obtained via relatively standardized Ge gamma-ray spectrometry in Marinelli geometry (the "D" and "S.x" notations refer to the sampling points).

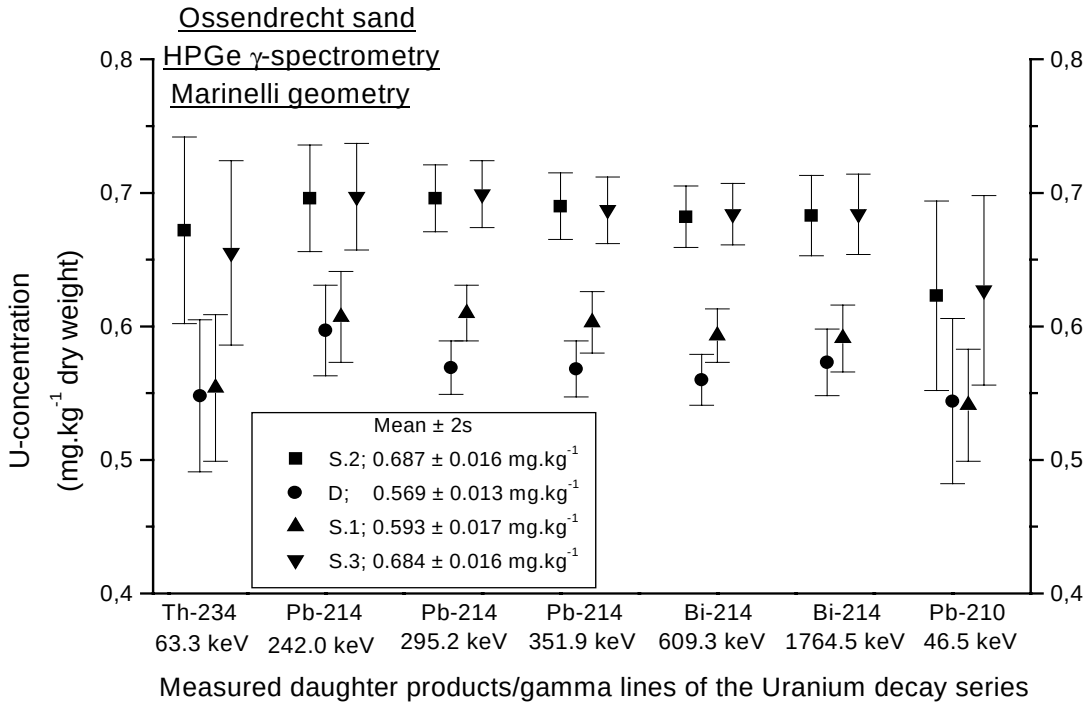

Fig. 5.6. Concentration of U (± 2s uncertainties) as obtained from the daughter nuclides in the ^{238}U decay chain, via relatively standardized Ge gamma-ray spectrometry in Marinelli geometry (the "D" and "S.x" notations refer to the sampling points).

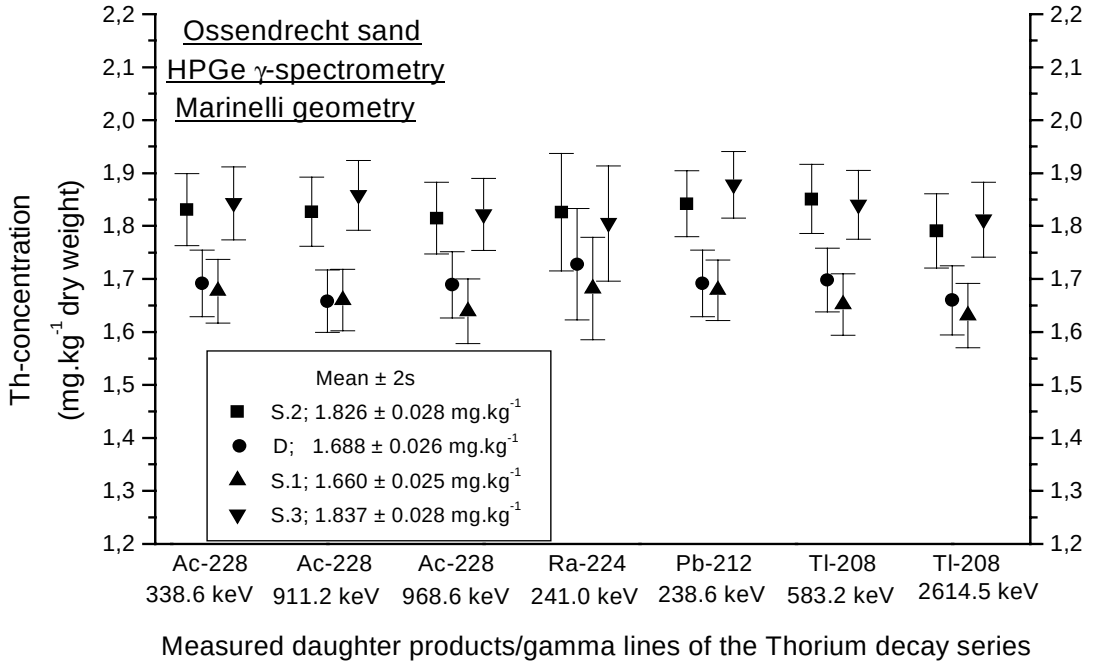

Fig. 5.7. Concentration of Th (± 2s uncertainties) as obtained from the daughter nuclides in the ^{232}Th decay chain, via relatively standardized Ge gamma-ray spectrometry in Marinelli geometry (the "D" and "S.x" notations refer to the sampling points).

5.3.2. k_0-NAA

For k_0-NAA [see Chapter 4 Section 4.7], the sample mass was increased to ~1 g (for loess ~ 500 mg material was used), due to its lower K, U and Th content. Unlike the situation experienced in the study of loess sediment [see Chapter 4], a large scatter between different sub-samples was now observed for the obtained concentrations of U, Th, and to a lesser extent for K. This is shown in Figs 5.8 – 5.10 for sample S.2. The same trend was found for the other samples as well. The scatter points at an inhomogeneous distribution of U and Th, at the gram level. Nevertheless, the average concentrations for each sampling point are in general consistent (within 2s) with the HPGe gamma spectrometry in Marinelli geometry measurements (representing 1.5 kg of dried raw material), as shown in Table 5.2.

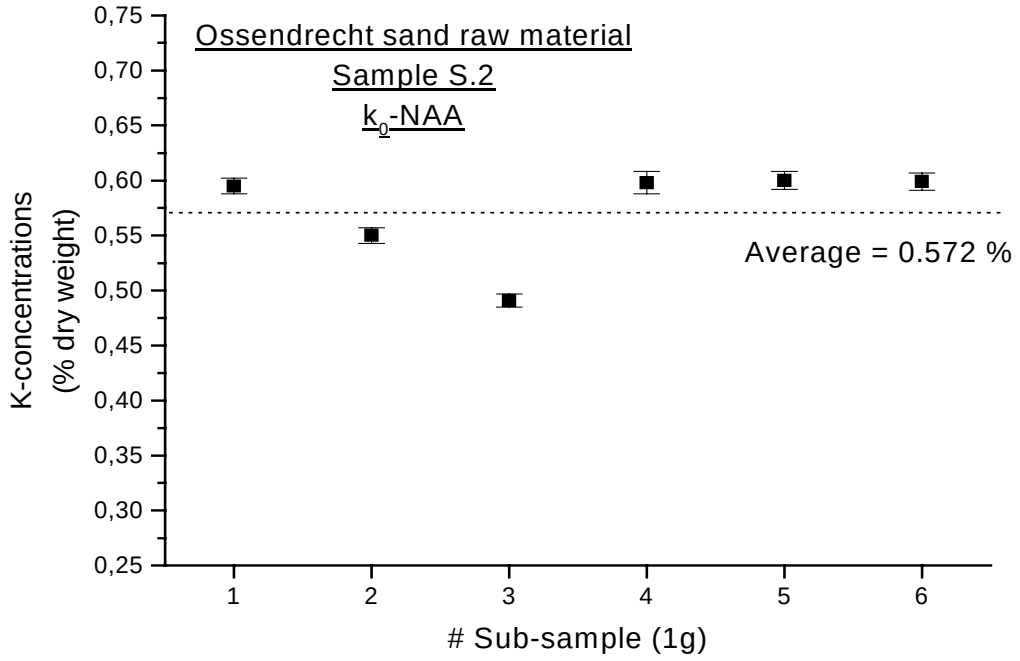

Fig.5.8. Demonstration of the inhomogeneity for K (± 2s uncertainties) in "raw" coversand sample S.2, using k_0-standardized instrumental neutron activation analysis on 1 gram sub-samples.

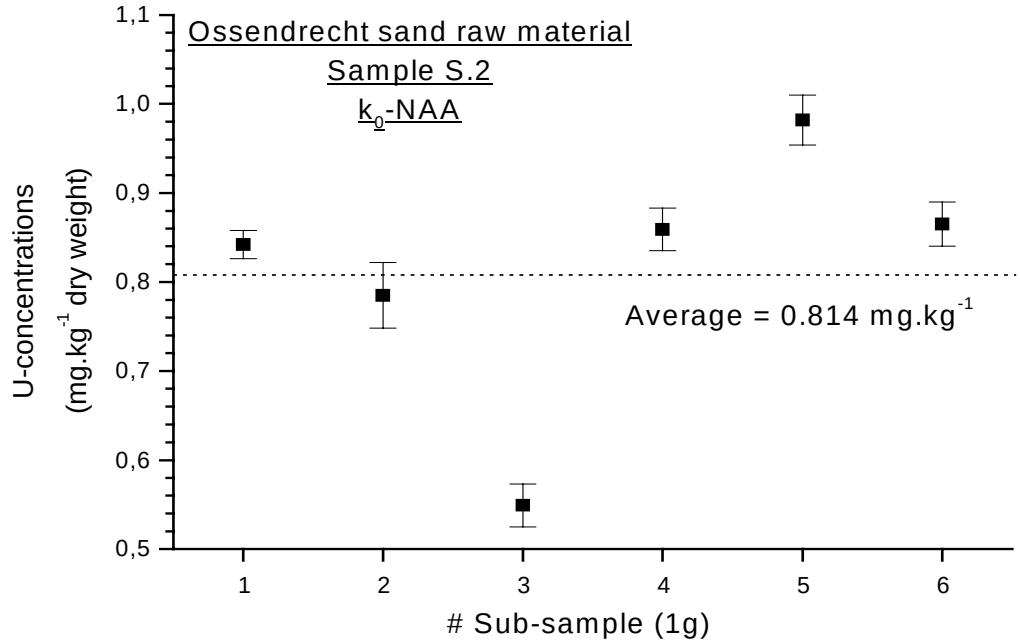

Fig. 5.9. Demonstration of the inhomogeneity for U (± 2s uncertainties) in "raw" coversand sample S.2, using k_0-standardized instrumental neutron activation analysis on 1 gram sub-samples.

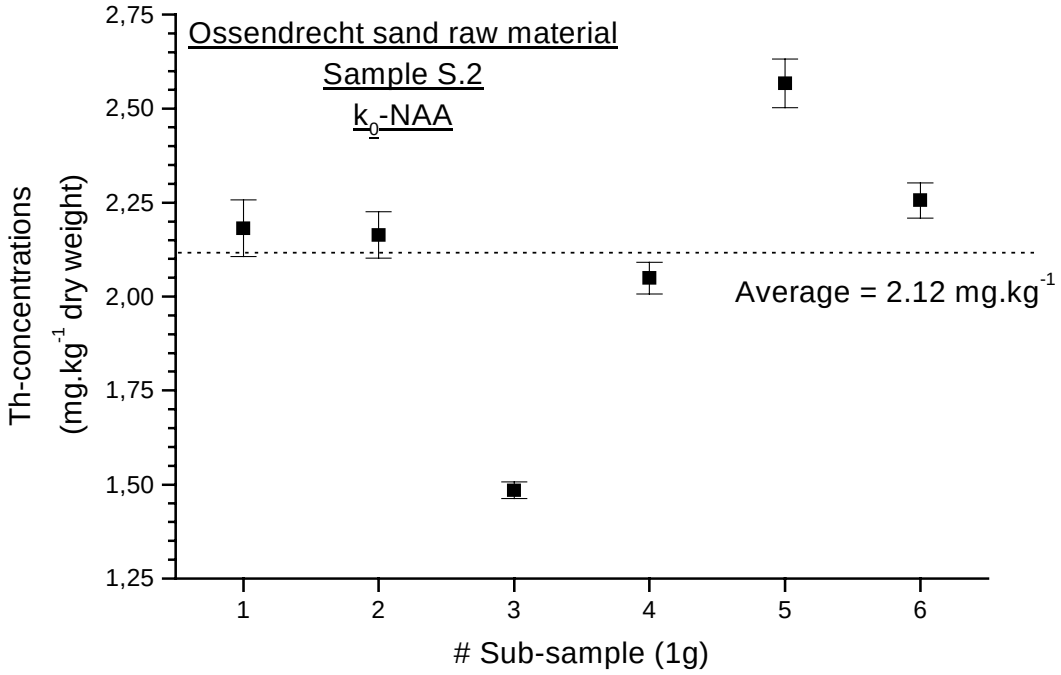

Fig. 5.10. Demonstration of the inhomogeneity for Th (± 2s uncertainties) in "raw" coversand sample S.2, using k_0-standardized instrumental neutron activation analysis on 1 gram sub-samples.

Table 5.2. The average concentrations of K, U and Th (± 2s standard deviation) measured for each sampling point ("step 1" material) as obtained via k_0-NAA and HPGe gamma spectrometry in Marinelli geometry.

Sample No.	K_0-NAA (raw material)			HPGe γ-spec. (raw material)		
	K (%) Dry weight	U (mg.kg^{-1}) dry weight	Th (mg.kg^{-1}) dry weight	K (%) dry weight	U (mg.kg^{-1}) Dry weight	Th (mg.kg^{-1}) dry weight
S.2	0.572 ± 0.088	0.81 ± 0.29	2.12 ± 0.71	0.561 ± 0.026	0.687 ± 0.039	1.826 ± 0.067
D	0.511 ± 0.049	0.723 ± 0.093	1.92 ± 0.32	0.552 ± 0.026	0.569 ± 0.032	1.688 ± 0.064
S.1	0.534 ± 0.034	0.622 ± 0.074	1.66 ± 0.11	0.517 ± 0.024	0.593 ± 0.042	1.660 ± 0.061
S.3	0.538 ± 0.039	0.59 ± 0.36	1.69 ± 0.53	0.561 ± 0.026	0.684 ± 0.039	1.837 ± 0.069

5.3.3. Need for homogenization

From the above findings it appears that the sample must be homogenized, for instance via manually grinding in a porcelain mortar. The grinding is not only necessary for homogenizing but also for having a smaller particle size to perform alpha and beta counting [see Chapter 4 Section 4.5.3]. It is worth mentioning that the sample is expected to be homogeneous at the 1.5 kg level, and the results from the gamma spectrometry in Marinelli geometry might therefore be considered as reliable.

5.4. Analysis of "step 2" material (manually ground sand)

5.4.1. k_0-NAA

k_0-NAA was performed in 3 fold for each sample. The obtained K, U and Th concentrations for these manually ground samples are shown in Table 5.3.

As seen, the standard deviations (2s) on the K, U, and Th concentrations are improved now, which indicates that the material became homogeneous. On the other hand, the concentrations became higher, especially for U and Th, and to a lesser extent for K.

Table 5.3. The concentrations of K, U and Th (± 2s standard deviation) determined via k_0-NAA in manually ground samples and HPGe gamma spectrometry in Marinelli geometry in "raw" material.

Sample No.	k_0-NAA (manually ground material)			HPGe γ-spec. (raw material)		
	K (%) dry weight	U ($mg.kg^{-1}$) dry weight	Th ($mg.kg^{-1}$) dry weight	K (%) dry weight	U ($mg.kg^{-1}$) dry weight	Th ($mg.kg^{-1}$) dry weight
S.2	0.667 ± 0.018	1.030 ± 0.058	2.90 ± 0.18	0.561 ± 0.026	0.687 ± 0.039	1.826 ± 0.067
D	0.520 ± 0.012	0.728 ± 0.021	2.13 ± 0.17	0.552 ± 0.026	0.569 ± 0.032	1.688 ± 0.064
S.1	0.5690 ± 0.0060	0.888 ± 0.053	2.202 ± 0.058	0.517 ± 0.024	0.593 ± 0.042	1.660 ± 0.061
S.3	0.615 ± 0.011	0.710 ± 0.042	2.258 ± 0.074	0.561 ± 0.026	0.684 ± 0.039	1.837 ± 0.069

5.4.2. Alpha counting

The low U and Th contents in the sand had their effect on the alpha counting time. Of each of the manually ground materials, 1 g was measured for as long as 2 weeks (cfr. 1 week in the case of loess) with the Elsec 7286 low-level α-counting system, as outlined in Chapter 4 Section 4.5. Due to the long counting times required, only one counting was performed, namely after the sample was sealed and stored for at least 4 weeks. The measured alpha dose-rates for the manually ground samples are significantly higher than the ones calculated from HPGe gamma-ray spectrometry in Marinelli geometry measurements (raw material), as shown in Table 5.4. For this comparison, conversion factors (concentrations → count rates → dose-rates) were taken from recent literature [Aitken, 1998].

Table 5.4. Comparison of measured and calculated α dose-rates for manually ground samples (± 2s uncertainties).

Sample No.	Measured α dose-rate (manually ground material) ($Gy.ka^{-1}$)	Calculated α dose-rate (HPGe γ-spec. of raw material) ($Gy.ka^{-1}$)	Ratio (measured / calculated)
S.2	0.417 ± 0.014	0.2763 ± 0.0042	1.510 ± 0.054
D	0.345 ± 0.013	0.2401 ± 0.0034	1.438 ± 0.058
S.1	0.350 ± 0.013	0.2439 ± 0.0041	1.434 ± 0.059
S.3	0.355 ± 0.014	0.2763 ± 0.0039	1.286 ± 0.054
	Mean		1.417 ± 0.095

5.4.3. Beta counting

In the case of beta counting, the measuring time for each sub-sample (~3 g) was maintained at 24 hours - the same as for loess - in each of the 5 counting positions of the Risø low-level GM-25-5 multicounter system (see Chapter 4 Section 4.6). Here also, the measured beta dose-rates for the manually ground samples are significantly higher than the ones calculated from the HPGe gamma ray spectrometry in Marinelli geometry measurements (raw material), as shown in Table 5.5.

Table 5.5. Comparison of measured and calculated β dose-rates for manually ground samples (± 2s uncertainties).

Sample No.	Measured β dose-rate (manually ground material) ($Gy.ka^{-1}$)	Calculated β dose-rate (HPGe γ-spec. of raw material) ($Gy.ka^{-1}$)	Ratio (measured / calculated)
S.2	0.833 ± 0.027	0.588 ± 0.020	1.417 ± 0.067
D	0.626 ± 0.021	0.560 ± 0.020	1.118 ± 0.055
S.1	0.681 ± 0.022	0.536 ± 0.019	1.271 ± 0.061
S.3	0.719 ± 0.024	0.588 ± 0.020	1.223 ± 0.059
	Mean		1.26 ± 0.12

5.4.4. Need for contamination-free homogenization method

The inhomogeneity effect could be eliminated by manually grinding the sample in a porcelain mortar, as is shown by the improved precision on the analysis results. However, the results also indicate that by doing so, the samples are seriously contaminated (concentrations increased ~ 8% for K, ~ 32% for U and ~ 35% for Th). Indeed, all techniques applied to the manually ground material yielded significantly higher dose-rates than when applied to the raw (dried, but otherwise untreated) sediment. Therefore, the source of the discrepancy must be sought in the grinding. Sand is harder than porcelain and can erode the mortar during the (sometimes quite lengthy) grinding process. Since the main constituent of porcelain is kaolin, which contains higher amounts of U and Th and lower of K, this will give rise to too high concentrations.

Taking into account the above mentioned contaminations in the case of Ossendrecht sand, and considering the higher elemental contents in Volkegem loess compared to Ossendrecht sand (~ 3.2 × higher for K, ~ 4.0 × higher for U and ~ 5.8 × higher for Th), one could at maximum expect contaminations of ~ 2.5% for K, ~ 8.2% for U and ~ 6.1% for Th in Volkegem loess after manually grinding it in a porcelain mortar. That this contamination did not happen (or was insignificant), is due to the fact that the abrasive action of sand (for which longer grinding times were necessary to obtain a powder passing through the 63 μm sieve) on porcelain is larger than that of loess.

In order to eliminate the inhomogeneity effect and to avoid contamination, a third approach for preparing the samples was therefore tested. The third approach consisted of "agate" ball-milling, followed by thorough mixing, of each sample, as described in Section 5.2.3.

5.5. Analysis of "step 3" material (ball-milled sand)

5.5.1. k_0-NAA

From the ball-milled homogenized material, 3 aliquots of 1g were analysed via k_0-NAA. The results for K, U and Th for the ball-milled homogenized material were not only much more reproducible (the standard deviation, when compared to the k_0-NAA results of the raw material, improved), but are also consistent with the HPGe gamma spectrometry in Marinelli geometry measurements, as shown in Table 5.6.

Table 5.6. The concentrations of K, U and Th (± 2s standard deviation) determined via k_0-NAA of the ball-milled material and HPGe gamma spectrometry in Marinelli geometry of the "raw" material.

.

Sample No.	k_0-NAA (ball-milled material)			HPGe γ-spec. (raw material)		
	K (%) dry weight	U ($mg.kg^{-1}$) dry weight	Th ($mg.kg^{-1}$) dry weight	K (%) dry weight	U ($mg.kg^{-1}$) dry weight	Th ($mg.kg^{-1}$) dry weight
S.2	0.558 ± 0.019	0.699 ± 0.032	1.91 ± 0.15	0.561 ± 0.026	0.687 ± 0.039	1.826 ± 0.067
D	0.4960 ± 0.0030	0.576 ± 0.011	1.66 ± 0.18	0.552 ± 0.026	0.569 ± 0.032	1.688 ± 0.064
S.1	0.5070 ± 0.0090	0.564 ± 0.011	1.583 ± 0.066	0.517 ± 0.024	0.593 ± 0.042	1.660 ± 0.061
S.3	0.541 ± 0.031	0.6100 ± 0.0090	1.703 ± 0.076	0.561 ± 0.026	0.684 ± 0.039	1.837 ± 0.069

5.5.2. Alpha counting

As is shown in Table 5.7, the measured alpha dose-rates for the ball-milled samples are consistent with the ones calculated from HPGe gamma ray spectrometry in Marinelli geometry.

Table 5.7. Comparison of measured and calculated α dose-rates (± 2s uncertainties) for ball-milled samples.

Sample No.	Measured α dose-rate (ball-milled material) ($Gy.ka^{-1}$)	Calculated α dose-rate (HPGe γ-spec. of raw material) ($Gy.ka^{-1}$)	Ratio (measured / calculated)
S.2	0.285 ± 0.012	0.2763 ± 0.0042	1.033 ± 0.046
D	0.238 ± 0.011	0.2401 ± 0.0034	0.992 ± 0.048
S.1	0.249 ± 0.010	0.2439 ± 0.0041	1.021 ± 0.046
S.3	0.273 ± 0.011	0.2763 ± 0.0039	0.989 ± 0.043
	Mean		1.009 ± 0.023

5.5.3. Beta counting

The beta dose-rates for ball-milled samples are also consistent with the ones calculated from HPGe gamma ray spectrometry in Marinelli geometry. This is shown in Table 5.8.

Table 5.8. Comparison of measured and calculated β dose-rates (± 2s uncertainties) for ball-milled samples.

Sample No.	Measured β dose-rate (ball-milled material) ($Gy.ka^{-1}$)	Calculated β dose-rate (HPGe γ-spec. of raw material) ($Gy.ka^{-1}$)	Ratio (measured / calculated)
S.2	0.610 ± 0.014	0.588 ± 0.020	1.037 ± 0.043
D	0.513 ± 0.010	0.560 ± 0.020	0.916 ± 0.038
S.1	0.545 ± 0.010	0.536 ± 0.019	1.017 ± 0.041
S.3	0.570 ± 0.010	0.588 ± 0.020	0.969 ± 0.038
	Mean		0.985 ± 0.054

5.5.4. Conclusion

For all samples, the concentrations and dose-rates obtained via k_0-NAA, alpha counting and beta counting are in good agreement with those predicted from gamma spectrometry, if ball-milling is used to prepare the samples. The precision improved greatly as well, when compared to the analyses of the untreated material.
It is therefore concluded that ball-milling (using an agate beaker and balls) yields a material that is homogeneous and not significantly contaminated, and that this material can be used for accurate and precise annual dose determination.

5.6. Evaluation of final results for the Ossendrecht site

As shown in Section 5.3.1, the U and Th decay series are in equilibrium in each of the samples. The trend of a lower ^{210}Pb content might point perhaps at ^{222}Rn escape in geological times, but if so, it is thought to be hardly significant.

The measured and calculated alpha and beta dose rates for each sampling point obtained via different analytical methods are shown in Figs 5.11 and 5.12, respectively. Dose conversion factors for the transformation of elemental concentrations or count rates to annual radiation doses [see Chapter 4 Section 4.9.2] were taken from recent literature [Aitken, 1998].

Whereas the HPGe gamma spectrometry measurement results are based on the raw materials, the results from ZnS alpha counting, GM beta counting and k_0-NAA are based on the ball-milled materials. The concentrations obtained from the field measurements were recalculated to the dry weight by introducing the moisture content, before converting to annual radiation doses.

It can be seen from Figs 5.11 and 5.12 that for the individual sampling point, the alpha and beta dose-rates obtained via the different analytical methods are consistent,

whereas the scatter between the sampling points is large. This might be due to a heterogeneous distribution of radionuclides throughout the profile. The large scatter in the k_0-NAA results of the raw sediment (see Section 5.3.2) supports this conclusion. Therefore, the results are plotted in Figs. 5.11 and 5.12 in another way as compared to Volkegem (the results from the different techniques are compared for each sample separately).

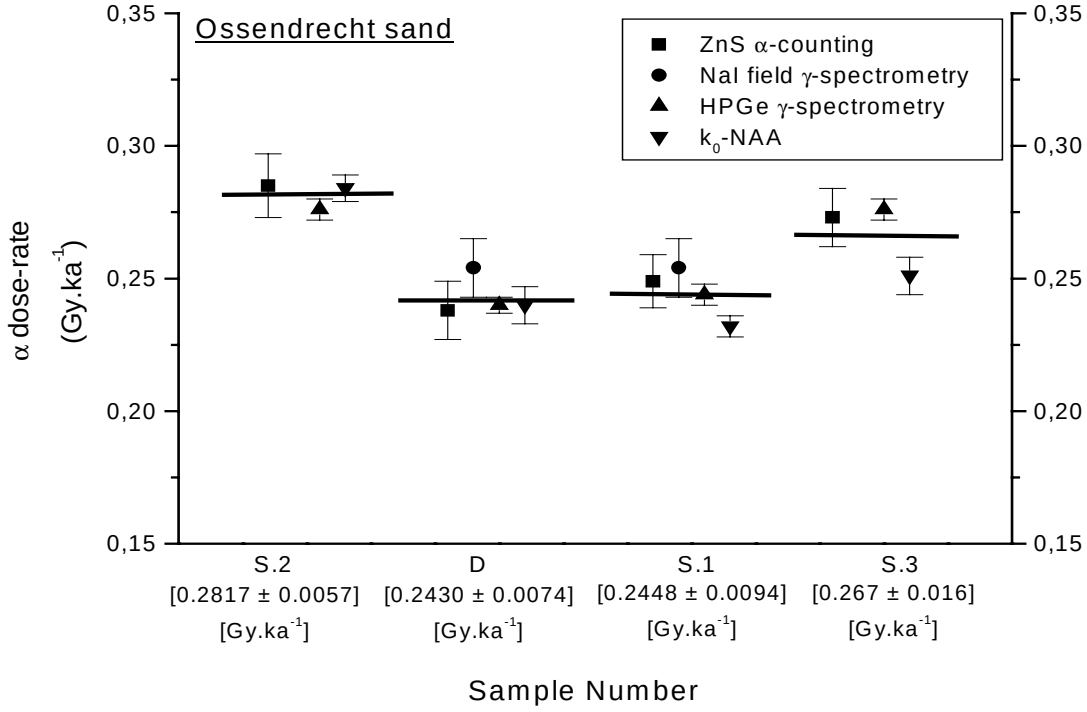

Fig. 5.11. The results of alpha dose-rate determinations (± 2s uncertainties) using different analytical techniques. The mean value for each sampling point is specified by a solid line and is also given in square brackets.

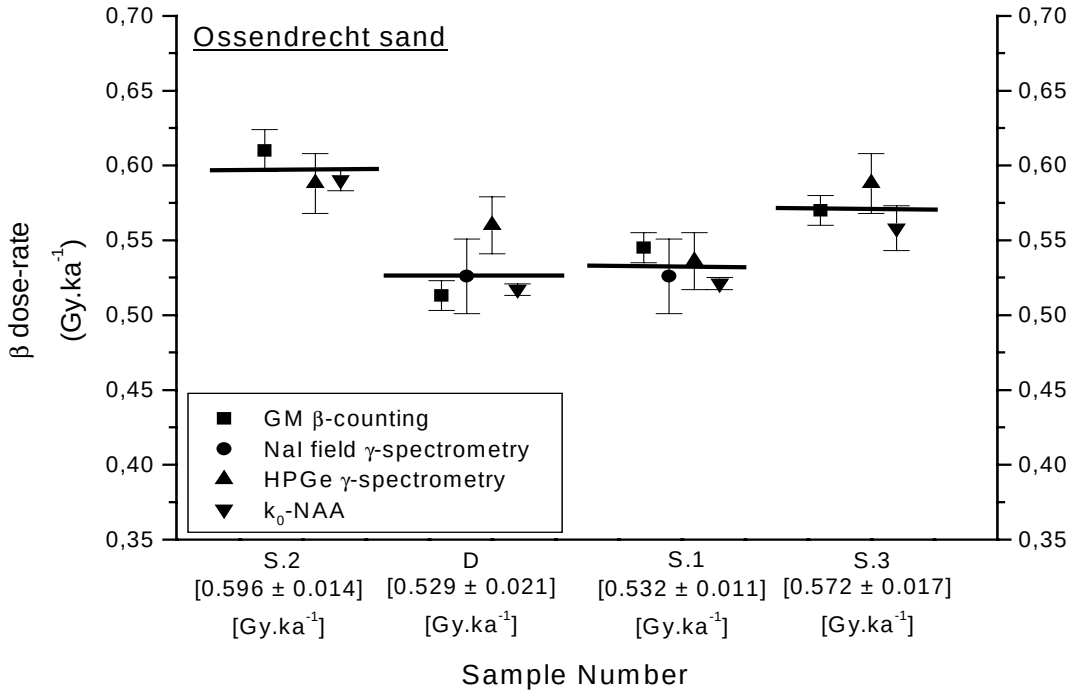

Fig. 5.12. The results of beta dose-rate determinations (± 2s uncertainties) using different analytical techniques. The mean value for each sampling point is specified by a solid line and is also given in square brackets.

In order to calculate the beta dose-rate from field measurements, the K concentration via the "Oxford" calibration was not taken into account, because this value is always on the lower side when comparing with other analytical methods (Fig. 5.13). This tendency was also observed in the case of Volkegem loess [see Chapter 4 Section 4.9.1]. The mean K concentration of sampling points D and S.1 is plotted because they are at the same height in the profile and originate from the same layer of sediment.

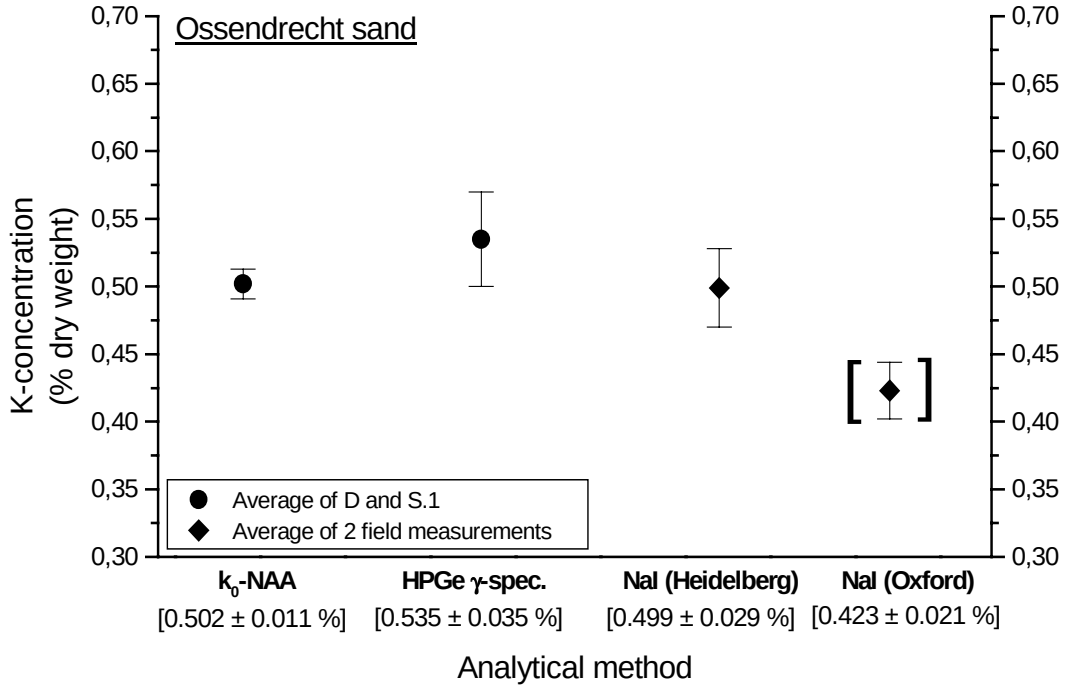

Fig. 5.13. The results of K concentration determinations (± 2s uncertainties) using different analytical methods. The mean vales are given in square brackets. The value obtained via the Oxford calibration block is put in bold square brackets. Note that all results are related to the same height in the profile (samples D and S.1).

The mean U and Th concentrations from the two field measurements obtained via the Heidelberg and the Oxford calibration are shown in Table 5.9.

Table 5.9. The results of U and Th concentrations from the field γ-spectrometry, calibrated via the Heidelberg natural granite block and the Oxford concrete blocks.

Calibration	U, $mg.kg^{-1}$ ± 2s	Th, $mg.kg^{-1}$ ± 2s
Heidelberg	0.574 ± 0.051	1.777 ± 0.072
Oxford	0.641 ± 0.022	1.748 ± 0.038
Mean	0.608 ± 0.067	1.762 ± 0.041

It should be noted that k_0-NAA also allowed the determination of Rb, for which values were found of 22.89 ± 0.36 mg.kg^{-1} in S.2, 19.67 ± 0.42 mg.kg^{-1} in D, 21.74 ± 0.91 mg.kg^{-1} in S.1 and 21.92 ± 0.31 mg.kg^{-1} in S.3. The uncertainties mentioned are 2s, and the largest of the internal or external uncertainty was adopted.

The alpha, beta and gamma dose-rates determined for each sampling point are shown in Table 5.10. The dose-rates were calculated from the concentrations determined via HPGe gamma spectrometry in Marinelli geometry, k_0-NAA and NaI(Tl) field gamma spectrometry (field gamma spectrometry results were considered only for the sampling points D and S.1), and from the alpha and beta count rates. The cosmic dose-rates for the sampling points S.2, D and S.3 at depths of 9.65 m, 9.45 m and 9.26 m, respectively, were calculated following Prescott and Hutton [1994], assuming an uncertainty (2s) of 15%.

Table 5.10. The alpha, beta and gamma dose-rates (± 2s uncertainties) in the Ossendrecht sand profile.

Sample Number	α dose-rate Gy.ka^{-1}	β dose-rate (K, U, Th) Gy.ka^{-1}	β dose-rate (Rb) Gy.ka^{-1}	γ dose-rate Gy.ka^{-1}	Cosmic dose-rate Gy.ka^{-1}	Total Dose-rate Gy.ka^{-1}
S.2	0.2817 ± 0.0057	0.596 ± 0.014	0.00870 ± 0.00014	0.3035 ± 0.0050	0.144 ± 0.022	1.335 ± 0.027
D	0.2430 ± 0.0074	0.529 ± 0.021	0.00747 ± 0.00016	0.2727 ± 0.0082	0.141 ± 0.021	1.194 ± 0.032
S.1	0.2448 ± 0.0094	0.532 ± 0.011	0.00826 ± 0.00035	0.2697 ± 0.0068	0.141 ± 0.021	1.196 ± 0.026
S.3	0.267 ± 0.016	0.572 ± 0.017	0.00833 ± 0.00012	0.292 ± 0.019	0.138 ± 0.021	1.277 ± 0.037

On the average, the alpha, beta, gamma and cosmic dose-rates contribute for 21%, 45%, 23% and 11%, respectively, to the total annual radiation dose. The contribution from Rb is negligible (less than 1%), whereas the contribution from cosmic radiation, due to the low activity of the sand, clearly is not. It is worth mentioning that, for coarse-grain luminescence dating of these deposits, the alpha contribution and the contribution from Rb should not be taken into account, and that the effective beta

dose-rate is 10% lower, as explained in Aitken [1998] in general, and in Vandenberghe et al. [2003a] more specific in the case of Ossendrecht. Furthermore, it must be realized that the dose-rates listed in Table 5.10 refer to the dry material. To obtain the effective "wet" dose-rates, allowance must be made for the fact that water in the pores of the sediment absorbs a part of the radiation that would otherwise reach the sample [Aitken, 1985].

In general, it is concluded that for each sample, all analytical techniques yielded consistent results. The results for samples S.1 and D are in perfect agreement, as expected since they were taken from the same height in the profile. The difference between the dose-rates for the vertically separated samples, points to an inhomogenous distribution of radio-nuclides throughout the profile. It is concluded that the results are of sufficient accuracy and precision and can be relied upon in dose-rate determination, on condition that proper care is taken during sampling and sample preparation.

- CHAPTER 6 -

SUMMARY AND CONCLUSIONS

The luminescence dating method is based on the measurement of the light (= luminescence) that crystalline minerals such as quartz or feldspars are emitting upon heating (TL - thermoluminescence) or when they are exposed to light (OSL - optically stimulated luminescence). The amount of luminescence emitted is proportional to the total received natural radiation dose. The latter, called the palaeodose, is built up by energy deposition by radiation (alpha, beta and/or gamma) emitted by the natural occurring radio-nuclides ^{232}Th, ^{235}U, ^{238}U (and their decay products) and ^{40}K - in addition to smaller contributions from ^{87}Rb and cosmic radiation - both from within the investigated mineral grains and from their surroundings. The luminescence dating method thus consists of two main analytical parts: i) the determination of the palaeodose - itself composed of a measurement of the natural luminescence signal and of the sensitivity, the latter via artificially adding a known radiation dose; and ii) the determination of the annual radiation dose, which is assumed to be constant with time. Comparison of the palaeodose with the annual radiation dose then permits the determination of the age of the sample. The age obtained is the time elapsed since the last "zeroing" of the luminescence signal, such as the moment of heating when producing ceramics, or the moment of exposure to sunlight during transport and deposition of sediments.

It is obvious that the experimental determination of the annual radiation dose is an important step in luminescence dating, since its uncertainty is linearly transferred to the age result. The aim of this thesis was to carry out an experimental study and a performance evaluation of some commonly applied methods for the determination of the annual radiation dose in luminescence dating of sediments. To this aim, two types of materials were investigated: a loess sediment, collected from a profile at Volkegem (southern part of East-Flanders, Belgium); and a coversand, collected from a deposit at Ossendrecht (south-western part of the Netherlands).

The material dealt with first was the Volkegem loess sediment, for which the following methods were investigated: NaI(Tl) gamma-ray spectrometry both in field (in-situ) and in low-background laboratory conditions for the measurement of K, U and Th; extended energy-range Ge gamma-ray spectrometry in low-background laboratory conditions for the measurement of K, U and Th, and also for the detection of possible disequilibria in the Th- and especially the U-decay series; thick source ZnS alpha counting, both in the integral mode for the measurement of U + Th and in the pair-counting mode for the discrimination between U and Th; low-background GM beta counting for the measurement of K + U + Th; instrumental reactor neutron activation analysis (INAA) for the determination of K, U, Th and Rb; and atomic absorption spectrometry (AAS) for the determination of K.

When determining the annual radiation dose, NaI(Tl) field measurements in auger hole geometry are very suitable since they are a true indicator of the environment surrounding the material to be dated. In the Volkegem loess profile, five field measurements were performed via a portable gamma spectrometry system (Canberra Portable Plus Model 1150) equipped with a 3×3″ NaI(Tl) detector, followed by collection of 15 samples which were then analysed in the lab (see further). From these field measurements, it was possible to get the number of counts (via window counting - using spectrum stripping, or via gamma spectrometry) associated with gamma-lines of ^{40}K at 1460.8 keV, of ^{214}Bi (in the ^{238}U decay chain) at 1764.5 keV and of ^{208}Tl (in the ^{232}Th decay chain) at 2614.5 keV. Then, using a calibration measurement, it was possible to obtain the K, U and Th content in the loess, which could be converted to the annual radiation doses. Calibration was done via measurements in blocks with an extended geometry of a material containing known amounts of K, U and Th, and having a borehole to insert the NaI(Tl) detector. Two sets of calibration blocks were used:

1) at the Forschungsstelle Archäometrie, MPI, Heidelberg, Germany, which is a natural granite block [Flossenburg Granite] of 1 × 1× 1 m, with K, U and Th concentrations (by weight) of 4.08 ± 0.11%, 18.8 ± 1.3 mg.kg^{-1} and 14.0 ± 0.9 mg.kg^{-1}, respectively;

2) at the Research Laboratory for Archaeology and the History of Art (RLAHA), Oxford University, UK, where there are three concrete blocks of 0.51×0.51×0.51 m doped with K, U and Th [plus one undoped "background" block], for which so called "effective" doping concentrations (by weight) are given of 5.71 % K, 117 $mg.k^{-1}$ U and 126 $mg.kg^{-1}$ Th (additionally including 4.8 $mg.kg^{-1}$ U), respectively, with no uncertainties specified.

The spectra measured in the field and in the calibration blocks were analyzed in two different ways according to the calibration type. For the "Heidelberg" calibration, gamma spectrometry was done in which all net peak area determinations of the relevant gamma-peaks were performed using the Hypermet-PC software package. On the other hand, the Oxford calibration blocks were rather developed for "window counting" with spectrum stripping, and - since in each a full spectrum was measured - the setting of the windows could be easily based on the location of the peaks, so that effects of possible temperature shift were minimized.

A study was made of the corrections that are needed in calibrating the field measurements via both the "Heidelberg" and the "Oxford" blocks. These corrections have to be introduced because of the different counting conditions of field and block measurements (with respect to geometry, composition and density of the material) and because of the non-infiniteness of the calibration blocks. It was found that the "Heidelberg" block can be considered as "quasi-infinite" and only requires "composition and density" corrections of a few percent; the "Oxford" concrete blocks, on the other hand, are far from infinite and this was in fact accounted for by working with "effective" concentrations of elements as reported to us by RLAHA, Oxford.

The cylindrical undisturbed loess samples collected from the field and brought to the laboratory were analysed with NaI(Tl) gamma-ray spectrometry (the instrument used is the same as the one in the field, except that the NaI(Tl) detector is mounted in a low-background lead castle) and with extended energy-range Ge gamma-ray spectrometry, by using a Canberra XtRa detector in a low-background lead castle. Both the NaI(Tl) and Ge gamma-ray measurements were calibrated in an absolute

way via introduction of peak detection efficiencies, of correction factors for true-coincidence effects and of nuclear data. For Ge gamma-ray spectrometry, also a relative calibration was performed, based on the use of IAEA radiometric reference materials RGK-1, RGU-1 and RGTh-1. Both the NaI(Tl) and the Ge measurements yielded K, U and Th concentrations, which could then be converted to annual radiation doses. In addition, with the Ge measurements various daughters in the U and Th decay chains could be measured, thus allowing to check if the decay series are in equilibrium.

After finishing the gamma-ray spectrometric measurements, the samples were dried at 110^{o}C until constant weight. The elemental composition of the dried loess material was determined via XRF analysis. This information on the elemental composition was required for the calculation of the effective solid angles in the gamma spectrometric measurements and also for k_0-NAA. For alpha and beta counting, the dried material was finely ground (manually in a porcelain mortar) and sieved (using a 63 μm sieve) to obtain a particle size of less than 63 μm

Thick source alpha counting was performed using two ELSEC 7286 low-level alpha counting systems each equipped with three scintillation/PM tube measuring units. Calibration of the six counters involved determination of the high voltage plateau and adjustment of the threshold voltage. Calibration was done via the granite standard GS-N. The validation of the calibration settings was performed via the measurement of several geo-standards (RGU-1, RGTh-1 and Biotite Mica, Fe) with known U and Th-contents. It not only allowed to determine the combined total alpha dose-rate from U and Th, but also – via built-in "pair counting" electronics - to discriminate between U and Th. Using proper conversion factors, the beta dose-rate originating from these radio-elements could be derived from alpha-counting as well.

Beta counting was performed using the Risø low-level GM-25-5 multicounter system. Calibration was done with U standards RGU-1 and CRM 105-A, Th standards RGTh-1 and CRM 109-A and a series of home-made K standards. It was found that the calibration factors were to a good approximation element-independent and did not

vary with the concentration of the element in the standard. Via the calibration factors, the results of beta counting could be converted to total beta dose-rates.

Instrumental neutron activation analysis was performed with the use of the k_0-standardization method. It involved irradiation of about 500 mg samples, together with a certified IRMM-530 Al-0.1% Au monitor, in a calibrated irradiation facility of reactor Thetis (Gent), followed by three countings on a calibrated HPGe gamma-ray spectrometer. The K-content was obtained via the measurement of ^{42}K (12.4 h) after a decay time of ~ 65 h, the U-content via the measurement of ^{239}Np (2.36 d) after a decay time of ~ 5 d, and the Th-content via the measurement of ^{233}Pa (27.0 d) after a decay time of ~ 3 weeks. Gamma-spectrum analysis was done via the Hypermet-PC software, and concentration calculation was based on the Kayzero/Solcoi software package. Noteworthy is the possibility of k_0-NAA to give "automatically" information on the Rb-content [via the measurement of ^{86}Rb (18.6 d) together with ^{233}Pa], for which otherwise a K:Rb ratio of 200 to 400 is tacitly assumed.

Atomic absorption spectrometry was applied to determine K. Use was made of a Varian SpectrAA-600 instrument, which is a double beam spectrometer equipped with a hollow cathode lamp and an acetylene-air flame ionization system. Calibration was done by measuring a series of home-made K standard (potassium biphtalate) solutions.

A comparative study of the above described methods for the determination of the annual radiation dose for Volkegem loess sediment indicated that consistent and sufficiently reliable results were obtained for: NaI(Tl) field gamma-ray spectrometry both via the "Heidelberg" and the "Oxford" calibration blocks, low-background NaI(Tl) gamma-ray spectrometry in the laboratory, low-background extended-range Ge gamma-ray spectrometry assisted by relative calibration (at the same time indicating equilibrium in both the U and Th decay series), k_0-standardized reactor neutron activation analysis, thick source ZnS alpha counting in the integral mode, and low-background GM beta counting. Methods yielding somewhat inconsistent or less precise results were found to be: absolutely calibrated Ge gamma-ray spectrometry,

ZnS alpha counting in the pair mode and atomic absorption spectrometry. For all three elements (K, U and Th), the best technique was found to be low-background extended-energy range Ge gamma-ray spectrometry with relative calibration, because it offers good precision and accuracy and simultaneously allows studying the radioactive equilibrium of the U and Th decay series.

The second material studied was the Ossendrecht coversand. In the profile, two NaI(Tl) gamma-ray field measurements were performed and four sampling points were chosen. From each sampling point about 3 kg material was collected and brought to the laboratory for analysis (after drying at 110°C until constant weight) with the following techniques: low-background extended-energy range (XtRa) HPGe gamma-ray spectrometry in Marinelli geometry, assisted by relative calibration; k_0-standardized instrumental reactor neutron activation analysis (k_0-INAA); low-background GM beta counting; and thick source ZnS alpha counting in the integral mode. Methods of somewhat poorer quality formerly observed in the analysis of loess sediment were cancelled for the analysis of Ossendrecht sand: absolutely calibrated XtRa HPGe gamma-ray spectrometry, ZnS alpha counting in the pair mode and atomic absorption spectrometry. Due to the low concentration of K, U and Th present in the here investigated sand samples (see further), low-background NaI(Tl) gamma-ray spectrometry in the laboratory was also cancelled.

Contrary to what was formerly experienced in the case of loess sediment, the determination of the annual radiation dose for the coversand deposit at Ossendrecht revealed two specific problems: 1) the low concentration of K, U and Th present in the sample, and 2) sample inhomogeneity at the gram level. Due to these problems, different approaches for sample preparation for the laboratory measurements had to be tried until satisfactory results were obtained.

In a first approach, the dried material was homogenized by simply stirring it in a bucket and was then analysed via low-background XtRa HPGe gamma spectrometry in Marinelli geometry and via k_0-NAA.

The encountered problems could be avoided by measuring a large volume of sample (1.5 kg) in Marinelli geometry with the low-background XtRa HPGe detector. Standardization was done in a relative way, and since such a large mass of standard is not easy to find commercially, use was made of the well-characterized Volkegem loess sediment. Whereas the counting geometry for the samples and the standards was identical, their chemical composition (determined via XRF analysis) and packing density were introduced when calculating the effective solid angle. The measurements yielded K, U and Th concentrations. The decay chains of U and Th show equilibrium, although a tendency of a small but systematic decrease can be observed for ^{210}Pb in the ^{238}U decay series. This might suggest a (hardly significant) disequilibrium caused by slight ^{222}Rn escape in geological times.

As for the K, U and Th concentrations obtained via k_0-NAA, a considerable scatter was now observed between different sub-samples [although the sample mass was increased from 500 mg to 1 g]. The scatter points at an inhomogeneous distribution of radionuclides at the gram level. Nevertheless, the average concentration for each sampling point was in general consistent with the results obtained via HPGe gamma spectrometry in Marinelli geometry. Since the sample is expected to be homogeneous at the 1.5 kg level, the results obtained via gamma spectrometry were considered as reliable.

To overcome the problem of inhomogeneity, a second approach for preparing the samples was tried. About 20 g dried sand material (for each sample) obtained in the first step was manually ground in a porcelain mortar, sieved (using a 63 μm sieve) and further homogenized. From this material gram-sized sub-samples were taken for k_0-NAA, ZnS alpha counting and GM beta counting.

The k_0-NAA results (for different sub-samples) from these manually ground samples were quite reproducible but consistently too high especially for U and Th, and to a lesser extent for K. Also the alpha and beta dose-rates for the manually ground samples, obtained via thick source alpha counting and GM beta counting, respectively, were significantly higher than the ones calculated from HPGe gamma spectrometry in Marinelli geometry.

These findings with the manually ground samples indicated that the inhomogeneity effect at the gram level could be eliminated by grinding the sample in a porcelain mortar, but that this also seriously contaminated the material.
On the basis of the above, one would also expect a contamination of the Volkegem loess, when manually ground in a porcelain mortar. That this contamination was insignificant was due to the fact that the abrasive action of sand on porcelain was larger than that of loess.

In order to eliminate the inhomogeneity effect at the gram level and to avoid contamination, the sampling approach for k_0-NAA, alpha counting and beta counting was adjusted. As a third step, about 200 g material obtained in the first step was randomly sampled from the bucket and was ground by ball-milling in a Pulverizer6 (Planetary Mono Mill, FRITSCH), followed by a further homogenizing step. This ball-milled material was again analyzed via k_0-NAA (in different sub-samples), alpha and beta counting. The k_0-NAA results of ball-milled homogenized material for K, U and Th were not only much more reproducible (the standard deviation improved when compared to the untreated material), but were also consistent with the results from HPGe gamma spectrometry in Marinelli geometry. Moreover, the measured alpha and beta dose-rates for the ball-milled samples were quite consistent with the ones calculated from HPGe gamma ray spectrometry in Marinelli geometry. These findings illustrated that the ball-milling (using an agate beaker and balls) yielded a material that was homogeneous and not significantly contaminated.

Due to inhomogeneity of the Ossendrecht profile, the results were presented in another way as compared to Volkegem, where the profile was homogeneous. In fact, in Volkegem the various analytical methods were investigated with respect to their performance, whereas for Ossendrecht they were applied to investigate the profile. The measured and calculated alpha and beta dose-rates, obtained via different analytical methods, were compared for each sampling point. The different methods yielded consistent results for each individual sampling point, whereas the scatter between the sampling points was large. This might be due to a heterogeneous distribution of radionuclides throughout the profile.

In general, it can be concluded that for the determination of the annual radiation dose in loess and sand sediments, dedicated procedures of calibration, sample preparation and measurement were worked out, and that application of them led to consistent and satisfactory results.

In the study of loess sediment, the various analytical methods were investigated and specific calibration procedures had to be developed for some of these analytical methods. The annual radiation dose determination for loess sediment did not cause special difficulties. An important observation concerning the Volkegem loess, following from the systematic investigation performed in this thesis, is that the material studied is quite homogeneous. The average concentrations ± 2s standard errors are: (1.784 ± 0.019) % for K, (2.516 ± 0.036) $mg.kg^{-1}$ for U and (10.221 ± 0.082) $mg.kg^{-1}$ for Th. In fact, the *a priori* assumption of its homogeneity was a criterion for the selection of the Volkegem loess site.

Methods that were found to be of poorer quality in the analysis of the loess were eliminated when performing the exercise to investigate the Ossendrecht sand profile, for which, however, specific problems were encountered. These were related to the low K, U and Th content in the samples, and to inhomogeneity of the material at the gram level. Both problems were solved when appropriate analytical methods were applied and proper care was taken for sampling and sample preparation.

As a general conclusion, it can be stated that in this work an experimental study is presented of methods that can be used for dose rate determination in the luminescence dating of sediments. Although the study was quite extensive, it will become clear from the following that there is still need for further research.

For both the loess and the coversand samples investigated in this work, the U and Th decay series were found to be in equilibrium. Thus, the annual radiation dose determination did not cause any special difficulties. There are many depositional environments, however, in which radioactive disequilibrium does occur. In such cases, the dose rate will vary as a function of time and if this variation is not taken

into account, a wrong luminescence age might be obtained. It is therefore necessary to carry out an investigation of samples showing disequilibrium (of different types and degrees) to gain experience with, and to be able to, assessing how the dose rate evolves as a function of the burial time (which is the time span that is being dated), and to determine how the variations will effect luminescence ages.

Besides gamma-spectrometry, also alpha-spectrometry can be used to estimate the degree of equilibrium of the U and Th decay chains. It would be worthwhile to investigate this technique to find out how it performs in addition, and compared to, low-level gamma-spectrometry. A combination of gamma and alpha-spectrometry would furthermore allow a complete examination of the state of equilibrium of the U and Th decay chains.

As was shown in Chapter 5 Section 5.3.2, a large scatter was found for the U and Th concentrations in the Ossendrecht sand, which was attributed to a heterogeneous distribution of radionuclides throughout the profile. Although grinding the sample in a pulverizer increased the precision of analysis, an important question this heterogeneity raises is how it influences the dose rate received by the individual mineral grains that are being used for equivalent dose determination. Vandenberghe et al. (2003) observed broad equivalent dose distributions for the Ossendrecht samples and attributed these to small-scale variations in annual dose. These so-called microdosimetric variations are at present a hot topic for those concerned with luminescence dating of sediments, and they need quantification, especially because the scale of D_e-analyses is reduced to a few or even single grains. It would also be very useful in this regard to find out where exactly the radioactivity is located (inside the grains, in a coating around them, etc).

The use of luminescence dosimeters is an interesting alternative to the techniques used in this work. The use of dosimeters would allow both equivalent and annual dose determination by luminescence measurements alone. This is very important because not everybody has easy access to, or the necessary expertise in, the sometimes complicated and expensive analytical facilities required for accurate dose rate

determination. Especially α-Al_2O_3:C is a very promising phosphor due to its high sensitivity. The use of α-Al_2O_3:C grains, mixed with sediment, furthermore has the potential to investigate microdosimetric variations (Kalchgruber, 2002).

Finally, it would be interesting to investigate how all techniques perform for the analysis of sediments with an even lower radionuclide content. It is worth mentioning that in these cases one would expect the cosmic dose rate to become more important, and a more precise evaluation of this component consequently poses a new challenge for further research.

- APPENDIX A -

FIELD NaI(Tl) GAMMA-RAY SPECTROMETRY WITH THE USE OF THE OXFORD CALIBRATION BLOCKS

As mentioned in Chapter 4 Section 4.2.1.3.1, calibration of the field NaI(Tl) gamma-ray measurements, in auger hole geometry, was done via the use of voluminous blocks with known contents of the radioelements K, U and Th and containing a "borehole" for inserting the NaI(Tl) detector. These blocks are in fact simulating the field measurement conditions. Two types of blocks were used: the one at the Forschungsstelle Archäometrie, MPI, Heidelberg, Germany, which is a natural granite block containing known concentrations of K, U and Th; and those at the Research Laboratory for Archaeology and the History of Art, Oxford University, UK, which are three concrete blocks doped with respectively K, U and Th [plus one undoped "background" block]. Whereas the Heidelberg block is suitable for performing true gamma-ray spectrometry, the Oxford calibration blocks were rather developed for "window counting" with spectrum stripping [Aitken, 1985], and – since in each case a full spectrum was measured anyhow - the setting of the windows could be easily based on the location of the peaks, so that effects of possible temperature shift were minimized. The spectra collected from the Oxford concrete blocks (K-, U-, Th-doped blocks and background block), with the selected windows for the respective elements, are shown in Figs A1 – A4.

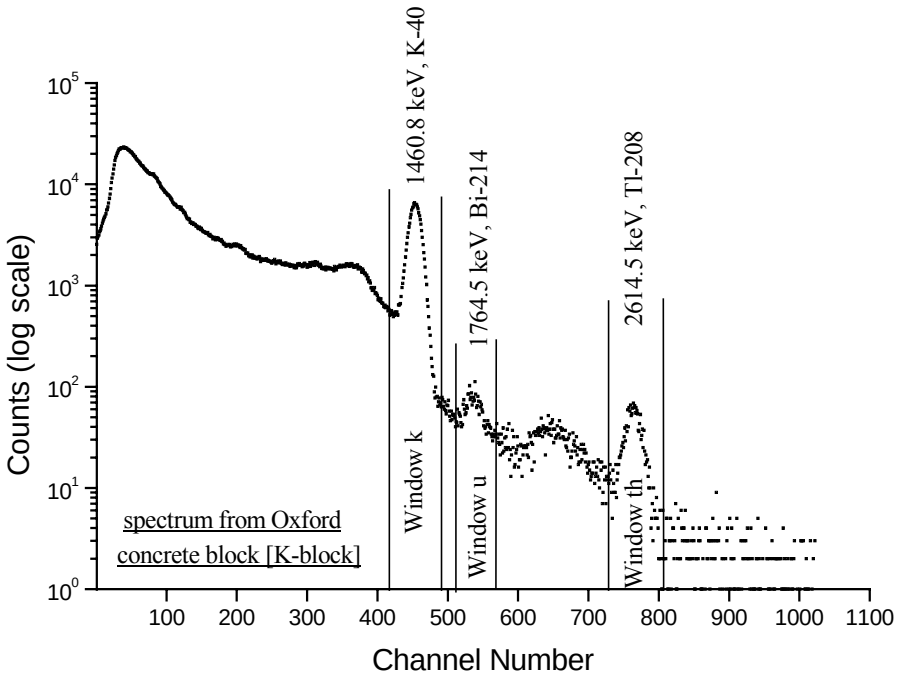

Fig. A1. NaI(Tl) spectrum collected from the Oxford concrete K-doped block during 45 min, showing the selected windows k, u and th of the radioelements K, U and Th, respectively.

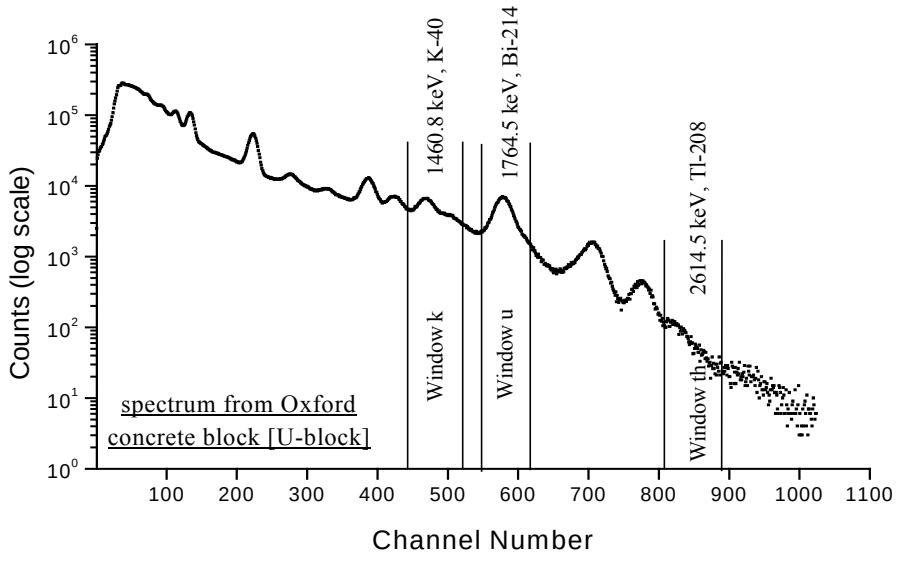

Fig. A2. NaI(Tl) spectrum collected from the Oxford concrete U-doped block during 45 min, showing the selected windows k, u and th of the radioelements K, U and Th, respectively.

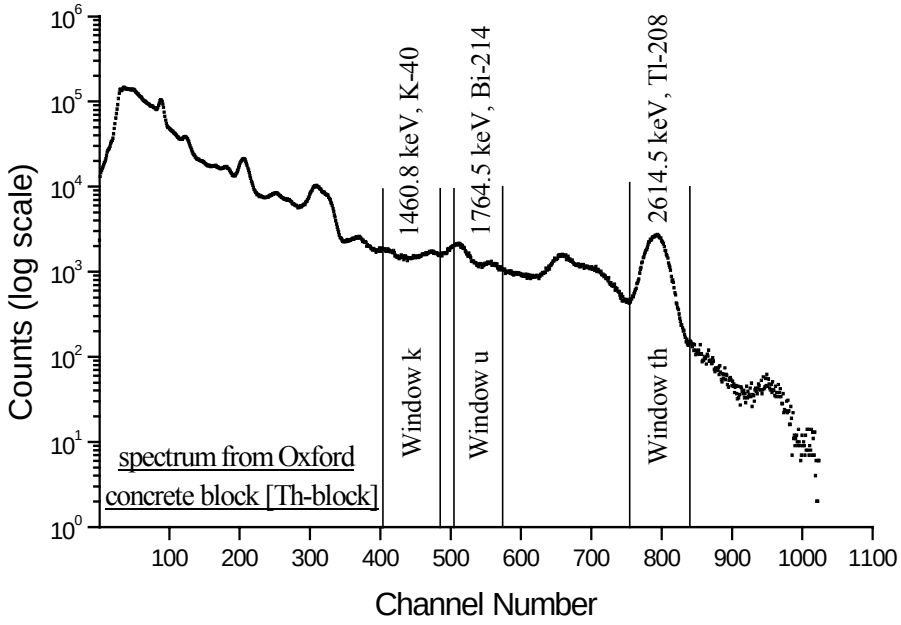

Fig. A3. NaI(Tl) spectrum collected from the Oxford concrete Th-doped block during 45 min, showing the selected windows k, u and th of the radioelements K, U and Th, respectively.

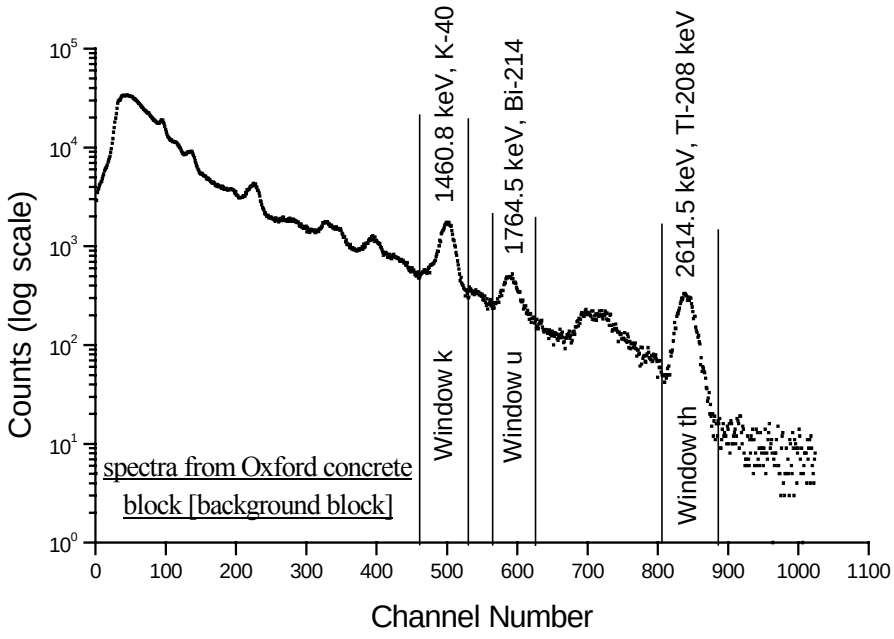

Fig. A4. NaI(Tl) spectrum collected from the Oxford concrete background-block during 3 h, showing the selected windows k, u and th of the radioelements K, U and Th, respectively.

A spectrum obtained from a field measurement (Volkegem loess), also indicating the three windows, is shown in Fig. A5.

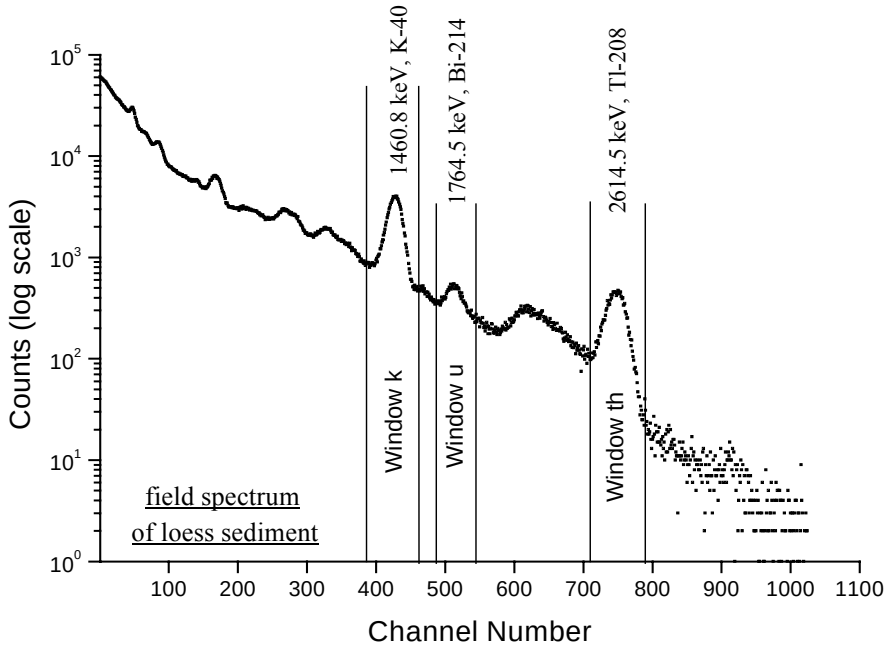

Fig. A5. NaI(Tl) field spectrum collected from Volkegem loess sediment during 2 h, showing the selected windows k, u and th of the radioelements K, U and Th, respectively.

In the spectra of the K-doped and background blocks and of the loess, the K, Th and U peaks are observed, and the corresponding "peak maximum" channel numbers can be defined. On the other hand, in the U- and Th-doped blocks only the U and Th peaks, respectively, can be seen. For these cases, the "maximum peak" channels for the unseen peaks of K and Th in the U-doped block were derived from the keV/channel ratio obtained from the U-peak, and the "maximum peak" channels for the unseen peaks of K and U in the Th-doped block were derived from the keV/channel ratio obtained from the Th-peak. Finally, based on the spectral shape for the block and field measurements, the peak widths were fixed (for all cases) as the "peak maximum" channel ± 35 channels for the K-window (window k), ± 26 channels for the U-window (window u) and ± 35 channels for the Th-window (window th).

For the measurement in the field the observed count rates in each window can be written as:

Field:

$$W_k = K(k) + Th(k) + U(k) + R_k \quad (A.1)$$

$$W_u = K(u) + Th(u) + U(u) + R_u \quad (A.2)$$

$$W_{Th} = K(th) + Th(th) + U(th) + R_{th} \quad (A.3)$$

where

W_k, W_u and W_{th} - the total count rates in the windows k, u and th, respectively;
K(k), Th(k), U(k) - the contribution from K, Th and U in the window k;
K(u), Th(u), U(u) - the contribution from K, Th and U in the window u;
K(th), Th(th), U(th) - the contribution from K, Th and U in the window th;
R_k, R_u and R_{th} - the contribution from cosmic rays and from the radioactivity in the detector itself, in the windows k, u and th.

For the measurements in the Oxford calibration blocks one can write:

K-block:

$$T(k) = B(k) + K(k) \quad (A.4)$$

$$T(u) = B(u) + K(u) \quad (A.5)$$

$$T(th) = B(th) + K(th) \quad (A.6)$$

U-block:

$$T(k) = B(k) + U(k) \quad (A.7)$$

$$T(u) = B(u) + U(u) \quad (A.8)$$

$$T(th) = B(th) + U(th) \quad (A.9)$$

Th-block (where the Th used for doping contained some U):

$$T(k) = B(k) + Th(k) + U(k) \quad (A.10)$$

$$T(u) = B(u) + Th(u) + U(u) \quad (A.11)$$

$$T(th) = B(th) + Th(th) + U(th) \quad (A.12)$$

where

T(k), T(u) and T(th) - total counts in the windows k, u and th, respectively;
B(k), B(u) and B(th) - contribution from background counts in the windows k, u and th, respectively;
K(k), K(u) and K(th) - contribution from K in the windows k, u and th, respectively;
U(k), U(u) and U(th) - contribution from U in the windows k, u and th, respectively;
Th(k), Th(u) and Th(th) - contribution from Th in the windows k, u and th, respectively.

The field measurement can be correlated with the block measurements as follows:

$$K(u)_{field} = \left[\frac{K(u)}{K(k)}\right]_{K-block} \times K(k)_{field} \quad (A.13)$$

$$K(th)_{field} = \left[\frac{K(th)}{K(k)}\right]_{K-block} \times K(k)_{field} \quad (A.14)$$

$$U(k)_{field} = \left[\frac{U(k)}{U(u)}\right]_{U-block} \times U(u)_{field} \quad (A.15)$$

$$U(th)_{field} = \left[\frac{U(th)}{U(u)}\right]_{U-block} \times U(u)_{field} \tag{A.16}$$

$$Th(u)_{field} = \left[\frac{Th(u)}{Th(th)}\right]_{Th-block} \times Th(th)_{field} \tag{A.17}$$

$$Th(k)_{field} = \left[\frac{Th(k)}{Th(th)}\right]_{Th-block} \times Th(th)_{field} \tag{A.18}$$

By replacing Eqns [(A.13) - (A.18)] into Eqns [(A.1) – (A.3)] one gets for the field:

$$W_k = K(k) + \left[\frac{Th(k)}{Th(th)}\right]_{Th-block} \times Th(th) + \left[\frac{U(k)}{U(u)}\right]_{U-block} \times U(u) + R_k \tag{A.19}$$

$$W_u = \left[\frac{K(u)}{K(k)}\right]_{K-block} \times K(k) + \left[\frac{Th(u)}{Th(th)}\right]_{Th-block} \times Th(th) + U(u) + R_u \tag{A.20}$$

$$W_{th} = \left[\frac{K(th)}{K(k)}\right]_{K-block} \times K(k) + Th(th) + \left[\frac{U(th)}{U(u)}\right]_{U-block} \times U(u) + R_{th} \tag{A.21}$$

From Eqns [(A.10) – (A.12)] one obtains:

$$Th(k)_{Th-block} = [T(k) - B(k)]_{Th-block} - \frac{U(k)_{U-block} \times 4.8}{117} \tag{A.22}$$

$$Th(u)_{Th-block} = [T(u) - B(u)]_{Th-block} - \frac{U(u)_{U-block} \times 4.8}{117} \tag{A.23}$$

$$Th(th)_{Th-block} = [T(th) - B(th)]_{Th-block} - \frac{U(th)_{U-block} \times 4.8}{117} \quad (A.24)$$

where 4.8 $mg.kg^{-1}$ and 117 $mg.kg^{-1}$ are the U-concentrations in the U-block and in the Th-block, respectively.

Now replacing Eqns [(A.22) and (A.23)] into Eqns [(A.19) and Eqns (A.20)], respectively, one gets:

$$W_k = K(k) + \frac{[T(k) - B(k)]_{Th-block} - \frac{U(k)_{U-block} \times 4.8}{117}}{[T(th) - B(th)]_{Th-block} - \frac{U(th)_{U-block} \times 4.8}{117}} \times Th(th) + \left[\frac{U(k)}{U(u)}\right]_{U-block} \times U(u) + R_k \quad (A.25)$$

$$W_k = \left[\frac{K(u)}{K(k)}\right]_{K-block} \times K(k) + \frac{[T(u) - B(u)]_{Th-block} - \frac{U(u)_{U-block} \times 4.8}{117}}{[T(th) - B(th)]_{Th-block} - \frac{U(th)_{U-block} \times 4.8}{117}} \times Th(th) + U(u) + R_u \quad (A.26)$$

$$W_{th} = \left[\frac{K(th)}{K(k)}\right]_{K-block} \times K(k) + Th(th) + \left[\frac{U(th)}{U(u)}\right]_{U-block} \times U(u) + R_{th} \quad (A.27)$$

Eqns [(A.7) – (A.9)] can be written as, respectively:

$$U(k)_{U-block} = [T(k) - B(k)]_{U-block} \quad (A.28)$$

$$U(u)_{U-block} = [T(u) - B(u)]_{U-block} \quad (A.29)$$

$$U(th)_{U-block} = [T(th) - B(th)]_{U-block} \quad (A.30)$$

and Eqns [(A.4) – (A.6)] can be written as, respectively:

$$K(k)_{K-block} = [T(k) - B(k)]_{K-block} \quad (A.31)$$

$$K(u)_{K-block} = [T(u) - B(u)]_{K-block} \quad (A.32)$$

$$K(th)_{K-block} = [T(th) - B(th)]_{K-block} \quad (A.33)$$

Now replacing Eqns [(A.28) – (A.33)] into Eqns [(A.25) – (A.27)] one obtains:

$$W_k = K(k) + \left[\frac{[T(k) - B(k)]_{Th-block} - \frac{[T(k) - B(k)]_{U-block} \times 4.8}{117}}{[T(th) - B(th)]_{Th-block} - \frac{[T(th) - B(th)]_{U-block} \times 4.8}{117}} \right] \times Th(th) + \left[\frac{T(k) - B(k)}{T(u) - B(u)} \right]_{U-block} \times U(u) + R_k \quad (A.34)$$

$$W_u = \left[\frac{T(u) - B(u)}{T(k) - B(k)} \right]_{K-block} \times K(k) + \left[\frac{[T(u) - B(u)]_{Th-block} - \frac{[T(u) - B(u)]_{U-block} \times 4.8}{117}}{[T(th) - B(th)]_{Th-block} - \frac{[T(th) - B(th)]_{U-block} \times 4.8}{117}} \right] \times Th(th) + U(u) + R_u \quad (A.35)$$

$$W_{th} = \left[\frac{T(th) - B(th)}{T(k) - B(k)} \right]_{K-block} K(k) + Th(th) + \left[\frac{T(th) - B(th)}{T(u) - B(u)} \right]_{U-block} \times U(u) + R_{th} \quad (A.36)$$

The coefficients of Th(th) in Eqns [(A.34) and (A.35)] are referred to as the stripping factors (hk) and (hu), respectively. The coefficients of U(u) in Eqns [(A.34) and (A.36)] are referred to as the stripping factors (uk) and (uh), respectively. The coefficients of K(k) in Eqns (A.35) and (A.36) are referred to as the stripping factors (ku) and (kh). Thus, these stripping factors can be written:

$$hk = \frac{[T(k) - B(k)]_{Th-b} - \left[\frac{[T(k) - B(k)]_{U-block} \times 4.8}{117}\right]}{[T(th) - B(th)]_{Th-block} - \left[\frac{[T(th) - B(th)]_{U-block} \times 4.8}{117}\right]} \quad \text{(A.37)}$$

$$hu = \frac{[T(u) - B(u)]_{Th-block} - \left[\frac{[T(u) - B(u)]_{U-block} \times 4.8}{117}\right]}{[T(th) - B(th)]_{Th-block} - \left[\frac{[T(th) - B(th)]_{U-block} \times 4.8}{117}\right]} \quad \text{(A.38)}$$

$$uk = \left[\frac{T(k) - B(k)}{T(u) - B(u)}\right]_{U-block} \quad \text{(A.39)}$$

$$uh = \left[\frac{T(th) - B(th)}{T(u) - B(u)}\right]_{U-block} \quad \text{(A.40)}$$

$$ku = \left[\frac{T(u) - B(u)}{T(k) - B(k)}\right]_{K-block} \quad \text{(A.41)}$$

$$kh = \left[\frac{T(th) - B(th)}{T(k) - B(k)}\right]_{K-block} \quad \text{(A.42)}$$

Introduction of Eqns [(A.37) – (A.42)] into Eqns [(A.34) – (A.36)] yields:

$$K(k) + (hk) \times Th(th) + (uk) \times U(u) + R_k - W_k = 0 \quad \text{(A.43)}$$

$$(ku) \times K(k) + (hu) \times Th(th) + U(u) + R_u - W_u = 0 \quad \text{(A.44)}$$

$$(kh) \times K(k) + Th(th) + (uh) \times U(u) + R_{th} - W_{th} = 0 \quad \text{(A.45)}$$

By measuring the window count-rates (W_k, W_u and W_{th}), the own contributions for K, U and Th can be determined from the following solutions of Eqns [(A.43) –(A.45)]:

$$K(k)=\frac{[W_u(uh)-(uh)R_u+R_{th}-W_{th}]\times[(hk)-(uk)(hu)]-[(uh)(hu)-1]\times[W_k-R_k-(uk)W_u+(uk)R_u]}{[(ku)(uh)-(kh)]\times[(hk)-(uk)(hu)]-[(uh)(hu)-1]\times[1-(uk)(ku)]} \quad (A.46)$$

$$U(u)=\frac{[(kh)(hk)-1][(W_k(ku)-(Ku)R_k+R_u-W_u]-[(kh)W_k+R_{th}-W_{th}-(kh)R_k]\times[(hk)(ku)-(hu)]}{[(kh)(hk)-1]\times[(ku)(uk)-1]-[(kh)(uk)-uh)]\times[(hk)(ku)-(hu)]} \quad (A.47)$$

$$Th(th)=\frac{W_{th}[1-(ku)(uk)]+W_k[(uh)(ku)-(kh)]+W_u[(kh)(uk)-(uh)]+R_{th}[(ku)(uk)-1]+R_k[(kh)-(uh)(ku)]+R_u[(uh)-(kh)(uk)]}{1-(ku)(uk)-(kh)(hk)+(hk)(ku)(uh)+(hu)(kh)(uk)-(hu)(uh)} \quad (A.48)$$

A numerical example of the calculations is given below.

Two measurements were performed for each of the K-, U- and Th- Oxford concrete blocks. The data obtained for the K-, U- and Th- windows for each block are shown in Table A.1.

The stripping factors hk, hu, uk, uh, ku and kh determined by using Eqns [(A.37) – (A.42)], are shown in Table A.2. Although the stripping factors ku and kh in principle should be zero, both factors are found here to be negative values, which were also taken into account for the calculation.

Window data for a field measurement in the Volkegem loess profile are shown in Table A.3.

The contribution from K, U and Th [K(k), U(u) and Th(th), respectively] into their own window determined by using Eqns [(A.46) – (A.48)], is shown in Table A.4. The

values of R_k (= 2.25 cpm), R_u (= 0.85 cpm) and R_{th} (= 1.12 cpm) were taken from the literature [Aitken, 1985].

Table A.1. Results of measurements in the Oxford concrete blocks.

Blocks	Measu-rement No.	K-window (peak channel ± 35 channels)		
		Window range Left–peak–right Channel	Total window counts	Window count rate (cpm)
K block	Meas.1	420 - 455 - 490	145946	3243
	Meas.2	448 - 483 - 518	146239	3250
U block	Meas.1	446 - 481 - 516	340514	7567
	Meas.2	454 – 489 - 524	339136	6970
Th block	Meas.1	409 - 444 - 479	112019	2489
	Meas.2	424 – 459 - 494	108790	2418
back-ground block	Meas.1	468 - 503 - 538	59504	330.6
	Meas.2	476 – 511 - 546	59824	332.4

Blocks	Measu-rement No.	U-window (peak channel ± 26 channels)		
		Window range Left–peak–right Channel	Total window counts	Window count rate (cpm)
K block	Meas.1	513 - 539 - 565	3082	64.49
	Meas.2	544 – 570 - 596	3067	68.16
U block	Meas.1	554 – 580 – 606	239864	5330
	Meas.2	565 – 591 - 617	239250	5317
Th block	Meas.1	510 – 536 – 562	77619	1725
	Meas.2	529 – 555 - 581	77227	1716
back-ground block	Meas.1	564 – 590 - 616	18255	101.42
	Meas.2	577 – 603 - 629	17696	98.31

Blocks	Measu-rement No.	Th-window (peak channel ± 35 channels)		
		Window range Left–peak–right Channel	Total window counts	Window count rate (cpm)
K block	Meas.1	729 - 764 - 799	1937	43.04
	Meas.2	778 – 813 - 848	1867	41.49
U block	Meas.1	825 – 860 – 895	3667	81.49
	Meas.2	839 – 874 - 909	3996	88.80
Th block	Meas.1	759 – 794 – 829	102927	2287
	Meas.2	787 – 822 - 857	103070	2290
back-ground block	Meas.1	807 – 842 – 877	10355	57.53
	Meas.2	819 – 854 - 889	10537	58.54

Table A.2. Stripping factors obtained from the measurements in the Oxford blocks.

	hk	hu	uk	uh	Ku	kh
Meas. 1	0.835330	0.632301	1.384009	0.004583	- 0.012680	- 0.004975
Meas. 2	0.802642	0.629351	1.380346	0.005798	- 0.010334	- 0.005844
Mean	0.818986	0.630826	1.382178	0.005191	- 0.011507	- 0.005410

Table A.3. Results of measurements in the Volkegem loess profile.

No. of field spectrum	K-window (peak channel ± 35 channels)		
	Window range Left–peak–right Channel	Total window counts	Window count rate W_k (cpm)
S.31	393 – 428 – 463	127472	1062
S.34	401 - 436 – 471	126520	1054
S.39	398 - 433 – 468	128319	1069
S.29	406 - 441 – 476	125334	1045
S.27	410 - 445 – 480	124085	1034

No. of field spectrum	U-window (peak channel ± 26 channels)		
	Window range Left–peak–right Channel	Total window counts	Window count rate W_u (cpm)
S.31	486 – 512 – 538	21735	181.1
S.34	496 – 522 – 548	22384	186.5
S.39	494 – 520 – 546	22161	184.7
S.29	502 – 528 – 554	22059	183.8
S.27	506 – 532 – 558	21772	181.4

No. of field spectrum	Th-window (peak channel ± 35 channels)		
	Window range Left–peak–right Channel	Total window counts	Window count rate W_{th} (cpm)
S.31	713 – 748 – 783	17653	147.1
S.34	713 – 748 – 783	18411	153.4
S.39	721 – 756 – 791	18077	150.6
S.29	734 – 769 – 804	18486	154.1
S.27	740 – 775 – 810	18231	151.9

Table A.4. Contributions from K, U and Th into their own window for the Volkegem loess field measurement.

No. of field spectrum	K(k) (cpm)		
	Meas. 1	Meas. 2	Mean
S.31	802	810	806
S.34	787	795	791
S.39	805	812	809
S.29	782	789	786
S.27	774	782	778

No. of field spectrum	U(u) (cpm)		
	Meas. 1	Meas. 2	Mean
S.31	95.9	94.1	95.0
S.34	97.2	95.5	96.4
S.39	97.2	95.5	96.4
S.29	94.0	92.3	93.2
S.27	92.9	91.2	92.1

No. of field spectrum	Th(th) (cpm)		
	Meas. 1	Meas.2	Mean
S.31	150	150	150
S.34	156	156	156
S.39	153	154	154
S.29	156	157	157
S.27	154	155	155

- APPENDIX B -

AVERAGES AND UNCERTAINTIES FOR MULTIPLE COUNTINGS OF REPLICATE SAMPLES

In various Chapters of this Thesis, results are obtained from repeated alpha, beta or gamma-ray countings of replicate samples.

In such cases, the following procedure was applied to arrive at the final result and its uncertainty.

First, the counting result per sub-sample (j) is calculated as an average over the n countings (i):

$$\overline{C}_j = \frac{1}{n}\sum_{i=1}^{n} C_{j,i} \quad \pm \quad s_{\overline{C}_j} \tag{B.1}$$

where:

$\overline{C}_j$ - the mean counting result for sub-sample j determined via n countings;

$s_{\overline{C}_j}$ - the largest of the internal (expected) or external (observed) uncertainty on $\overline{C}_j$, i.e.

$s_{\overline{C}_j}$ = largest [$(s_{\overline{C}_j})_{int}$ or $(s_{\overline{C}_j})_{ext}$]

with:

$$(s_{\overline{C}_j})_{int} = \frac{\sqrt{\sum_{i=1}^{n} s_{C_{j,i}}^2}}{n} \tag{B.2}$$

$s_{C_{j,i}}$ - counting statistics;

$$(s_{\bar{C}_j})_{ext} = \sqrt{\frac{\sum_{i=1}^{n}(C_{j,i} - \bar{C}_j)^2}{n(n-1)}} \qquad (B.3)$$

As a second and final step, the grand mean and its uncertainty is calculated by averaging over the means of the N sub-samples.

$$\bar{C} = \frac{1}{N}\sum_{j=1}^{N}\bar{C}_j \quad \pm \quad s_{\bar{C}} \{\text{largest}\,[(s_{\bar{C}})_{int} \text{ or } (s_{\bar{C}})_{ext}]\} \qquad (B.4)$$

where:

$$(s_{\bar{C}})_{int} = \frac{\sqrt{\sum_{j=1}^{N} s^2_{\bar{C}_j}}}{N} \qquad (B.5)$$

and

$$(s_{\bar{C}})_{ext} = \sqrt{\frac{\sum_{j=1}^{N}(\bar{C}_j - \bar{C})^2}{N(N-1)}} \qquad (B.6)$$

As an illustration of the above, an example is given for beta counting of Volkegem loess sample S.31 (Chapter 4, Section 4.6), 5 sub-samples (replicates) of which were measured in each of the 5 counting positions of the Risø GM-25-5 system. Table B.1 summarizes the count rates and counting statistics.

Table B.1. Beta count rates for different sub-samples via different counters.

Sub-sample j	Counter I				
	1 cpm ± s	2 cpm ± s	3 cpm ± s	4 cpm ± s	5 cpm ± s
1	6.93 ± 0.07	6.50 ± 0.07	6.71 ± 0.07	7.01 ± 0.07	6.21 ± 0.07
2	6.96 ± 0.07	6.66 ± 0.07	6.89 ± 0.07	7.19 ± 0.07	6.31 ± 0.06
3	6.85 ± 0.07	6.70 ± 0.07	6.95 ± 0.07	7.21 ± 0.07	6.33 ± 0.06
4	6.87 ± 1.0	6.63 ± 1.0	6.94 ± 1.0	7.36 ± 1.0	6.37 ± 0.06
5	6.90 ± 1.0	6.56 ± 1.0	6.74 ± 1.0	7.27 ± 1.0	6.21 ± 0.06

According to the above equations, the data processing is then as follows:

$$\overline{C}_1 = 6.67\ \text{cpm} \pm 0.15\ \text{cpm};\ [\,(s_{\overline{C}_1})_{\text{int}} = 0.03\ \text{cpm and}\ (s_{\overline{C}_1})_{\text{ext}} = 0.15\ \text{cpm}\,]$$

$$\overline{C}_2 = 6.80\ \text{cpm} \pm 0.15\ \text{cpm};\ [\,(s_{\overline{C}_2})_{\text{int}} = 0.03\ \text{cpm and}\ (s_{\overline{C}_2})_{\text{ext}} = 0.15\ \text{cpm}\,]$$

$$\overline{C}_3 = 6.81\ \text{cpm} \pm 0.15\ \text{cpm};\ [\,(s_{\overline{C}_3})_{\text{int}} = 0.03\ \text{cpm and}\ (s_{\overline{C}_3})_{\text{ext}} = 0.15\ \text{cpm}\,]$$

$$\overline{C}_4 = 6.83\ \text{cpm} \pm 0.17\ \text{cpm};\ [\,(s_{\overline{C}_4})_{\text{int}} = 0.03\ \text{cpm and}\ (s_{\overline{C}_4})_{\text{ext}} = 0.17\ \text{cpm}\,]$$

$$\overline{C}_5 = 6.74\ \text{cpm} \pm 0.18\ \text{cpm};\ [\,(s_{\overline{C}_5})_{\text{int}} = 0.03\ \text{cpm and}\ (s_{\overline{C}_5})_{\text{ext}} = 0.18\ \text{cpm}\,]$$

and the grand mean:

$$\overline{C} = 6.770\ \text{cpm} \pm 0.072\ \text{cpm};\ [\,(s_{\overline{C}})_{\text{int}} = 0.072\ \text{cpm and}\ (s_{\overline{C}})_{\text{ext}} = 0.029\ \text{cpm}\,]$$

The background was determined in the same way, resulting in:

$$\overline{C}_{\text{Bkg}} = 0.153\ \text{cpm} \pm 0.008\ \text{cpm}$$

Finally, the net count rate for sample S.31 is then (with quadratic summation of uncertainties):

$$\overline{C}_{\text{net}} = \left[(\overline{C} - \overline{C}_{\text{Bkg}}) \pm \sqrt{(s^2_{\overline{C}} + s^2_{\overline{\text{Bkg}}})} \right] = 6.617\ \text{cpm} \pm 0.072\ \text{cpm}$$

Note:

In the present work mostly uncertainties of random origin are quoted. That systematic uncertainties were as a rule not taken into account, was because the elaboration of the complete uncertainty budget for the analytical results obtained in the present work was not always possible. For instance, whereas k_0-NAA offers a well-established uncertainty budget, this is not the case for field gamma-ray spectrometry with calibration via the "Oxford" blocks, for which no uncertainties on the K, U and Th concentrations are known.

NEDERLANDSE SAMENVATTING

De luminescentiedateringsmethode is gebaseerd op de meting van het licht (= luminescentie) dat wordt uitgezonden door kristallijne mineralen zoals kwarts en veldspaat wanneer ze verhit worden (TL – thermoluminescentie) of wanneer ze blootgesteld worden aan licht (OSL – optisch gestimuleerde luminescentie). De hoeveelheid geëmitteerde luminescentie is evenredig met de totaal ontvangen natuurlijke stralingsdosis. Deze laatste, de paleodosis genoemd, is opgebouwd door energiedepositie van straling (alfa, beta en/of gamma) uitgestuurd door de natuurlijk voorkomende radionucliden ^{232}Th, ^{235}U, ^{238}U (en hun vervalproducten) en ^{40}K – naast kleinere bijdragen van ^{87}Rb en kosmische straling – zowel van binnen de onderzochte mineraalkorrels als vanuit hun omgeving. De luminescentiedateringsmethode bestaat dus in hoofdzaak uit twee analytische luiken: i) de bepaling van de paleodosis – zelf samengesteld uit een meting van het natuurlijk luminescentiesignaal en van de gevoeligheid, via artificiele toediening van een gekende stralingsdosis; en ii) de bepaling van de jaarlijkse stralingsdosis, die verondersteld wordt constant te zijn met de tijd. Vergelijking van de paleodosis met de jaarlijkse stralingsdosis laat dan de bepaling toe van de ouderdom van het monster. De verkregen ouderdom is de tijd verlopen sinds de laatste "opnulstelling" van het luminescentiesignaal, zoals het moment van verhitting bij de productie van keramiek, of het moment van blootstelling aan zonlicht gedurende het transport en de afzetting van sedimenten.

Het is duidelijk dat de experimentele bepaling van de jaarlijkse stralingsdosis een belangrijke stap is in de luminescentiedatering, aangezien de onzekerheid ervan lineair getransfereerd wordt naar het ouderdomsresultaat. De bedoeling van deze thesis is het uitvoeren van een experimentele studie en een performantie-evaluatie van enkele courant gebruikte methoden voor de bepaling van de jaarlijkse stralingsdosis in de luminescentiedatering van sedimenten. Met dit doel voor ogen, werden twee materiaaltypes onderzocht: een loess-sediment, gecollecteerd in een profiel te Volkegem (in het zuidelijk deel van Oost-Vlaanderen, België); en een dekzand,

gecollecteeerd in een afzetting te Ossendrecht (in het zuidwestelijk deel van Nederland).

Het eerst bestudeerde materiaal was het Volkegem loess sediment, waarvoor de volgende methoden onderzocht werden: NaI(Tl) gamma-spectrometrie zowel in het veld (in-situ) als in lage-achtergrond laboratoriumcondities, voor de meting van K, U en Th; Ge gamma-spectrometrie met uitgebreid energiebereik, in lage-achtergrond laboratoriumcondities, voor de meting van K, U en Th alsook voor de detectie van mogelijke onevenwichten in de Th- en vooral in de U-vervalreeks; "thick source" ZnS alfa telling, zowel in de integrale mode voor de meting van U + Th als in de paartelling mode voor de discriminatie tussen U en Th; lage-achtergrond GM beta telling voor de meting van K + U + Th; instrumentele reactorneutronenactiverings-analyse (INAA) voor de bepaling van K, U, Th en Rb; en atomaire absorptie-spectrometrie (AAS) voor de bepaling van K.

Bij de bepaling van de jaarlijkse stralingsdosis zijn NaI(Tl) veldmetingen in boorgat-geometrie zeer geschikt omdat zij een echte indicator zijn voor de omgeving van het te dateren materiaal. In het Volkegem loessprofiel werden vijf veldmetingen uitgevoerd met een draagbaar gamma-spectrometrie systeem (Canberra Portable Plus Model 1150) uitgerust met een 3 × 3'' NaI(Tl) detector, waarna 15 monsters gecollecteerd werden voor analyse in het laboratorium (zie verder). Uit deze veldmetingen was het mogelijk het aantal tellen te bekomen (via telling in vensters met gebruik van spectrum-"stripping", of via gamma-spectrometrie) die geassocieerd zijn met de gamma-lijnen van ^{40}K bij 1460,8 keV, van ^{214}Bi (in de ^{238}U vervalketen) bij 1764,5 keV en van ^{208}Tl (in de ^{232}Th vervalketen) bij 2614,5 keV. Met gebruik van een kalibratiemeting was het dan mogelijk het K, U en Th gehalte in het loess te bekomen, dat geconverteerd kon worden naar jaarlijkse stralingsdosissen. De kalibratie werd uitgevoerd via metingen in blokken met een uitgebreide geometrie, die bestaan uit een materiaal met gekende hoeveelheden K, U en Th, en die een "boorgat" hebben waar de detector kan ingeschoven worden. Twee sets van dergelijke kalibratieblokken werden gebruikt:

1) aan de Forschungsstelle Archäometrie, MPI, Heidelberg, Duitsland: een natuurlijk granietblok [Flossenburg graniet] van 1 × 1 × 1 m, met K, U en Th (gewichts)-concentraties van respectievelijk 4,08 ± 0,11 %, 18,8 ± 1,3 mg.kg^{-1} en 14,0 ± 0,9 mg.kg^{-1};
2) aan het Research Laboratory for Archaeology and the History of Art (RLAHA), Oxford University, UK: drie betonblokken van 0,5 × 0,5 × 0,5 m gedopeerd met K, U en Th [plus een ongedopeerd "achtergrond" blok], waarvoor respectievelijk "effectieve" (gewichts)concentraties opgegeven waren van 5,71 % K, 117 mg.kg^{-1} U en 126 mg.kg^{-1} Th (met additioneel 4,8 mg.kg^{-1} U), zonder specificatie van onzekerheden.

De spectra gemeten in het veld en in de kalibratieblokken werden geanalyseerd op twee verschillende manieren, overeenkomstig het type van de kalibratie. Voor de "Heidelberg" kalibratie werd gamma-spectrometrie uitgevoerd waarbij, voor de relevante gamma-pieken, de bepalingen van het netto piekoppervlak gebeurden met behulp van het Hypermet-PC softwarepakket. De Oxford kalibratieblokken, daarentegen, werden ontwikkeld voor "venster"-metingen met spectrum-"stripping" en aangezien telkens een volledig spectrum geregistreerd werd, kon de instelling van de vensters gemakkelijk gebaseerd worden op de locatie van de pieken, zodat het mogelijk was effecten van mogelijke temperatuurvariaties te minimaliseren.

Er werd een studie uitgevoerd van de correcties die nodig zijn bij de kalibratie van de veldmetingen via de "Heidelberg" en de "Oxford" blokken. Deze correcties moeten ingevoerd worden vanwege de verschillende telcondities bij de veld- en blok-metingen (met betrekking tot geometrie, samenstelling en dichtheid van het materiaal) en ook omdat de kalibratieblokken niet echt oneindige afmetingen hebben. Het kon besloten worden dat het "Heidelberg" blok beschouwd kan worden als "quasi-oneindig" en dat enkel "samenstelling en dichtheid"-correcties van een paar procent vereist zijn; de "Oxford" blokken, daarentegen, zijn ver van oneindig en dit werd in feite in rekening gebracht door te werken met "effectieve" elementconcentraties zoals ze ons gerapporteerd werden door RLAHA, Oxford.

De cylindrische ongestoorde loessmonsters die in het veld gecollecteerd en naar het laboratorium gebracht werden, werden geanalyseerd met NaI(Tl) gamma-spectrometrie (hetzelfde instrument dat gebruikt werd in het veld, behalve dat de NaI(Tl) detector gemonteerd is in een lage-achtergrond loodkasteel) en met Ge gamma-spectrometrie met uitgebreid energiebereik (met gebruik van een Canberra XtRa detector in een lage-achtergrond loodkasteel). Zowel de NaI(Tl) als de Ge gamma-metingen werden gekalibreerd op een absolute manier via de introductie van piek-detectie efficiënties, van correctiefactoren voor echte-coincidentie effecten en van nucleaire gegevens. Voor Ge gamma-spectrometrie werd eveneens een relatieve kalibratie uitgevoerd, gebaseerd op het gebruik van de IAEA radiometrische referentiematerialen RGK-1, RGU-1 en RGTh-1. De NaI(Tl) en de Ge metingen leverden beide K, Th en U concentraties op, die dan konden geconverteerd worden naar jaarlijkse stralingsdosissen. Bovendien konden met de Ge metingen verschillende dochters in de U en Th vervalreeksen bepaald worden, zodat het mogelijk was een controle uit te voeren van het evenwicht in de vervalreeksen.

Na het beeindigen van de gamma-spectrometrie, werden de monsters gedroogd bij 110 °C tot constant gewicht. De elementsamenstelling van het gedroogde loessmateriaal werd bepaald via XRF analyse. Deze informatie over de elementaire compositie is vereist voor de berekening van de effectieve ruimtehoeken in de gamma-spectrometrie alsook voor k_0-NAA. Voor alfa en beta telling werd het gedroogde materiaal fijn gemalen (manueel in een porceleinen mortier) en gezeefd (met gebruik van een 63 μm zeef) om een deeltjesgrootte van minder dan 63 μm te bekomen.

“Thick source” ZnS alfa-telling werd uitgevoerd met behulp van twee ELSEC 7286 lage-achtergrond alfa telsystemen, elk uitgerust met drie scintillatie/PM-buis meeteenheden. Kalibratie van de zes tellers hield de bepaling in van het hoogspanningsplateau en regeling van de drempelspanning, en werd uitgevoerd met behulp van de granietstandaard GS-N. De validatie van de kalibratie-instellingen gebeurde via de meting van verschillende geo-standaarden (RGU-1, RGTh-1 en Biotiet Mica, Fe) met gekende U en Th gehaltes. Dit leverde niet enkel de gecombineerde totale alfa dosissnelheid van U en Th op, maar het liet ook toe om –

via ingebouwde "paartelling" electronica – een discriminatie te maken tussen U en Th. Met gebruik van aangepaste conversiefactoren, kon eveneens de beta dosissnelheid gerelateerd aan deze elementen verkregen worden.

GM beta-telling werd uitgevoerd met gebruik van het "Risø low-level GM-25-5 multicounter system". Kalibratie gebeurde met behulp van de U standaarden RGU-1 en CRM 105-A, de Th standaarden RGTh-1 en CRM 109-A en met een serie van zelfbereide K standaarden. Er werd gevonden dat de kalibratiefactoren met een goede benadering element-onafhankelijk waren en ook niet varieerden met de concentratie van het element in de standaard. Via de kalibratiefactoren konden de resultaten van de beta-telling omgezet worden naar totale beta dosissnelheden.

Instrumentele neutronenactiveringsanalyse werd uitgevoerd met behulp van de k_0-standaardisatiemethode. Dit behelsde de bestraling van ~500 mg monsters, samen met een gecertificeerde IRRM-530 Al-0,1%Au monitor, in een gekalibreerde bestralingsfaciliteit van reactor Thetis (Gent), gevolgd door drie metingen op een gekalibreerde HPGe gamma-spectrometer. Het K-gehalte werd bekomen via de meting van ^{42}K (12,4 h) na een vervaltijd van ~ 65 h, het U-gehalte via de meting van ^{239}Np (2,36 d) na een vervaltijd van ~ 5 d, en het Th-gehalte via de meting van ^{233}Pa (27,0 d) na een vervaltijd van ~ 3 weken. Gamma-spectrum analyse werd uitgevoerd via de Hypermet-PC software, en de concentratie-berekening was gebaseerd op het Kayzero/Solcoi softwarepakket. Vermeldenswaardig is de mogelijkheid van k_0-NAA om "automatisch" informatie op te leveren over het Rb-gehalte [via de meting van ^{86}Rb (18,6 d) samen met ^{233}Pa], waarvoor anders een K:Rb verhouding van 200 tot 400 wordt aangenomen.

Atomaire absorptie-spectrometrie werd toegepast voor de bepaling van K. Er werd gebruik gemaakt van een Varian SpectrAA-600 instrument, dit is een dubbele-bundel spectrometer uitgerust met een holle kathode lamp en een acetyleen-lucht vlam ionisatie systeem. De kalibratie werd uitgevoerd door meting van een reeks zelfbereide K (kaliumbiftalaat) standaardoplossingen.

Een vergelijkende studie van de hierboven beschreven methoden ter bepaling van de jaarlijkse stralingsdosis voor Volkegem loess toonde aan dat consistente en betrouwbare resultaten werden verkregen met behulp van: NaI(Tl) veld gamma-spectrometrie zowel via de "Heidelberg" als de "Oxford" kalibratieblokken; lage-achtergrond NaI(Tl) gamma-spectrometrie in het laboratorium; lage-achtergrond Ge gamma-spectrometrie met uitgebreid energiebereik gebaseerd op de relatieve kalibratie (waarbij tevens een indicatie werd bekomen over het evenwicht in zowel de U als de Th serie); k_0-gestandaardiseerde reactorneutronenactiveringsanalyse; "thick source" ZnS alfa telling in de integrale mode; en lage-achtergrond GM beta telling. De volgende methodes leverden enigszins inconsistente of minder preciese resultaten op: absoluut gekalibreerde Ge gamma-spectrometrie; ZnS alfa telling in de paartelling mode; en atomaire absorptie spectrometrie. De beste techniek voor de drie elementen (K, U en Th) bleek relatief gestandaardiseerde, lage-achtergrond Ge gamma-spectrometrie te zijn, aangezien het een goede precisie en accuratesse opleverde, waarbij het bovendien toeliet om het radioactief evenwicht in de U en Th vervalreeksen te bestuderen.

Het tweede materiaal dat bestudeerd werd was het Ossendrecht dekzand. In het profiel werden twee NaI(Tl) gamma veldmetingen uitgevoerd en er werden vier bemonsteringspunten uitgekozen. Van ieder punt werd ongeveer 3 kg materiaal gecollecteeerd en naar het laboratorium gebracht voor analyse (na drogen bij 110°C tot constant gewicht) met de volgende technieken: lage-achtergrond HPGe gamma-spectrometrie met uitgebreid energiebereik (XtRa) in Marinelli geometrie, met behulp van relatieve kalibratie; k_0-gestandaardiseerde instrumentele reactorneutronen-activeringsanalyse (k_0-INAA); lage-achtergrond GM beta telling; en "thick source" ZnS alfa telling, in de integrale mode. Methoden van ietwat mindere kwaliteit zoals eerder geobserveerd bij de analyse van loess sediment, werden niet toegepast op de analyse van het Ossendrecht zand: absoluut gekalibreerde XtRa HPGe gamma-spectrometrie, ZnS alfa telling in de paartelling mode, en atomaire absorptie spectrometrie. Wegens de lage concentratie van K, U en Th in de hier onderzochte zandmonsters (zie verder), werd ook lage-achtergrond NaI(Tl) gamma-spectrometrie in het laboratorium geschrapt.

In tegenstelling tot wat vroeger vastgesteld werd bij de analyse van loess sediment, bracht de bepaling van de jaarlijkse stralingsdosis voor de dekzandafzetting in Ossendrecht twee specifieke problemen aan het licht: 1) de lage concentratie van K, U en Th aanwezig in het materiaal, en 2) monsterinhomogeniteit op het gram niveau. Omwille van deze problemen dienden voor de mostervoorbereiding voor de laboratoriummetingen verschillende benaderingen uitgeprobeerd te worden teneinde aanvaardbare resultaten te bekomen.

In een eerste benadering werd het gedroogde materiaal gehomogeniseerd door eenvoudig omroeren in een emmer, waarna het geanalyseerd werd via lage-achtergrond XtRa HPGe gamma-spectrometrie in Marinelli geometrie en via k_0-NAA.

De vermelde problemen konden vermeden worden door het meten van een grote hoeveelheid monster (1,5 kg) in Marinelli geometrie met de lage-achtergrond XtRa HPGe detector. Er werd op een relatieve manier gestandardiseerd, en aangezien zulk een grote massa van een standaard niet eenvoudig te vinden is in de handel, werd gebruik gemaakt van het goed-gekarakteriseerde Volkegem loess sediment. Alhoewel de telgeometrie voor de monsters en de standaarden identiek was, dienden hun chemische samenstelling (bepaald via XRF analyse) en hun pakkingsdichtheid in aanmerking genomen te worden bij de berekening van de effectieve ruimtehoeken. De metingen leverden K, U en Th concentraties op. De vervalketens van U en Th vertoonden evenwicht, alhoewel er een aanduiding was van een geringe maar systematische verlaging van ^{210}Pb in de ^{238}U vervalserie. Dit kan in de richting wijzen van een (nauwelijks significant) onevenwicht veroorzaakt door een kleine ^{222}Rn emanatie in geologische tijden.
Wat betreft de K, U en Th concentraties verkregen via k_0-NAA, werd thans een aanzienlijke strooiing waargenomen tussen de verschillende submonsters [alhoewel het monstergewicht was opgetrokken van 500 mg naar 1 g]. Deze variatie wijst op een inhomogene verdeling van de radionucliden op het gram niveau. Toch was de gemiddelde concentratie voor ieder bemonsteringspunt in het algemeen consistent met de resultaten bekomen via HPGe gamma-spectrometrie in Marinelli geometrie.

Aangezien verwacht wordt dat het monster homogeen is op het 1,5 kg niveau, worden de resultaten verkregen via gamma-spectrometrie als betrouwbaar beschouwd.

Om het probleem van de inhomogeniteit uit de weg te ruimen, werd een tweede benadering voor de bereiding van de monsters uitgeprobeerd. Ongeveer 20 g gedroogd zandmateriaal (per monster) verkregen in de eerste stap, werd manueel gemalen in een porceleinen mortier, gezeefd (met gebruik van een 63 μm zeef) en verder gehomogeniseerd. Van dit materiaal werden submonsters van de orde van een gram genomen voor k_0-NAA, ZnS alfa telling en GM beta telling.
De k_0-NAA resultaten (voor de verschillende submonsters) bekomen voor deze manueel gemalen monsters waren zeer reproduceerbaar maar systematisch te hoog vooral voor U en Th, en in mindere mate voor K. Tevens waren de alfa dosissnelheden voor de manueel gemalen monsters, verkregen via alfa telling van dikke monsters, systematisch hoger dan deze berekend uit HPGe gamma-spectrometrie in Marinelli geometrie. In het geval van beta telling, waren de gemeten beta dosissnelheden voor de handgemalen monsters eveneens significant hoger dan deze berekend uit HPGe gamma-spectrometrie in Marinelli geometrie.
Deze bevindingen wezen er op dat de inhomogeneiteit op het gram niveau kon geëlimineerd worden door manueel malen in een porceleinen mortier, maar dat deze bewerking tevens het materiaal ernstig contamineerde.
Op basis van het bovenstaande, zou men eveneens een contaminatie verwachten van het Volkegem loess, bij manueel malen ervan in een porceleinen mortier. Dat deze contaminatie insignificant was, kan toegeschreven worden aan het feit dat de abrasieve actie van zand op porcelein groter is dan deze van loess.

Om zowel de inhomogeniteit op het gram niveau weg te werken als om contaminatie te vermijden, werd de benadering voor de bemonstering voor k_0-NAA, alfa telling en beta telling aangepast. In deze derde stap werd ongeveer 200 g materiaal uit de eerste stap random bemonsterd en nadien gemalen via “ball-milling” in een Pulverizer6 (Planetary Mono Mill, Fritsch), gevolgd door verdere homogenisatie. Het aldus gemalen materiaal werd opnieuw geanalyseerd via k_0-NAA (in verschillende submonsters), alfa telling en beta telling. De k_0-NAA resultaten voor K, U en Th

waren niet allen veel reproduceerbaarder (verbeterde standaarddeviatie vergeleken met het onbehandelde materiaal), maar tevens consistent met de resultaten van HPGe gamma-spectrometrie in Marinelli geometrie. Bovendien waren thans de gemeten alfa en beta dosissnelheden volledig consistent met deze berekend uit HPGe gamma-spectormetrie in Marinelli geometrie. Deze bevindingen tonen aan dat het gebruik van "ball-milling" (met een agaat beker en ballen) een materiaal opleverde dat homogeen was en niet significant gecontamineerd.

Wegens de inhomogeniteit van het Ossendrecht profiel, werden de resultaten anders voorgesteld dan voor Volkegem, waar het profiel homogeen was. In feite werden in het geval van Volkegem de verschillende analytische methoden onderzocht op hun performantie, terwijl ze in het geval van Ossendrecht toegepast werden om het profiel te onderzoeken. De gemeten en berekende alfa en beta dosissnelheden, verkregen via verschillende analytische technieken, werden voor ieder bemonsteringspunt vergeleken. De verschillende methoden leverden per bemonsteringspunt consistente resultaten op, maar de variatie tussen de bemonsteringspunten was groot. Dit wijst op een heterogene verdeling van de radio-elementen in het profiel.

In het algemeen kan gesteld worden dat er in dit werk voor de bepaling van de jaarlijkse stralingsdosis in loess en zand sedimenten, specifieke procedures voor kalibratie, monstervoorbereiding en meting uitgewerkt werden, en dat de toepassing ervan leidde tot consistente en bevredigende resultaten.
In de studie van het loess sediment, werden de verschillende analytische methoden onderzocht, en voor sommige ervan dienden specifieke kalibratieprocedures ontwikkeld te worden. De bepaling van de jaarlijkse dosis stelde in dit geval geen speciale problemen. Een belangrijke vaststelling, volgend uit de hier uitgevoerde systematische studie van Volkegem loess, is dat dit materiaal zeer homogeen is. De gemiddelde concentraties ± 2s standaardfouten zijn: (1,784 ± 0,019) % voor K, (2,516 ± 0,036) $mg.kg^{-1}$ voor U en (10,221 ±0,082) $mg.kg^{-1}$ voor Th. In feite was de *a priori* assumptie van de homogeniteit een criterium voor de selectie van de Volkegem loess site.

Methoden die bij de analyse van loess van mindere kwaliteit bleken te zijn, werden geëlimineerd bij het onderzoek van het Ossendrecht zandprofiel. Bij het onderzoek van het zand kwamen echter specifieke problemen aan het licht. Deze hadden betrekking op het laag K, U en Th gehalte in de monsters, en op de inhomogeniteit van het materiaal op het gram niveau. Beide problemen konden opgelost worden door het aanwenden van geschikte analytische methodes en door het toepassen van aangepaste technieken voor monstervoorbereiding.

Als een algemene conclusie kan gesteld worden dat in dit werk een experimentele studie werd voorgesteld van methoden voor de bepaling van de jaarlijkse stralingsdosis in de luminescentiedatering van sedimenten. Alhoewel de studie behoorlijk uitgebreid was, zal blijken uit hetgeen volgt dat er een behoefte is aan verder onderzoek.

Voor zowel de monsters van loess als dekzand die in dit werk onderzocht werden, bleken de U en Th vervalseries in evenwicht te zijn. Daarom stelde de jaarlijkse dosisbepaling geen speciale problemen. Er zijn evenwel talrijke afzettingen waarin wel degelijk radioactief onevenwicht optreedt. In deze gevallen zal de dosissnelheid variëren als een functie van de tijd, en indien deze variatie niet in rekening gebracht wordt, zou een verkeerde luminescentie-ouderdom kunnen bekomen worden. Het is daarom noodzakelijk om een bijkomend onderzoek uit te voeren van monsters die onevenwichten vertonen (van verschillende types en graad) met het doel ervaring op te doen en te komen tot oplossingen betreffende de vaststelling hoe de dosissnelheid varieert met de begravingstijd (d.i. de tijdsspanne die gedateerd wordt) en hoe deze variaties de luminescentie-ouderdommen beïnvloeden.

Naast gamma-spectrometrie kan ook alfa-spectrometrie gebruikt worden voor de schatting van de graad van onevenwicht in de U en Th vervalseries. Het zou de moeite waard zijn om ook deze techniek te onderzoeken om te bepalen wat de performantie ervan is, naast, en in vergelijking met, lage-achtergrond gamma-spectrometrie. Een combinatie van gamma- en alfa-spectrometrie zou verder een volledig onderzoek toelaten van de evenwichten in de U en Th vervalreeksen.

Zoals aangetoond werd in Hoofdstuk 5, Sectie 5.3.2, werd een grote variatie gevonden van de U en Th concentraties in het Ossendrecht zand, hetgeen toegeschreven werd aan een heterogene distributie van radionucliden doorheen het profiel. Alhoewel het vermalen van het monster de precisie van de analyse verbeterde, blijft het een belangrijke vraag hoe dit de dosissnelheid beïnvloedt die ontvangen wordt door de individuele mineraalkorrels die gebruikt worden voor de bepaling van de equivalente dosis. Vandenberghe et al. (2003) observeerden brede distributies voor de equivalente dosis in de Ossendrecht monsters, en schreven deze toe aan variaties op kleine schaal in de jaarlijkse dosis. Deze zogeheten microdosimetrische variaties zijn thans een "hot topic" voor degenen die werken in de luminescentiedatering van sedimenten, en een kwantificatie van het effect is noodzakelijk, vooral omdat de schaal van D_e-analyses gereduceerd werd tot een paar of zelfs tot individuele korrels. In deze context zou het eveneens zeer nuttig zijn om uit te zoeken waar de radioactiviteit exact is gelokaliseerd (binnenin de korrels, in een coating er omheen, enz.).

Het gebruik van luminescentiedosimeters is een interessant alternatief voor de technieken die in dit werk gebruikt werden. De toepassing ervan zou de bepaling toelaten van zowel de equivalente dosis als de jaarlijkse dosis, enkel via luminescentiemetingen. Dit is zeer belangrijk aangezien niet iedereen toegang heeft tot, of de noodzakelijke expertise heeft in, de soms complexe en dure analytische faciliteiten die vereist zijn voor een accurate bepaling van de dosissnelheid. Vooral α-Al_2O_3:C is een veelbelovend materiaal vanwege zijn grote gevoeligheid. Het gebruik van α-Al_2O_3:C korrels, gemengd met sediment, geeft bovendien de mogelijkheid om microdosimetrische variaties te onderzoeken (Kalchgruber, 2002).

Tenslotte zou het zeer interessant zijn om te onderzoeken wat de performantie is van alle technieken bij de analyse van sedimenten met een nog geringer gehalte aan radionucliden. Het kan vermeld worden dat in deze gevallen verwacht wordt dat de bijdrage van de kosmische straling belangrijker wordt, en dat bijgevolg een meer precieze evaluatie van deze component een nieuwe uitdaging wordt voor verder onderzoek.

References

Aitken M. J. (1968)
Low-level environmental radiation measurements using natural calcium fluoride, Proc. of the 2nd Int. Conf. on Lumin. Dosim., Gatlinburg, editted by Auxier J.A., Becker K, Robinson E.M. (Eds), CONF-680920, pp. 281-290, U.S. National Bureau Standards, Washington D.C.

Aitken (1969)
Thermoluminescent dosimetry of environmental radiation on archaeological sites, Archaeometry, **11**, 109-114.

Aitken M. J. (1985)
Thermoluminescence Dating, Academic Press, New York, pp. 359.

Aitken M. J. (1998)
An Introduction to Optical Dating, Oxford University Press, Oxford, pp. 267.

Aitken M. J., Tite, M. S., and Reid, J. (1964)
Thermoluminescent dating of ancient ceramics, Nature, **202**, 1032-1033.

Akselrod M.S., Kortov V. S., Kravetsky D. J. and Gotlib V. L. (1990)
Highly sensitive thermoluminescent anion-defective Al_2O_3:C single crystal detector, Radiat. Prot. Dosim., **32,** 15-29.

Akselrod M. S. and Gorelova E. A. (1993)
Deep traps in highly sensitive α-Al_2O_3:C TLD crystals, Nucl. Tracks Radiat. Meas., **21**, 143-146.

Allsop A.
RLAHA, University of Oxford, UK, private communication.

Bailiff J. K. (1976)
Some new techniques in thermoluminescence dating, M.Sc. thesis, Oxford University. UK.

Bailiff J. K. and Aitken M. J. (1980)
Use of thermoluminescence dosimetry for evaluation of internal beta dose-rate in archaeological dating, Nucl. Instr. Methods, **173**, 423-429.

Bøtter-Jensen L. (2000)
Development of Optically Stimulated Luminescence Techniques using Natural Minerals and Ceramics, and their Application to Retrospective Dosimetry, D.Sc. Thesis, University of Copenhagen, Denmark.

Bøtter-Jensen L. and Mejdahl V. (1985)
Determination of Potassium in feld-spars by beta counting using a GM multicounter system, Nucl. Tracks, **10**, 663-666.

Bøtter-Jensen L. and Mejdahl V. (1988)
Assessment of beta dose-rate using a GM multicounter system, Nucl. Tracks Radiat. Meas., **14**, 187-191.

Bowman S. G. E., (1976)
Thermoluminescent Dating: The Evaluation of Radiation dosage, Ph.D. Thesis, University of Oxford, UK.

Bowman S. G. E., (1982)
Alpha particle ranges in pottery, PACT **6**, 61-66.

Brown C. K., Bolch W. E. and Poston J. W. Sr (1993)
Characterization of Al_2O_3:C thermoluminescent dosimeter response to beta radiation, Hlth Phys. **64** (6 Suppl.) S41.

Chiozzi P., Pasquale V., Verdoya M. and De Felice P. (2000)
Practical applicability of field γ-ray scintillation spectrometry in geophysical surveys, Appl. Radiat. Isot., **53**, 215-220.

Chowdhury P., Hildebrandt U. and Ney J. (1982)
High resolution Ge-Li gamma spectroscopy and ceramic phase analysis in TL-dating of a medieval castle, PACT J. **6**, 116-131.

Cox K. G., Bell J. D. and Pankhurst R. J (1981)
The interpretation of igneous rocks, Allen and Unwing, London.

Chu S. Y., Nordberg H., Firestone R. B. and Ekström L. P. (1999)
Isotope Explorer, Version 2.23.

Daniels F., Boyd C. A. and Saunders D. F. (1953)
Thermoluminescence as a research tool, Science, **117**, 343-349.

Debenham N. C. and Aitken M. J. (1984)
Thermoluminescence dating of stalagmitic calcite, Archaeometry **26**, 155-170.

De Corte F. (1987a)
The k_0-standardization method: a move to the optimization of neutron activation analysis, Aggregate thesis, University of Ghent.

De Corte F. (1987b)
The traceability of the neutron activation analysis (NAA) k_0-standardization method, J. Trace Microprobe Techn., **5/2-3**, 115-134.

De Corte F. (1992)
Problems and solutions in the standardization of reactor neutron activation analysis, J. Radioanal. Nucl. Chem., **160**, 63-75.

De Corte F. (2001)
The standardization of standardless NAA, J. Radioanal. Nucl. Chem., **248**, 13-20.

De Corte F., Demeter A., Lin Xilei, Moens L., Simonits A., De Wisplaere A. and Hoste J.(1984)
Evaluation of the k_0-Method by its Application to (n,γ) RNAA of Geological, Environmental and Clay Reference Materials, Isotopenpraxis, **20**, 223-226.

De Corte F., Simonits A., De Wispelaere A. and Hoste J. (1987)
Accuracy and applicability of the k_0-standardization method, J. Radioanal. Nucl. Chem., **113**, 145-161.

De Corte F. and Simonits A. (1989)
k_0-Measurements and related nuclear data compilation for (n,γ) reactor neutron activation analysis; IIIb: Tabulation, J. Radioanal. Nucl. Chem., **133**, 43-130.

De Corte F., Simonits A., De Wispelaere A. and Elek A. (1989)
Measurements and related nuclear data compilation for (n,γ) reactor neutron activation analysis, J. Radioanal. Nucl. Chem., **133**, 3-41.

De Corte F., Simonits A., Bellemans F., Freitas M. C., Jovanović S., Smodiš B., Erdtman G., Petri H. and De Wispelaere A. (1993)
Recent advantages in the k_0-standardization of neutron activation analysis: Extensions, applications, prospects, J. Radioanal. Nucl. Chem., **169**, 125-158.

De Corte F. and Simonits A. (1994)
Vademecum for k_0-users, addendum to the Kayzero/Solcoi Report, DSM Research, Gellen (NL).

De Corte F., De Wispelaere A., Vancraeynest L., De Neve P. and Van den haute P. (1994)
True-coincidence correction for field gamma-ray spectrometry in auger hole counting geometry, Nucl. Instr. Methods A, **353**, 539-541.

De Corte F., Bellemans F., De Neve P. and Simonits A. (1994a)
The use of a modified WESTCOTT-FORMALISM in the k_0-standardization of NAA: the state of affairs, J. Radioanal. Nucl. Chem., **179**, 93-103.

De Corte F and Van Lierde S. (2000)
Determination and evaluation of fission k_0-factors for correction of the $^{235}U(n,f)$ interference in k_0-NAA, Presented at MARC-V, Kona, HI, USA.

De Corte F., Hossain S.M., Jovanović S., Dlabać A, De Wispelaere A., Vandenberghe D. and Van den haute P. (2001)
The introduction of Marinelli effective solid angles for correcting the calibration of NaI(Tl) field gamma-ray spectrometry in TL/OSL dating, J. Radioanal. Nucl. Chem., in press.

De Corte F., Hossain S. M., Vandenberghe D. and Van den haute P. (2002)
Alpha, beta and gamma-ray counting in the evaluation of the annual radiation dose in luminescence dating of sediments, Nucl. Instr. Methods, in press.

De Wispelaere A. and De Corte F. (1997)
A refinement of true coincidence correction factor calculation for large cylindrical samples. Proceed. 2nd Intern. k_0-users Workshop, Ljubljana, Slovenië, 168-171.

De Wispelaere A. and De Corte F. (2001)
Recalibration of the irradiation facilities in the Thetis reactor, with an examination of the α vs E behaviour in the keV neutron energy range, J. Radioanal. Nucl. Chem., in press.

Desai V. S. (1975)
Studies in radon emanation relevant to thermoluminescent dating, M.Sc. thesis, Oxford University, UK.

Duchesne J. C.
Deptment of Geology – Petrology – Geochemistry, Université de Liége, private communication.

ELSEC 7286 (1993)
Low level alpha counter User Manual, Littlemore Scientific Engineering, UK.

Fazekas B., Molnár G. Belgya T., Dabolczi L. and Simonits A. (1997)
Introducing HYPERMET-PC for automatic analysis of complex gamma-ray spectra, J. Radioanal. Nucl. Chem. **215**, 271-277.

García-Orellana I. and García-León M. (2002)
An easy method to determine ^{210}Po and ^{210}Pb by alpha spectrometry in marine environmental samples.

Goedicke C. (1988)
Determination of natural uranium and thorium content by α-spectrometry, Nucl. Tracks Radiat. Meas., **14**, 219-222.

Göksu H. Y., Fremlin J. H, Irwin H. T. and Fryxell R. (1974)
Age determination of burnt flint by a thermoluminescent method, Science **183**, 651-654.

Govindaraju K. (1988)
Compilation Report (1966-1987) on Trace Elements in five CRPG Geochemical Reference Samples: Basalt BR; Granites, GA and GH; Micas, Biotite Mica-Fe and Phlogopite Mica-Mg, Geostandards Newsletter, **12**, 119-201.

Govindaraju K. (1989)
1988 Compilation report on trace elements in six ANRT rock reference samples: Diorite DR-N, Surpentine UB-N, Bauxite BX-N, Disthene DT-N, Granite GS-N and Potash Feldspar FK-N, Geostandards Newsletter, **13**, 5-67.

Guibert P. and Schvoerer M. (1991)
TL dating: low background gamma spectrometry as a tool for the determination of the annual dose, Nucl. Tracks Radiat. Meas., **18**, 231-238.

Huntley D. J. and Wintle A.G. (1981)
The use of alpha scintillation counting for measuring Th-230 and Pa-231 contents of ocean sediments, Can. J. Earth Sci., **18**, 419-432.

Huntley D. J., Godgrey-Smith D. I. and Thewalt M. L. W. (1985)
Optical dating of sediments, Nature, **313**, 105-107.

Hütt G., Jaek I. and Tchonka J. (1988)
Optical dating: K-feldspars optical response stimulation spectra, Quaternary Science Review, **7**, 381-385.

Hutton J. T. and Prescott J. R. (1992)
Field and laboratory measurement of low-level thorium, uranium and potassium, Nucl. Tracks Radiat. Meas., **20**, 367-370.

Ingelbrecht C., Peetermans F., De Corte F., De Wispelaere A., Vandecasteele C., Courtijn E. and D'Hondt P. (1991)
Aluminium-gold reference material for the k_0-standardization of neutron activation analysis, Nucl. Instr. Methods **A303**, 119-122.

IAEA reference material (1987)
Preparation and Certification of IAEA Gamma Spectrometry Reference Materials RGU-1, RGTh-1 and RGK-1, Report IAEA/RL/148, Vienna, Austria.

Jovanović S., Mihaljević N, De Corte F., Vancraeynest L., Faltejsek J., Vukotić P., Dapčevic S., Kučera J., De Wispelaere A, Carrot F., Dardenne-Deschamps C. and Deschamps N. (1992)
Experimental test of "MARSANGLE", a computer code to calculate detection efficiencies of Ge detectors for Marinelli sources, Proc. Intern. k_0 Users Workshop – Gent, 59-62.

Jovanović S., Dlabać A., Mihaljević N. and Vukotić P. (1997)
ANGLE: A PC-code for semiconductor detector efficiency calculations, J. Radioanal. Nucl. Chem., **218**, 13-20.

Kalchgruber R. (2002)
α-Al_2O_3:C als Dosimeter zur Bestimmung der Dosisleistung bei der Lumineszenzdatierung, PhD Thesis, Ruprecht-Karls-Univ. Heidelberg, Germany, 2002, pp. 130.

Kayzero/Solcoi (1996)
For reactor neutron activation analysis (NAA) using the k_0-standardization method, User's Manual. Version 4, DSM Research, Geleen.

Kitis G., Papadopoulos J. G., Charalambous S. and Tuyn J. W. (1994)
The influence of heating rate on the response and trapping parameters of α-Al_2O_3:C, Radiat. Prot. Dosim., **55**, 183-190.

Korotov V. S., Milman I. I., Kirpa V. I. and Lesz J. (1994)
Some features of α-Al_2O_3:C dosimetric thermoluminescence crystals, Radiat. Prot. Dosim., **55**, 279-283.

Krbetschek M. R., Rieser U., Zöller L. and Heinicke J. (1994)
Radioactive disequilibria in palaeodosimetric dating of sediments, Radiation Measurements, **23**, 485-489.

Mangini A., Pernicka E. and Wagner G.A. (1983)
Dose-rate determination by radiochemical analysis, PACT **9**, 49-56.

Marechal R. (1992)
Geologische kaart: Kwartairgeologie, lithologie van de oppervlakkige lagen, carthografische voorstelling en druk in het National Geografisch Instituut, Nationale Atlas.

Meakins R. L., Dickson B. L. and Kelly J. C. (1979)
Gamma-ray analysis of K, U and Th for dose-rate estimation in thermoluminescence dating, Archaeometry, **21**, 79-86.

Mejdahl V. (1969)
Thermoluminescence dating of ancient Danish Ceramics, Archaeometry, **11**, 99-104.

Mejdahl V. (1978)
Thermoluminescence dating: a thermoluminescence technique for beta-ray dosimetry, in "A Specialist Seminar on Thermoluminescence Dating", Oxford, PACT, Council Europe.

Miallier D., Fain J., Sanzelle S., Daugas J. P. and Raynal J. P. (1983)
Dating of the Butte de Clermont basaltic maar by means of the quartz inclusion method, PACT **9**, 487-498.

Moens L. De Donder J., Xilei Lin, De Corte F., De Wispelaere, Simonits A. and Hoste J. (1981)
Calculation of the absolute peak efficiency of gamma-ray detectors for different counting geometries, Nucl. Instr. Meth., **187**, 451-472.

Morozov G. V. (1968)
The relative dating of Quaternary Ukrainian sediments by the thermoluminescence method, 8th International Quaternary Association Congress, Paris, p. 167, U.S. Geological Survey Library, Washington D.C., Cat. No. 208M8280.

Moscovitch M., Tawil R. A. and Svinkin M. (1993a)
Light induced fading in α-Al_2O_3:C, Radiat. Prot. Dosim., **47**, 251-253.

Moscovitch M., Kaufman M. M., Rodgers J. E. and Nirroomand-Rad A. (1993b)
Ultra-low dose (100 nGy-100μGy) response of α-Al_2O_3:C, Radiat. Prot. Dosim., **47**, 173-176

Mukherje B. and Lucas A. C. (1993)
Light conversion efficiency of aluminium oxide dosemeters irradiation with ^{241}Am alpha particles, Radiat. Prot. Dosim., **47**, 177-179.

Murray A. S. (1981)
Environmental Radioactivity Studies Relevant to Thermoluminescence Dating, Ph.D. Thesis, University of Oxford, UK.

Murray A. S. (1982)
Studies of the stability of radioisotope concentrations and their dependence on grain size, PACT **6**, 216-223.

Murray A. S., Marten R., Johnston A. and Martin P. (1987)
Analysis for naurally occuring radionuclides at environmental concentrations by gamma spectrometry, J. Radioanal. Nucl. Chem., Articles, **115**, 263-288.

Murray A. S. and Aitken M. J. (1988)
Analysis of low-level Natural Radioactivity in Small Mineral Samples for use in Thermoluminescence Dating, using High-resolution Gamma Spectrometry, Appl. Radiat. Isot., **39**, 145-158.

Musk J. H. (1993)
Time-dependent and light-induced fading in Victoreen Model 2600-80 aluminium oxide thermoluminescence dosemeters, Radiat. Prot. Dosim., **47**, 247-249.

NBL (February, 1981a)
New Brunswick Laboratory Certified Reference Materials, Certificate of Analysis, CRM 105-A/Uranium Standard.

NBL (February, 1981b)
New Brunswick Laboratory Certified Reference Materials, Certificate of Analysis, CRM 109-A/Thorium Standard.

O'Brien T. J., Dooremus S. W., Moscovitch M., Rodgers J. E. and Popescu G. F. (1993)
Thermoluminescent response of aluminium oxide (α-Al_2O_3:C) to alpha particles, Hlth Phys., **64** (6 Suppl.) S41.

Olley Jon M., Roberts Richard G., and Murray Andrew S. (1997)
Disequilibria in the uranium decay series in sedimentary deposits at Allen's Cave, Nullarbor Plain, Australia: implications for dose rate determinations, Radiation Measurements, **27**, 433-443.

Pernicka E.
MPI, Heidelberg, Germany, private communication.

Pernicka E. and Wagner G. A. (1982)
Radioactive equilibrium and dose-rate determination in TL dating, PACT **6**, 132-144.

Prescott J. R. and Hutton J. T. (1994)
Cosmic ray contributions to dose rates for luminescence and ESR dating: large depths and long-term time variations, Radiation Measurements, **23**, 497-500.

Prescott J. R. and Hutton J. T. (1995)
Environmental dose rates and radioactive equilibrium from some Australian luminescence dating sites, Quaternary Science Reviews (Quaternary Geochronology), **14**, 439-448.

Preusser Frank and Uwe Kasper Haino (2001)
Comparison of dose rate determination using high-resolution gamma spectrometry and inductively coupled plasma-mass spectrometry, Ancient TL, **19**, 19-23.

Robouch P., Eguskiza M., Maguregui M. I., Pommé S. and Pauwels J. (2001)
k_0-NAA, a valuable tool for reference-material producers, Fresenius J. Anal. Chem., **370**, 255-258.

Sanderson D. C. W. (1988)
Thick source beta counting (TSBC): a rapid method for measuring beta dose-rates, Nucl. Tracks Radiat. Meas., **14**, 203-207.

Sanzelle S., Erramli H., Faïn J. and Miallier D. (1988)
The assessment of gamma dose-rate by gamma-ray field spectrometer, Nucl. Tracks Radiat. Meas., **14**, 209-213.

Tite M. S. and Waine J. (1962)
Thermoluminescent dating: a re-appraisal, Archaeometry, **5**, 53-79.

Vancraeynest L. (1998)
Bijdrage tot de studie van de thermoluminescentie-dateringsmethode en toepassing op archeologisch keramiek en eolische sedimenten, Ph.D. thesis, University of Ghent.

Van Lierde S., De Corte F., Bossus D., Van sluijs R., Pommé S. (1999)
Determination of k_0 and related nuclear data for short-lived radionuclides to be used in KAYZERO-NAA at DSM research, Nucl. Instr. Methods A, **422**, 874-879.

Vandenberghe D., Hossain S. M., De Corte F., Van den haute P. (2003)
Investigations on the origin of the equivalent dose distribution in the Dutch coversand, Radiation Measurements [in press].

Vandenberghe D., Kasse C., Hossain S. M., De Corte F., Van den haute P., Fuch M. and Murray A. S. (2003a)
Exploring the methodology of optically stimulated luminescence dating and comparison of optical and ^{14}C ages of late weichselian coversands in the southern Netherlands, Journal of Quaternary Science [submitted].

Warren S. E. (1978)
Thermoluminescence dating of pottery: an assessment of the dose rate from rubidium, Archaeometry, **20**, 69-71.

Wintle A. G. and Huntley D. J. (1979)
Themoluminescence dating of a deep-sea ocean core, Nature, **279**, 710-712.

Wintle A. G. and Huntley D. J. (1980)
Thermoluminescence dating of ocean sediments, Canadian Journal of Earth Sciences, **17**, 348-360.

Wintle A. G. and Dijkmans J. W. A. (1988)
Dose-rate comparisons of sands for thermoluminescence dating, Acient TL **6**, 15-17.

Zöller L.and Pernicka E. (1989)
A note on overcounting in alpha-counters and its elimination, Ancient TL **7**, 11-14.